Technical Report
for
Research Project T9902-11
"Multi-Column Bridge Retrofit"

ANALYTICAL EVALUATION OF RETROFIT STRATEGIES FOR MULTI-COLUMN BRIDGES

by

William F. Cofer
Associate Professor
Washington State University

David I. McLean
Associate Professor
Washington State Univesity

Yi Zhang
Graduate Research Assistant
Washington State University

Washington State Transportation Center (TRAC)
Washington State University
Department of Civil & Environmental Engineering
Pullman, WA 99164-2910

Washington State Department of Transportation
Project Manager
Keith W. Anderson

Prepared for

Washington State Transportation Commission
Department of Transportation
and in cooperation with
U.S. Department of Transportation
Federal Highway Administration

May 1997

TECHNICAL REPORT STANDARD TITLE PAGE

1. REPORT NO.	2. GOVERNMENT ACCESSION NO.	3. RECIPIENT'S CATALOG NO.
WA-RD 427.1		

4. TITLE AND SUBTITLE	5. REPORT DATE
Analytical Evaluation of Retrofit Strategies for Multi-Column Bridges	May 1997
	6. PERFORMING ORGANIZATION CODE
7. AUTHOR(S)	8. PERFORMING ORGANIZATION REPORT NO.
William F. Cofer, David I. McLean, and Yi Zhang	
9. PERFORMING ORGANIZATION NAME AND ADDRESS	10. WORK UNIT NO.
Washington State Transportation Center (TRAC) Civil and Environmental Engineering; Sloan Hall, Room 101 Washington State University Pullman, Washington 99164-2910	11. CONTRACT OR GRANT NO. T9902-11
12. SPONSORING AGENCY NAME AND ADDRESS	13. TYPE OF REPORT AND PERIOD COVERED
Washington State Department of Transportation Transportation Building, MS 7370 Olympia, Washington 98504-7370	Technical Report
	14. SPONSORING AGENCY CODE

15. SUPPLEMENTARY NOTES

This study was conducted in cooperation with the U.S. Department of Transportation, Federal Highway Administration.

16. ABSTRACT

Many retrofit measures have been proposed and then implemented into existing highway bridges. The goal of seismic strengthening is not intended to retrofit a bridge to be "earthquake-proof", but to minimize the likelihood of structural collapse. An amount of acceptable damage may occur during a design level earthquake. The combination of retrofit measures and the acceptable damage greatly complicates the structural properties for a bridge. It is necessary to use analytical and experimental means to verify the effectiveness of various retrofit combinations.

The objectives of this research are: (1) to investigate analytically the feasibility and advantages of applying the retrofit measures developed for single-column bent bridges to multi-column bent bridges; (2) to evaluate analytically the effects and benefits of current column retrofit strategies for multi-column bridges and propose the most effective measures for strengthening bridges; (3) to evaluate the performance of earthquake restrainers and find the change of seismic loads and displacements caused by their installation.

To achieve the objectives, an existing nonlinear dynamic bridge analysis program with elastic-perfectly plastic column behavior and a conventional hysteresis model was modified in order to include softening behavior and a more realistic hysteresis rule for cyclic loading.

Both two- and three-dimensional structural models for two actual bridges from Washington were analyzed by inputting a typical seismic record. The two-dimensional models were used to evaluate column retrofitting measures, and the three-dimensional model was used to evaluate the performance of longitudinal earthquake restrainers. Both partial and full column retrofit strategies were shown to result in decreased maximum earthquake response and decreased plastic deformation of columns for the bridge bent compared to the case without retrofitting. Therefore, it was concluded that the partial column retrofit strategies were feasible after a ductility capacity of the bridge is exactly defined. The opening displacements at expansion joint hinges were decreased due to the installation of longitudinal restrainers. Additionally, the redistribution of earthquake forces caused by their installation was not significant.

17. KEY WORDS	18. DISTRIBUTION STATEMENT
Key words: Bridge, earthquake, retrofit, analysis, column	No restrictions. This document is available to the public through the National Technical Information Service, Springfield, VA 22616

19. SECURITY CLASSIF. (of this report)	20. SECURITY CLASSIF. (of this page)	21. NO. OF PAGES	22. PRICE
None	None		

DISCLAIMER

The contents of this report reflect the views of the authors, who are responsible for the facts and the accuracy of the data presented herein. The contents do not necessarily reflect the official views or policies of the Washington State Transportation Commission, Department of Transportation, or the Federal Highway Administration. This report does not constitute a standard, specification, or regulation.

Table of Contents

List of Figures

List of Tables

Chapter 1

Introduction

1.1 History of Seismic Bridge Design and Retrofitting in the United States

Many bridges have been built since the beginning of this century. Not only do highway bridges serve as convenient and effective transportation tools, they are also important components for modern life. As one of the most developed countries, the United States is also one that has borne the most severe earthquake damage to highway bridges. Prior to the San Fernando earthquake of February 9, 1971, permanent ground displacement had been considered as the primary factor for earthquake damage (Iwasaki, Penzien, and Clough, 1972). Through analysis by researchers, it was found that the damage of superstructures was primarily caused by foundation failures resulting from large ground displacements, settlements, and loss of bearing capacity (Imbsen and Penzien, 1986). Therefore, it was little related to the deficiencies in the design provisions of that time.

The 1971 San Fernando earthquake caused substantial damage to highway bridges. During that earthquake, significant damage resulted from the dynamic behavior of the bridge superstructures, substructures, and their interactions (Tan and Wilson, 1987). Bridge designers concluded that seismic design provisions, which at that time did not include dynamic analysis, were insufficient for structures to resist potential earthquakes, especially those of the magnitude of the San Fernando earthquake. Dynamic

analysis, considering the properties of superstructures, substructures, and site-dependent characteristics, was added to the seismic design provisions for bridges along with other modifications. Several noteworthy techniques were also subsequently developed to increase the seismic capabilities of existing bridges as retrofit measures. On one hand, new design provisions for bridges were developed for future structural designs. On the other hand, the proposed retrofit measures were intended for bridges that were designed before 1971 and could not be replaced totally by new ones for reasons of economy and time.

1.1.1 Evolution of Seismic Design Provisions

The 1933 Long Beach earthquake increased the awareness that seismic design for buildings or bridges should be considered because of the occurrence of severe damage to public schools. In 1958, seismic loadings on highway bridges appeared in the Standard Specifications for Highway Bridges by the American Association of State Highway Officials (AASHTO), the first seismic design provision for highway bridges in the United States. In the design provisions, the equivalent lateral earthquake loading was expressed as a product of a lateral force coefficient and the dead load of the structure. The lateral force coefficient depended on the type of foundation and soil bearing capacity that supported it. It was obvious that the geographical conditions and structural vibrational properties were considered as influential factors on the lateral earthquake loading. The provisions remained in effect in the AASHTO specifications until 1973.

Because of the deficiencies in the existing design provisions, in 1968 the California State Division of Highways adopted the AASHTO specifications. In the new provisions, a new coefficient was included in the equation that was used to compute the lateral earthquake loading. The coefficient represented the energy absorption of the structure and therefore depended on the structural system and dimensions that resisted horizontal forces. Moreover, the lateral force coefficient was modified on the basis of the natural period of vibration of the structure. The adopted equation of lateral earthquake loading was better able to consider structural properties and vibrational effects than that of the earlier code. However, structures founded in soft soil must be given special consideration.

Many bridges collapsed and were severely damaged during the San Fernando earthquake. Most of the collapses and damage were primarily due to the failure of supporting columns due to moment and shear strength insufficiency and to inadequate seat width for bridge decks. These collapses and damage reflected the fact that the seismic design criteria before 1971 were not adequate. Immediately after the San Fernando earthquake, researchers and designers from the State of California began to update the seismic design provisions and seismic construction details. The new specifications after the San Fernando earthquake had significant enhancements relative to the old ones. The main enhancements included (Imbsen and Penzien, 1986):

- The geographical location of a bridge relative to an active fault;
- The effects of the maximum credible earthquake expected to occur on an active fault;

- The effect on surface motions of overlying soils at a site;
- The dynamic response of a bridge to ground motion;
- The reduction in design forces to account for ductility and risk considerations.

Based on the above criteria, a normalized elastic response spectrum and the maximum expected earthquake acceleration map across the entire United States were developed. The normalized elastic response spectrum was a family of curves of the normalized acceleration vs. basic period of a structure for various site categories. The product of the value from the response spectrum for a designed structure and the maximum expected acceleration obtained from the acceleration map where the structure was located was the lateral earthquake force coefficient. Finally, the lateral earthquake force was defined as the lateral earthquake force coefficient multiplied by the equivalent static load of the structure.

The criteria were designed to be open for the inclusion of future developments in various areas of earthquake engineering. The modification of construction details included (Roberts, 1995):

1) Improved design of bridge columns (Figure 1.1-1);
   - provide adequate confinement and shear reinforcing steel for columns
   - tie all main column reinforcing into the footing and superstructure
   - weld lap splices both in the main and transverse reinforcing
2) Beam-column joint confinement;
3) Improved edge beam-column-bent cap joint detail (Figure 1.1-2).

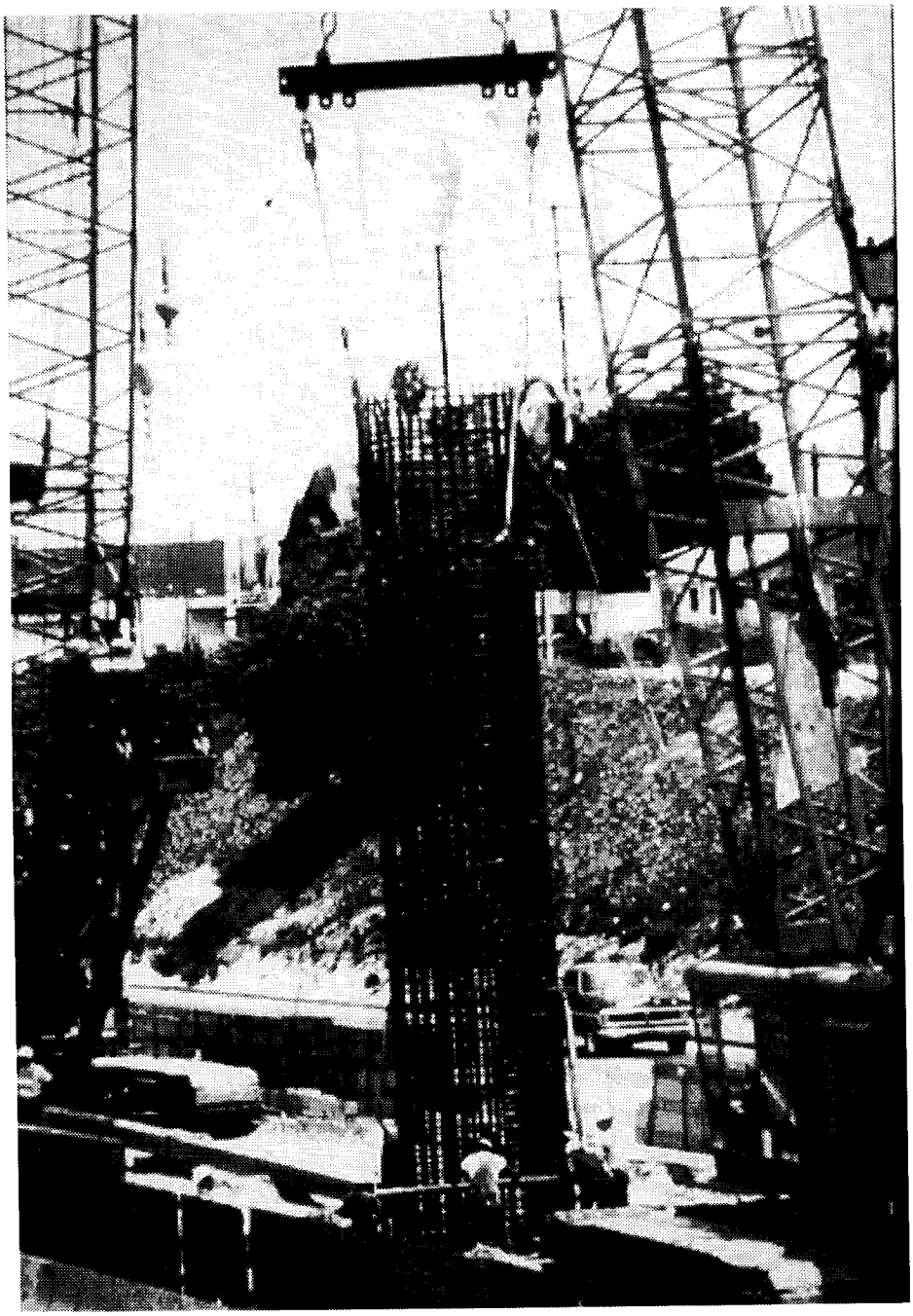

Figure 1.1-1: Reinforcing Steel Pattern for Ductile Column

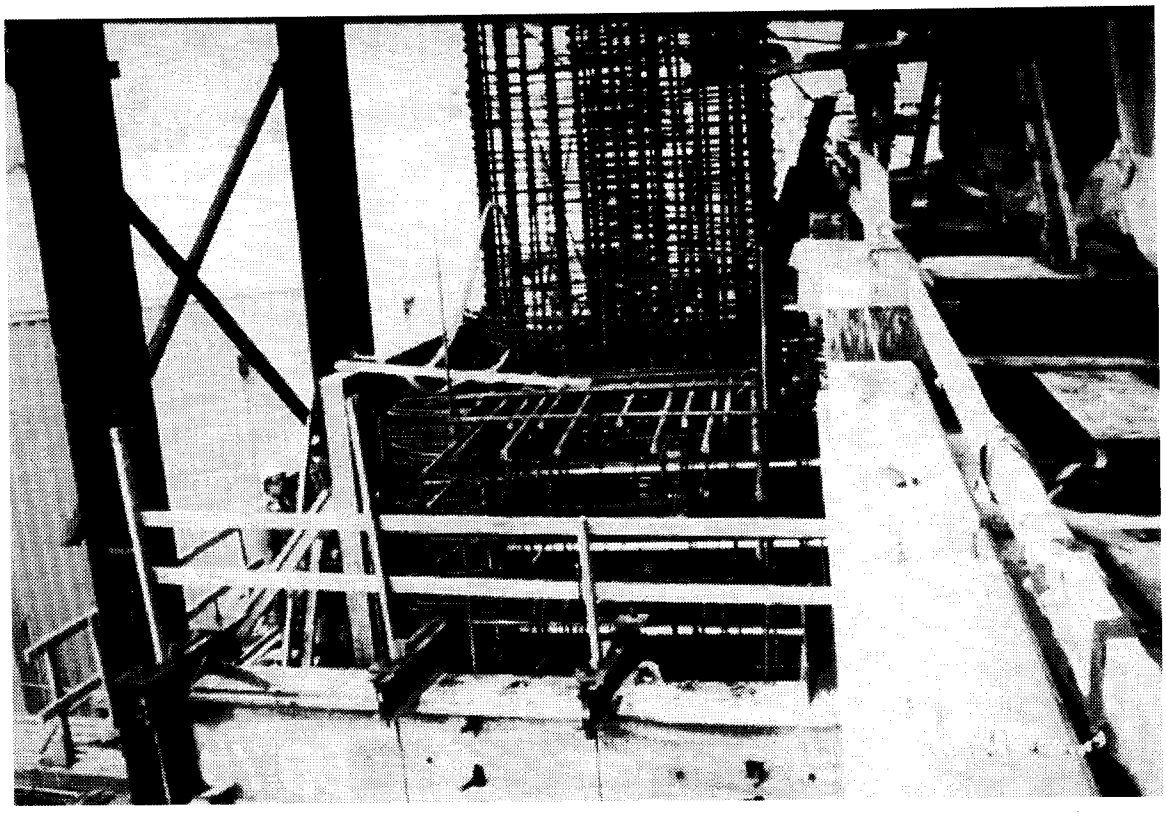

Figure 1.1-2: Reinforcing Steel Pattern for Beam-Column Joint

Because the updated seismic design provisions in the State of California considered the dynamic behavior of the bridges and site characteristics, and were proved to be effective for the earthquake resistance of bridges based on the new design guidelines in the post San Fernando earthquakes, AASHTO adopted the design criteria nationally in 1983. Following the update by AASHTO, many other states in the United States have used the California seismic design provisions for bridge designs.

1.1.2 Retrofit Measures Used for Improvement of Existing Highway Bridges

After the pre-1971 seismic design provisions were updated, the highway bridges designed using the new design guidelines in California performed very well without collapse or serious damage during several significant earthquakes that occurred in this state, such as the 1987 Whitter earthquake, the 1989 Loma Prieta earthquake, and the 1994 Northridge earthquake. However, the highway bridges constructed prior to the 1971 San Fernando earthquake suffered collapse and major damage. It was found by researchers that the separation of deck expansion joints and the failure of older non-ductile columns contributed to the causes of collapse and damage for highway bridges (Roberts, 1995). For example, during the 1994 Northridge earthquake, the failure of all six failed bridges and four badly damaged ones resulted primarily from the failure of the supporting columns that had been designed and constructed before 1971 (Cooper, *et al.*, 1994).

It has been identified that 37 of the 50 States in the US have a 1-in-10 chance of a significant earthquake occurring within the next 50 years. Relatively high levels of ground shaking are possible in fifteen of these States. Because of the numerous highway bridges that were built before 1971, and the large possibility that they will be subjected to relatively high levels of shaking for most states in the United States, necessary programs should be formulated to identify seismically deficient bridges, evaluate the consequences of seismic damage, and reduce the seismic risk to a minimum degree. One problem that bridge designers have confronted is that the bridges designed before 1971 can not be replaced totally by new ones for reasons of economy and time. Therefore, seismic retrofitting techniques for existing bridges have been developed and that are practical and feasible methods for reducing the risk that currently exists. The benefits of retrofit measures were evident in the 1989 Loma Prieta earthquake and 1994 Northridge earthquake. Currently, the California State Department of Transportation (Caltrans) has completed seismic retrofit upgrading on over 1/4 of the bridges that have been identified as requiring seismic retrofitting (Roberts, 1995). Most of the retrofitted bridges have performed very well in significant earthquakes.

The primary goal of seismic retrofitting is to minimize the risk of unacceptable damage during a design-level earthquake. This means that a considerable amount of structural damage during major earthquakes is acceptable but that collapse of the bridge is prevented. The acceptable damage is defined according to the importance of the bridge. This consideration that an acceptable amount of damage may occur for a bridge during an

earthquake is due to the difficulty and cost involved in strengthening an existing bridge to new design standards. Generally, the procedures for evaluating and upgrading the seismic resistance of existing highway bridges are described as follows (Buckle, and Friedland, 1995):

- A preliminary screening is performed to identify and prioritize bridges that need to be evaluated for seismic retrofitting;
- A methodology is applied for quantitatively evaluating the seismic capacity of an existing bridge and determining the overall effectiveness of alternative seismic retrofit measures, including cost and ease of installation;
- Retrofit measures and design requirements are identified for increasing the seismic resistance of existing bridges.

The above standards for evaluating and upgrading the seismic resistance of existing highway bridges are not straightforward because of the complexity and subjectivity of retrofitting decisions and the many non-engineering factors involved. Therefore, engineering judgment is required during that process. On the other hand, this also forces researchers to do further investigation and research, so that the retrofitting decisions can be made more scientifically, with fewer man-made factors.

Many bridges collapsed in the 1971 San Fernando earthquake. The major cause for many of the failures was separation of the deck joint due to an insufficient seat width. Therefore, early retrofit efforts in the State of California concentrated on providing restrainers between bridge deck sections. Moreover, the installation of devices to fasten

the superstructure elements to the substructure in order to resist vertical acceleration and prevent superstructure elements from falling off their supports was also included in this phase. While the hinge and joint restrainers performed well following the 1987 Whittier Narrows earthquake and the 1989 Loma Prieta earthquake, extensive damage occurred to many columns during these two earthquakes. In the moderate 1987 Whittier Narrows earthquake, shear failure of columns designed based on pre-1971 specifications on the I-605/I-5 bridges was found. The collapse of the Cypress Street Viaduct on I-880 in Oakland in the 1989 Loma Prieta earthquake was also a result of pre-1971 designed, non-ductile column damage. It became apparent that retrofit measures in which only partial components were strengthened were not sufficient; retrofit efforts must address the entire bridge structure. Subsequently, column and foundation retrofit strategies were developed, and the retrofit measures, especially the column retrofit measures, were observed to be effective in recent earthquakes. For example, in the 1994 Northridge earthquake, the 63 bridges strengthened by post-Loma Prieta retrofit details in this area performed extremely well (Roberts, 1995). In general, the main failure patterns of bridges and corresponding retrofit measures to overcome these types of failure include (Priestley, and Seible, 1988; Cooper, *et al.*, 1994; Buckle, and Friedland, 1995):

1) Superstructure failure due to inadequate force or displacement capacities and flexural strength (Figure 1.1-3).

Retrofit:

- Install longitudinal joint restrainers, transverse bearing restrainers, or vertical restrainers if necessary to increase displacement capacity (Figure 1.1-4);
- Extend bearing seat width;
- Replace bearing seats if their failure will result in collapse or loss of function of the superstructure.

2) Column failure due to deficiencies in flexural ductility, shear strength, and flexural strength, when affected by lap splices in critical regions (Figures 1.1-5 and 1.1-6).

Retrofit:

- Provide steel jacketing if there is inadequate confinement in the column and /or there are splices or laps in the hinge zone (Figure 1.1-7);
- Wrap prestressing wire under tension around a column;
- Place confinement consisting of composite fiberglass/epoxy as a column jacket;
- Add a comparatively thick layer of reinforced concrete in the form of a jacket to existing deficient circular and rectangular columns; or
- Insert external steel hoops tensioned onto the column by a turn-buckle arrangement.

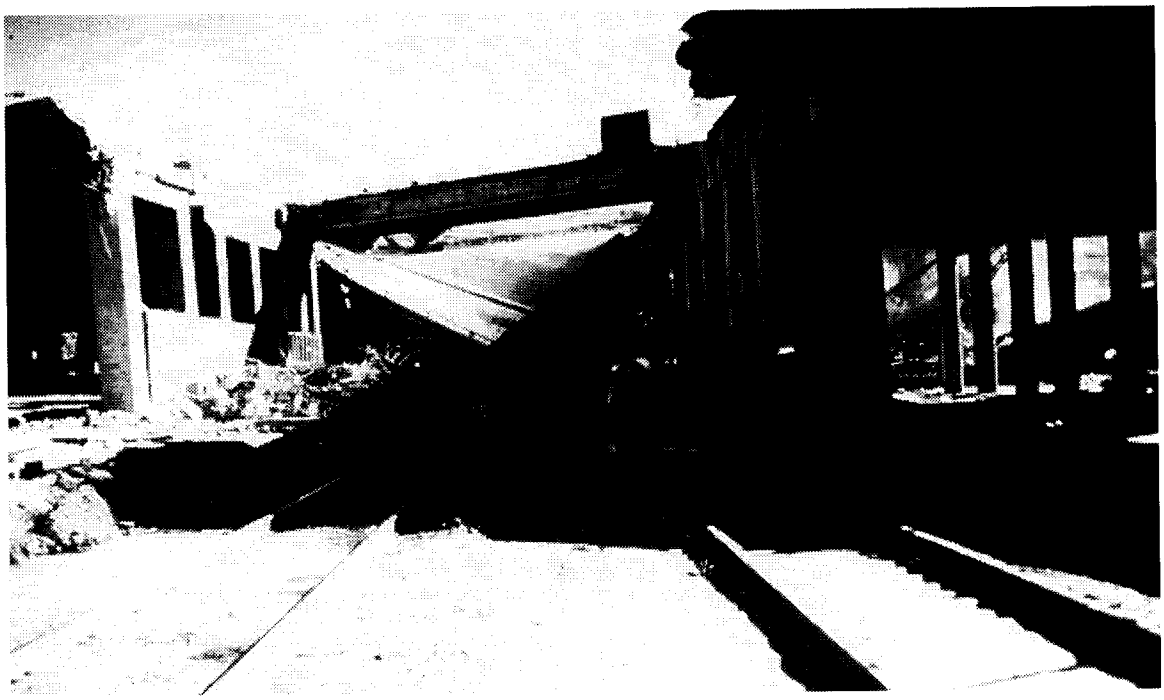

Figure 1.1-3: Spans Dropped off Narrow Support Seat

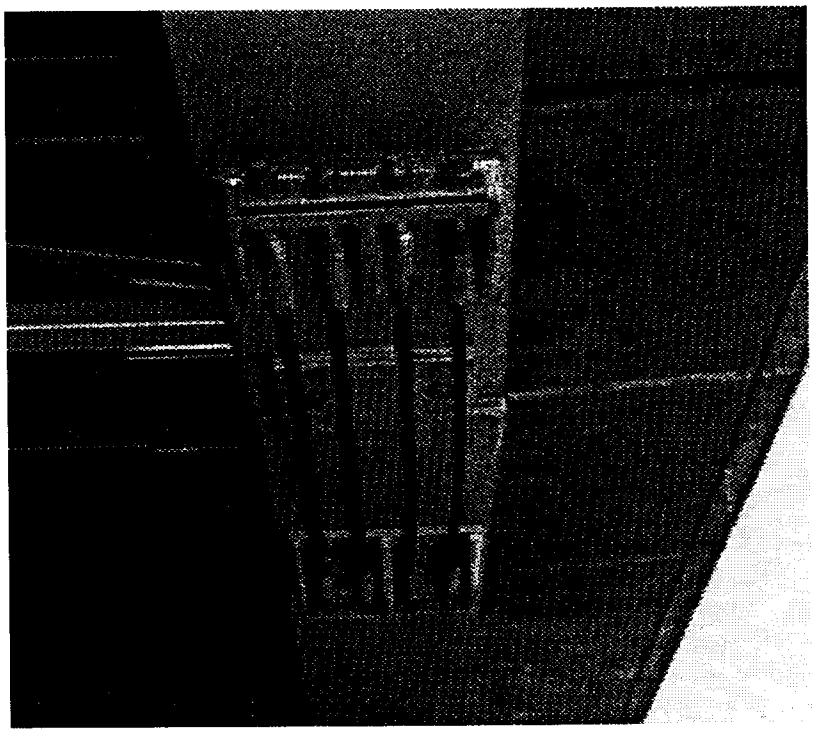

Figure 1.1-4: Cable Restrainers

Figure 1.1-5: Column Shear Failure

Figure 1.1-6: Column Flexural Failure

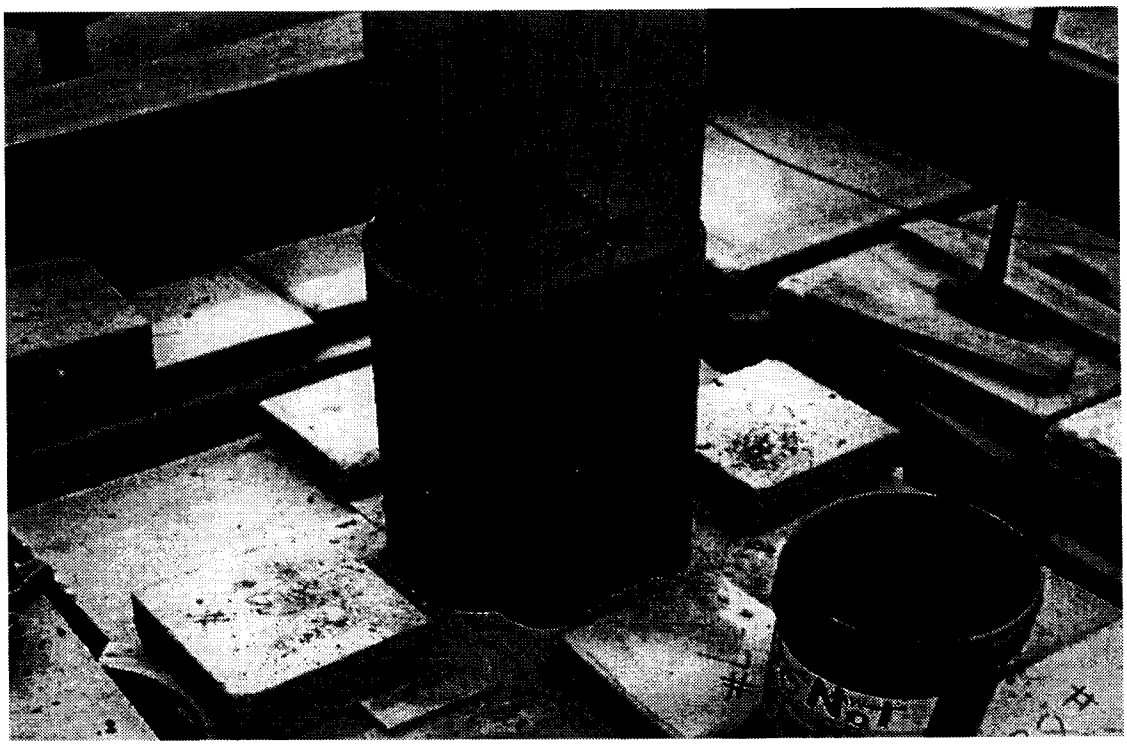

Figure 1.1-7: Steel Jacket Column Retrofit

3) Cap beam failure due to deficiencies in flexure, shear, joint shear, and torsion (Figure 1.1-8).

Retrofit:

- Add reinforced bolsters to the sides of the cap beam after roughening the interface if flexural strength and ductility need to be increased;
- Provide full-depth bolsters to the sides of cap beam and increase the depth of the flexural companion if shear strength is inadequate;
- Replace the existing joint of the column/cap beam or add reinforced concrete to the sides of the joint region if joint shear strength is deficient in integral column/cap beams;
- Add an edge beam (or supergirder) in the plane of the columns from bent to bent if the torsion strength of the cap beam needs to enhanced.

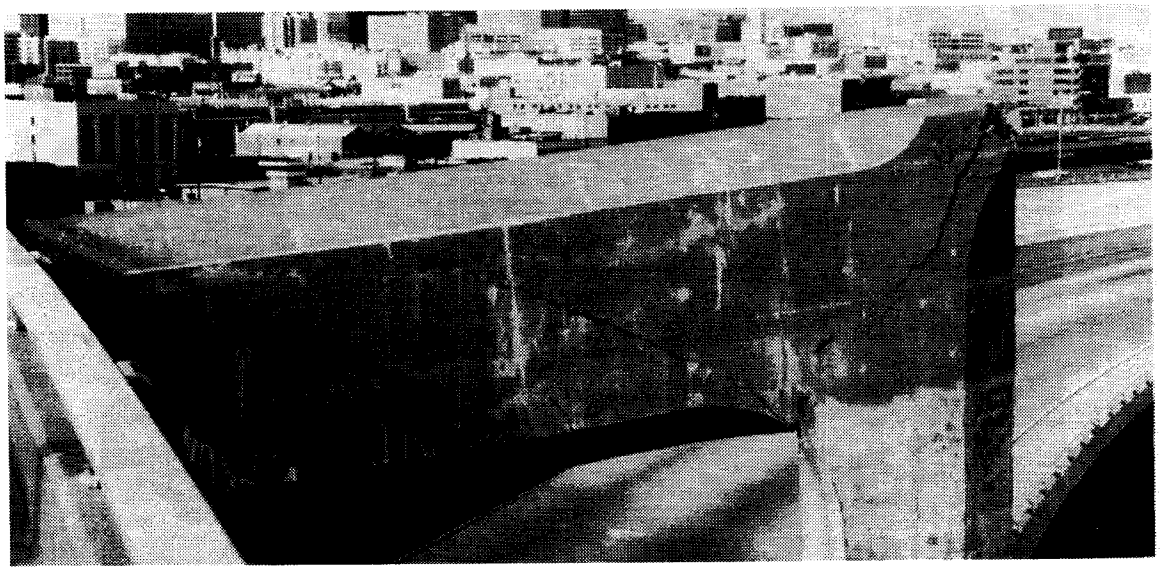

Figure 1.1-8: Cap Beam Flexure/Shear Failure

4) Footing failure due to deficiencies in footing flexural strength, shear strength, footing/column shear, anchorage of column rebar, pile capacity, and overturning resistance.

Retrofit:

- Dowel an overlay of reinforced concrete to the existing footing, or increase the depth of the footing if flexural strength of the footing is inadequate;
- Increase the footing depth, drill vertically through the footing and anchor vertical rebar, or drill longitudinally through the footing, preferably prestressed if increased shear strength of the footing is required;
- Increase the footing plan dimensions, add tension piles; or use soil or rock anchors if the footing overturning resistance needs to be improved;
- Replace the damaged footing after an earthquake.

5) Abutment failure due to abutment fill slumping from soil failure behind the abutment or permanent abutment movement (Figure 1.1-9).

Retrofit:

- Place settlement slabs tied to the abutment to provide continuity between the bridge deck and the abutment fill in the case of approach fill settlement;
- Add soil or gravity anchors to prevent or minimize displacement of abutment normal or parallel to the abutment face.

It should be noted that here only conventional retrofit strategies were discussed. Earthquake protective systems, such as seismic isolation, or the installation of mechanical energy dissipation devices, were not considered.

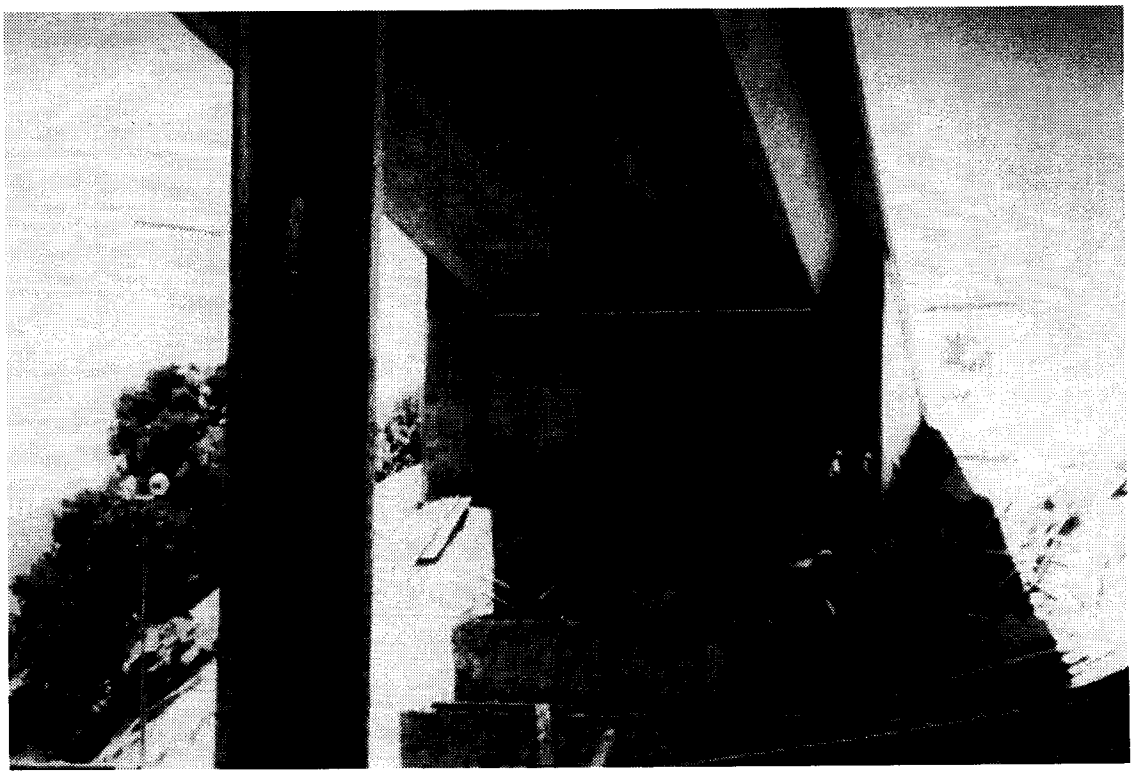

Figure 1.1-9: Abutment Failure for Large Displacements

1.2 Current Research on Retrofit Strategies

The 1989 Loma Prieta earthquake and the 1994 Northridge earthquake have provided important information for future highway bridge strengthening. Much research has been conducted in both the US and around the world. Priestley and Seible (1991) established widely used procedures for the assessment and retrofit procedures of bridges. The new procedures simplified global analysis procedures for seismic assessment and retrofit. Based on a large number of experiments that they have conducted, the new approaches are more realistic in predicting member and section performance than previous practice. It was pointed out that retrofit protection should be increased, particularly for connection regions which were not typically considered in earlier procedures. In recent years, the new procedures have been applied to a large number of real assessment and retrofit situations. As a result, considerable savings have been realized through the reduced need for retrofit (Priestley and Seible, 1994). In general, current research efforts toward retrofit strategies have stressed effectiveness and economics.

1.2.1 Analytical Procedures

Powell defined the main steps for structural analysis, whether linear or nonlinear, at the Third Caltrans Workshop, 1994. They are:

1) Create an analysis model of the structure;

2) Perform numerical computation on the model; and

3) Interpret the results.

The second step is a key step in the process because the results will not be correct or cover the overall structural behavior if the numerical analysis is not appropriate. Although the analysis may be linear or nonlinear, nonlinear analysis is particularly useful for predicting structural behavior under strong earthquakes. Therefore, an important consideration in structural analysis should be placed on the selection of an appropriate computer program. The program should have the ability to handle all types of elements, from linear elements to nonlinear, three-dimensional elements.

When researchers tried to describe and explain the failure mechanism of highway bridges by existing linear theories, they met many difficulties. The main reason is that the performance of bridges under strong earthquakes exhibits a complex nonlinear and inelastic behavior. However, capabilities of modern computers and workstations allow the consideration of numerous nonlinear effects. For instance, beam-column members during potential major earthquakes will develop many mechanisms, such as (Powell, 1994):

- Concrete crushing, and cracking;
- Yield and strain hardening of longitudinal reinforcement;
- Buckling of longitudinal reinforcement;
- Spread of concrete crushing, concrete cracking and reinforcement yield, both along the length of the column and through the depth of the cross section at any longitudinal location;

- Diagonal shear cracking in the concrete;
- Yield of transverse reinforcement, caused by shear forces and/or by the need to provide concrete confinement;
- Diagonal concrete cracking and yield of transverse reinforcement due to torsional moments;
- Deformations, especially bond slip, in the connection regions at the column ends;
- Bond slip of transverse reinforcement;
- Interaction between axial force, biaxial bending, biaxial shear force and torsional moment, especially in hinge regions;
- Degradation of stiffness and strength under cyclic loads;
- $P-\Delta$ and $P-\delta$ effects.

Obviously, it is nearly impossible to develop a practical model to accurately capture the complete details of these behavioral aspects in even a nonlinear and inelastic structural analysis of bridges. However, an important goal in nonlinear and inelastic analysis is to help structural engineers make design decisions, that is, to identify the main modes of behavior of the structure without worrying about the detailed numerical values. Thus, it need not be "exact," but only accurate enough for practical design purposes. Such a release allows researchers to model only the significant behavioral aspects in analyses, and then build equations and rules that define nonlinear and inelastic behavior by an empirical approach. The empirical approach is to develop equations and rules to capture complex nonlinear and inelastic behavior, with little or no attempt to model the

underlying mechanisms directly. It requires ensuring that the nonlinear and inelastic solutions that form the basis of the equations is accurate enough for engineering purposes.

In general, the criteria to identify the effectiveness of a nonlinear and inelastic analysis method depend on the following:

1) The nonlinear and inelastic models should be rational with model parameters that can be easily identified and specified;
2) An effective nonlinear and inelastic numerical solution method is very important to ensure that the nonlinear and inelastic solution will converge to the physically correct solution;
3) An intuitive and efficient post-processing tool is required to handle the large amount of information that arises from the nonlinear and inelastic dynamic analysis of a complex structure.

Tseng and Penzien developed a nonlinear mathematical model for bridge structural systems in 1973 in which an elasto-perfectly plastic beam-column element and bridge expansion joint element were presented. Based on this computer program called NEABS (Nonlinear Earthquake Analysis of Bridge System), case studies on long, multiple-span highway bridges that suffered heavy damage during the 1971 San Fernando earthquake were conducted. They concluded that a nonlinear mathematical model that represented the structural system should be used in dynamic analysis for major highway bridge design (Tseng and Penzien, 1973). In 1975, another analytical

investigation of the dynamic response of short, single-span and multiple-span highway overcrossings of the type which suffered heavy damage during the 1971 San Fernando earthquake was conducted by using the NEABS program (Chen and Penzien, 1975). Again, in 1978 Imbsen, Nutt, and Penzien investigated analytically the seismic response of bridges by conducting case studies in order to evaluate seismic design provisions and methodology and to aid in formulating recommendations for changes in the design provisions. All three investigations were part of the project entitled "An Investigation of the Effectiveness of Existing Bridge Design Methodology in Providing Adequate Structural Resistance to Seismic Disturbance," under the sponsorship of U.S. Department of Transportation, Federal Highway Administration.

In 1986, Imbsen and Penzien modified the nonlinear beam-column element and expansion joint element to include kinematic hardening in the beam-column element and a bilinear force-displacement relationship for the tie bar in the expansion joint element in order to analytically evaluate the energy characteristics of highway bridges under seismic conditions. The case studies included assessments of energy absorption, comparisons between the results obtained using elastic and nonlinear analyses, and a correlation with a documented earthquake failure (Imbsen and Penzien, 1986). Several major and significant conclusions and suggestions were drawn. Saiidi, *et al.*(1996) conducted a parameter study on bridge restrainer design for seismic retrofit by using the modified NEABS program when the change of cross-sectional area of restrainers and the restrainer gap was considered. They recommended that restrainer design should be based on cases

with and without restrainer gaps to encompass all the critical forces, stresses, and displacements.

In addition to NEABS, a number of computer programs have been developed in the past several years for nonlinear cyclic analysis of reinforced concrete structures, for instance, SARCF-II by Rodriguez-Gomez, *et al.* (1990); DRAIN-2DX by Prakash, *et al.* (1992); and IDARC by Kunnath, *et al.* (1992). Each of these programs has achieved some measure of success in predicting the inelastic dynamic response of reinforced concrete structures. Compared to NEABS, these programs have advantages in that they use hysteretic models to model reinforced concrete component behavior. However, these programs were not specifically designed for highway bridge dynamic analysis. Some special elements that only highway bridges possess, such as an expansion joint element and a curved beam element, were not included in these programs. At the same time, these programs also were limited to two-dimensional frames.

In 1990, the National Institute of Standards and Technology (NIST) developed a consistent, integrated approach to the seismic design, retrofit, and repair of structures. Based on the method presented by NIST, an integrated seismic design procedure (ISDP) that focused on the behavior of reinforced concrete bridge columns was proposed (Stone and Taylor, 1994). In this procedure, first, bedrock earthquake motions are filtered through the soil overburden using a wave-propagation model. Each filtered earthquake acceleration record was then applied to the structure individually for nonlinear dynamic analysis, and the record causing the greatest damage was taken as the controlling design

case. The damage index was compared with a predetermined acceptable level of damage. If the damage index exceeded the acceptable level of damage, then for the column being designed, the structural configuration needed to be altered, but for an existing column, retrofit should be used to increase its strength. The analysis was repeated until an acceptable level of damage was obtained. Various changes of structural configuration and various levels of retrofit might be checked on the basis of minimum cost of construction. In case studies, the one dimensional shear-wave model program SHAKE91 (Idriss, *et al.*, 1992) and the inelastic dynamic analysis program IDARC (Kunnath, *et al.*, 1992) were used. The damage index model was the model that was presented by Park and Ang (1985).

1.2.2 NEABS Computer Program

To realize the research objectives presented in this dissertation, the modification of NEABS was required. Therefore, it is necessary to have an introduction to this nonlinear dynamic analysis program.

The computer program NEABS was originally developed by Tseng and Penzien in 1973 for performing three-dimensional nonlinear dynamic analyses of long, multi-span bridges (Tseng and Penzien, 1973). The program was later modified in 1976 by Kawashima and Penzien, and again in 1978 by Imbsen, Nutt, and Penzien. To study energy absorption characteristics of highway bridges under seismic conditions, Imbsen and Penzien presented a new nonlinear beam-column element that added kinematic

hardening effects to NEABS in 1986. At the same time, a gapped tension-compression, tie-bar element was also developed for inclusion in the NEABS nonlinear expansion joint element.

Using plastic flow theory, the structural elasto-plastic stiffness matrix for beam-column elements was derived for the original program. It was assumed that the material behavior of the beam-column element was elastic-perfectly plastic, in which plastic hinges were point hinges (zero-length hinges), and the yield function was similar to that proposed by Bresler (1960). A nonlinear expansion joint element was included in this program to simulate the effects of impacting when the expansion joint closes, of sliding friction of bearings when joint movements exceed the bearing capacities, and of yielding of earthquake restrainer cables. Because the continuous bridge deck sections are usually strong enough to remain elastic during a severe earthquake, they may be modeled by elastic straight and curved beam elements. Support conditions of structures were modeled by three-dimensional boundary spring elements.

NEABS can evaluate a discrete bridge system subjected to applied dynamic loadings or prescribed support motions. The concentrated masses, or mass moments of inertia, may be assigned to structural nodes directly, but the distributed masses of beams or columns are equivalently placed on the two end nodes by computing consistent masses of beams or columns. Moreover, multiple dynamic loadings or support motions can be applied simultaneously.

The equation of motion in NEABS is solved by a step-by-step direct integration procedure. Either the constant acceleration or the linear acceleration method may be chosen for integration depending on which one can lead to convergence. To increase the speed of convergence at each time step, an option is provided through subdividing the time step.

Recently, it has been recognized that the effect of soil-structure interaction is important and cannot, in general, be neglected. Therefore, to enhance its capacities, Cofer, *et al.* (1994) modified the 1978 version of NEABS to include the effect of soil-structure interaction in the program. In the modified version of NEABS, a Discrete Foundation (DF) element was developed to allow a variety of discrete foundation models that include the energy dissipation associated with the soil domain. These models may range in complexity from simple linear elastic spring supports to those employing a number of internal nodes, masses, dampers, and nonlinear springs. This research was conducted using the modified version of NEABS.

1.3 Aims of This Research

Many retrofit measures have been proposed and then implemented into existing highway bridges. The goal of seismic strengthening is not to retrofit a bridge to be "earthquake-proof", but to minimize the likelihood of structural collapse. Some level of acceptable damage may occur during a design level earthquake. An option in current retrofit strategies is to retrofit only some of the columns for a bridge bent rather than all of them, providing economic benefits when compared to a full retrofit. Retrofitted single-

column bents perform very well in laboratory tests and have performed well in recent earthquakes. Thus, these retrofit measures developed for single columns may be applied to multi-column bent bridges. The combination of unretrofitted and retrofitted columns in a multi-column bridge bent complicates the structural properties compared with a single-column bridge bent. It is necessary to use analytical and experimental means to verify the effectiveness for various combinations, so that the most economical and technically feasible ones can be found. The analytical evaluations are especially important because any future experimental research requires guidelines from the results of the analysis.

It may be said that the installation of restrainers between bridge deck sections is the earliest and simplest retrofit technique to avoid catastrophic collapse of bridges due to a loss of support at their bearing seats. This retrofit effort performed very well in several major earthquakes. However some problems still remain. One important lesson that was learned in the recent Kobe earthquake was the necessity to assure that the destructive force is transmitted by restrainers to the strongest structural elements rather than the weakest ones. The inappropriate use and/or installation of restrainers can defeat their purpose and perhaps trigger a collapse (Cooper and Buckle, 1995). Thus, a precise prediction of the seismic force path during an earthquake will help to determine the need for retrofitting the weakest member when the restrainers are installed.

The objectives of this research are:

1) To investigate analytically the feasibility and advantages of applying the retrofit measures developed for single-column bent bridges to multi-column bent bridges;

2) To evaluate analytically the effects and benefits of current column retrofit strategies for multi-column bridges and propose the most effective measures for strengthening bridges;

3) To improve nonlinear beam-column element capabilities in NEABS; including

- softening behavior, in which the bending moment capacity is allowed to degrade, and
- a more accurate hysteretic rule for cyclic loading

4) To evaluate the performance of earthquake restrainers and find the change of seismic loads and displacements caused by their installation;

5) To provide guidelines in selecting safe and economical retrofit measures and define future research orientation to verify the recommended measures.

1.4 A Reconnaissance of the Recent Northridge Earthquake

At 4:31 a.m. PST on Monday, January 17, 1994, an earthquake with a Richter magnitude of 6.8 occurred in the Northridge section of the San Fernando Valley in Los Angeles. The ground shaking lasted approximately 20 seconds and fifty-seven people lost their lives during the quake. The economic loss from the earthquake was tremendous because the epicenter of this quake was directly beneath a suburban area of houses, apartment buildings, shopping malls, hospitals, schools, and a university campus.

Generally speaking, the majority of the bridges in this earthquake area performed well. However, because of some failures of highway overpasses, the normal order of work and life was significantly disrupted after the earthquake occurred. Six bridges collapsed and 157 other highway bridges were damaged. Among those damaged bridges, four were so badly damaged that they had to be replaced. The estimated cost to replace and repair these bridges is $1.5 billion.

The lessons learned through the performance of bridges in this earthquake are valuable for future studies. The following is a brief overview of the significant failures of bridges in this quake. It is based on the publication entitled "1994 Northridge Earthquake, Performance of Structures, Lifelines, and Fire Protection System" (Todd, *et al.*, 1994).

1.4.1 Bridge Damage in the Northridge Earthquake

Interstate 5 (the Golden State Freeway)

The bridge at Interstate 5 over Gavin Canyon failed because three of the four end spans of the bridge fell off the hinge seats (Figure 1.3-1). This bridge was designed in

1964, constructed in 1967, and cable restrainers were later installed at the hinges in order to prevent the failure of the superstructure. The bridge has four two-pier bents, and there is a structural hinge near each of the two center bents (Figure 1.3-2). The superstructure consists of reinforced concrete box girders. The skewed alignment of the bridge was reputed to be an important factor in this failure (Todd, *et al.* 1994). The skewed alignment permitted rotation of the superstructure; however, the tall, flexible piers of the two center bents offered relatively small resistance to rotation in the horizontal plane. Therefore, large displacements resulted at the hinges due to the rotation of the superstructure. Eventually, the end spans were unseated.

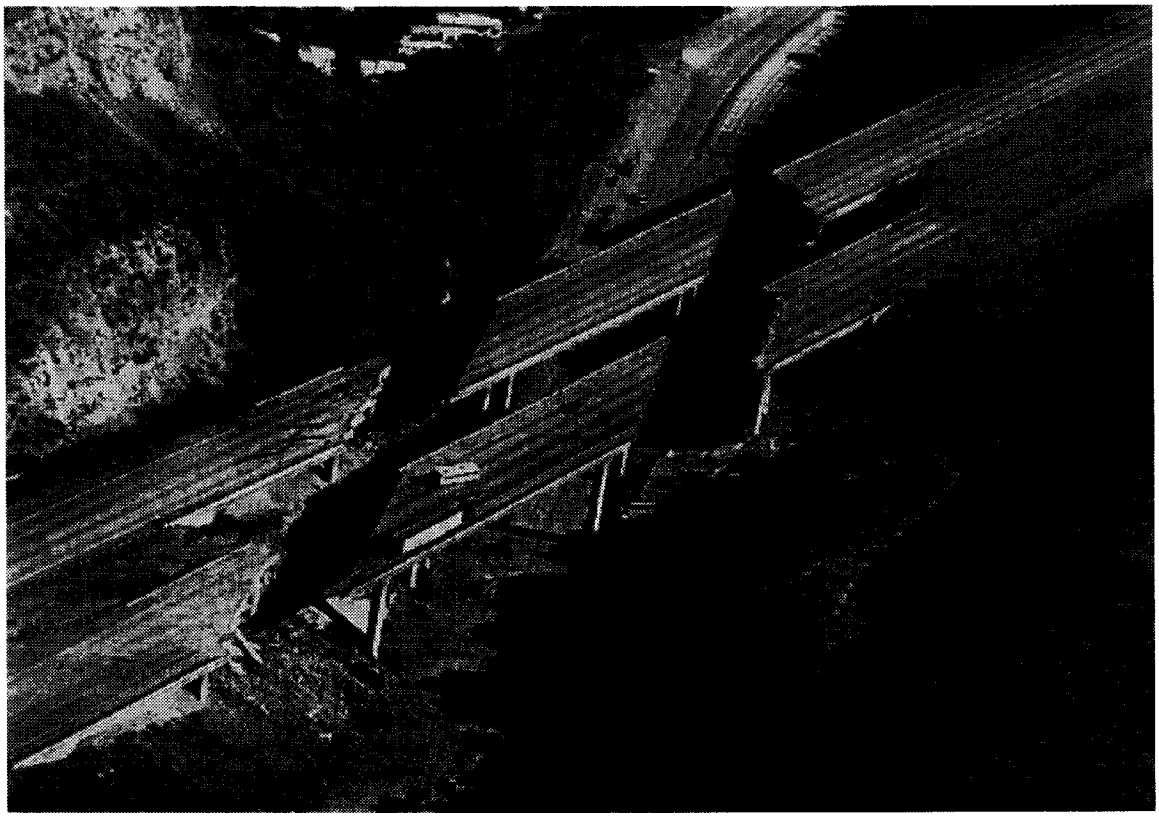

Figure 1.3-1: Aerial View of the Damaged Bridge at Interstate 5 (the Golden State Freeway (from Todd, *et al.*, 1994)

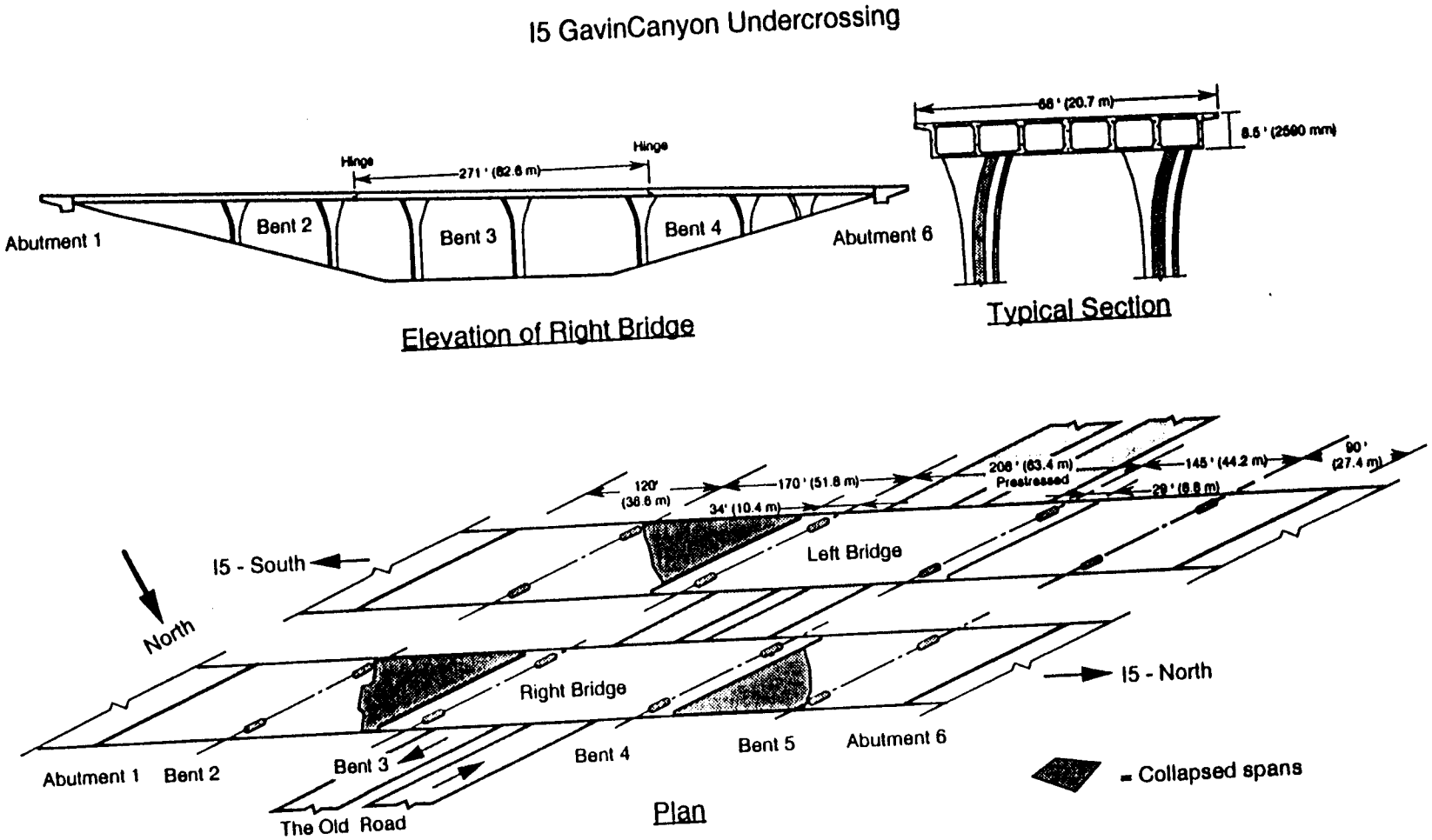

Figure 1.3-2: Plan and Elevation Views of Gavin Canyon Undercrossing (Todd, *et al.*, 1994)

State Route 14 (the Antelope Valley Freeway) Interchange

Two bridges partially collapsed at the State Route 14 Interchange. The two bridges are the 14/I5 Separation and Overhead Ramp C (Figure 1.3-3) and the North Connector Overcrossing Ramp M (Figure 1.3-4). Figures 1.3-5 and 1.3-6 show the collapse of the two bridges. Both bridges were designed in 1968 and constructed in 1971. The structures consist of multiple-cell concrete box girders, supported on single pier bents. The quantities of transverse reinforcement are considered inadequate by current standards. Because of the topography, the height of the piers was not the same for the two bridges. The piers located at the middle portion of the ramps were higher than the piers located at both ends. The portions of the two bridges that collapsed were three continuous spans starting from an abutment. The possible explanation for the two bridge failures are nearly the same (Todd, *et al.* 1994). The shortest and stiffest pier at an end of the ramp attracted a large share of the horizontal seismic forces. Thus, the pier was first damaged and collapsed, and then, it pulled the superstructure off the seat at the abutment.

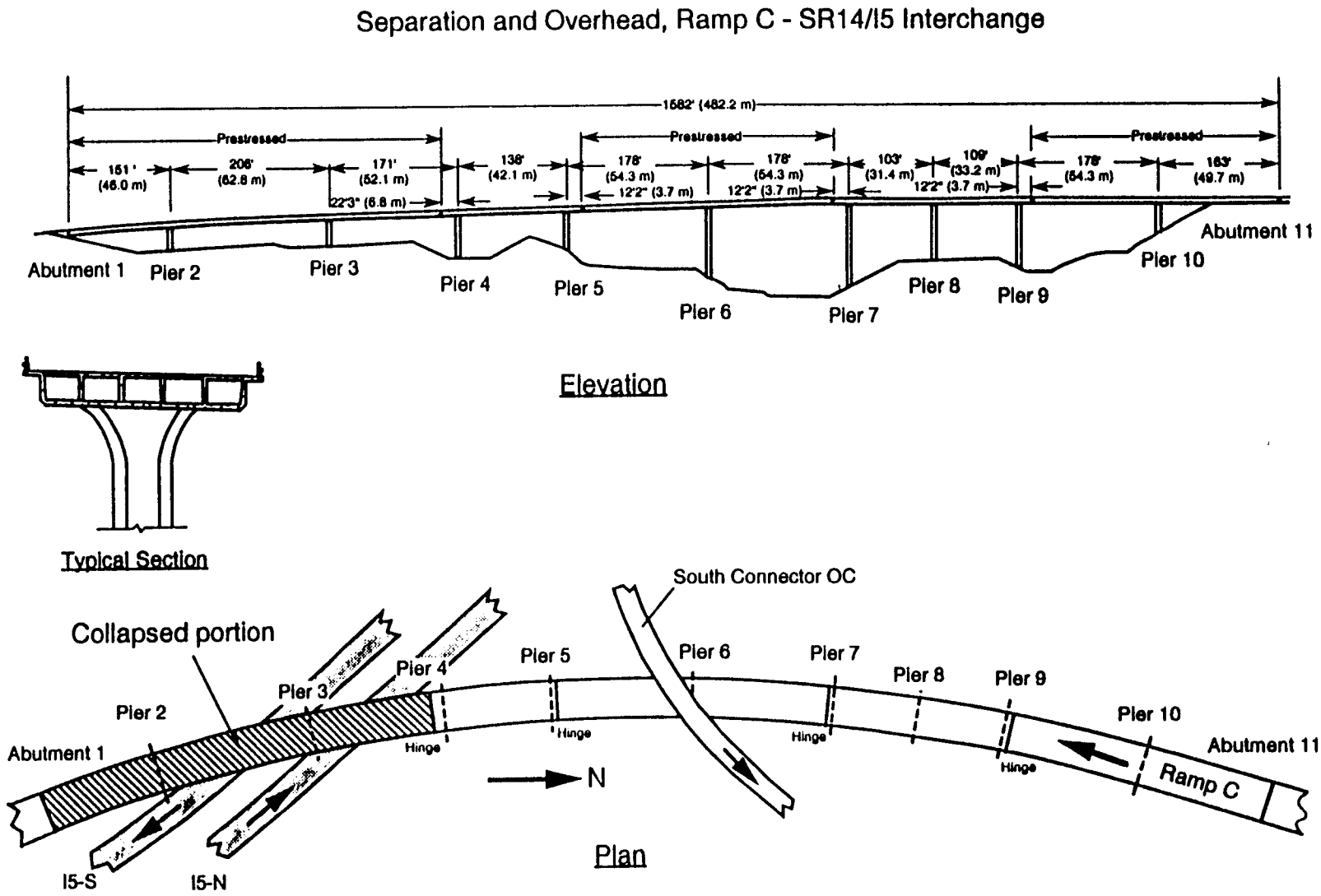

Figure 1.3-3: Plan and Elevation Views of the SR 14/I5 Separation and Overhead, Ramp C (Todd, *et al.*, 1994)

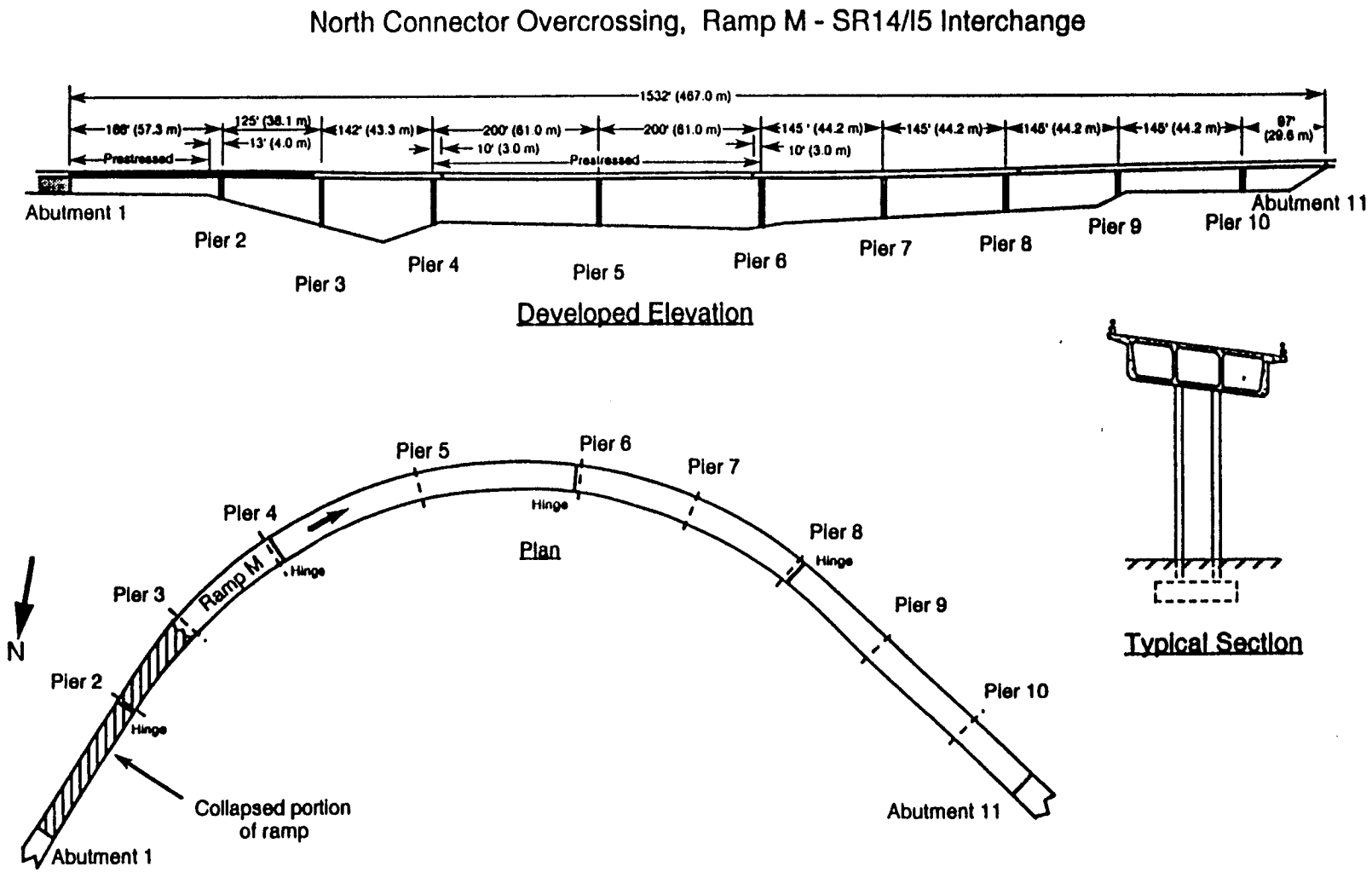

Figure 1.3-4: Plan and Elevation Views of the SR 14/I5 North Connector Overcrossing (Todd, *et al.*, 1994)

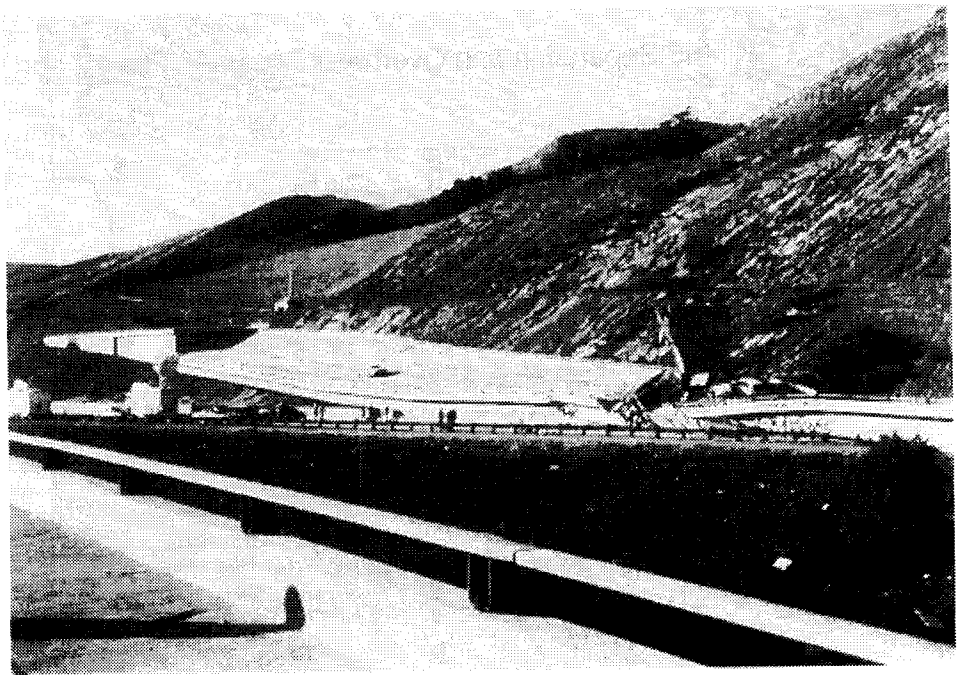

(a)

(b)

Figure 1.3-5: The Collapse of the SR 14/I5 Separation and Overhead, Ramp C: (a) Overview; (b) Damage of Pier 3 (Todd, *et al.*, 1994)

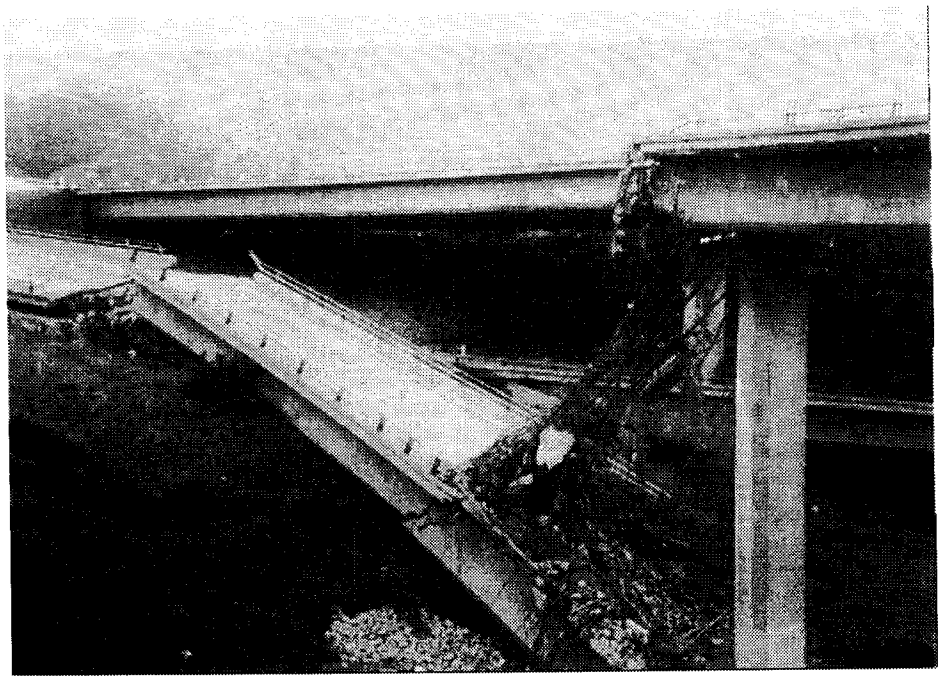

(a)

(b)

Figure 1.3-6: Collapse of the SR 14/I5 North Connector Overcrossing, Ramp M: (a) Collapsed Portion; (b) Crushed Pier (Todd, *et al.*, 1994)

State Route 118 (the Simi Valley Freeway)

Three bridges received significant damage, but two bridges, at the intersection of San Fernando Mission Boulevard and Gothic Avenue (Figure 1.3-7), and Bull Creek Canyon Channel (Figure 1.3-8), were damaged severely. The bridge at the Ruffner Avenue Overcrossing had repairable damage.

Because of severe damage to piers (Figure 1.3-9) and abutments, the eastbound lanes of the Mission-Gothic Undercrossing collapsed. The bridge was designed in 1972, after the San Fernando earthquake. Thus, the seismic details in this bridge were improved by the modified design codes. The most notable improvement is that the spiral hoops in the bridge piers were spaced closely together. Damage and collapse were attributed to two main sources: the geometry of the overall structure, and the geometry of the bridge piers. As shown in Figure 1.3-7, the plan shape of the bridge is a trapezoid. The orientation of the abutments constrains the structure to move only in the lateral direction during an earthquake; thus, diagonal shear failures were observed in many of the piers. Compared to the geometry of the overall structure, the geometry of the piers was a more important factor in causing the bridge failure. The relatively short piers, roughly 24 ft tall and 6 ft across, with the architectural flares, resulted in an aspect ratio of only 3:1. Thus, the piers were very stiff laterally, and many shear rather than bending failures were observed in the piers (Todd, *et al* 1994).

Many of the piers of the bridge at Bull Creek Canyon Channel were severely damaged (Figure 1.3-10) though the bridge did not collapse completely. The bridge was designed just after the 1971 San Fernando earthquake, and it contains some seismic

detailing. However, since the seismic design codes were not significantly updated at that time, the design of this bridge was not sufficient when compared with current seismic design standards. The failure of the piers was observed to result from combined shear and compression near their bases and tops. The inadequate confining reinforcement in the piers and the asymmetric plan geometry of the bridge were main factors in causing these failures.

The bridge at the Ruffner Avenue Overcrossing, designed in 1971, after the San Fernando earthquake, was not damaged seriously during the earthquake. The only significant damage suffered by the bridge was extensive spalling at one of the centers, as shown in Figure 1.3-11. Two factors contributed to the favorable seismic performance of this bridge: (1) adequate confining reinforcement in the piers and the adequate slenderness of the piers; (2) fairly compact overall geometry of the bridge.

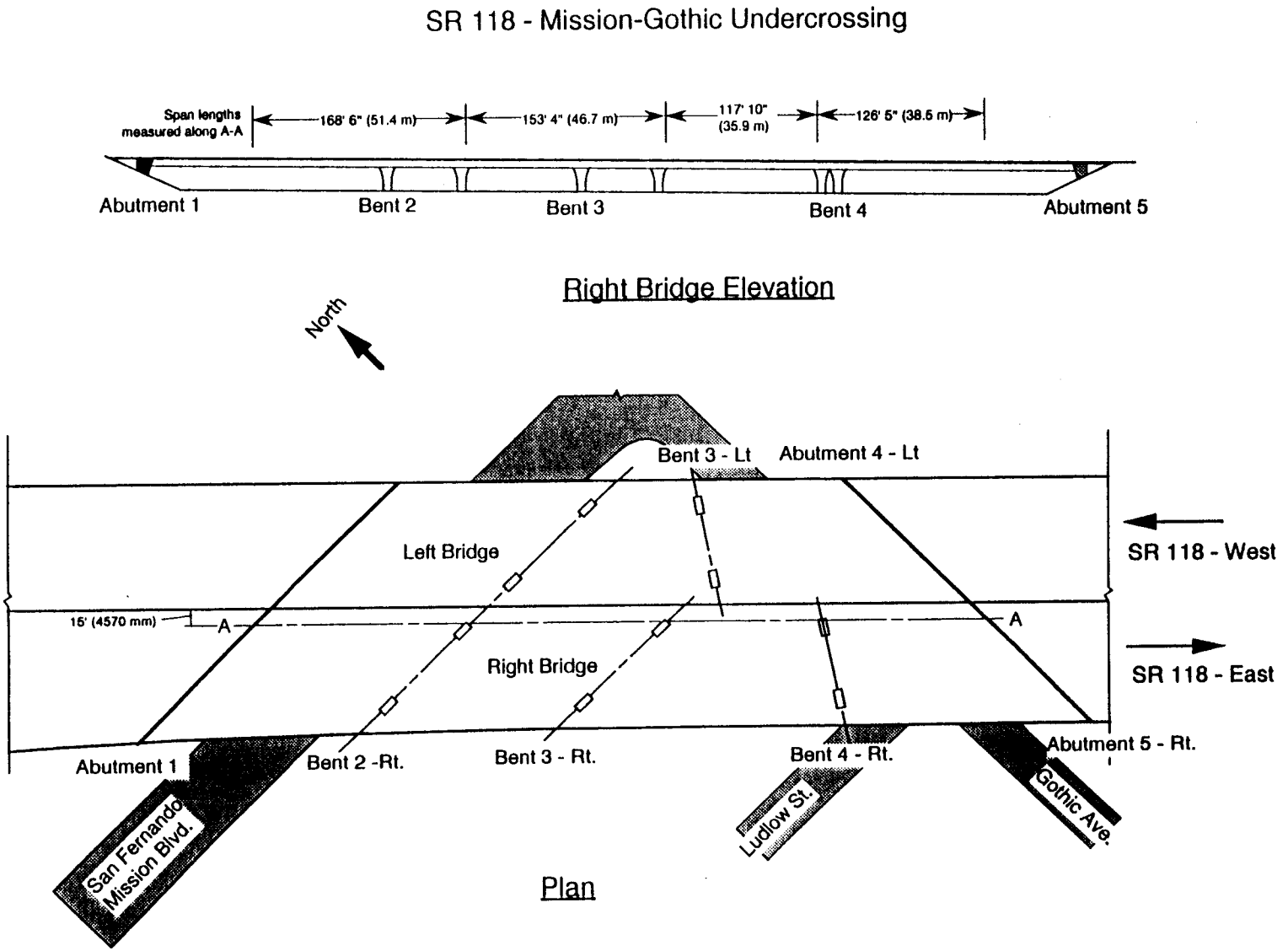

Figure 1.3-7: Plan and Elevation Views of the SR 118 Mission-Gothic Undercrossing (Todd, *et al.*, 1994)

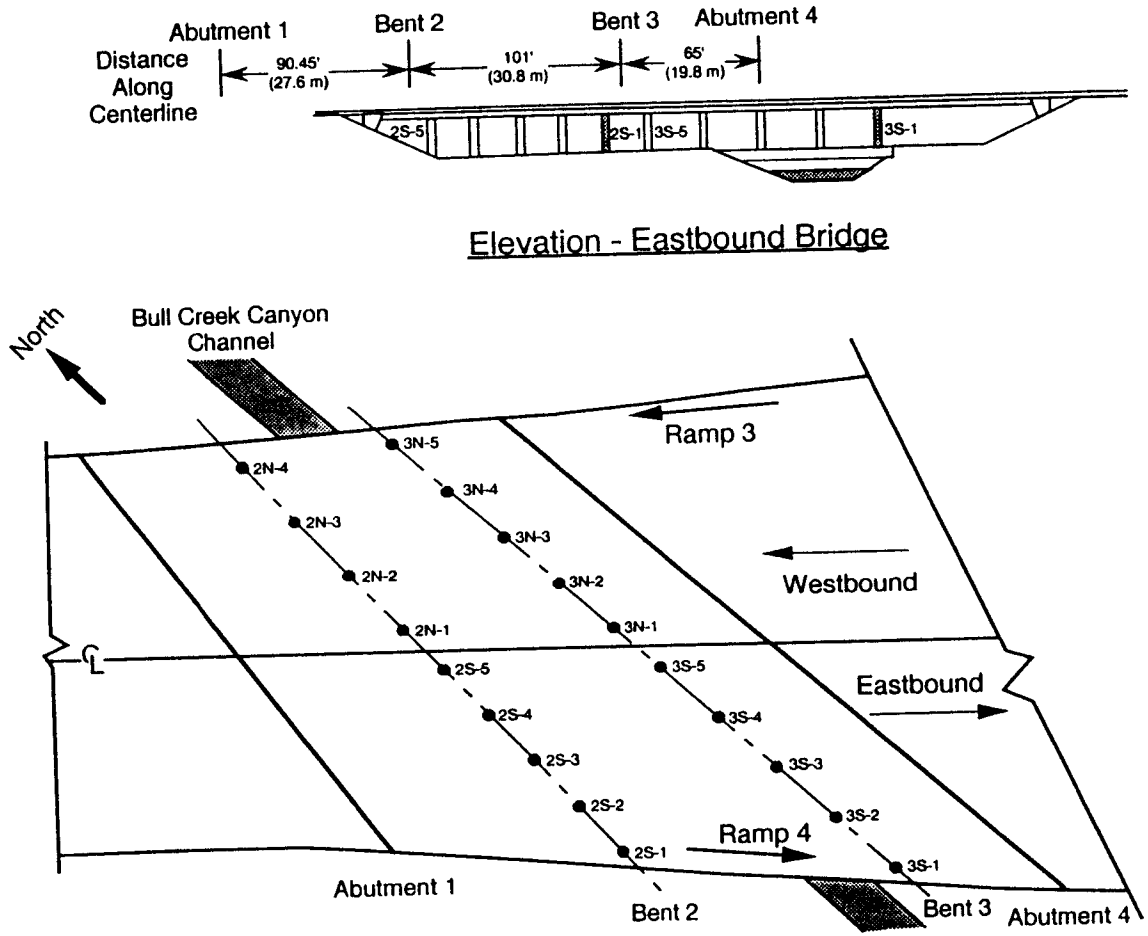

Figure 1.3-8: Plan and Elevation Views of State Route 118 at Bull Creek Canyon Channel (Todd, *et al.*, 1994)

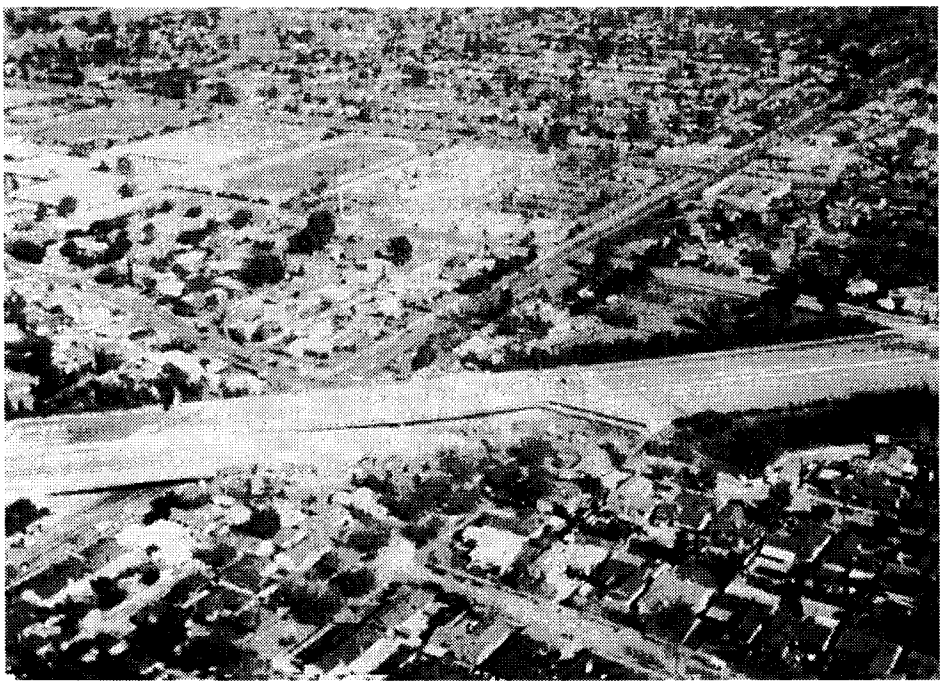

(a)

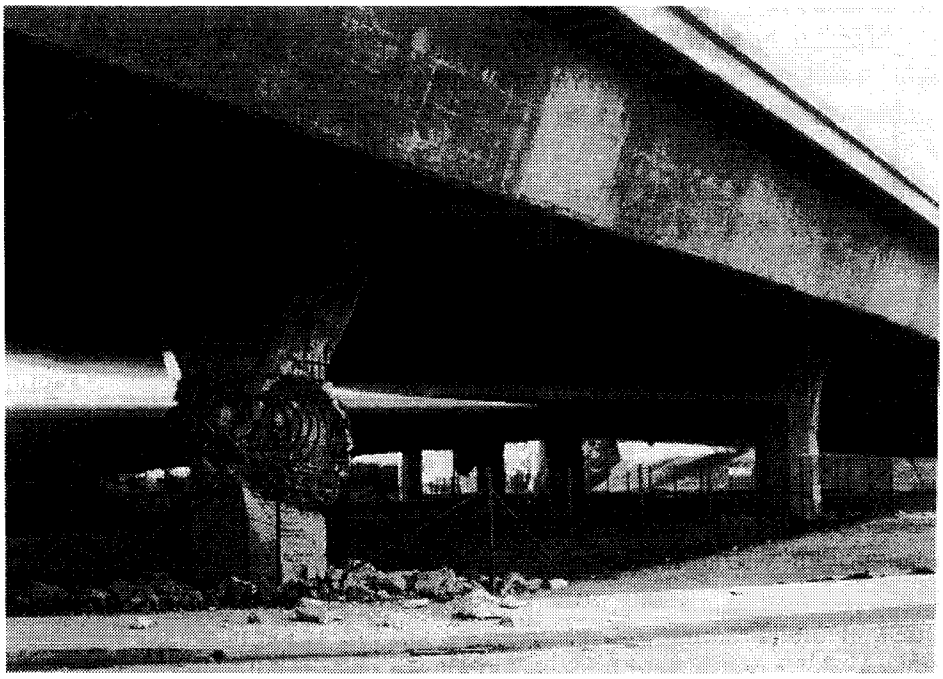

(b)

Figure 1.3-9: Collapse of the SR 118 Mission-Gothic Undercrossing: (a) Aerial View; (b) Damage of the Piers (Todd, *et al.*, 1994)

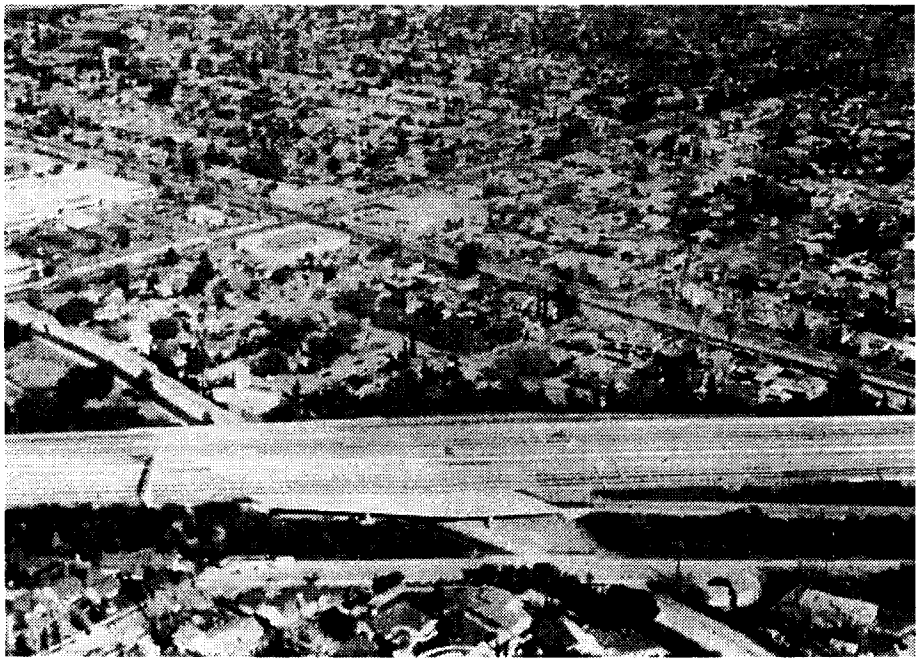

(a)

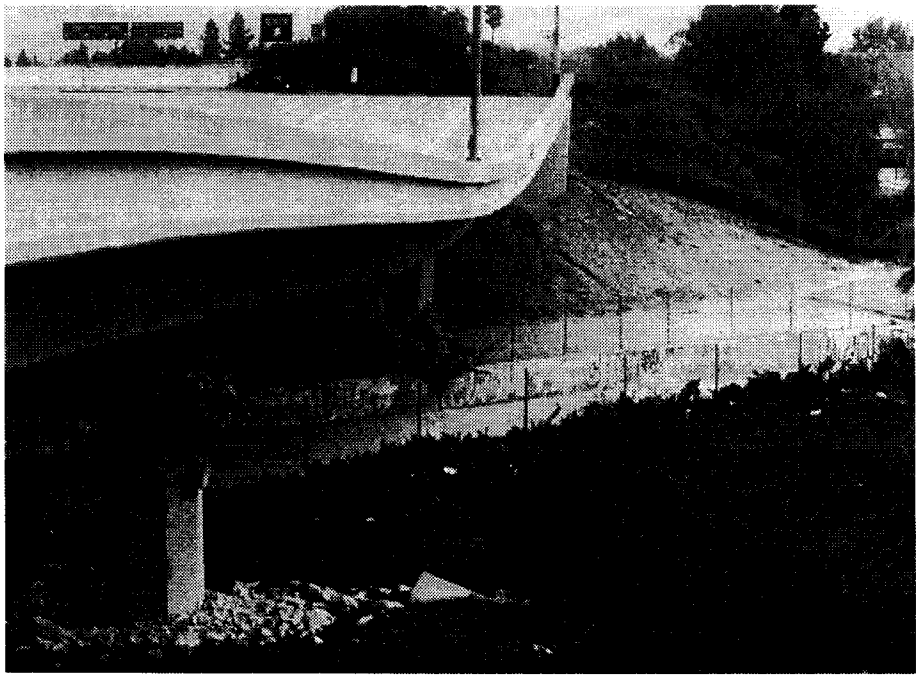

(b)

Figure 1.3-10: Failure of SR 118 at Bull Creek Canyon Channel: (a) Aerial View; (b) Damage of the Piers (Todd, *et al.*, 1994)

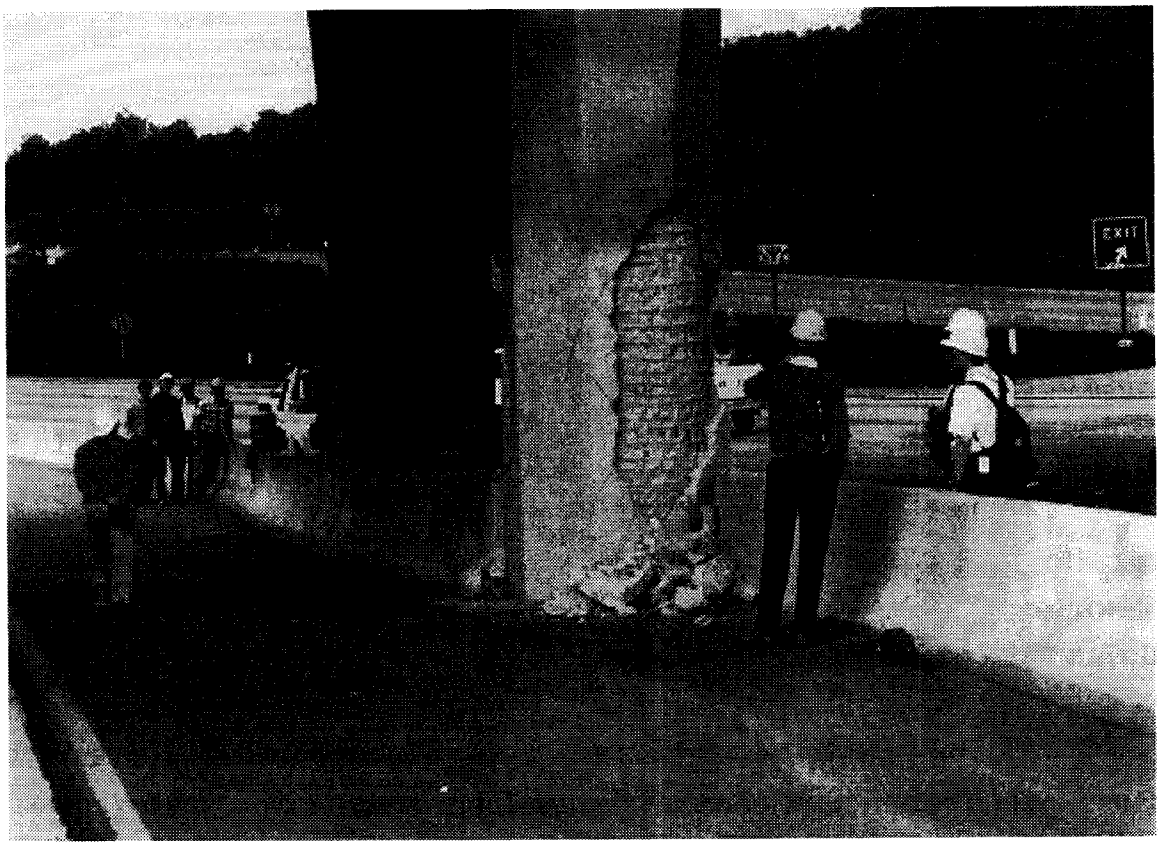

Figure 1.3-11: Spalling of the Concrete at Easternmost Central Pier (Todd, *et al.*, 1994)

Interstate 10

Two major bridges on Interstate 10 collapsed. One of the bridges was located at the La Cienega Blvd.-Venice Blvd. Separation (Figure 1.3-12), and the other was located at the Fairfax Ave.-Washington Blvd. Undercrossing (Figure 1.3-15). Both bridges at the two locations were designed before 1971.

Figure 1.3-13 is an aerial view of the bridge at the La Cienega Blvd.-Venice Blvd. Separation. The portion of the westbound lane collapsed to ground level, and most of the supporting piers of the bridges had extensive damage (Figure 1.3-14). The failure was attributed to the pre-1971 column designs. As the lateral earthquake loading was applied to the structure, the piers cracked. However, because of the inadequate confinement in the piers the vertical load capacity was significantly reduced so that the core concrete was crushed and the longitudinal bars buckled.

Two spans of the eastbound and westbound lanes at the Fairfax Ave.-Washington Blvd. Undercrossing were partially collapsed during the earthquake (Figure 1.3-16), and the piers in Bent 3 had extensive damage (Figure 1.3-17a). The failure mode is similar to that observed at the Venice Blvd. and La Cienega Blvd. Separation. A minor difference is that the cable restrainers at the hinge west of Bent 4 prevented the girders from falling off of the hinge seats (Figure 1.3-17a).

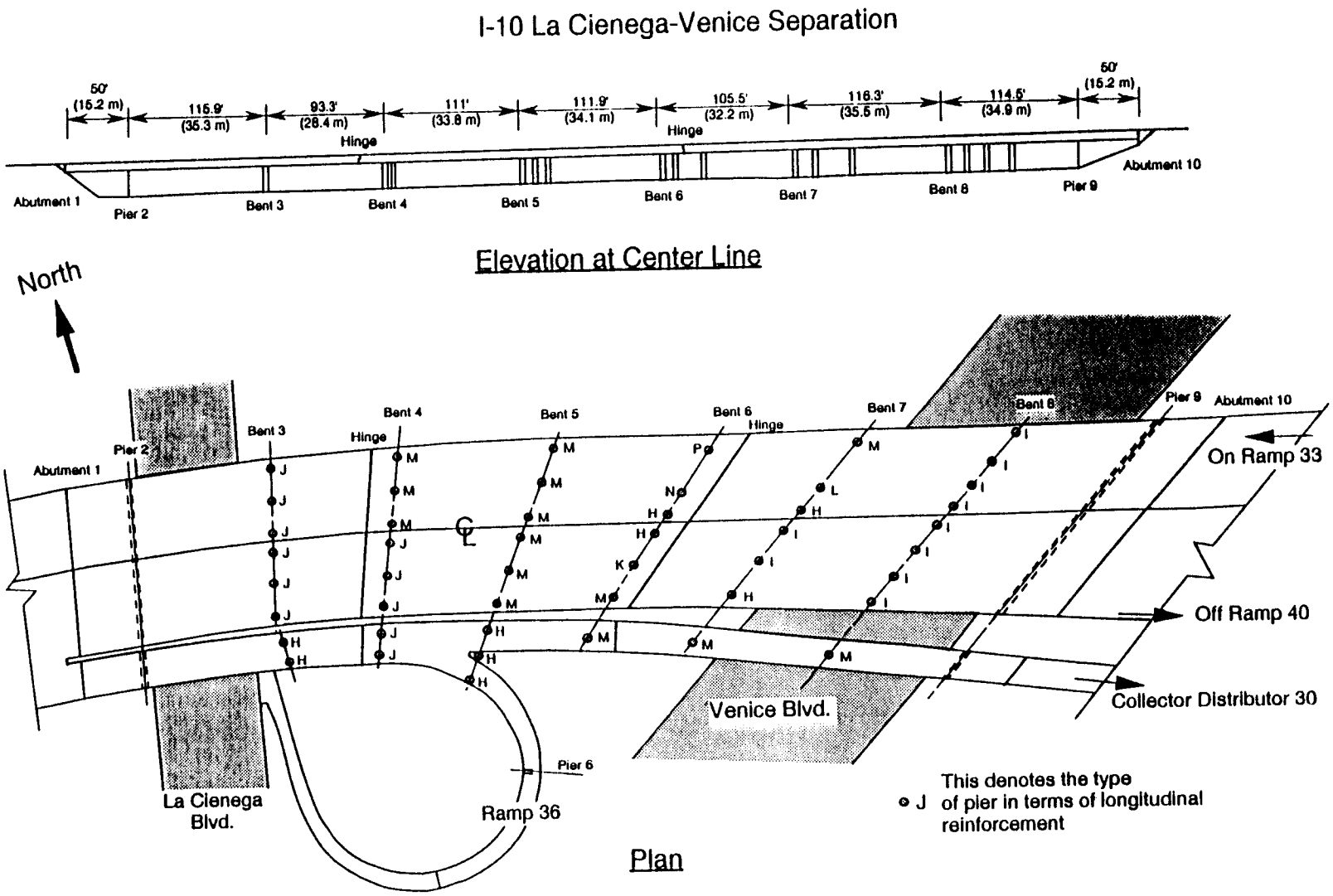

Figure 1.3-12: Elevation and Plan of I10 Separation at La Cienega Blvd. and Venice Blvd. (Todd, *et al.*, 1994)

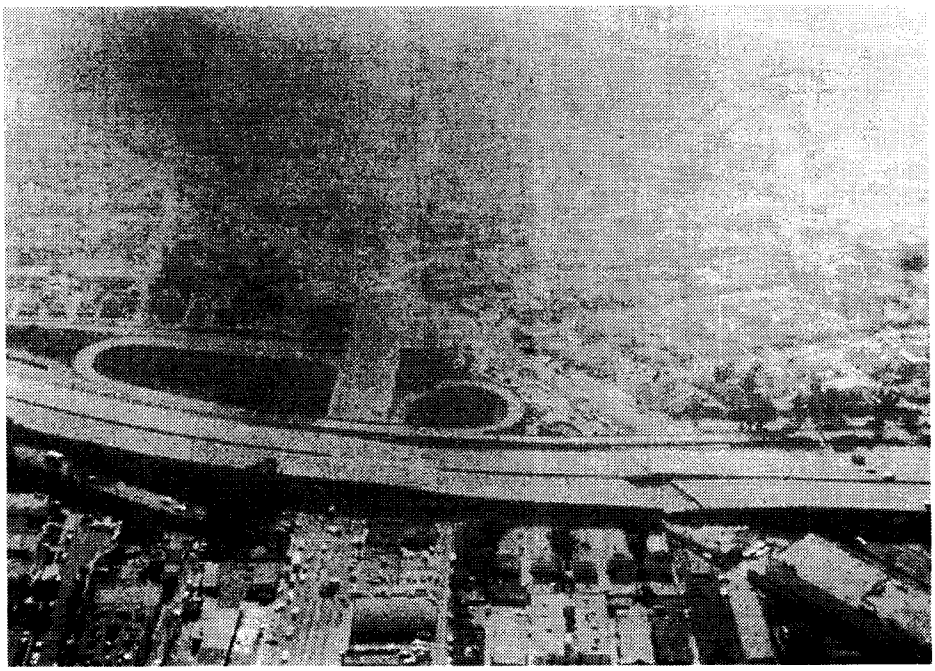

Figure 1.3-13: Aerial View of I10 Separation at La Cienega Blvd. and Venice Blvd. (Todd, *et al.*, 1994)

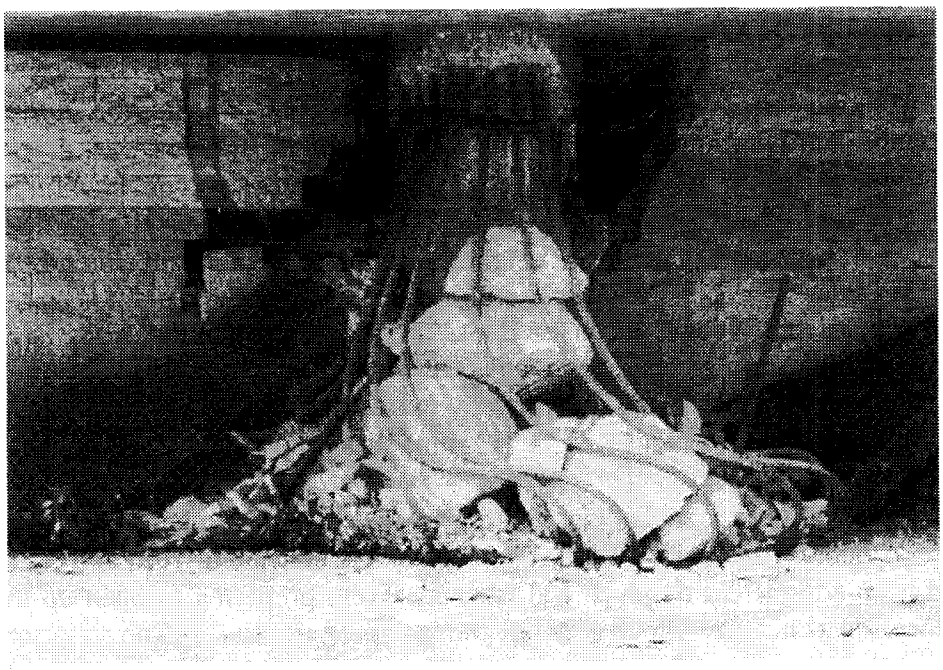

(a)

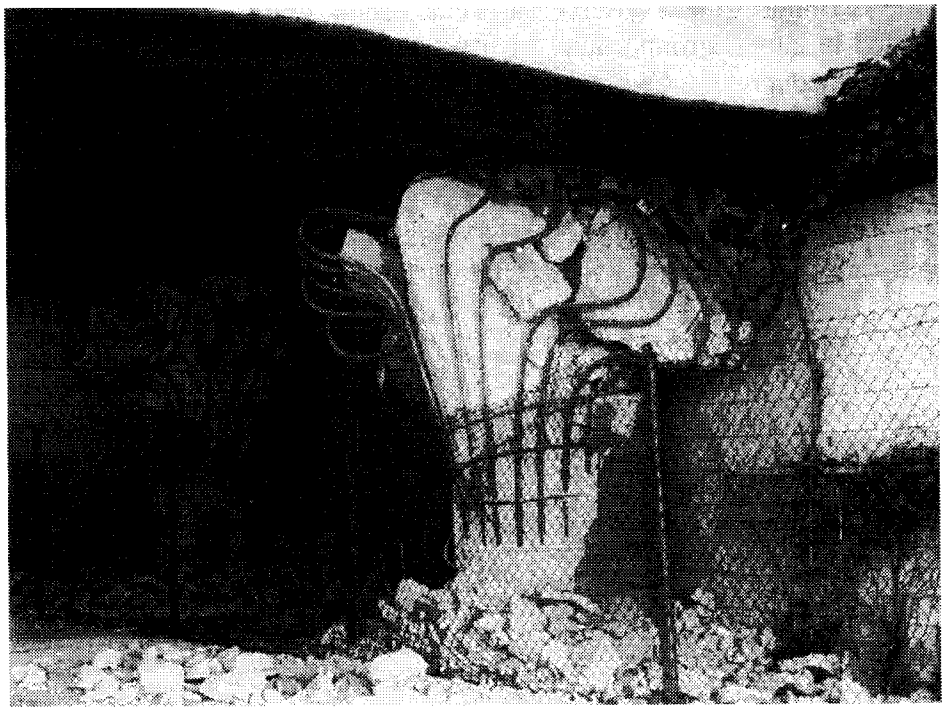

(b)

Figure 1.3-14: Damage of the Piers (Todd, *et al.*, 1994)

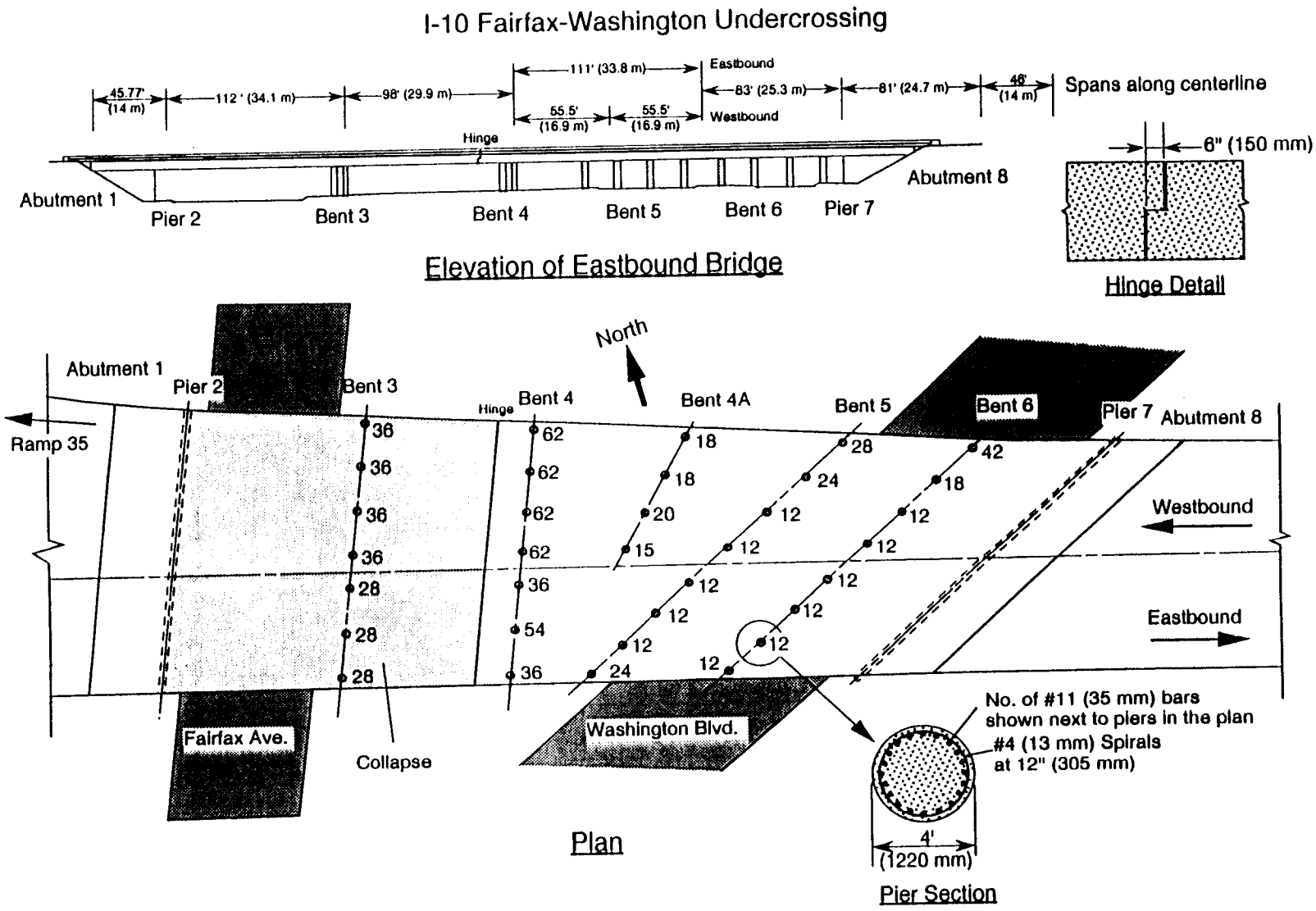

Figure 1.3-15: Elevation and Plan of I10 Separation at the Fairfax Ave.-Washington Blvd. Undercrossing (Todd, *et al.*, 1994)

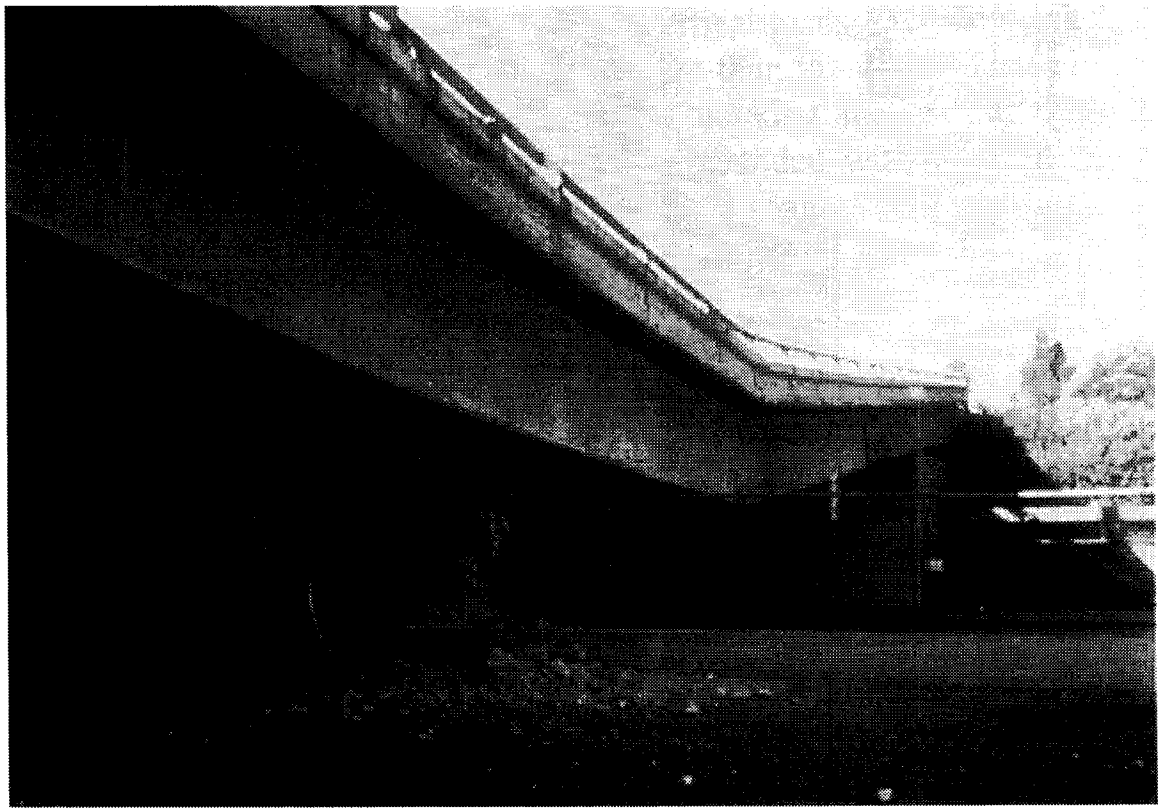

Figure 1.3-16: View of Collapsed Span of I 10 over Fairfax Avenue (Todd, *et al.*, 1994)

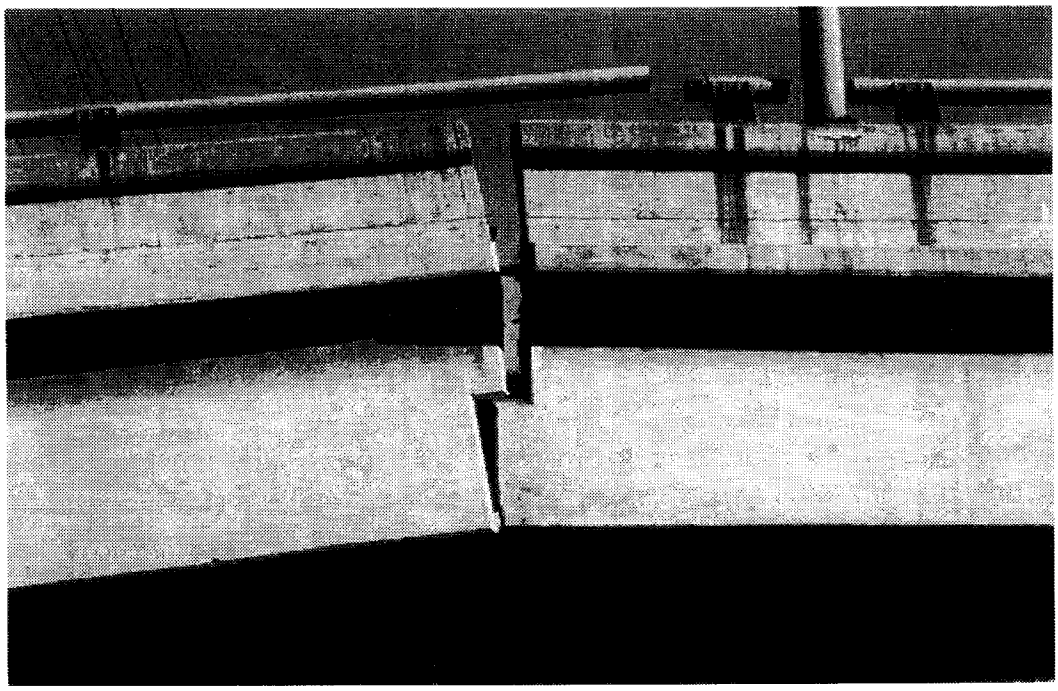

(a)

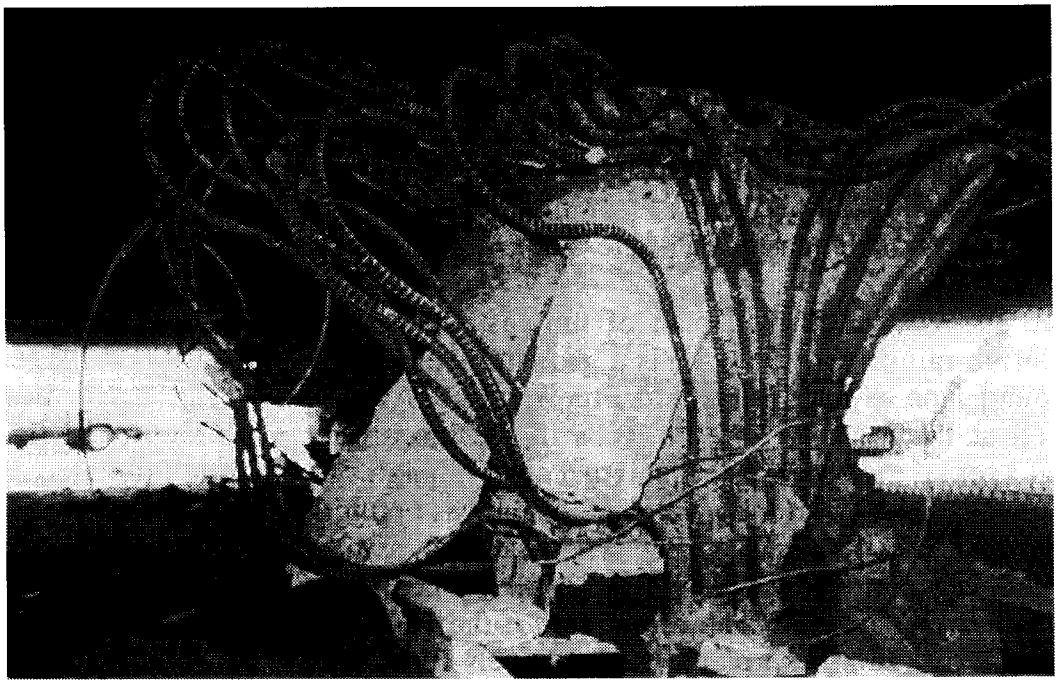

(b)

Figure 1.3-17: Failure of the Hinge Adjacent to Bent 4 and Pier In bent 3: (a) Hinge; (b) Pier (Todd, *et al.*, 1994)

State Route 134

At the abutment of the eastbound lane of the Ventura Freeway, the bearings were seriously damaged. A simplified plan of the eastbound lane of the Ventura Freeway and Riverside Drive ramp, and the bearing details used at the abutment, are shown in Figure 1.3-18. The interchange of the Ventura Freeway and Hollywood Freeway was designed in the late 1950's. The bridges are made of multiple-cell reinforced concrete box girders supported by multiple-pier bents. The girders are supported by sliding-type bearings and rocker-type bearings at the abutments.

Four sliding-type bearings were installed at the north side of the eastbound lane of the Ventura Freeway, and the remainder of bearings supporting the eastbound lane and the Riverside Drive ramp were of the rocker type. Figure 1.3-19a shows the damage of the sliding-type bearings. The force resulting from the dynamic frictional resistance of the bearing spalled off the shell of the abutment. The damage of the rocker-type bearings is shown in Figure 1.3-19b. The bolts for the restraining plates were sheared off at many locations. Although the bridge did not collapse during the earthquake because of redundancy, it must be kept in mind that the multiple bearing failures could drastically alter the forces in the girder and result in serious damage to the girder.

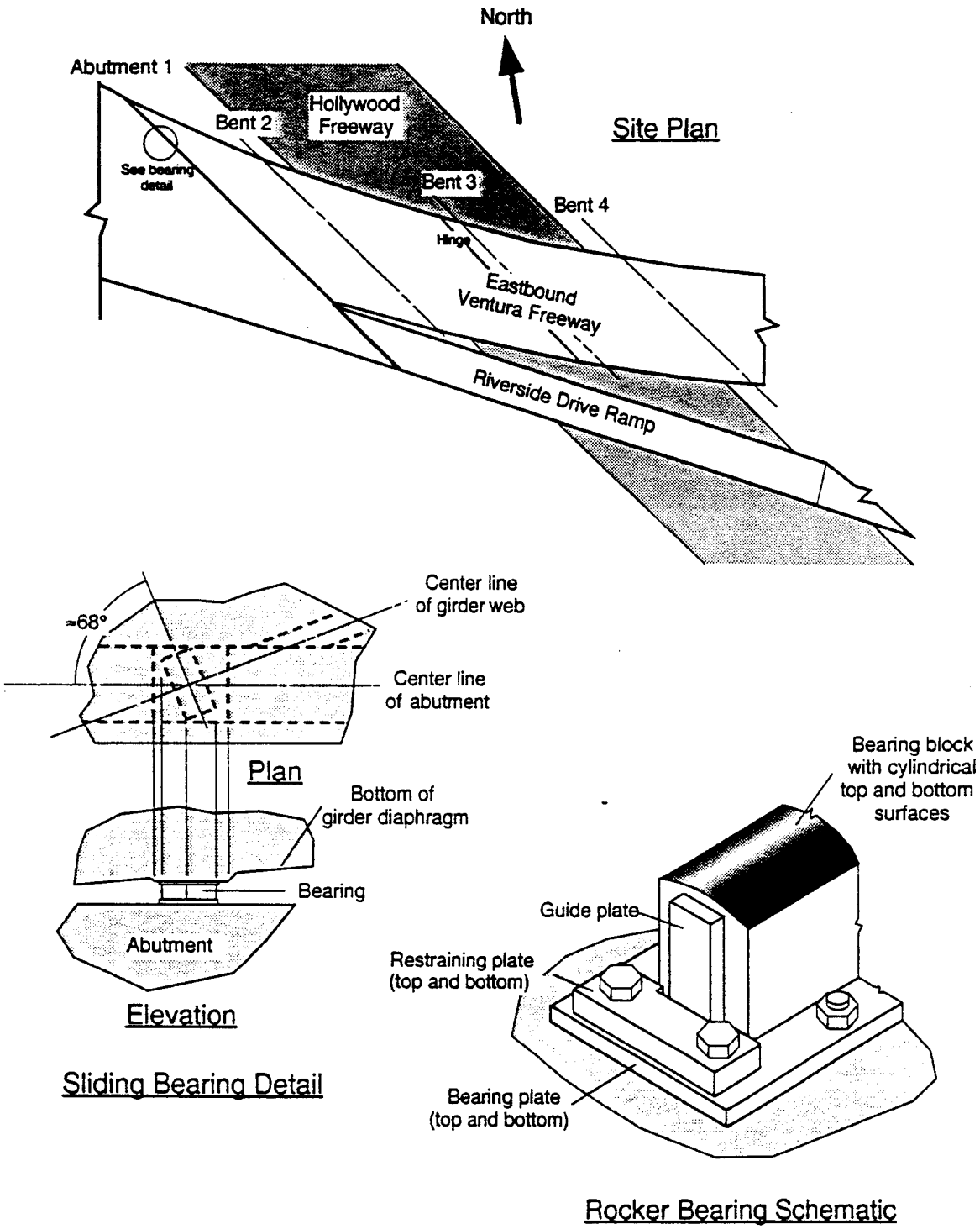

Figure 1.3-18: Eastbound Lane of Ventura Freeway Crossing over Hollywood Freeway; Site Plan and Bearing Details (Todd, *et al.*, 1994)

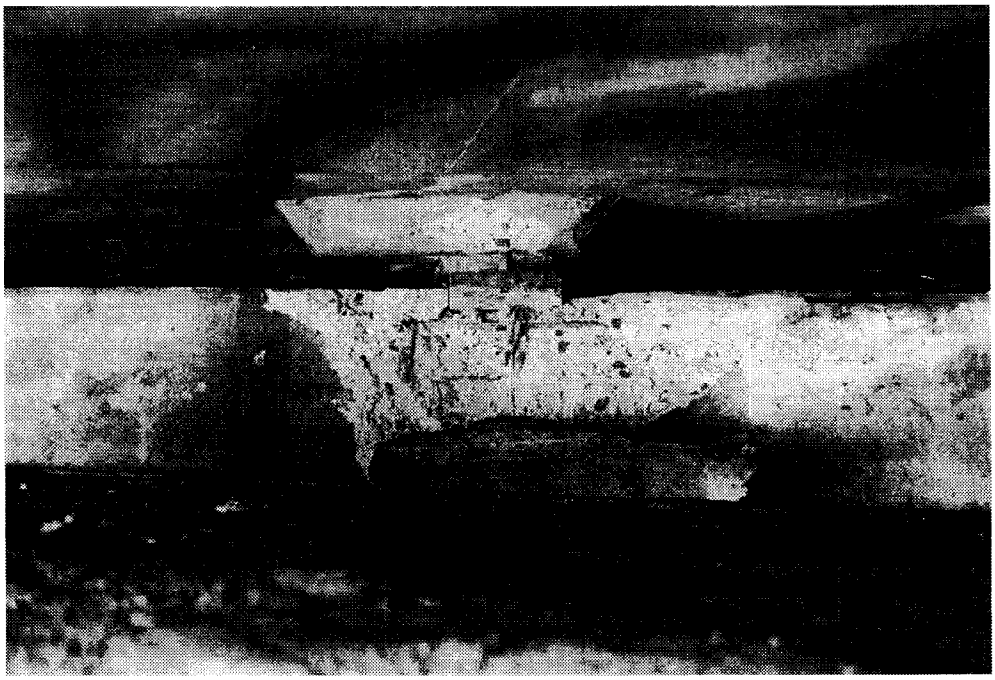

(a)

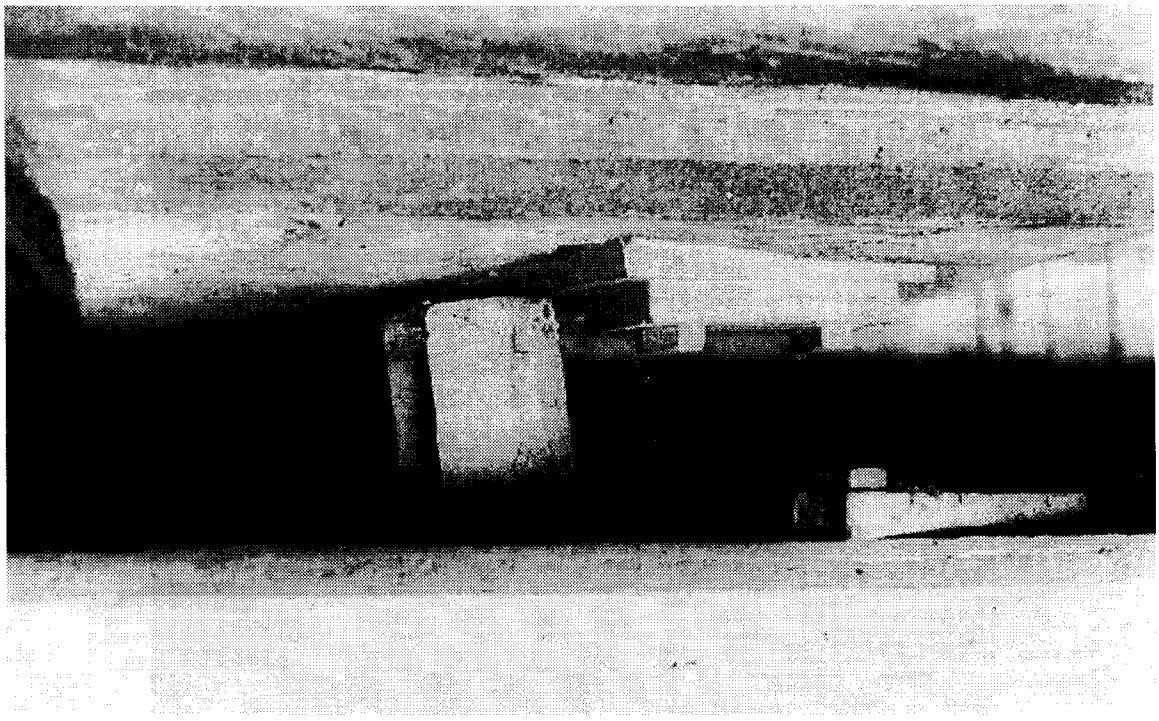

(b)

Figure 1.3-19: Abutment Damage: (a) Sliding-type Bearing; (b) Rocker-type Bearing (Todd, *et al.*, 1994)

State Route 90 / Interstate 405 Interchange, Jefferson Blvd. Undercrossing

The bridge was constructed in 1961 with an inadequate seismic design. Three six-pier bents support the four-span bridge. A special aspect of the bridge is that the outer piers of each bent are located outside of the bridge girders, creating an "outrigger" configuration, as shown in Figure 1.3-20a. Diagonal cracks were observed in all six outrigger joints at the ends of the three bents (Figure 1.3-20b). Three possible factors are attributed to the damage: (1) the reinforcement at the joint regions is not sufficient according to the current design standard; (2) the structural hinges at the bases of most outrigger piers tended to increase the moments imposed on the outrigger joints; (3) the upper SR 90 structure is more flexible than the lower structure, resulting in further concentrations of moment at the outrigger joints.

(a)

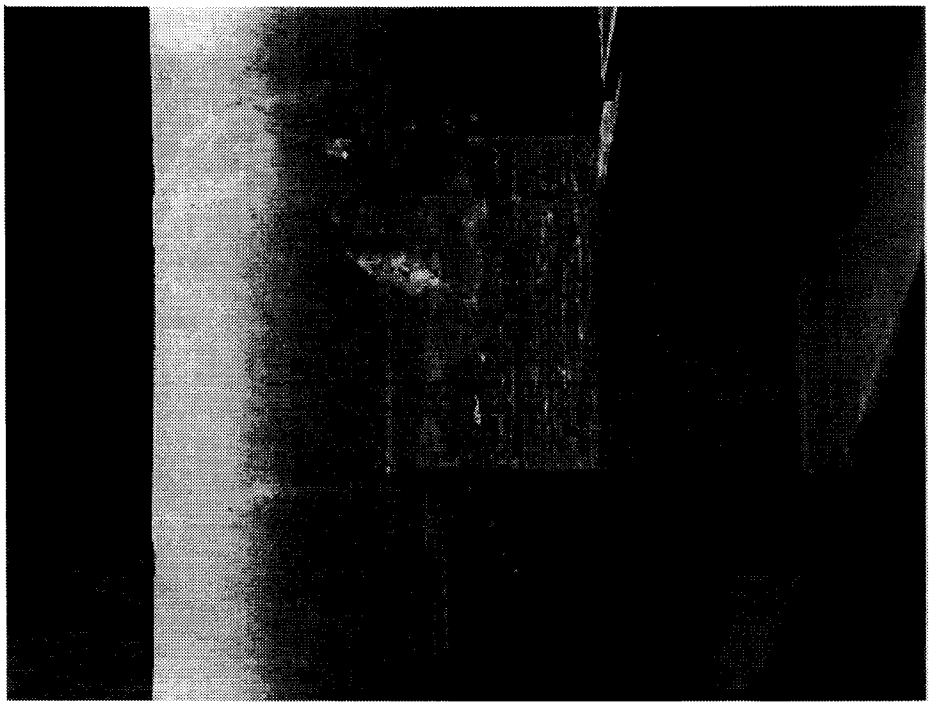

(b)

Figure 1.3-20: Overview and Damage of the Outrigger Joint at the SR90/I405 Interchange, Jefferson Blvd. Undercrossing (Todd, *et al.*, 1994)

1.4.2 Summary

There were about 2000 bridges in the epicentral region of the Northridge earthquake. Of these, only a few bridges failed or were badly damaged. However, the performance of these bridges has taught us much about seismic retrofit and the seismic research program.

1) Most of the bridges that were heavily damaged were those with unusual geometries and large skews and, usually, these bridges were designed by pre-1971 design standards.
2) New bridges designed to current specifications performed well.
3) Generally speaking, retrofitting techniques improve a bridge's earthquake resistance. However, significant damage to older bridges which had been seismically retrofit also was occasionally observed. Therefore, it is necessary to continue the detailed studies of these retrofit methods. For example, the cable restrainers installed at the bridge at Gavin Canyon were unable to prevent parts of the bridge deck from falling off the supports.
4) Older bridge bearings of the steel rocker type are highly susceptible to damage in strong shaking. The failures caused by the loss of rocker bearing support can include cracked girders, loss of roadway elevation alignment, and complete collapse of the superstructure.
5) Many failures were associated with short piers with flares on the top, even for those with high levels of confining reinforcement. Hence, a better understanding of the seismic performance of short piers, including piers with flares, is needed.

6) Unusually high vertical accelerations were recorded at several locations near bridge structures during this earthquake. This phenomenon and its implication on structural performance need further investigation.

7) Bridge abutments had widespread damage. The seismic behavior of bridge abutments is relatively unknown. Therefore, effective seismic design codes for bridge abutments need to be developed.

8) Many of the bridges with multiple-pier bents were damaged. At the present time, most seismic retrofit efforts have been directed toward retrofitting isolated piers as opposed to the strengthening of multiple-pier bents. Further research is required to develop cost-effective seismic retrofit guidelines for multiple-pier bridge bents.

Chapter 2

Beam Column Element with Softening Hinges and Degradation of Stiffness

2.1 Introduction and Problem Statement

The computer program, NEABS, is a good tool to investigate the dynamic characteristics of highway bridges having inelastic beam-columns, expansion joint hinges, and bearing support conditions that exhibit complex nonlinear behavior. However, this program has a major shortcoming, in that the softening behavior of beam-columns due to damage is not considered. Reinforced concrete members exhibit damage and softening behavior, i.e., decreasing bending moment at advanced flexural deformations before failure. The softening is relatively important to the dynamic analysis of pre-1971 designed highway bridges. Because most columns designed before 1971 had inadequate confinement and were lap-spliced at the connection zone between columns and footings (plastic hinge region) , the flexural strength of columns in the potential plastic hinge region degrades rapidly. The decrease of flexural strength of columns will cause a redistribution of structural element forces, so that the seismic response of the entire highway bridge is significantly influenced.

However, a more important aspect to dynamic column behavior is the degradation of stiffness when members are subjected to cyclic loadings, in which structural stiffness will decrease with reloading. The hysteresis rule used in the original version of NEABS

is a conventional elastic-plastic model that does not represent very well the degradation of stiffness with increasing deformations for reinforced concrete. Therefore, NEABS is not typically appropriate in evaluating earthquake response for the highway bridges that were constructed before 1971.

Wood (1968) pointed out that the simple elastic bending theory for structural members meets with difficulties when considering softening because of the inelastic effect. Darvall (1985) developed a beam stiffness matrix using a finite-length hinge concept and later performed inelastic analyses of R/C frames in which the softening effect was included (Darvall and Mendis, 1985). In 1988, Sanjayan also used the finite-length hinge concept to analyze the dynamic response of R/C structures with softening behavior and an idealized hysteretic model. Although acceptable values are available from experimental observations (Sanjayan and Darvall, 1995), it has not been possible, so far, to theoretically determine the hinge length for R/C members. Moreover, this method is typically not used in earthquake engineering for highway bridges.

To overcome this deficiency of NEABS and provide a realistic and practical method for the assessment of the effectiveness of different retrofit measures, a model for softening behavior of beam-column elements based on an isotropic softening model and with degradation of stiffness is proposed and then implemented into NEABS. In the following sections, the moment-curvature relationship, the yield function, and the derivation of the stiffness of the beam-column element with softening and degradation behavior are described. Finally, a computational example using the modified NEABS program is presented.

2.2 Review of Previous Models

For the elastic-perfectly plastic R/C beam-column element used in NEABS, the moment-curvature relationship in a one-dimensional force space is shown in Figure 2.2-1. In the model, when the moment reaches its yielding value (M_y), it is assumed to remain unchanged as the load continues to increase. Strain hardening is, therefore, neglected. The hysteretic model (Figure 2.2-2) in NEABS is a simple one, and it is based on the assumption that no stiffness degradation occurs for loading and unloading. However, most experimental results for R/C beams or columns subject to cyclic loading exhibit rather complicated behavior that includes such effects as rounding, pinching, and stiffness degradation (Imbsen and Penzien, 1986). The most significant influence on structural analysis is stiffness degradation. According to experiments conducted by Priestley and Seible (1994), the elastic-perfectly plastic model cannot represent the actual behavior if the plastic deformation is allowed to increase without limit. When plastic deformation at an end grows beyond a certain value (called critical curvature, ϕ_c), the material may undergo damage, which is represented by softening. In this stage, the moment decreases with an increase in plastic rotation.

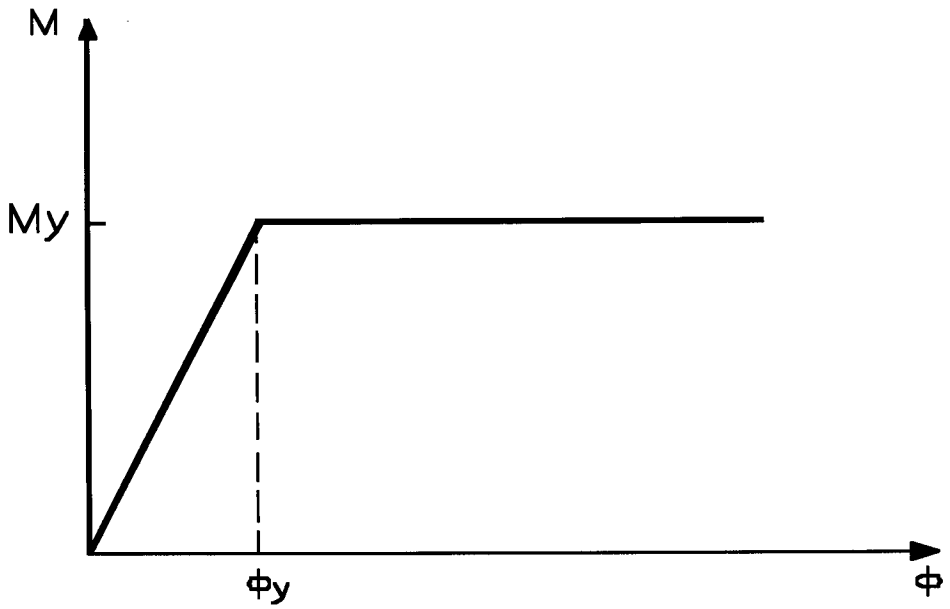

Figure 2.2-1: Moment vs Curvature Diagram for Elastic-Perfectly Plastic Beam

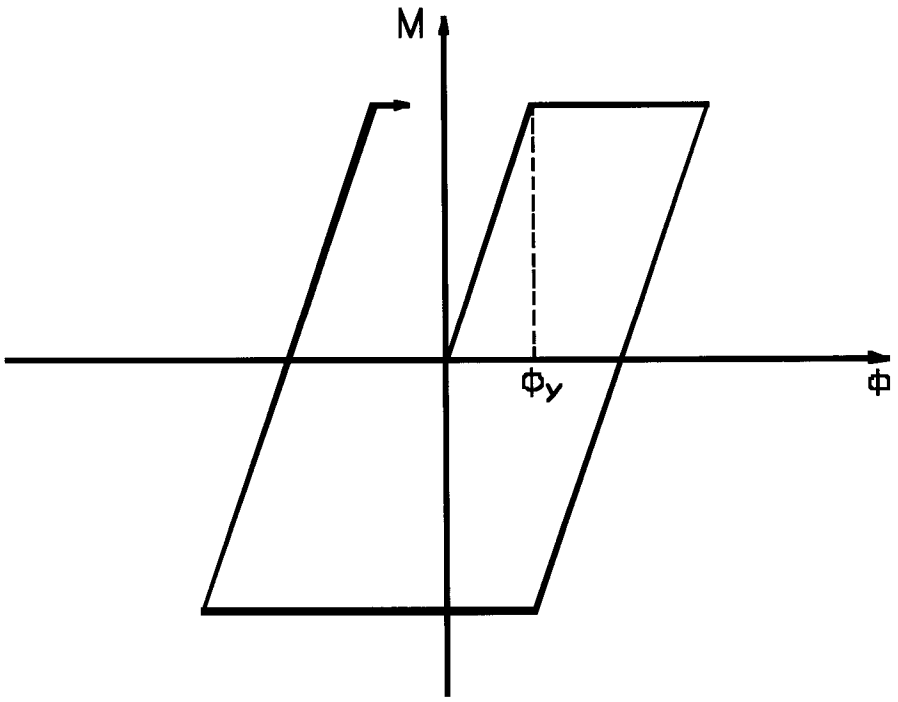

Figure 2.2-2: Conventional Elastic-Plastic Model

2.3 A Proposed Beam Column Element with Softening Hinges

The softening stage of the M-ϕ curve cannot be followed in a load-control test of a statically determinate structure, and it is only obtained in displacement-control tests if the relative stiffness of the testing machine with respect to the concrete specimen is reasonable, which is why experimental data in this area is not extensive (Darvall and Mendis, 1985). Figure 2.3-1 shows three approximations for a real M-ϕ curve that were proposed by Darvall and Mendis in 1985. In this research, a model that is similar to that of Figure 2.3-1(b), shown in Figure 2.3-2, is described. It should be noted that strain hardening in this model is neglected. The hysteretic rule will be discussed in 2.4.

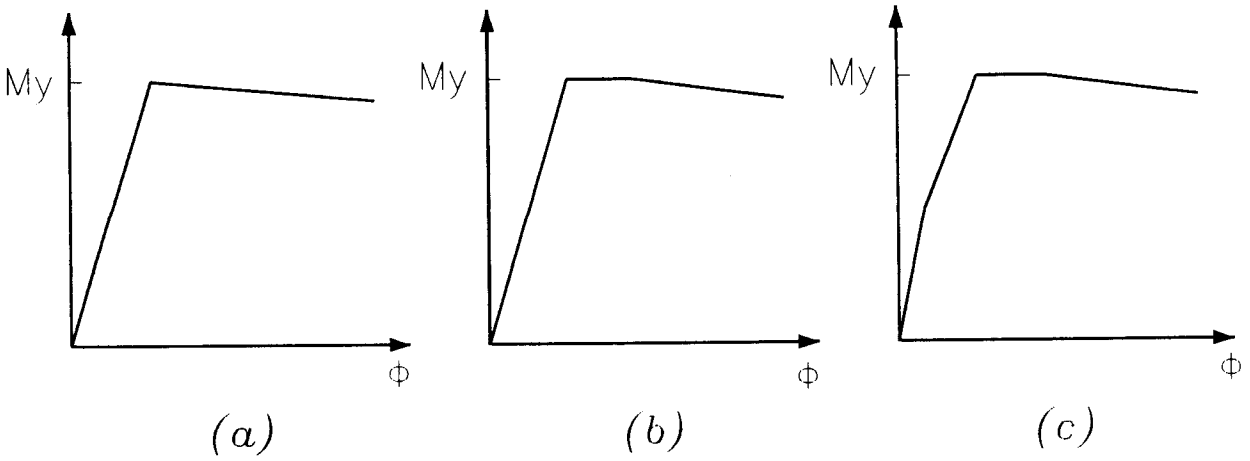

Figure 2.3-1: Approximations for Moment vs Curvature Curves: (a) Elastic-Softening; (b) Elastic-Plastic-Softening; (c) Elastic-Reduced Elastic-Plastic-Softening

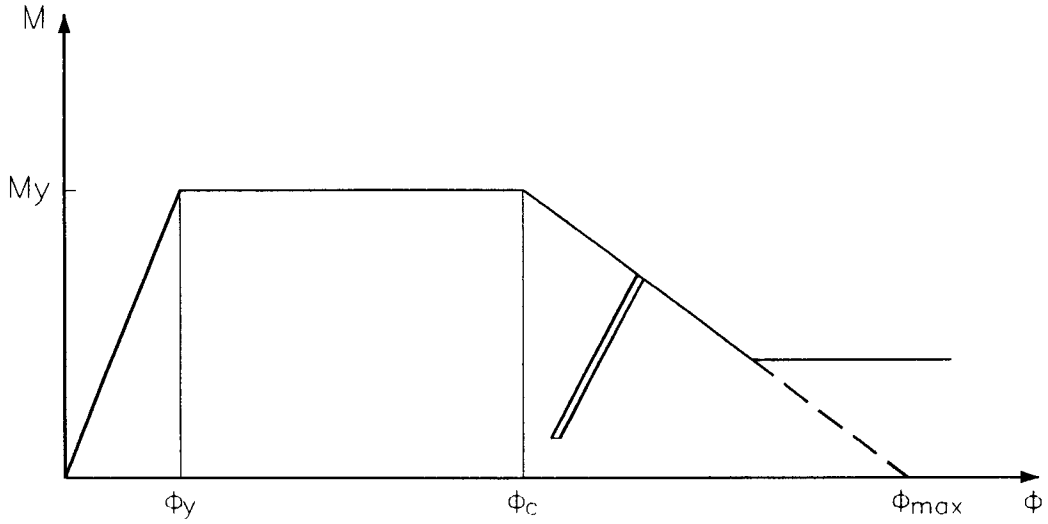

Figure 2.3-2: Moment vs Curvature Relation of the Element

2.3.1 Damage Coefficient

To derive the stiffness matrix for the softening stage, a damage coefficient, D, is introduced. The damage coefficient is defined such that a value of 0 indicates no damage while a value of 1 means total damage. Failure of actual components is observed to occur at an intermediate value of damage, D_{max}. Therefore, during the evolution of softening, the damage coefficient is equal to

$$\boldsymbol{D = \frac{\theta_p - \theta_{cp}}{\theta_{max} - \theta_{cp}}, 0 \le D \le D_{max} \le 1} \quad \text{.....(2.3-1)}$$

where θ_p is total plastic rotation angle, θ_{cp} is the critical plastic rotation angle that indicates the point at which softening begins, and $\theta_{\max}$ is the maximum theoretical plastic rotation angle. θ_{cp} and $\theta_{\max}$ may be calculated through the following formula:

$$\theta_{cp} = l_p \cdot (\phi_c - \phi_y) \quad \text{.....(2.3-2)}$$

$$\theta_{\max} = l_p \cdot (\phi_{\max} - \phi_y) \quad \text{.....(2.3-3)}$$

where l_p is plastic hinge length and $\phi_{\max}$ is the curvature for which the maximum moment capability is equal to zero, theoretically. Thus, according to the definition of the damage coefficient, at any point during the softening stage, the maximum moment capacity is

$$M = (1 - D)M_y \quad \text{.....(2.3-4)}$$

where M_y is the yielding moment.

2.3.2 Yield Function

The generalized yield surface used in NEABS has a form similar to that proposed by Bresler (1960) for biaxial bending. The formula is given as

$$\left(\frac{M_{yu}}{M_{yp}}\right)^2 + \left(\frac{M_{zu}}{M_{zp}}\right)^2 = 1 \quad \text{.....(2.3-5)}$$

where M_{yu} and M_{zu} are the bending moment values about the y and z axes, respectively, on the interaction surface for a fixed value of axial force, P_u. M_{yp} and M_{zp} are the ultimate bending moment values about the y and z axes, respectively, for the same fixed

value of P_u when M_y and M_z are applied separately. To consider the influence of axial force P_u, the following cubic equations are used to compute M_{yp} and M_{zp}:

$$M_{yp} = M_{y0} \cdot \left[1 + a_1 \left(\frac{P_u}{P_0} \right) + a_2 \left(\frac{P_u}{P_0} \right)^2 + a_3 \left(\frac{P_u}{P_0} \right)^3 \right], -P_0 \langle P_u \langle P_t \quad \text{.....(2.3-6)}$$

$$M_{zp} = M_{z0} \cdot \left[1 + b_1 \left(\frac{P_u}{P_0} \right) + b_2 \left(\frac{P_u}{P_0} \right)^2 + b_3 \left(\frac{P_u}{P_0} \right)^3 \right], -P_0 \langle P_u \langle P_t \quad \text{.....(2.3-7)}$$

where P_t is the ultimate axial tensile force, P_0 is the ultimate axial compressive force, M_{y0} and M_{z0} are yielding moments about the y and z axes, respectively, in pure bending, and a_1, a_2, a_3, b_1, b_2, and b_3 are constants. Figure 2.3-3 shows the generalized yield surface.

One should note that the yield function mentioned above is only suitable for a perfectly plastic material, while the yield stress level does not depend in any way on the degree of plastification. This means that the yield surface is fixed, as shown in Figure 2.3-4 for a cross-section of the yield surface for a fixed value of P_u. For softening behavior, however, the yield surface is no longer unchanged in size, shape, or position with increasing plastification. The selected model for the evolution of softening in this report is isotropic, in which the subsequent yield surface is a uniform contraction of the original one, as shown in Figure 2.3-5. The cause of the yield surface contraction is that the yield stress level at a point decreases with increasing plastic deformation.

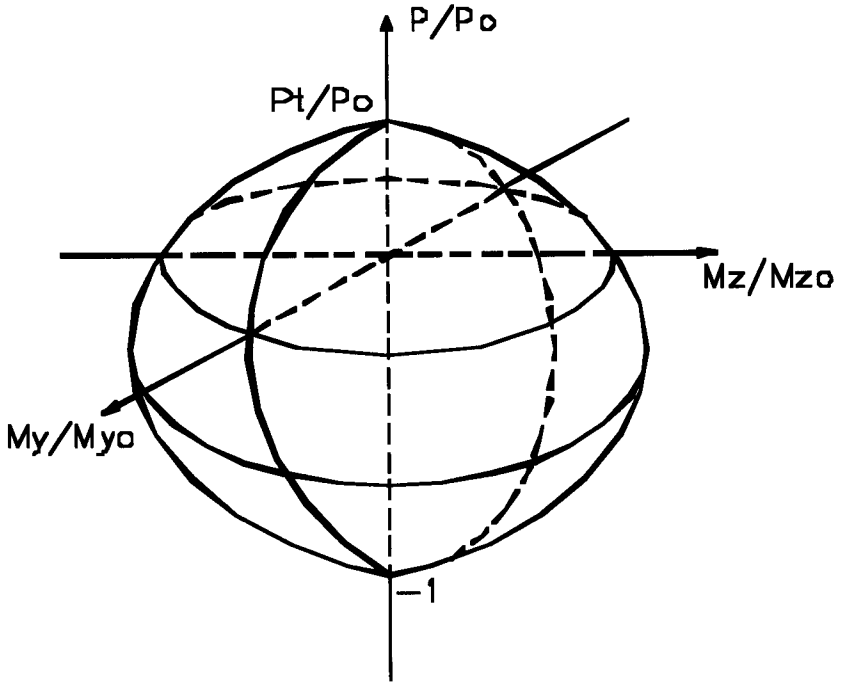

Figure 2.3-3: Generalized Yield Surface

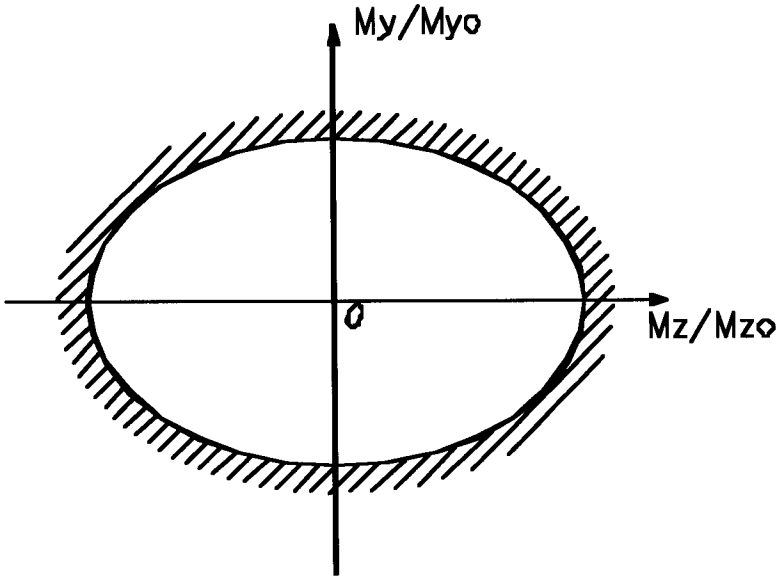

Figure 2.3-4: Yield Curve of Elastic-Perfectly Plastic Material for a Fixed Axial Force

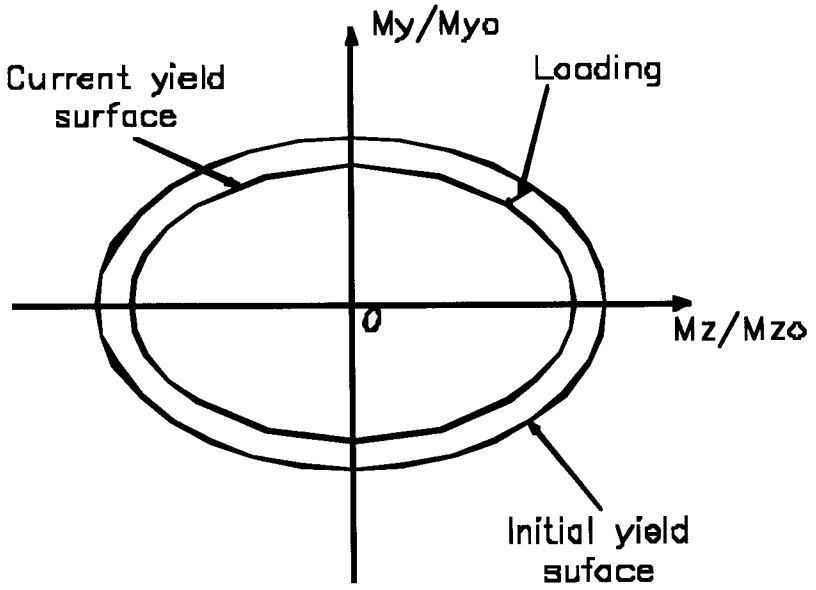

Figure 2.3-5: Yield Curve of Isotropic Strain Softening Material for a Fixed Axial Force

The yield function that also includes softening is defined as

$$\left(\frac{M_{yu}}{M_{yp}}\right)^2 + \left(\frac{M_{zu}}{M_{zp}}\right)^2 = (1-D)^2 \quad \text{.....(2.3-8)}$$

where D is the aforementioned damage coefficient and it is a function of plastic deformation. Because $(1-D)^2$ is less than or equal to one, the yield surface shrinks. To further explain the meaning of the yield function, it may be written in another way as:

$$f(\underline{s}_k) = \kappa \quad \text{.....(2.3-9)}$$

where, $f(\underline{s}_k) = \left(\frac{M_{yu}}{M_{yp}}\right)^2 + \left(\frac{M_{zu}}{M_{zp}}\right)^2$, $\kappa = (1-D)^2$, and $\underline{s}_k$ represents the generalized force vector.

The generalized force state is never allowed to go outside the yield surface. Therefore, it only falls inside or on the yield surface. Generalized force states for which $f = \kappa$ denote plastic states, while elastic behavior is characterized by $f \langle \kappa$. Chen and Han (1988) have noted that the generalized force space formulation presents difficulties in distinguishing between a reduction of generalized forces from softening and one due to elastic unloading. To overcome this dilemma, the following procedures are used to distinguish unloading and loading. First, the change in incremental generalized forces, $d\underline{s}_k$ which is calculated by using the **elastic stiffness**, is substituted into the following equation:

$$df = \frac{\partial f}{\partial \underline{s}_k} d\underline{s}_k \quad \text{.....(2.3-10)}$$

Then, if

$df \langle 0$, elastic unloading occurs (elastic behavior) and the generalized force point returns inside the yield surface;

$df = 0$, neutral loading occurs and the generalized force point remains on the yield surface;

$df \rangle 0$, plastic loading occurs and the generalized force point remains on the contracting yield surface.

2.3.3 Elastic-Plastic-Damage Tangent Stiffness Matrix

After the yield function for the softening stage is defined, the next step is to form the incremental elastic-plastic-damage tangent stiffness matrix, $\underline{k}^{epd}$, using the **flow rule,**

which relates the element generalized force increments, $d\underline{s}$, to the element nodal displacement increments, $d\underline{r}$, for an elasto-plastic flexural beam-column element. For this approach, a plastic node (plastic hinge) is assumed to be inserted into one or both ends of the beam-column element when the combination of generalized forces falls on the yield surface. According to the flow rule, the element nodal displacement increment, $d\underline{r}$, is assumed to be the sum of the elastic and plastic displacement increments:

$$d\underline{r} = d\underline{r}^{e} + d\underline{r}^{p} \quad \text{.....(2.3-11)}$$

where,

$$d\underline{r}^{e} = \begin{pmatrix} d\underline{r}_i^{e} \\ d\underline{r}_j^{e} \end{pmatrix}, \text{ and } d\underline{r}^{p} = \begin{pmatrix} d\underline{r}_i^{p} \\ d\underline{r}_j^{p} \end{pmatrix} \quad \text{.....(2.3-12)}$$

and i and j indicate the left and right ends of the element, respectively, as shown in Figure 2.3-6. The generalized forces can be determined uniquely by the elastic displacement increment, i.e.,

Figure 2.3-6: Nodes of the Elasto-Plastic Beam-Column Element

$$d\underline{s} = \underline{k}^{e} \cdot d\underline{r}^{e} \quad \text{.....(2.3-13)}$$

where $\underline{k}^e$ is the elastic stiffness matrix of the element. The plastic deformation is defined by the flow rule, which can be written in the form:

$$d\underline{r}_k^p = \left[\frac{\partial f_k}{\partial \underline{s}_k}\right] \cdot d\lambda_k, k = i, j \quad \text{.....(2.3-14)}$$

where λ_k is a positive proportionality constant termed the plastic multiplier, which is nonzero only when plastic deformations occur. Using equation (2.3-9), the incremental change in the yield function is:

$$df_k = \left[\frac{\partial f_k}{\partial \underline{s}_k}\right]^T \cdot d\underline{s}_k = -2(1 - D_k) \cdot dD_k, \; k = i, j \quad \text{.....(2.3-15)}$$

From (2.3-14) and (2.3-15), the incremental plastic displacement vector and incremental change in yield function for a beam-column element become:

$$d\underline{r}^p = \begin{Bmatrix} d\underline{r}_i^p \\ \\ d\underline{r}_j^p \end{Bmatrix} = \begin{bmatrix} \frac{\partial f_i}{\partial \underline{s}_i} & \underline{0} \\ \underline{0} & \frac{\partial f_j}{\partial \underline{s}_j} \end{bmatrix} \cdot \begin{Bmatrix} d\lambda_i \\ \\ d\lambda_j \end{Bmatrix} = \left[\frac{\partial \underline{f}}{\partial \underline{s}}\right] \cdot d\underline{\lambda} \quad \text{.....(2.3-16)}$$

and

$$d\underline{f} = \begin{Bmatrix} df_i \\ \\ df_j \end{Bmatrix} = \begin{bmatrix} \frac{\partial f}{\partial \underline{s}_i} & \underline{0} \\ \underline{0} & \frac{\partial f}{\partial \underline{s}_j} \end{bmatrix}^T \cdot \begin{Bmatrix} d\underline{s}_i \\ \\ d\underline{s}_j \end{Bmatrix} = \begin{bmatrix} -2(1 - D_i) & 0 \\ 0 & -2(1 - D_j) \end{bmatrix} \cdot \begin{Bmatrix} dD_i \\ dD_j \end{Bmatrix}$$

$$= \left[\frac{\partial \underline{f}}{\partial \underline{s}}\right]^T \cdot d\underline{s} = [D] \cdot d\underline{D} \quad \text{.....(2.3-17)}$$

From (2.3-11) and (2.3-13),

$$d\underline{s} = \underline{k}^e \cdot d\underline{r}^e = \underline{k}^e \cdot (d\underline{r} - d\underline{r}^p) \quad \text{.....(2.3-18)}$$

Therefore,

$$\left[\frac{\partial \underline{\underline{f}}}{\partial \underline{s}}\right]^T \cdot d\underline{s} = \left[\frac{\partial \underline{\underline{f}}}{\partial \underline{s}}\right]^T \cdot \underline{k}^e \cdot (d\underline{r} - d\underline{r}^p) = [D] \cdot d\underline{D} \quad \text{.....(2.3-19)}$$

Substituting (2.3-16) into (2.3-19),

$$d\underline{\lambda} = \left(\left[\frac{\partial \underline{\underline{f}}}{\partial \underline{s}}\right]^T \cdot \underline{k}^e \cdot \left[\frac{\partial \underline{\underline{f}}}{\partial \underline{s}}\right]\right)^{-1} \cdot \left\{\left[\frac{\partial \underline{\underline{f}}}{\partial \underline{s}}\right]^T \cdot \underline{k}^e \cdot d\underline{r} - [D] \cdot d\underline{D}\right\} \quad \text{.....(2.3-20)}$$

Thus, using (2.3-16) and substituting into (2.3-20) for $d\underline{\lambda}$ leads to the following relation:

$$d\underline{r}^p = \left[\frac{\partial \underline{\underline{f}}}{\partial \underline{s}}\right] \cdot \left(\left[\frac{\partial \underline{\underline{f}}}{\partial \underline{s}}\right]^T \cdot \underline{k}^e \cdot \left[\frac{\partial \underline{\underline{f}}}{\partial \underline{s}}\right]\right)^{-1} \cdot \left\{\left[\frac{\partial \underline{\underline{f}}}{\partial \underline{s}}\right]^T \cdot \underline{k}^e \cdot d\underline{r} - [D] \cdot d\underline{D}\right\} \quad \text{.....(2.3-21)}$$

In the relation above, only $d\underline{D}$ is unknown. Actually, the damage coefficient D has been defined in equation (2.3-1), in which it is related to plastic deformation. Since the θ_p used in (2.3-1) is defined in one-dimensional force space, it must be generalized to three dimensions. Here, θ_p is assumed to be the square root of the sum of plastic rotations in both axial directions. That is:

$$\theta_p = \sqrt{\theta_{yp}^2 + \theta_{zp}^2} \quad \text{.....(2.3-22)}$$

Therefore,

$$dD_k = \frac{1}{(\theta^k_{\max} - \theta^k_{cp})} \cdot \frac{\theta^k_{yp} \cdot d\theta^k_{yp} + \theta^k_{zp} \cdot d\theta^k_{zp}}{\sqrt{\left(\theta^k_{yp}\right)^2 + \left(\theta^k_{zp}\right)^2}},\ k = i, j \quad \text{.....(2.3-23)}$$

Using (2.3-23), then

$$d\underline{D} = \begin{Bmatrix} dD_i \\ dD_j \end{Bmatrix} = \begin{bmatrix} 0 & 0 & 0 & 0 & b_5 & b_6 & 0 & 0 & 0 & 0 & 0 & 0 \\ 0 & 0 & 0 & 0 & 0 & 0 & 0 & 0 & 0 & 0 & b_{11} & b_{12} \end{bmatrix} \cdot d\underline{r}^p = [B] \cdot d\underline{r}^p \ldots.$$

$$\text{.....(2.3-24)}$$

where,

$$b_5 = \frac{1}{\theta^i_{\max} - \theta^i_{cp}} \cdot \frac{\theta^i_{yp}}{\sqrt{\left(\theta^i_{yp}\right)^2 + \left(\theta^i_{zp}\right)^2}},\ b_6 = \frac{1}{\theta^j_{\max} - \theta^j_{cp}} \cdot \frac{\theta^i_{zp}}{\sqrt{\left(\theta^i_{yp}\right)^2 + \left(\theta^i_{zp}\right)^2}},$$

$$b_{11} = \frac{1}{\theta^j_{\max} - \theta^j_{cp}} \cdot \frac{\theta^j_{yp}}{\sqrt{\left(\theta^j_{yp}\right)^2 + \left(\theta^j_{zp}\right)^2}},\ b_{12} = \frac{1}{\theta^j_{\max} - \theta^j_{cp}} \cdot \frac{\theta^j_{zp}}{\sqrt{\left(\theta^j_{yp}\right)^2 + \left(\theta^j_{zp}\right)^2}}$$

Substituting (2.3-24) into (2.3-21) and solving for $d\underline{r}^p$, one obtains:

$$d\underline{r}^p = \left\{ I + \left[\frac{\partial \underline{f}}{\partial \underline{s}}\right]\left(\left[\frac{\partial \underline{f}}{\partial \underline{s}}\right]^T \underline{k}^e \left[\frac{\partial \underline{f}}{\partial \underline{s}}\right]\right)^{-1} [D][B] \right\}^{-1} \left[\frac{\partial \underline{f}}{\partial \underline{s}}\right]\left(\left[\frac{\partial \underline{f}}{\partial \underline{s}}\right]^T \underline{k}^e \left[\frac{\partial \underline{f}}{\partial \underline{s}}\right]\right)^{-1} \left[\frac{\partial \underline{f}}{\partial \underline{s}}\right]^T \underline{k}^e d\underline{r}$$

$$\text{.....(2.3-25)}$$

Substituting (2.3-25) into (2.3-18), the relationship between incremental generalized forces and incremental displacement is obtained:

$$d\underline{s} = \underline{k}^{epd} \cdot d\underline{r} \quad \text{.....(2.3-26)}$$

where,

$$\underline{k}^{epd} = \underline{k}^{e} - \underline{k}^{e}\left\{I + \left[\frac{\partial \underline{f}}{\partial \underline{s}}\right]\left(\left[\frac{\partial \underline{f}}{\partial \underline{s}}\right]^{T}\underline{k}^{e}\left[\frac{\partial \underline{f}}{\partial \underline{s}}\right]\right)^{-1}[D][B]\right\}^{-1}\left[\frac{\partial \underline{f}}{\partial \underline{s}}\right]\left(\left[\frac{\partial \underline{f}}{\partial \underline{s}}\right]^{T}\underline{k}^{e}\left[\frac{\partial \underline{f}}{\partial \underline{s}}\right]\right)^{-1}\left[\frac{\partial \underline{f}}{\partial \underline{s}}\right]^{T}\underline{k}^{e}$$

.....(2.3-27)

and I is the 12×12 unit matrix.

Equations (2.3-25) and (2.3-26) are in the final form to compute incremental plastic deformation and incremental generalized forces in the softening stage. However, from equation (2.3-27), one may note that the elasto-plastic-damage stiffness matrix is no longer symmetric, which violates a requirement of the NEABS program. To avoid this problem, a symmetric approximation to $\underline{k}^{epd}$ can be obtained by letting $[B] = [0]$. Then the symmetric stiffness matrix will be used for solving the dynamic equilibrium equation at the current time step or iteration. The equilibrium unbalance caused by the symmetric stiffness matrix will be corrected by applying the equilibrium unbalance within the next time step or iteration to restore equilibrium. Therefore, the original asymmetrical $\underline{k}^{epd}$ is used to compute generalized force increments and convergence is readily obtained. A detailed description of the computational procedure is given in Section 2.4.2.

2.4 Review of Previous Hysteresis Rules

When cyclic loading is applied to a reinforced concrete member, its hysteretic behavior is relatively complex. The load history, axial load, shear force, and lateral and longitudinal reinforcement are the primary factors that influence the hysteresis of

reinforced concrete (Sanjayan, 1988; Imbsen and Penzien, 1986). Considerable research has been done over the last several decades. The earliest proposed hysteresis model is the conventional elastic-plastic model (Figure 2.2-2). In this model, no stiffness change is included for unloading and reloading. The model was considered to be accurate for representing the hysteresis rule of metals, especially steel, but not for reinforced concrete. Clough (1966) improved this model by incorporating stiffness degradation--a significant characteristic of reinforced concrete (Figure 2.4-1), in which the response point during loading moved toward the previous maximum response, while the unloading slope remained unchanged relative to the initial elastic slope. However, this model did not include the softening effect.

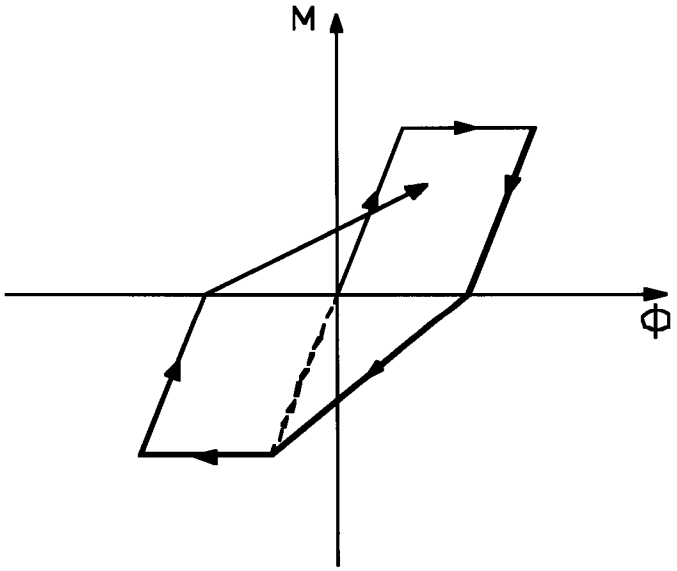

Figure 2.4-1: Clough 's Hysteresis Model

Based on twelve tests, Atalay and Penzien (1975) proposed a complex hysteretic model (Figure 2.4-2). In this model, the investigators defined several curve functions that represented reloading, unloading, and softening. However, it was suggested by the investigators that application of these functions to more general loading conditions needs further research.

Al-Sulaimani and Roesset (1985) defined a more refined hysteretic model with softening in a study to examine the effect of stiffness and strength degradation of hysteresis on the inelastic design spectra. They concluded that the stiffness would decrease during reloading and unloading (Figure 2.4-3). The reduction factor for stiffness during the unloading was a function of the ratio of maximum displacement and yield displacement. The reduction factor for stiffness during the reloading was determined by connecting the load-reversal point to the yield point or to the maximum load/deformation experienced if the system has already yielded in the new loading direction.

To investigate the influence of softening on the dynamic response of structures, Sanjayan (1988) extended the hysteresis model proposed by Clough (1966), in which the model consisted of several approximately straight lines. The unloading paths were considered to be parallel to the initial elastic slope, but the reversed loading followed a path in a direction pointing toward the previously-attained maximum deformation point (Figure 2.4-4).

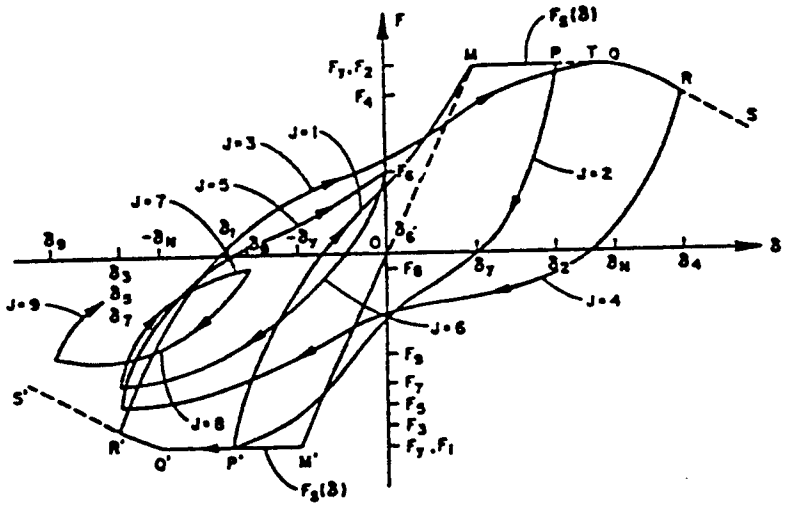

Figure 2.4-2: Atalay and Penzien (1975) Model (from Sanjayan, 1988)

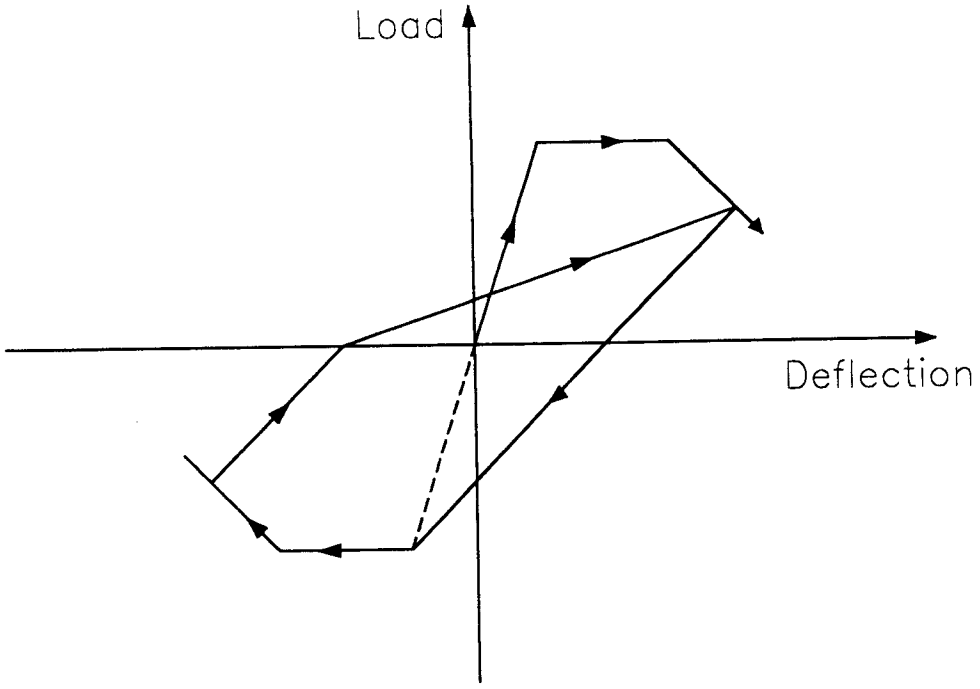

Figure 2.4-3: Al-Sulaimani and Roesset (1985) Model

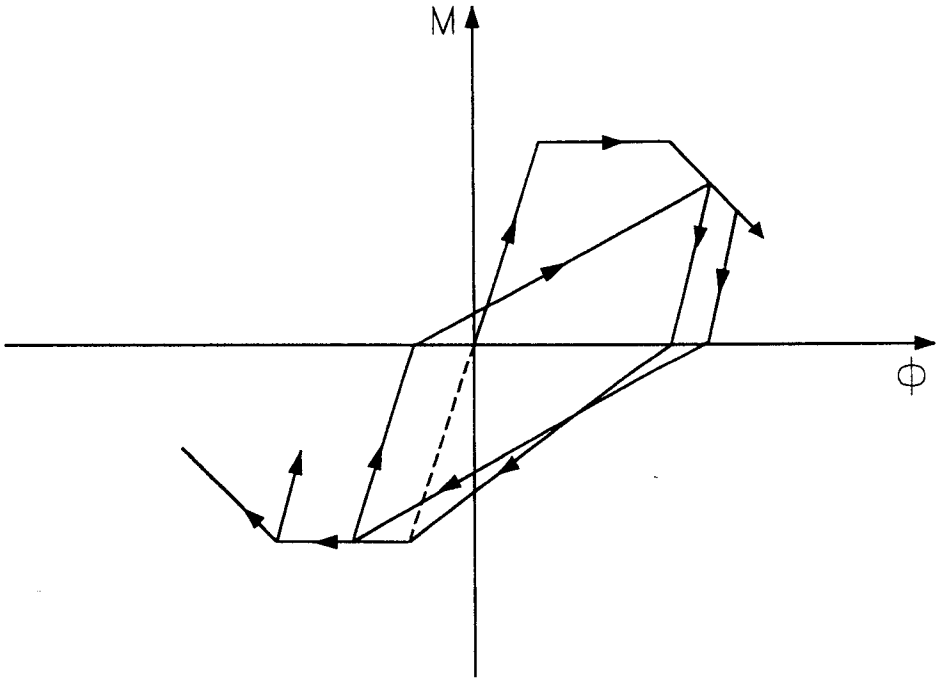

Figure 2.4-4: An Idealized Hysteresis Model Used By Sanjayan (1985)

2.5 Hysteresis Model for the Beam-Column Element

In this research, to imitate the actual behavior of reinforced concrete members subjected to cyclic deformation, a degradation of stiffness is considered. It is assumed that the degradation of stiffness can only occur within the yield surface. If the generalized forces are on the yield surface, the elasto-plastic-damage stiffness matrix, $\underline{k}^{epd}$ previously derived, is still used in the dynamic equilibrium equation for the current time step. The application of stiffness degradation is illustrated by the moment vs curvature curve in Figure 2.5-1. The loading, unloading, and reloading behavior are defined by the curve. The stiffness during unloading is assumed to be the same as the initial elastic stiffness, but the stiffness during reloading is allowed to degrade.

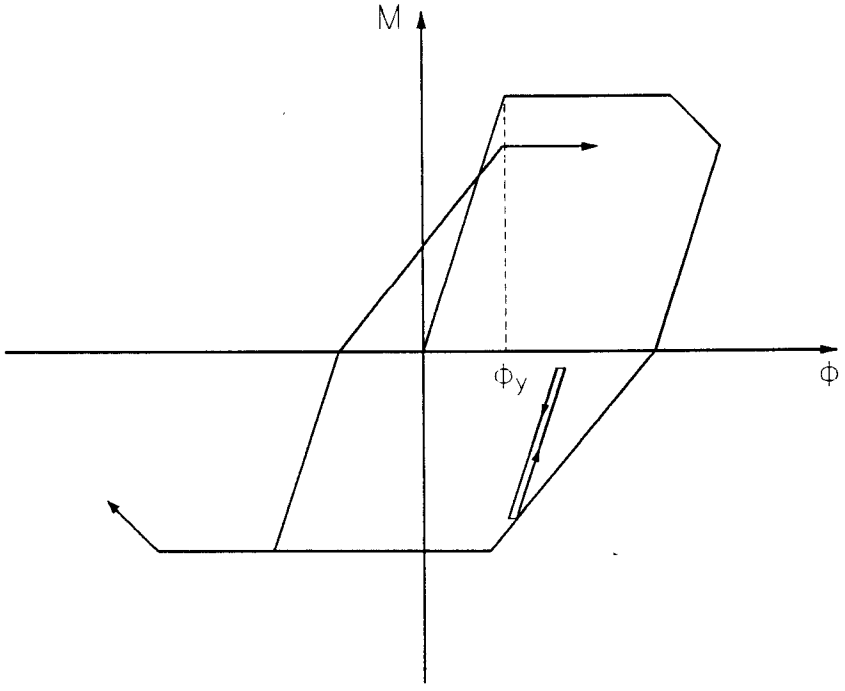

Figure 2.5-1: Hysteresis Model for the Beam-Column Element

The beam-column element is a three dimensional element. During the elastic loading or unloading stage, as shown in Figure 2.5-1, the flexural capacities about the y and z-axes are modeled as being fully continuous with no stiffness degradation. However, during the elastic reloading stage, the end conditions about the y and z-axes are considered to be between fully continuous and fully hinged conditions, in which the degradation of stiffness is produced due to the damage. One should note that the approach is also based on the assumption that the shear and axial capacities remain intact. To obtain the degradation stiffness during the elastic reloading stage, the damage coefficient is used again to define the loss of elastic stiffness of the member due to damage.

Let $\underline{k}^e{}_{miy}$, $\underline{k}^e{}_{miz}$, $\underline{k}^e{}_{mjy}$, and $\underline{k}^e{}_{mjz}$ be the release matrices about the y and z-axes at the i and j ends, respectively. The difference between the elastic stiffness matrix and any one of these release matrices equals the elastic matrix for pinned end conditions. For instance, the matrix $\underline{k}^e - \underline{k}^e_{miz}$ is the elastic matrix for which the rotational stiffness about the z-axis at the i-end is released. The $\underline{k}^e_{miy}$, $\underline{k}^e_{miz}$, $\underline{k}^e_{mjy}$ $\underline{k}^e{}_{mjz}$, and $\underline{k}^e$ matrices can be found in Appendix B. The $\underline{k}^e{}_{miy}$ and $\underline{k}^e{}_{miz}$, or $\underline{k}^e_{mjy}$ and $\underline{k}^e_{mjz}$ matrices are independent, and they can be used simultaneously to obtain pinned conditions about the y and z-axes at the i or j-ends. However, $\underline{k}^e_{miy}$ and $\underline{k}^e_{mjy}$, or $\underline{k}^e_{miz}$ and $\underline{k}^e_{mjz}$ are coupled, and thus they cannot be used to define the hinge conditions at the i and j-ends. To derive the degradation stiffness, this problem may be avoided by using the matrix condensation technique. First, the beam- column element, as shown in Figure 2.3-6, is divided into two

sub-elements (Figure 2.5-2) that are called element (1) and element (2), in which only the i and j-ends are allowed to develop damage.

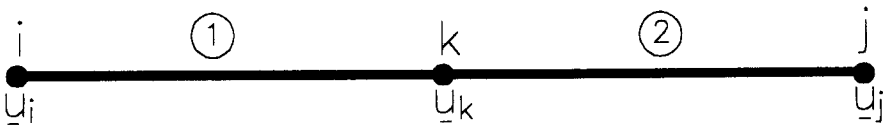

Figure 2.5-2: A Sub-Divided Beam-Column Element

Therefore, the degradation stiffness for element (1) and element (2) may be expressed:

$$\underline{k}_1^{ed} = \underline{k}_1^{e} - D_1 \cdot \underline{k}_{miy}^{e} - D_1 \cdot \underline{k}_{miz}^{e} \quad \text{.....(2.5-1)}$$

$$\underline{k}_2^{ed} = \underline{k}_2^{e} - D_2 \cdot \underline{k}_{mjy}^{e} - D_2 \cdot \underline{k}_{mjz}^{e} \quad \text{.....(2.5-2)}$$

where $\underline{k}_1^{ed}$ and $\underline{k}_2^{ed}$ are degradation stiffness matrices for elements (1) and (2), and $\underline{k}_1^{e}$ and $\underline{k}_2^{e}$ are the usual elastic stiffness matrices for elements (1) and (2). Further, $\underline{k}_1^{ed}$ and $\underline{k}_2^{ed}$ may be written as follows:

$$\underline{k}_1^{ed} = \begin{bmatrix} \underline{k}_{aa}^{1} & \underline{k}_{ab}^{1} \\ \underline{k}_{ba}^{1} & \underline{k}_{bb}^{1} \end{bmatrix} \quad \text{.....(2.5-3)}$$

and

$$\underline{k}_2^{ed} = \begin{bmatrix} \underline{k}_{aa}^{2} & \underline{k}_{ab}^{2} \\ \underline{k}_{ba}^{2} & \underline{k}_{bb}^{2} \end{bmatrix} \quad \text{.....(2.5-4)}$$

If $\underline{u}_i$, $\underline{u}_j$, and $\underline{u}_k$ are node displacement vectors at nodes i, j, and k (shown on Figure 2.5-2), then the end displacements of elements (1) and (2) are related by the following equations:

$$\begin{bmatrix} \underline{k}_{aa}^{1} & \underline{0} & \underline{k}_{ab}^{1} \\ \underline{0} & \underline{k}_{bb}^{2} & \underline{k}_{ba}^{2} \\ \underline{k}_{ba}^{1} & \underline{k}_{ab}^{2} & \underline{k}_{bb}^{1} + \underline{k}_{aa}^{2} \end{bmatrix} \cdot \begin{Bmatrix} \underline{u}_i \\ \underline{u}_j \\ \underline{u}_k \end{Bmatrix} = \begin{Bmatrix} \underline{p}_i \\ \underline{p}_j \\ \underline{p}_k \end{Bmatrix} \quad \text{.....(2.5-5)}$$

where $\underline{p}_i$, $\underline{p}_j$, and $\underline{p}_k$ are force vectors at nodes i, j, and k, respectively. The node k is the inner-node. Thus

$$\underline{p}_k = \underline{0} \quad \text{.....(2.5-6)}$$

Substituting (2.5-6) into (2.5-5), one can get:

$$\underline{k}_{\alpha\alpha} \cdot \underline{u}_\alpha + \underline{k}_{\alpha\beta} \cdot \underline{u}_\beta = \underline{p}_\alpha \quad \text{.....(2.5-7)}$$

and

$$\underline{k}_{\beta\alpha} \cdot \underline{u}_\alpha + \underline{k}_{\beta\beta} \cdot \underline{u}_\beta = \underline{0} \quad \text{.....(2.5-8)}$$

where,

$$\underline{k}_{\alpha\alpha} = \begin{bmatrix} \underline{k}_{aa}^{1} & \underline{0} \\ \underline{0} & \underline{k}_{bb}^{2} \end{bmatrix}, \quad \underline{k}_{\alpha\beta} = \begin{Bmatrix} \underline{k}_{ab}^{1} \\ \underline{k}_{ba}^{2} \end{Bmatrix}, \quad \underline{k}_{\beta\alpha} = \begin{bmatrix} \underline{k}_{ba}^{1} & \underline{k}_{ab}^{2} \end{bmatrix} \quad \underline{k}_{\beta\beta} = \begin{bmatrix} \underline{k}_{bb}^{1} + \underline{k}_{aa}^{2} \end{bmatrix}, \quad \underline{u}_\alpha = \begin{Bmatrix} \underline{u}_i \\ \underline{u}_j \end{Bmatrix},$$

and $\underline{u}_\beta = \{\underline{u}_k\}$

Using equations (2.5-7) and (2.5-8), the inner-node displacements $\underline{u}_\beta$ can be eliminated to solve $\underline{u}_\alpha$. Finally, the equation expressing end forces and displacements for node i and j becomes:

$$\left(\underline{k}_{\alpha\alpha} - \underline{k}_{\alpha\beta} \cdot \underline{k}_{\beta\beta}^{-1} \cdot \underline{k}_{\beta\alpha}\right) \cdot \underline{u}_\alpha = \underline{p}_\alpha \quad \text{.....(2.5-9)}$$

Let

$$\underline{k}^{ed} = \underline{k}_{\alpha\alpha} - \underline{k}_{\alpha\beta} \cdot \underline{k}_{\beta\beta}^{-1} \cdot \underline{k}_{\beta\alpha} \quad \text{.....(2.5-10)}$$

The $\underline{k}^{ed}$ matrix is thus the degradation stiffness matrix of the condensed, 2-node beam-column element.

2.6 Computational Procedures

After the derived elastic-plastic-damage tangent stiffness and the degradation stiffness are implemented into NEABS, the dynamic response is determined by step-by-step integration with a constant or linear acceleration assumption within any step. The information about an element yielding, softening, unloading, or reloading must be obtained in advance to determine which kind of tangent stiffness is to be used. Most of the computational procedures used in the original NEABS program remain. A major enhancement was required to correct the error which may arise from the equilibrium unbalance caused by using the symmetric stiffness matrix instead of the asymmetrical stiffness matrix for softening on the current iteration or time step. The method is to apply a corrective load within the next equilibrium iteration or time step to restore equilibrium.

The dynamic equation of motion may be expressed mathematically for the i^{th} equilibrium iteration at time t_n as:

$$\delta \underline{Q}_I^{(i)}(\ddot{t}_n) + \delta \underline{Q}_D^{(i)}(\dot{t}_n) + \delta \underline{Q}_S^{(i)}(t_n) = \delta \underline{F}^{(i)}(t_n) \quad \text{.....(2.6-1)}$$

where $\delta \underline{Q}_I^{(i)}(\ddot{t}_n)$, $\delta \underline{Q}_D^{(i)}(\dot{t}_n)$, $\delta \underline{Q}_S^{(i)}(t_n)$, and $\delta \underline{F}^{(i)}(t_n)$ are corrective inertia force, damping force, internal restoring force, and external applied dynamic force for the i^{th} iteration at time t_n, respectively. If softening occurs, the internal restoring force, $\delta \underline{Q}_S^{(i)}(t_n)$ is calculated approximately by using a symmetric stiffness

matrix, $\delta \underline{Q}_{Sym}^{(i)}(t_n)$, because of the symmetry requirement of NEABS for triangularizing the matrix. Thus, an equilibrium unbalance arises. This unbalance can be represented in terms of a corrective unbalanced internal restoring force

$\delta \underline{Q}_{U}^{(i)}(t_n) = \delta \underline{Q}_{Sym}^{(i)}(t_n) - \delta \underline{Q}_{S}^{(i)}(t_n)$. The true corrective internal restoring force is then $\delta \underline{Q}_{Sym}^{(i)}(t_n) - \delta \underline{Q}_{U}^{(i)}(t_n)$. Hence, equation (2.6-1) must be rewritten as:

$$\delta \underline{Q}_{I}^{(i)}(\ddot{t}_n) + \delta \underline{Q}_{D}^{(i)}(\dot{t}_n) + \delta \underline{Q}_{Sym}^{(i)}(t_n) - \delta \underline{Q}_{U}^{(i)}(t_n) = \delta \underline{F}^{(i)}(t_n) \quad \textbf{.....(2.6-2)}$$

For computational purposes, the unbalanced force, $\delta \underline{Q}_{U}^{(i)}(t_n)$, is moved to the right-hand-side of equation (2.6-2), resulting in the following:

$$\delta \underline{Q}_{I}^{(i)}(\ddot{t}_n) + \delta \underline{Q}_{D}^{(i)}(\dot{t}_n) + \delta \underline{Q}_{Sym}^{(i)}(t_n) = \delta \underline{F}^{(i)}(t_n) + \delta \underline{Q}_{U}^{(i)}(t_n) \quad \textbf{.....(2.6-3)}$$

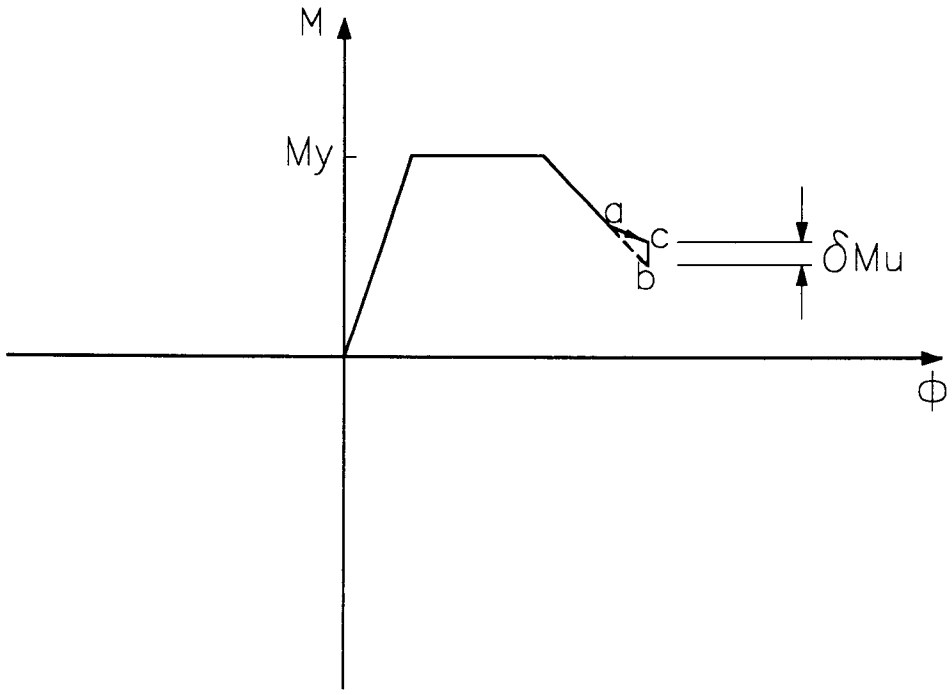

Figure 2.6-1: Unbalance Moment

To explain the procedure clearly, an example is presented here. Figure 2.6-1 shows the exact moment vs curvature curve for a bending member (note that only moment is dealt with here). The correct path for an equilibrium iteration should be from a-b if the asymmetrical elastic-plastic-softening stiffness matrix is used in solving the corrective dynamic equation of motion (2.6-1). However, because an approximate symmetric stiffness matrix replaces the asymmetrical stiffness matrix to solve equation (2.6-1), the path a-b will deviate to a-c. The equilibrium unbalance caused by the deviation is δM_U. In order to avoid errors from the equilibrium unbalance, δM_U is added to the corrective external load.

2.7 Examples

Once the aforementioned derivations were implemented into NEABS, example studies were conducted. The purpose of the examples was to test the derivations in the above sections and to assess the performance of the modified program. A total of three examples were analyzed. The first example analysis was performed by hand computation in order to check the derivation. The other two examples were analyzed by the modified program, in which static monotonic loading conditions were applied. The purpose of the first example for the computer analysis was to check the influence of the softening effect. The second example was to test the procedure that was used for the implementation of the degradation of stiffness.

2.7.1 Example 1

Although the derivation of the elasto-plastic damage stiffness matrix is in a three dimensional domain, it is straightforward to adopt the derivation to a planar problem. Figure 2.7-1 shows a plane beam element, for which the axial force is neglected. The definition of the damage coefficient is the same as that of equation (2.3-1) in Section 2.3.1. However, only one plastic rotation in the z-direction contributes to the total plastic rotation. Moreover, the yield function is also simplified as:

$$f(s_k) = \frac{M_k}{M_p} = 1 - D_k,\ k = i, j \qquad \text{(2.7-1)}$$

Figure 2.7-1: Plane Beam-Column Element

Thus, for the plane problem the following relations may be obtained:

$$D_k = \frac{\theta^k - \theta^k_{cp}}{\theta^k_{\max} - \theta^k_{cp}},\ k = i, j \qquad \text{(2.7-2)}$$

$$\underline{B} = \begin{bmatrix} 0 & \dfrac{1}{\theta^i_{\max} - \theta^i_{cp}} & 0 & 0 \\ 0 & 0 & 0 & \dfrac{1}{\theta^j_{\max} - \theta^j_{cp}} \end{bmatrix} \qquad \text{(2.7-3)}$$

$$\underline{D} = \begin{bmatrix} -1 & 0 \\ 0 & -1 \end{bmatrix} \qquad \text{(2.7-4)}$$

For computation purposes in this example, it is assumed that only node j is allowed to develop a plastic hinge. Thus,

$$\left[\frac{\partial \underline{f}}{\partial \underline{s}}\right] = \begin{bmatrix} 0 & 0 \\ 0 & 0 \\ 0 & 0 \\ 0 & \frac{1}{M_p} \end{bmatrix} \quad \text{.....(2.7-5)}$$

The well known incremental elastic tangent stiffness matrix for the plane beam element is

$$\underline{k}^e = \begin{bmatrix} \frac{12EI}{l^3} & \frac{6EI}{l^2} & -\frac{12EI}{l^3} & \frac{6EI}{l^2} \\ \frac{6EI}{l^2} & \frac{4EI}{l} & -\frac{6EI}{l^2} & \frac{2EI}{l} \\ -\frac{12EI}{l^3} & -\frac{6EI}{l^2} & \frac{12EI}{l^3} & -\frac{6EI}{l^2} \\ \frac{6EI}{l^2} & \frac{2EI}{l} & -\frac{6EI}{l^2} & \frac{4EI}{l} \end{bmatrix} \quad \text{.....(2.7-6)}$$

Substituting equations (2.7-3), (2.7-4), (2.7-5), and (2.7-6) into (2.3-25) and (2.3-27) in Section 2.3.3, one can get the following:

$$d\underline{r}^p = c \begin{bmatrix} 0 & 0 & 0 & 0 \\ 0 & 0 & 0 & 0 \\ 0 & 0 & 0 & 0 \\ \frac{3}{2l} & \frac{1}{2} & -\frac{3}{2l} & 1 \end{bmatrix} \cdot d\underline{r} \quad \text{.....(2.7-7)}$$

$$\underline{k}^{epd} = \begin{bmatrix} \frac{(12-9c)EI}{l^3} & \frac{(6-3c)EI}{l^2} & -\frac{(12-9c)}{l^3} & \frac{(6-6c)EI}{l^2} \\ \frac{(6-3c)EI}{l^2} & \frac{(4-c)EI}{l} & -\frac{(6-3c)EI}{l^2} & \frac{(2-2c)EI}{l} \\ -\frac{(12-9c)EI}{l^3} & -\frac{(6-3c)EI}{l^2} & \frac{(12-9c)EI}{l^3} & -\frac{(6-6c)EI}{l^2} \\ \frac{(6-6c)EI}{l^2} & \frac{(2-2c)EI}{l} & -\frac{(6-6c)EI}{l^2} & \frac{(4-4c)EI}{l} \end{bmatrix} \quad \text{.....(2.7-8)}$$

where,

$$c = \frac{1}{1 - \dfrac{M_p l}{4EI(\theta^j_{\max} - \theta^j_{cp})}} \qquad \text{(2.7-9)}$$

The $\underline{k}^{epd}$ matrix is the incremental elastic-plastic-damage tangent stiffness matrix for the plane beam element when only end j is allowed to develop a plastic hinge. Because only one end is allowed to develop a plastic hinge, the matrix is symmetric. It is straightforward to obtain the incremental tangent stiffness matrix from (2.7-8) for an elastic-perfectly plastic beam element by simply letting $c = 1$. The particular incremental tangent stiffness matrix for the elastic-perfectly plastic beam element is:

$$\underline{k}^{ep} = \begin{bmatrix} \frac{3EI}{l^3} & \frac{3EI}{l^2} & -\frac{3EI}{l^3} & 0 \\ \frac{3EI}{l^3} & \frac{3EI}{l} & -\frac{3EI}{l^2} & 0 \\ -\frac{3EI}{l^3} & -\frac{3EI}{l^2} & \frac{3EI}{l^3} & 0 \\ 0 & 0 & 0 & 0 \end{bmatrix} \qquad \text{(2.7-10)}$$

This incremental tangent stiffness matrix is exactly the same as the incremental stiffness matrix of an element when end i is fixed and end j is pinned.

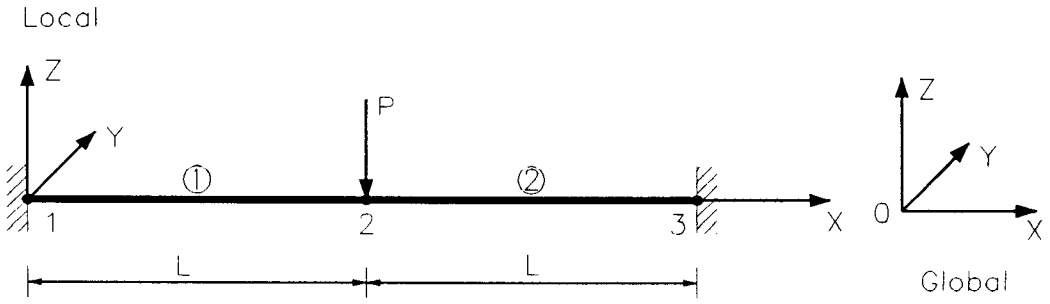

Figure 2.7-2: Structural Model of Beam

Using (2.7-8) and (2.7-10), a simple beam with two fixed ends, as shown in Figure 2.7-2, is analyzed. The beam is divided into two elements. It is assumed that only node 2 in element (1) is allowed to develop a plastic hinge and that other nodes remain elastic. The assumption is made purely for test purposes. Assuming that the beam is subjected to force P in the middle of the beam, two cases are computed, in which for Case 1, the plastic hinge at node 2 is allowed to develop without softening, and for Case 2, the plastic hinge is allowed to develop with softening.

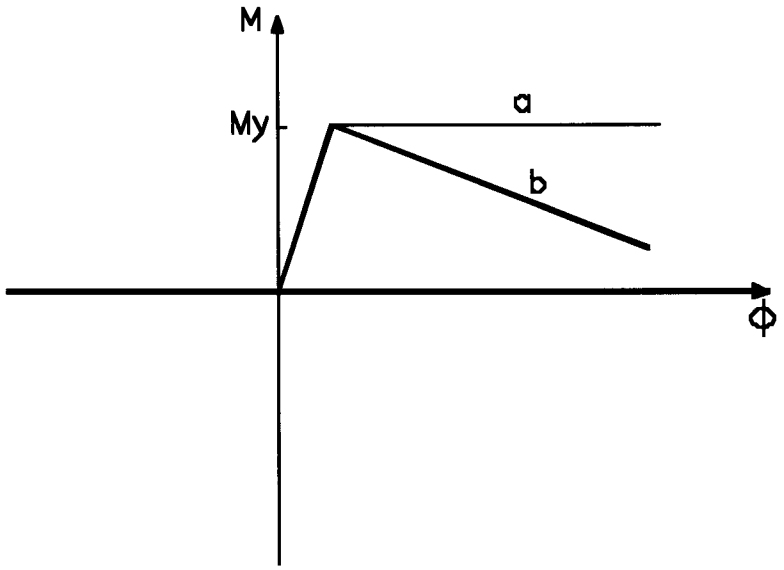

Figure 2.7-3: Moment vs Curvature

Case 1 (Without Softening)

Because of the assumption of no softening at node 2 of element (1), the curve of moment vs. curvature is elastic-perfectly plastic, represented by curve a in Figure 2.7-3.

For the first step, $P = P_1$, where P_1 just makes node 2 in element (1) yield, so that the beam is in the elastic stage. Assembling the incremental elastic tangent stiffness matrices and total incremental external forces of elements (1) and (2), the incremental displacements and external forces may be written as:

$$\begin{bmatrix} \frac{12EI}{l^3} & \frac{6EI}{l^2} & -\frac{12EI}{l^3} & \frac{6EI}{l^2} & 0 & 0 \\ \frac{6EI}{l^2} & \frac{4EI}{l} & -\frac{6EI}{l^2} & \frac{2EI}{l} & 0 & 0 \\ -\frac{12EI}{l^3} & -\frac{6EI}{l^2} & \frac{24EI}{l^3} & 0 & -\frac{12EI}{l^3} & \frac{6EI}{l^2} \\ \frac{6EI}{l^2} & \frac{2EI}{l} & 0 & \frac{8EI}{l} & -\frac{6EI}{l^2} & \frac{2EI}{l} \\ 0 & 0 & -\frac{12EI}{l^3} & -\frac{6EI}{l^2} & \frac{12EI}{l^3} & -\frac{6EI}{l^2} \\ 0 & 0 & \frac{6EI}{l^2} & \frac{2EI}{l} & -\frac{6EI}{l^2} & \frac{4EI}{l} \end{bmatrix} \begin{Bmatrix} \delta u_1^1 \\ \delta\theta_1^2 \\ \delta u_2^2 \\ \delta\theta_2^2 \\ \delta u_3^3 \\ \delta\theta_3^3 \end{Bmatrix} = \begin{Bmatrix} 0 \\ 0 \\ -P_1 \\ 0 \\ 0 \\ 0 \end{Bmatrix} \quad \text{.....(2.7-11)}$$

Substituting the boundary conditions, $\delta u_1^1 = \delta\theta_1^1 = \delta u_3^3 = \delta\theta_3^3 = 0$, into (2.7-11), and solving equation (2.7-11) for unknown incremental displacements δu_2^2, $\delta\theta_2^2$, one gets:

$$\delta u_2^2 = -\frac{P_1 l^3}{24EI}$$

$$\delta\theta_2^2 = 0$$

Using (2.7-6), the moment in node 2 is:

$$\delta M_2 = -\frac{6EI}{l^2}\delta u_2^2 = \frac{1}{4}P_1 l$$

Assuming no initial displacements and forces, when $P = P_1$ for node 2 the total displacements are:

$$u_2 = \delta u_2^1 = -\frac{P_1 l^3}{24EI}$$

$\theta_2 = \delta\theta_2^1 = 0$

Then, by using (2.7-6)

$M_2 = \delta M_2^1 = \frac{1}{4} P_1 l$ and

the following is obtained:

$$M_p = \frac{1}{4} P_1 l \quad \text{.....(2.7-12)}$$

In the next step, the force is increased to $P_1 + P_2$. Because the total external force $P_1 + P_2$ has exceeded the yield force P_1, node 2 in element (1) will enter the plastic region without softening. By using the incremental elastic-perfectly plastic tangent stiffness matrix (2.7-10) for element (1) and the elastic tangent stiffness matrix (2.7-6) for element (2), the relation of displacements and forces becomes:

$$\begin{bmatrix} \frac{3EI}{l^3} & \frac{3EI}{l^2} & -\frac{3EI}{l^3} & 0 & 0 & 0 \\ \frac{3EI}{l^2} & \frac{3EI}{l} & -\frac{3EI}{l^2} & 0 & 0 & 0 \\ -\frac{3EI}{l^3} & -\frac{3EI}{l^2} & \frac{15EI}{l^3} & \frac{6EI}{l^2} & -\frac{12EI}{l^3} & \frac{6EI}{l^2} \\ 0 & 0 & \frac{6EI}{l^2} & \frac{4EI}{l} & -\frac{6EI}{l^2} & \frac{2EI}{l} \\ 0 & 0 & -\frac{12EI}{l^3} & -\frac{6EI}{l^2} & \frac{12EI}{l^3} & -\frac{6EI}{l^2} \\ 0 & 0 & \frac{6EI}{l^2} & \frac{2EI}{l} & -\frac{6EI}{l^2} & \frac{4EI}{l} \end{bmatrix} \begin{Bmatrix} \delta u_1^2 \\ \delta\theta_1^2 \\ \delta u_2^2 \\ \delta\theta_2^2 \\ \delta u_3^2 \\ \delta\theta_3^2 \end{Bmatrix} = \begin{Bmatrix} 0 \\ 0 \\ -P_2 \\ 0 \\ 0 \\ 0 \end{Bmatrix} \quad \text{.....(2.7-13)}$$

Solving equation (2.7-13) as was done for equation (2.7-11), one obtains:

$$\delta u_2^2 = -\frac{P_2 l^3}{6EI}$$

$$\delta\theta_2^2 = \frac{P_2 l}{4EI}$$

Thus, when $P = P_1 + P_2$ the total displacements at node 2 are:

$$u_2 = \delta u_2^1 + \delta u_2^2 = -\frac{P_1 l^3}{24EI} - \frac{P_2 l^3}{6EI} \quad \text{.....(2.7-14)}$$

$$\theta_2 = \delta\theta_2^1 + \delta\theta_2^2 = \frac{P_2 l^2}{4EI} \quad \text{.....(2.7-15)}$$

Using (2.7-7) by letting $c = 1$, it is straightforward to obtain the plastic deformations for node 2 at the force increment step. The computational results are:

$$\delta u_2^p = 0$$

$$\delta\theta_2^p = \frac{P_2 l^2}{2EI}$$

Total plastic deformations for node 2 are:

$$u_2^p = \delta u_2^p = 0 \quad \text{.....(2.7-16)}$$

$$\theta_2^p = \delta\theta_2^p = \frac{P_2 l^2}{2EI} \quad \text{.....(2.7-17)}$$

Case 2 (With Softening)

It is assumed that the critical plastic rotation θ_{cp} at node 2 of element (1) is zero in the example. Thus the curve of moment vs. curvature may be specified by curve b in Figure 2.7-3 with softening. When the beam is subjected to the force $P = P_1$, node 2 of element (1) is in the elastic stage. Thus, the results of analysis in this stage are the same as those for Case 1. As soon as the force is increased to $P_1 + P_2$, the plastic hinge with softening in node 2 is formed because the critical plastic rotation θ_{cp} is assumed to be zero. The incremental force- displacement analysis in this secondary load stage is

influenced by a combination of elasticity and plasticity and softening. The incremental elastic-plastic-damage tangent stiffness matrix $\underline{k}^{epd}$ is used for element (1).

Assuming that

$$\theta_{\max} = \frac{mlM_p}{4EI} \quad \text{(2.7-18)}$$

where m is an undetermined coefficient, and substituting (2.7-18) and $\theta_{cp} = 0$ into (2.7-9), the coefficient c is expressed as:

$$c = \frac{m}{m-1} \quad \text{(2.7-19)}$$

Assembling the incremental elastic-plastic-damage tangent stiffness matrix (2.7-8) for element (1) and the incremental elastic tangent stiffness matrix (2.7-6) for element (2), the displacement-force relation is:

$$\begin{bmatrix} \frac{(12-9c)EI}{l^3} & \frac{(6-3c)EI}{l^2} & -\frac{(12-9c)EI}{l^3} & \frac{(6-6c)EI}{l^2} & 0 & 0 \\ \frac{(6-3c)EI}{l^2} & \frac{(4-c)}{l} & -\frac{(6-3c)EI}{l^2} & \frac{(2-2c)}{l} & 0 & 0 \\ -\frac{(12-9c)EI}{l^3} & -\frac{(6-3c)EI}{l^2} & \frac{(24-9c)EI}{l^3} & \frac{6cEI}{l^2} & -\frac{12EI}{l^3} & \frac{6EI}{l^2} \\ \frac{(6-6c)EI}{l^2} & \frac{(2-2c)EI}{l} & \frac{6cEI}{l^2} & \frac{(8-4c)EI}{l} & -\frac{6EI}{l^2} & \frac{2EI}{l} \\ 0 & 0 & -\frac{12EI}{l^3} & -\frac{6EI}{l^2} & \frac{12EI}{l^3} & -\frac{6EI}{l^2} \\ 0 & 0 & \frac{6EI}{l^2} & \frac{2EI}{l} & -\frac{6EI}{l^2} & \frac{4EI}{l} \end{bmatrix} \begin{Bmatrix} \delta u_1^2 \\ \delta\theta_1^2 \\ \delta u_2^2 \\ \delta\theta_2^2 \\ \delta u_3^2 \\ \delta\theta_3^2 \end{Bmatrix} = \begin{Bmatrix} 0 \\ 0 \\ -P_2 \\ 0 \\ 0 \\ 0 \end{Bmatrix} \quad \text{(2.7-20)}$$

Applying boundary constraints and solving the equations, the incremental displacements for node 2 are:

$$\delta u_2^2 = -\frac{P_2 l^3}{6EI} \cdot \frac{(2-c)}{(8-7c)} = -\frac{P_2 l^3}{6EI} \cdot \left(1 + \frac{6}{m-8}\right)$$

$$\delta\theta_2^2 = \frac{P_2 l^2}{4EI} \cdot \frac{c}{(8-7c)} = \frac{P_2 l^2}{4EI} \cdot \left(1 + \frac{8}{m-8}\right)$$

Substituting the above incremental displacements into (2.7-7), the incremental plastic deformations for node 2 are:

$$\delta u_2^p = 0$$

$$\delta\theta_2^p = \frac{P_2 l^2}{2EI} \cdot \left(1 + \frac{8}{m-8}\right)$$

Thus, when the force, P, is $P_1 + P_2$ for the case of a plastic hinge with softening, the total displacements and plastic deformations for node 2 are:

$$\boldsymbol{u_2 = -\frac{P_1 l^3}{24EI} - \frac{P_2 l^3}{6EI} \cdot \left(1 + \frac{6}{m-8}\right)} \quad \textbf{(2.7-21)}$$

$$\boldsymbol{\theta_2 = \frac{P_2 l^2}{4EI} \cdot \left(1 + \frac{8}{m-8}\right)} \quad \textbf{(2.7-22)}$$

$$\boldsymbol{u_2^p = \delta u_2^p = 0} \quad \textbf{(2.7-23)}$$

$$\boldsymbol{\theta_2^p = \delta\theta_2^p = \frac{P_2 l^2}{2EI} \cdot \left(1 + \frac{8}{m-8}\right)} \quad \textbf{(2.7-24)}$$

Using (2.7-2), (2.7-12), (2.7-18), and (2.7-24), when $P = P_1 + P_2$, the damage coefficient at node 2 in element (1) is expressed as:

$$\boldsymbol{D_2 = \frac{P_2}{P_1} \cdot \frac{8}{(m-8)}} \quad \textbf{(2.7-25)}$$

From (2.7-21) to (2.7-25), it is found that the displacements, plastic deformations, and damage coefficient become infinite when $m = 8$. The main reason is that the incremental stiffness matrix, given in equation (2.7-20), becomes singular, so that the

equation (2.7-20) is invalid. Further, for values of $m < 8$, the displacements (2.7-21) and (2.7-22) and plastic deformations (2.7-23) and (2.7-24) for the plastic hinge with softening are less than those for the plastic hinge without softening. This result implies that the stiffness of the beam with a softening hinge is larger than that for the beam with a perfectly plastic hinge. This is not acceptable because softening results in a smaller stiffness for a structure. In fact, values of $m \leq 8$ represent very large softening slopes with almost vertical unloading; thus an instability of the structure may be expected. A similar phenomenon was noted by Sanjayan (1988) when a parameter that defined the softening slope reached a critical value. A solution to the singularity was proposed in his Ph.D. dissertation. Further investigation of the dilemma is not a part of this research. However, it is strongly recommended for future study.

Comparing to the displacements and plastic deformations between Case 1 and Case 2 when $m > 8$, it is found that the displacements and deformations for the beam with softening are always larger than those for the beam without softening. In order to identify the influence of the softening slope on displacements, plastic deformations, and the damage coefficient, plots may be considered. When $P_2 = nP_1$, where n is a coefficient, the displacements, plastic deformations, and damage coefficient become:

For Case 1

$$u_2 = -\frac{P_1 l^3}{24EI}(1+4n)$$

$$\theta_2 = \frac{P_1 l^2}{4EI}n$$

$$u_2^p = 0$$

$$\theta_2^p = \frac{P_1 l^2}{2EI} n$$

For Case 2

$$u_2 = -\frac{P_1 l^3}{24EI}\left(1 + 4n + \frac{24n}{m-8}\right)$$

$$\theta_2 = \frac{P_1 l^2}{4EI}\left(n + \frac{8n}{m-8}\right)$$

$$u_2^p = 0$$

$$\theta_2^p = \frac{P_1 l^2}{2EI}\left(n + \frac{8n}{m-8}\right)$$

$$D_2 = \frac{8n}{m-8}$$

From the definition of m, it is shown that m is a parameter that defines the softening slope, which means that a large value of m represents a small softening slope, while a small value represents a large softening slope. When the value of m is infinite, a plastic hinge with elastic-perfectly plastic behavior will be obtained. In that case, all results derived in Case 2 are the same as the results in Case 1. Figures 2.7-4 through 2.7-7 show the significant influence of the softening slope on displacements, plastic deformations and the damage coefficient. The steeper the softening slope, the larger the displacements, plastic deformations, and damage coefficient. A small value of m, i.e. a large softening slope, and a large load cause a larger difference of displacements and deformations between the two cases (Figures 2.7-4, 2.7-5, and 2.7-6). This phenomenon

can be explained by Figure 2.7-7, where the difference between the damage coefficients for different values of load is much more obvious when the softening slope is large than that when the softening slope is small. A limitation to the damage coefficient is that it must be less than or equal to one; that is $D_2 \leq 1$. There is no physical meaning when $D_2 \rangle 1$. When the damage coefficient equals one, that means that the plastic hinge totally loses flexural resistance and is assured to behave as a pin. Therefore, the equations that express displacements and plastic deformations cannot be used to calculate the displacements and plastic deformations when the damage coefficient theoretically exceeds one.

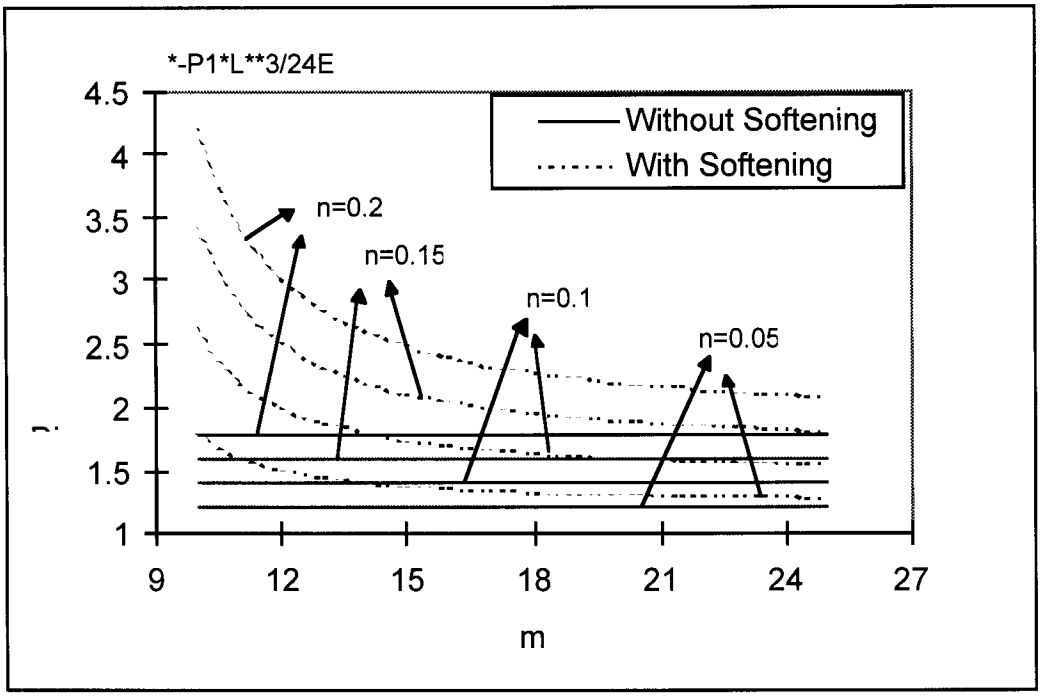

Figure 2.7-4: Displacement

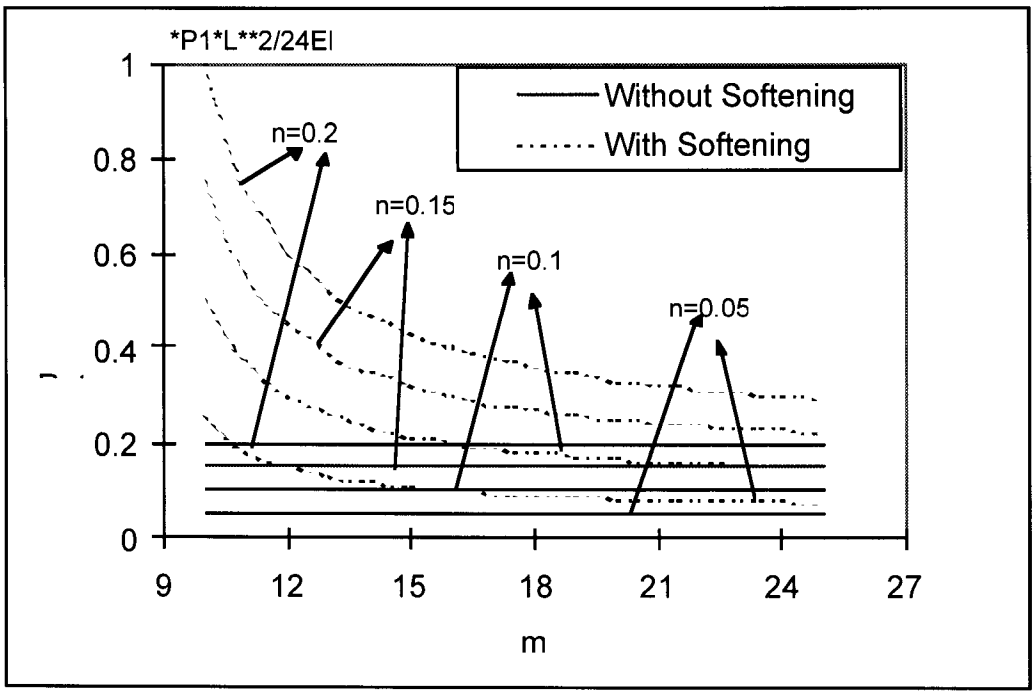

Figure 2.7-5: Rotation

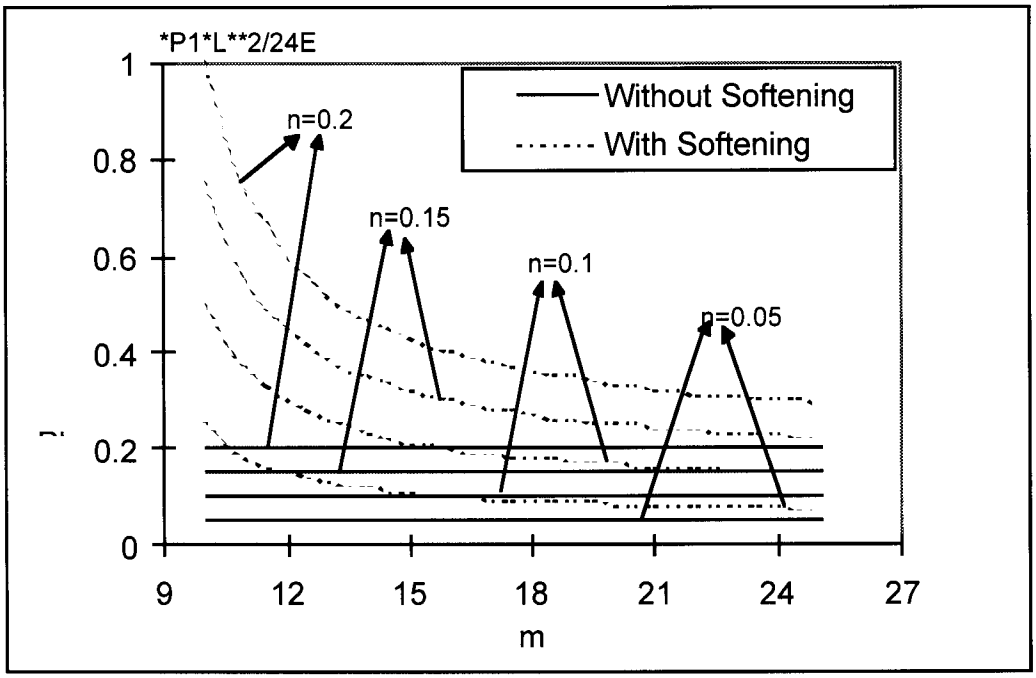

Figure 2.7-6: Plastic Rotation

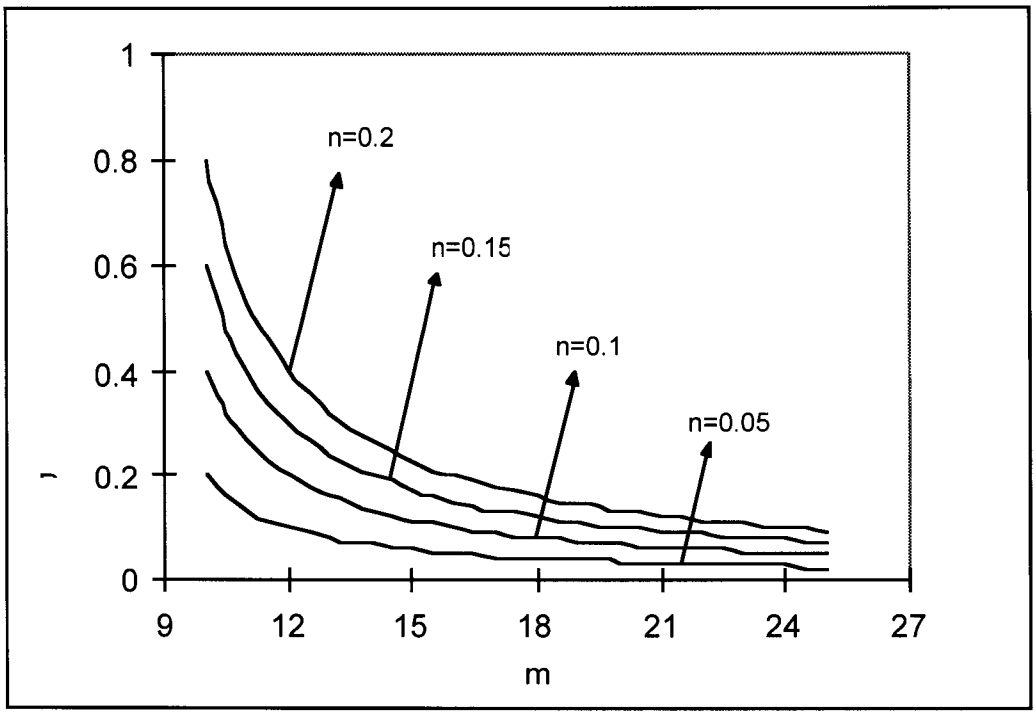

Figure 2.7-7: Damage Coefficient

2.7.2 Example 2

Dimensions and numbers of nodes and members are shown in Figure 2.7-8, where both ends of the beam are fixed. Other element properties are shown in Table 2.7-1. To reach the desired result, two artificial actions were used in the selections of some parameters. Firstly, the values of θ_{cp} and $\theta_{\max}$ were chosen for testing purposes, in which $\theta_{cp} = 0$ and $\theta_{\max} = 0.75 \times 10^{-2} rad$. Secondly, the yield moments about the y and z-axes, M_{y0} and M_{z0} for element (2), were much larger than those for element (1). The purpose was to let element (1) undergo softening, but not element (2). Figure 2.7-9 is the bilinear monotonic loading vs. time diagram that was applied to node 2, as shown in Figure 2.7-8.

Table 2.7-1: Structural Properties of the Beam

Element No.	Young's Modulus (kN/cm^2)	Poisson Ratio	Unit Weight (kN/cm^3)	M_{y0} ($kN-m$)	P_0	P_t/P_0	a_1	a_2	a_3
1	3169	0.18	0.0	1016	21709	0.122	-6.97	-9.44	-1.47
2	3169	0.18	0.0	2145	21709	0.122	-6.97	-9.44	-1.47

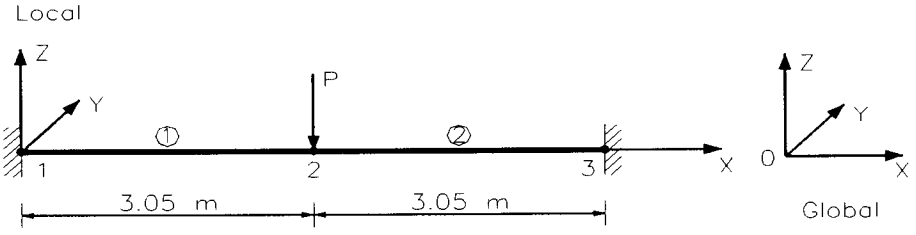

Figure 2.7-8: Structural Model of Beam

The results at node 2 are shown in Figures 2.7-10 to 2.7-13, where solid lines represent the results for which no damage effects are included (i.e., all plastic hinges are perfectly plastic.), and dashed lines indicate the results for which the plastic hinges are considered as plastic-softening.

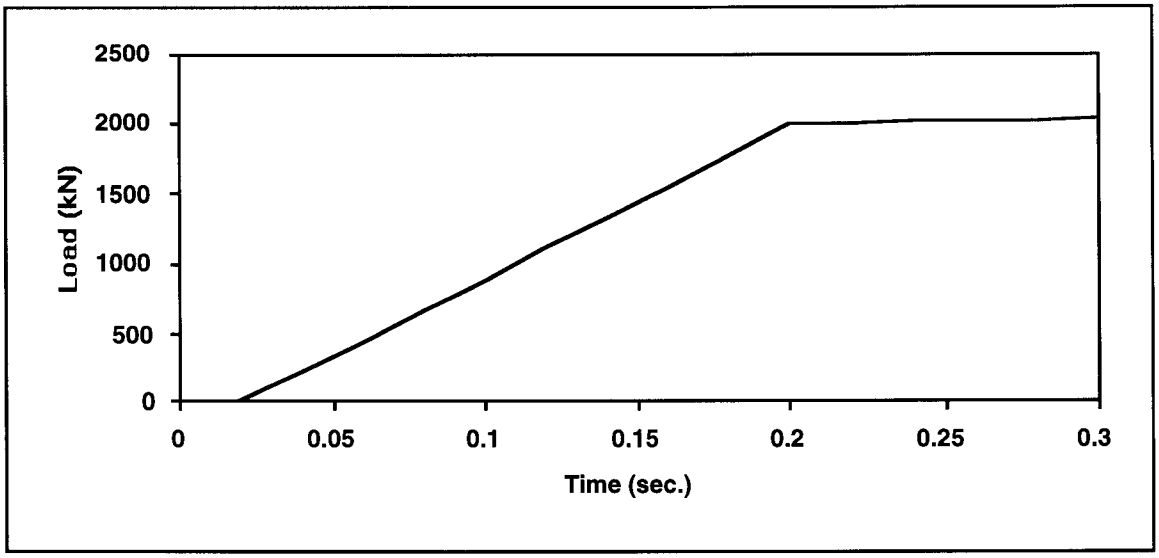

Figure 2.7-9: Load vs Time Curve

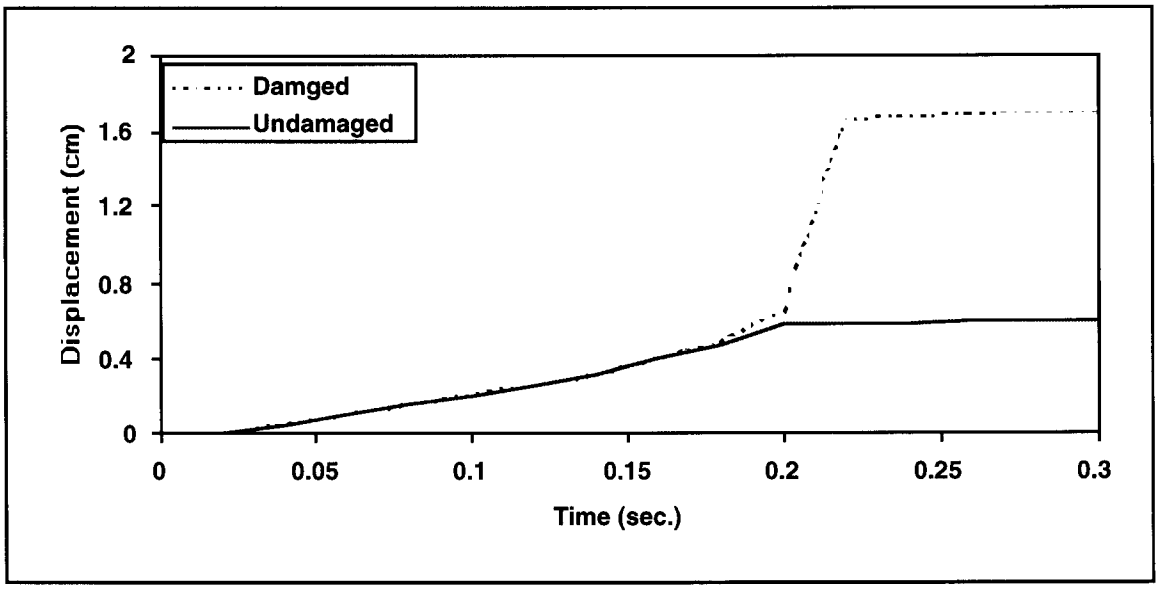

Figure 2.7-10: Displacement vs Time Curve

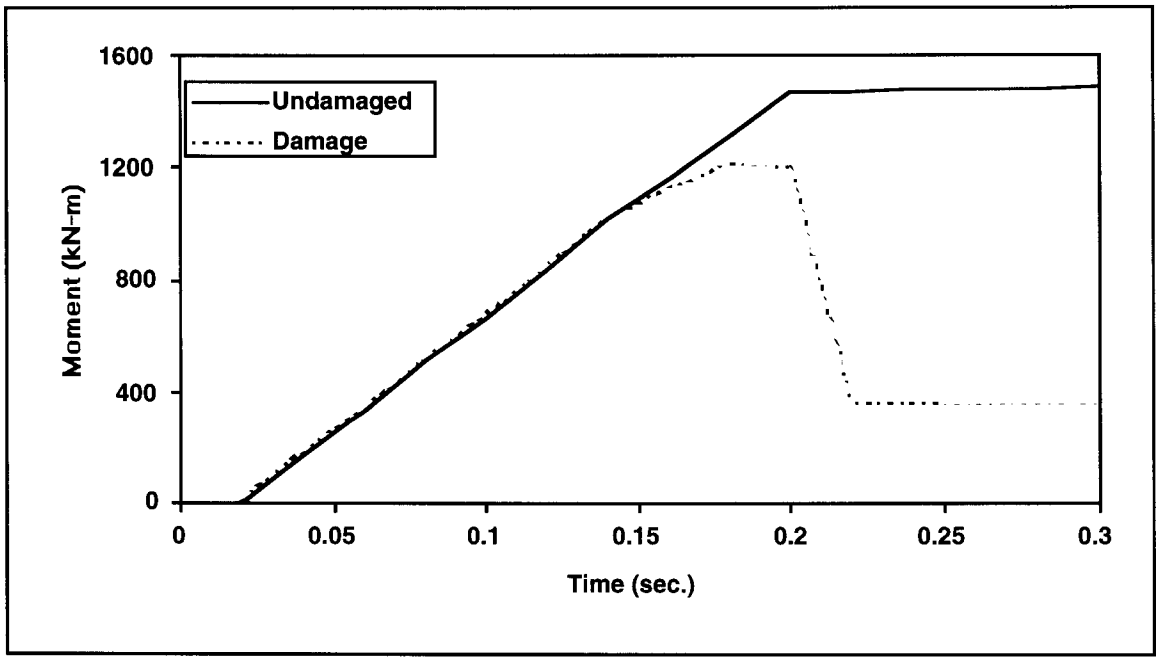

Figure 2.7-11: Moment vs Time Curve

Figure 2.7-10 shows that a plastic hinge is formed at node 2 when the displacement is corresponding to a load of 1334 kN. With the increase of the load, the displacement continues to increase, but the plastic rotation is not beyond the critical value that makes the plastic hinge enter the softening stage, so that the displacements from both calculations remain the same until the damage effect (softening) occurs. Because of the softening, the displacement results from both analyses diverge with the increase of load. The influence due to the softening on displacement is quite considerable. The moment behavior (Figure 2.7-11) at node 2 is similar to that of displacements. Comparing maximum displacements and plastic rotations, as shown in Figures 2.7-10, 2.7-12, and 2.7-13, the maximum displacement with softening is increased by 18.5 times, and the maximum plastic rotation is increased by 12.2 times.

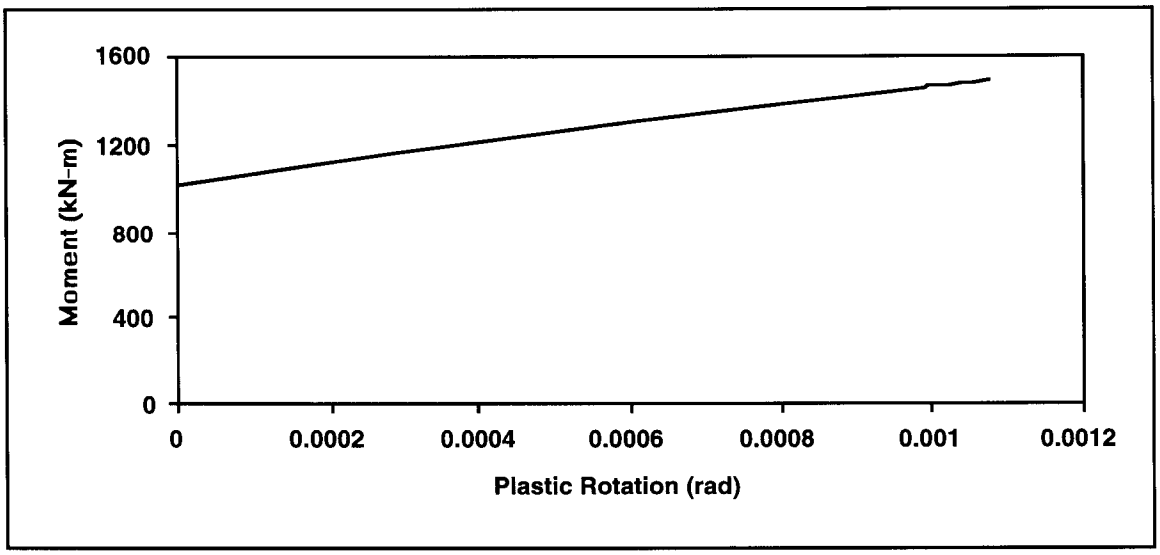

Figure 2.7-12: Moment vs Plastic Rotation Curve without Softening

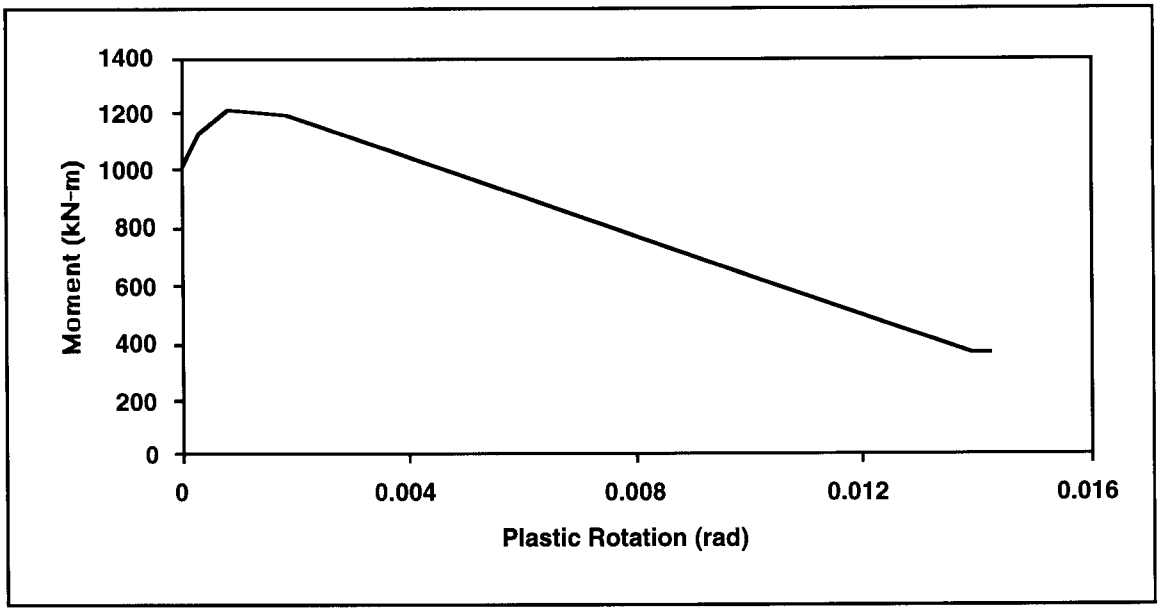

Figure 2.7-13: Moment vs Plastic Rotation Curve with Softening

2.7.3 Example 3

In this example, a single-column model was analyzed in order to test the hysteresis rule used in this dissertation. The column was fixed at the bottom, while the top of the column was connected to an elastic spring (Figure 2.7-14). The role of the elastic spring was to absorb the extra force that was released by the column when it was forced to soften by a horizontal load.

All structural properties of the column were tabulated in Table 2.7-2 except that the height of the column was 4.575 m. The elastic stiffness of the spring was set equal to the lateral stiffness of the fixed column. That is

$$k_s = \frac{3EI}{l^3} = \frac{3 \times 2635 \times 306263}{457.5^3} = 25.28\ kN / cm.$$

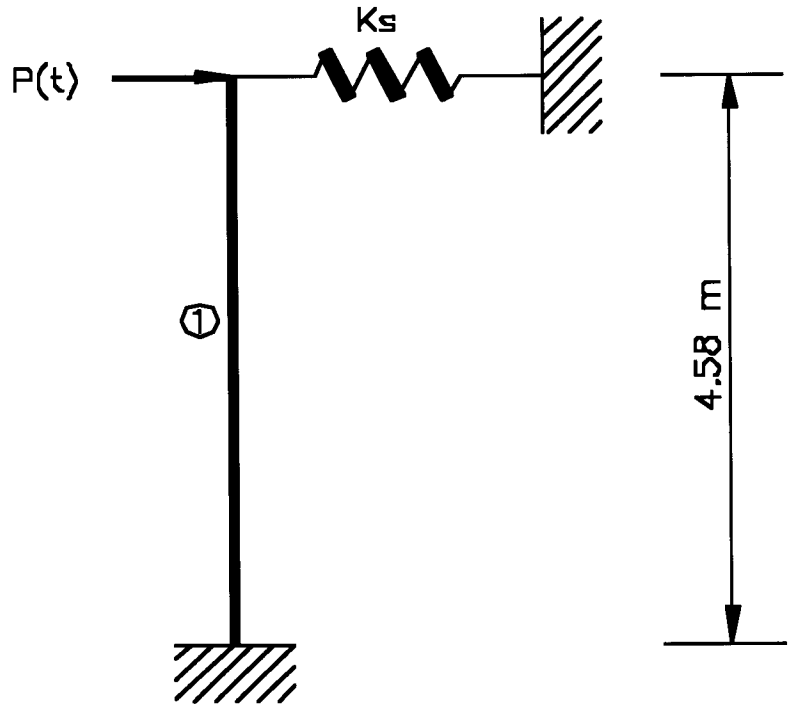

Figure 2.7-14: Structural Model of Single-Column System

Table 2.7-2: Structural Properties of the Column

Young's Modulus (kN/cm^2)	Poisson Ratio	Unit Weight (kN/cm^3)	M_{y0} ($kN-m$)	P_0 (kN)	P_t / P_0	a_1	a_2	a_3
2635	0.18	0.0	207	7174	0.1143	-7.597	-9.933	-1.226

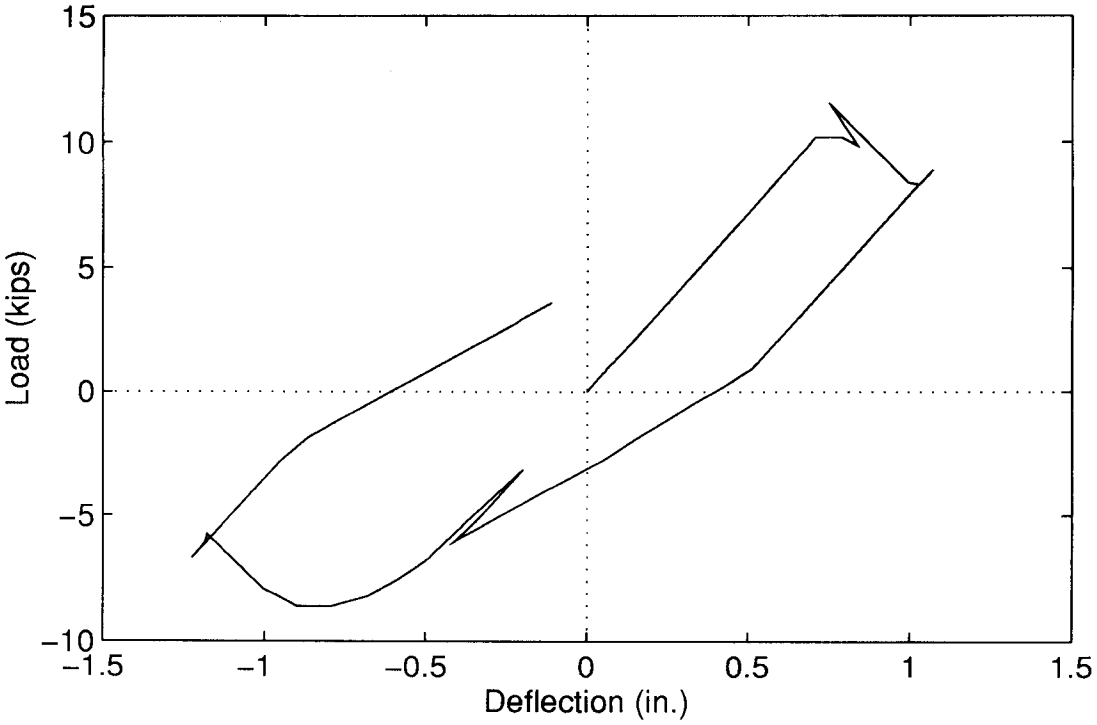

Figure 2.7-15: Load vs Deflection

Figure 2.7-15 shows a computed hysteresis path followed by the structural system. The force in the curve of load vs deflection was the difference between the total lateral load and force in the elastic spring. A degradation of stiffness was observed during the reversed reloading.

Chapter 3

Expansion Joints of Highway Bridges

3.1 Introduction

Most of the bridge failures in the 1971 San Fernando earthquake were caused by the loss of support at their bearing seats and/or expansion joints. Therefore, the retrofit effort in the first phase of retrofitting implemented in California was directed toward tying bridges together at their bearings and expansion joints, through the placement of earthquake restrainers, extension of bearing seats, replacement of bearings, etc. These retrofitting methods for the superstructure are relatively simple and inexpensive compared to other retrofitting methods. For research purposes, only restrainers are discussed in detail in this dissertation.

Generally, when tying the various parts of a bridge together, restrainers are used for the following three different purposes (Buckle and Friedland, 1995):

- Longitudinal joint restraint;
- Transverse bearing restraint;
- Vertical motion restraint.

Figure 3.1-1 shows a typical placement of longitudinal restrainers. The orientation of longitudinal restrainers should be along the principal direction of expected movement. The goal is to limit the relative displacement at joints and thus decrease the chance of a loss of support at these locations. An ideal restrainer should be capable of

resisting appropriate force, resisting movements of bridge segments, dissipating energy, and returning the structure segments to their relative pre-earthquake positions. Thus, restrainers for a joint should be placed symmetrically to minimize eccentric movement. An adequate gap is also necessary to allow the normal in-service movements, such as the opening and closing due to temperature change at expansion joints. The most frequently used materials for longitudinal restrainers are steel cables and bars.

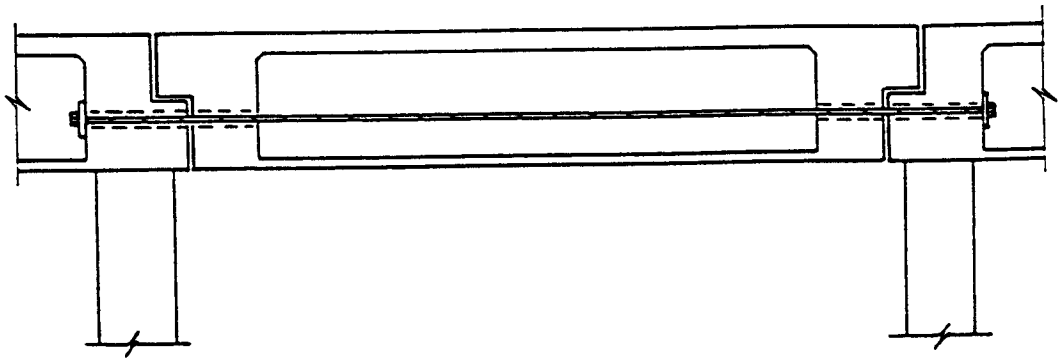

Figure 3.1-1: Longitudinal Restrainer for Retrofitting a Suspended Span (Buckle and Friedland, 1995)

Figure 3.1-2 shows a cross section of an expansion joint with a transverse restrainer to keep the superstructure from sliding off its support if the bearing fails in the transverse direction. This kind of failure occurs easily, especially when high concrete pedestals serve as bearing seats under individual girders, when bearing seats are narrow

and highly skewed, and in two-girder bridges where the transverse distance between the bearing and the edge of the seat is small. One method commonly used as the transverse restraint in concrete structures is to employ a double extra-strong steel pipe filled with concrete that passes through the expansion joint (Buckle and Friedland, 1995).

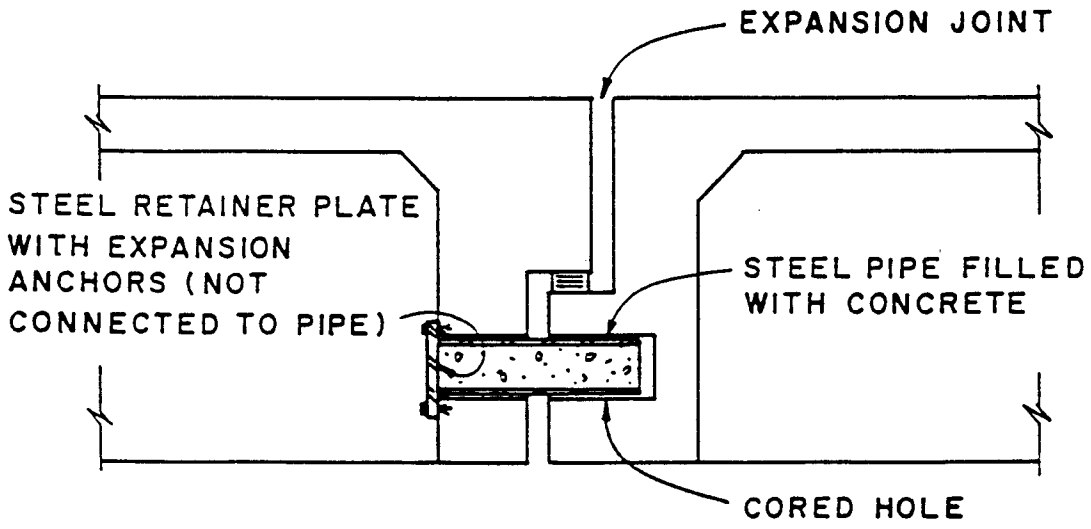

Figure 3.1-2: Transverse Restrainer for an Expansion Joint (Buckle and Friedland, 1995)

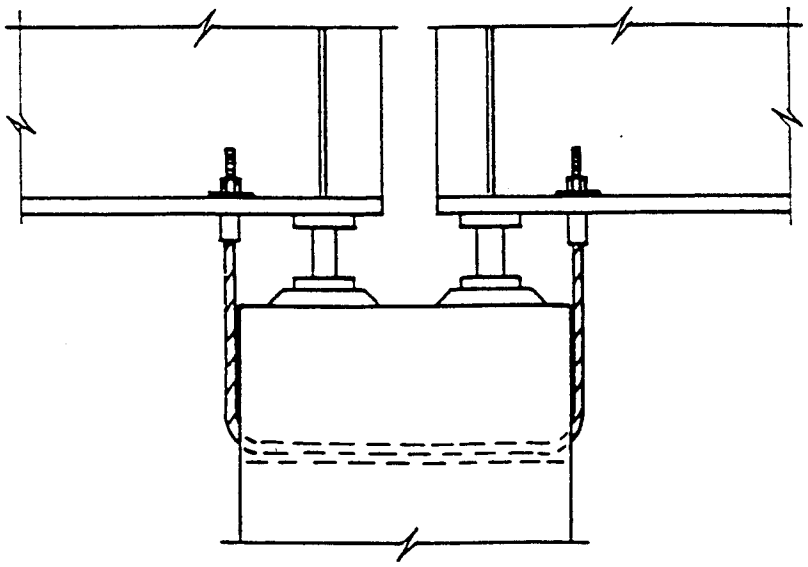

Figure 3.1-3: Expansion Joint with Vertical Motion Restrainer (Buckle and Friedland, 1995)

Although vertical motion is not usually included in a seismic design for bridges, the failure caused by the vertical motion cannot be neglected. Uplift is a type of failure caused by the vertical motion, which can result in damage or loss of stability. Thus if the uplift is an issue in potential earthquakes, vertical hold-down devices (i.e. vertical restrainers) should be considered. An expansion joint with a vertical motion restrainer is shown in Figure 3.1-3.

3.2 Restrainer Design Method

Although the response of expansion joints is highly nonlinear, which will be shown in a later section, an equivalent static analysis for restrainer forces and

deformations is used to design restrainers in order to simplify their design. In the equivalent static analysis, some assumptions and primary features of the design are as follows: (Buckle and Friedland, 1995):

- The mass of one section (i.e. the portion of the superstructure between expansion joints) is used for computing the earthquake force.
- Each section on either side of the joint is used to evaluate the restrainers but, for curved bridges, an extra evaluation of the joint opening from lateral earthquakes will be required. Usually the analysis which requires the fewest number of restrainers will govern the design.
- One end of the restrainer is assumed to be fixed and the other end is assumed to be attached to the superstructure section moving away from the joint.
- The longitudinal stiffness of the adjacent section in addition to the longitudinal stiffness of the section under consideration will be included only when the joint gap is closed. The abutment may be considered as part of the adjacent section when the gap considerations permit.
- Expansion joint gaps without expansion joint filler in the joint are not capable of transmitting any appreciable force until the joint is closed.
- For multiple simple spans, if the bearings are identified as inadequate to transfer the earthquake forces to the substructure, then only the restrainers can be used to determine the longitudinal stiffness of the system. Moreover, the stiffness of the

adjacent section should not be considered when the stiffness of multiple simple span systems is computed.

- The formation of plastic hinge and flexural softening in columns, and the resulting reduction in the stiffness, need to be accounted for.
- Restrainers should be designed to resist the maximum earthquake forces in the elastic range.
- The longitudinal earthquake deflection for both of the sections adjacent to the joint under consideration is determined using the response spectrum method.
- The basis for the design of restrainers is that the deflection capacity of a restrainer does not exceed the available seat width and maximum joint opening.

3.3 Nonlinear Behavior of Expansion Joints During Earthquakes

Studies on expansion joints of highway bridges during dynamic loading conditions show that the components exhibit many sources of nonlinearity in their behavior. Usually, these nonlinearities interact during the dynamic loading of bridges, and the interaction of these nonlinearities is not easily verified by physical testing (Imbsen and Penzien, 1986). To investigate the failure of the 5/14 South Connector Overcrossing, California in the 1971 San Fernando earthquake, a 1/30-scale hybrid model of this bridge was built and tested by Williams and Godden (1976), in which the bridge contained two intermediate expansion joints. Several conclusions were drawn from the tests:

1. The discontinuity caused by the presence of the expansion joints had a great influence on the overall dynamic response of the bridge.
2. The impacting between decks, sliding friction between decks, or decks and bent caps, and yielding of earthquake restrainers were primary reasons for the expansion joints exhibiting the nonlinear behavior.
3. The earthquake cable restrainers which were capable of resisting tension only also exhibited nonlinear behavior.

3.4 Expansion Joint Element

Because of the complication of modeling the expansion joint and the limited amount of physical test results, it is difficult to model the expansion joint behavior accurately. In this research, an expansion joint element provided by NEABS that was initially developed to investigate the main features of the expansion joint was used. The element included impact forces, tie bars, bearing pads, and a shear key. A typical expansion joint is shown in Figure 3.4-1 (Tseng and Penzien, 1973).

To model the expansion joint, as shown in Figure 3.4-1, with all the features previously described, the expansion joint element is divided into several subelements. The detailing that comprises the element is shown in Figure 3.4-2. The element has two nodes, I and J, and the distance between I and J is assumed to be infinitesimally small. The main features, such as impact force and the effects of longitudinal restrainers, bearing pads, and a shear key, are represented by the subelement properties, as shown in Figure 3.4-2.

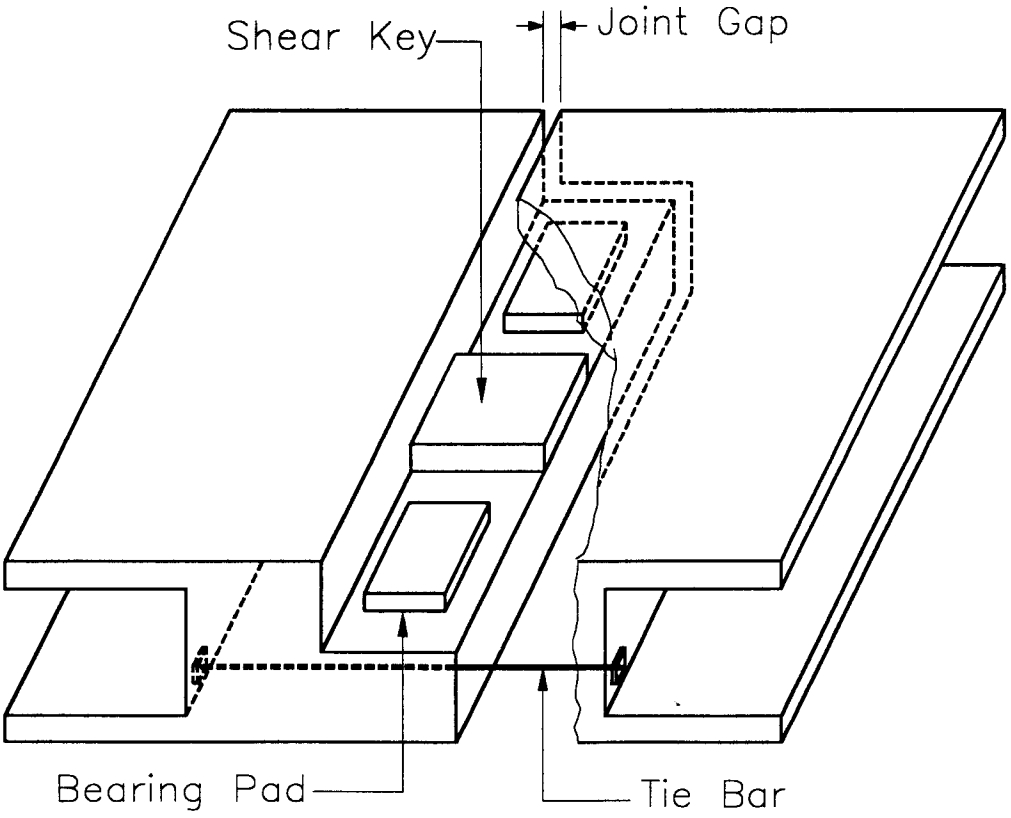

Figure 3.4-1: A Typical Bridge expansion Joint

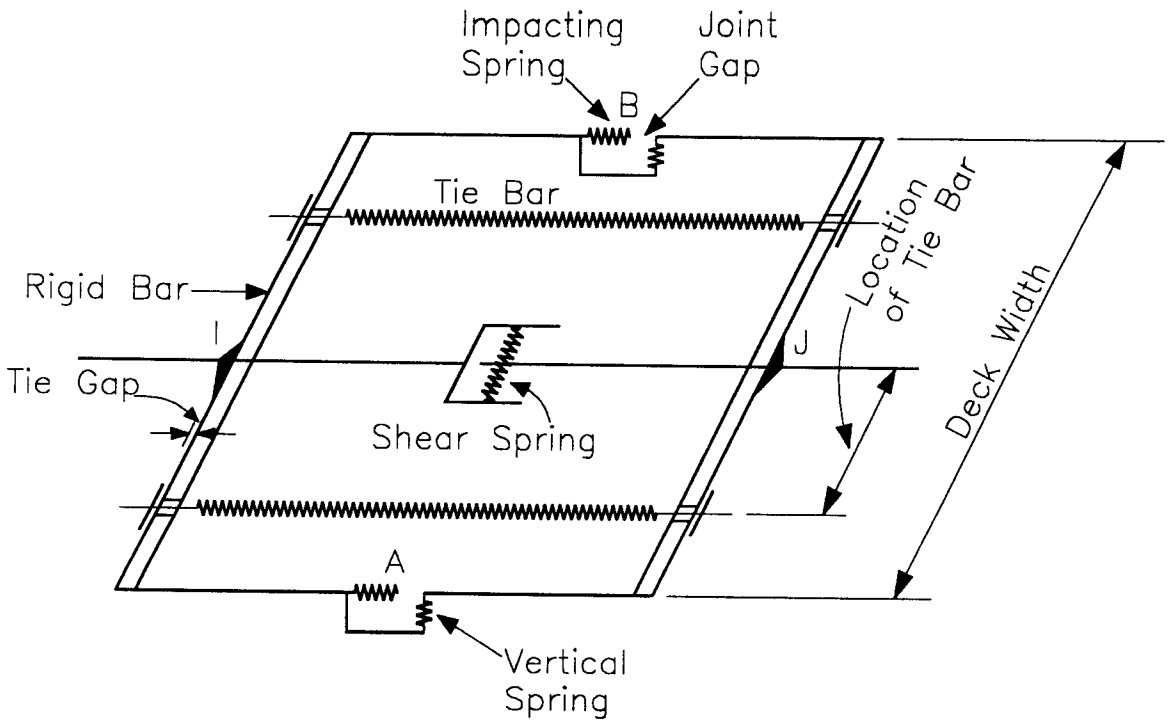

Figure 3.4-2: An Idealized Expansion Joint Element

3.4.1 Basic Assumptions

Since extensive difficulties exist in idealizing mathematically the nonlinear expansion joint, many assumptions were made in deriving the numerical model. They included (Tseng and Penzien, 1973):

1. The end diaphragms of the deck in the transverse or skewed direction along the centerline of bearing of the hinge seat at each expansion joint are assumed to be rigid.
2. Contact within the expansion joint can develop at only two points, A and B, located at the ends of the rigid diaphragms (Figure 3.4-2).

3. The impact upon closure of the gap is imitated by two longitudinally gapped linear compressive springs that are attached to points A and B individually.
4. The two joints are free to rotate relative to one another in a direction oriented along the skew (i.e., parallel to the rigid link) unless a linear spring is superimposed on the joint to resist it.
5. Relative slippage between the two diaphragms in the longitudinal direction at points A and B is modeled by Coulomb friction.
6. The shear which controls relative transverse motions of the two rigid diaphragms is modeled by a shear spring aligned perpendicular to the direction of the centerline of the bridge deck.
7. The bearing pad is modeled as a vertical spring connecting the two rigid links to each other at points A and B.
8. Longitudinal restrainer ties may be placed through the two rigid diaphragms in the longitudinal centerline direction of the deck with tie gaps at one end of each bar.
9. Linear springs may be superimposed on each one of the nonlinear springs as necessary.

3.4.2 Parameter Explanation

The expansion joint is characterized by a number of sources of nonlinear behavior. Therefore, an extensive discussion on the components that cause this nonlinear behavior is relatively important to define reasonable parameters in the dynamic analysis of highway bridges with expansion joints.

3.4.2.1 Sliding Friction

The contact between two neighboring superstructure sections, or a superstructure section and a substructure member that supports the superstructure section, will produce friction resistance at sliding surfaces. Sometimes, to keep the superstructure from sliding off its supports, bearing pads are placed between superstructure sections, or superstructure section and a substructure member, as shown in Figure 3.4-3.

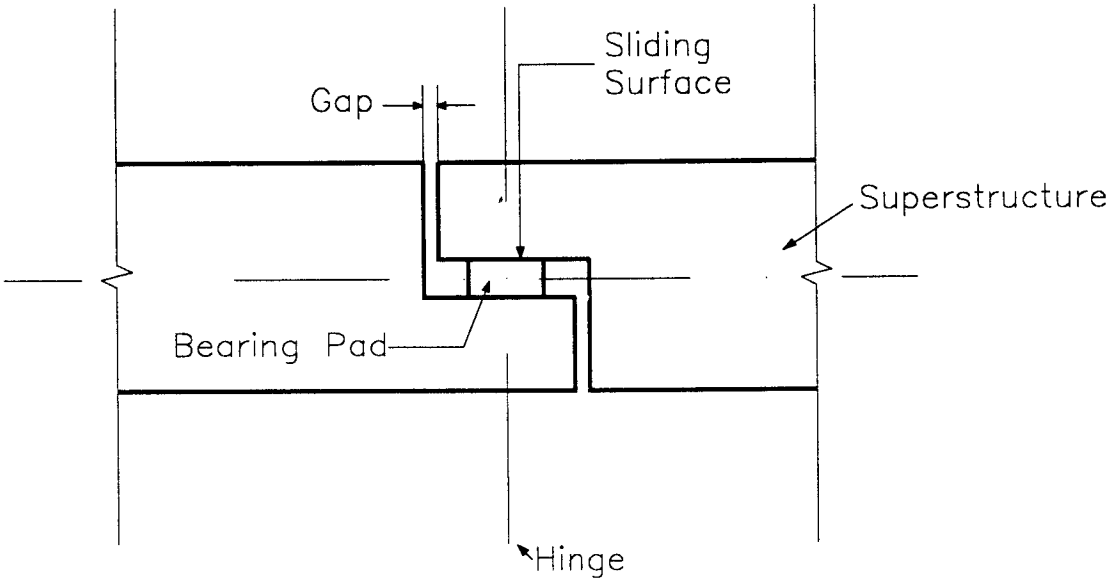

Figure 3.4-3: Expansion Joint with Bearing Pad

In NEABS, the bearings are idealized as bearing subelements and they are assumed to be concentrated at points A and B only (Figure 3.4-2). The bearing subelements provide the interface through which vertical gravity forces are transmitted. The bearing subelement is deformed, as shown in Figure 3.4-4, until the Coulomb friction is exceeded. Then, relative slippage between the two diaphragms takes place. The elastic

deformation is calculated in NEABS by defining the friction stiffness of the bearing. Coulomb friction is obtained by multiplying the coefficient of friction and the respective vertical contact forces between the two diaphragms. It is also assumed in NEABS that the dead load reaction will exceed the uplift earthquake forces.

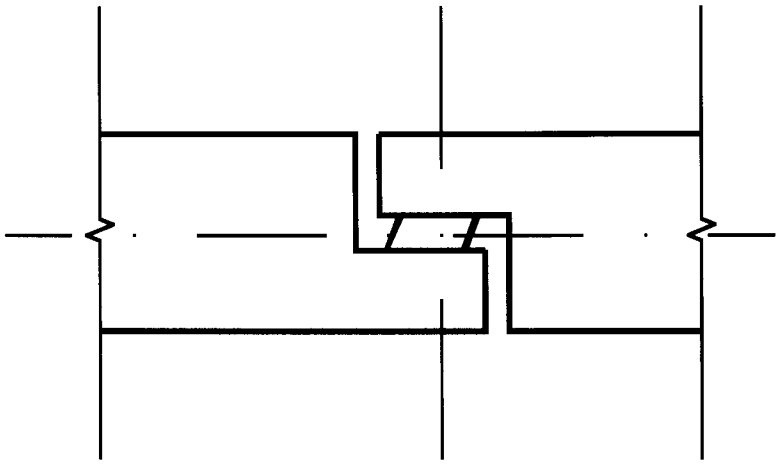

Figure 3.4-4: Elastic Deformation for the Bearing Subelement

3.4.2.2 Impacting Effect

Longitudinal impact starts when the relative displacements of the two diaphragms close the gap. The impacting effect on the structural response of bridges is considerable when a major earthquake takes place. The effect is imitated by two impacting springs in NEABS, located at points A and B (Figure 3.4-2). It is assumed that the impact spring is activated only when the gap is closed. That means that when the gap is open, the impact spring will not contribute any resistance. The function of this spring may be explained by

Figure 3.4-5. One should note that the impact spring usually is very rigid when the gap is closed. The magnitude of the stiffness of the impact spring may be related to the quantity of axial stiffness of the bridge deck.

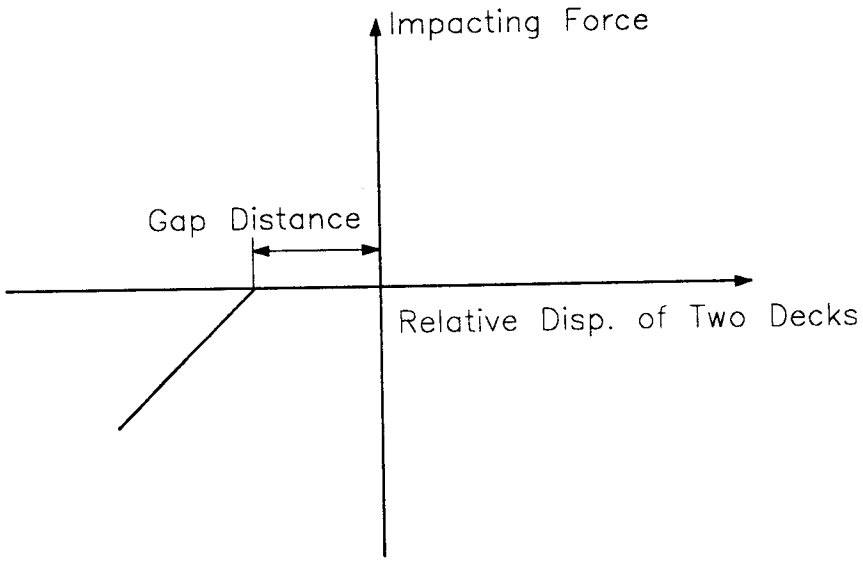

Figure 3.4-5: Force vs Displacement Relationship of the Impact Spring

3.4.2.3 Tie Bars

Steel bars and cables are two types of restrainer materials that are most often used. Here, the steel bars and cable are called tie bars in accordance with NEABS. Usually, the tie bars are connected to the decks and aligned perpendicular to the end diaphragms of the deck, as shown in Figure 3.4-1. To model the tie bars, a tie bar subelement was developed in NEABS. The tie bar is allowed to have a gap in order to let the superstructure section move freely due to temperature and shrinkage so that no stresses are produced in the tie bars. Contrary to the impact spring, the tie bar element is a

tensile spring without compressive stiffness. That means that the tie bar shows resistance only when the two end diaphragms of the deck are open and the opening is larger than the tie bar gap.The force-displacement relationship of the tie bar is assumed to be bilinear. After the yield force is reached, perfectly plastic behavior is assumed. Figure 3.4-6 gives the force-displacement relationship of the tie bar.

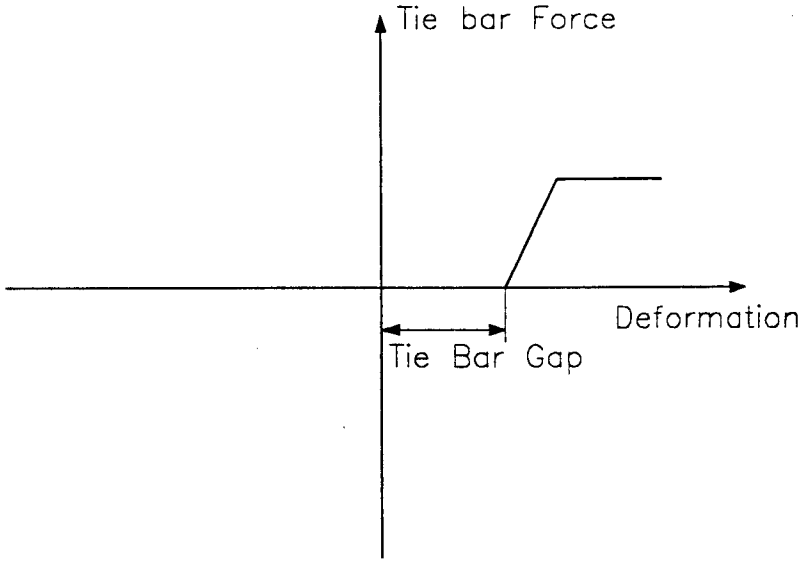

Figure 3.4-6: Force vs Displacement Relationship of the Tie Bar

Chapter 4

Analytical Assessment of Ductility and Strength for Bridge Members

4.1 Introduction

Bridges designed in accordance with pre-1971 codes have shown insufficient ductility and strength to resist earthquakes. As a result, the emphasis in new design criteria is placed on increasing ductility and avoiding strength degradation of various bridge components. The current design philosophy is to allow bridges to have an acceptable level of damage in a major earthquake because the construction cost of fully elastic bridges is too high to be feasible. Thus, the ductile behavior of bridge members after an acceptable failure is very important to ensure that the bridge will survive major earthquakes and be repairable after moderate earthquakes. Therefore, an effective and accurate evaluation of section ductility and strength degradation can provide retrofitting suggestions to engineers for ensuring bridge serviceability even though the current design provisions do not require these calculations. In this chapter, a review of the evaluation of column ductility and flexural strength capacity is conducted.

4.2 Flexural Ductility

For the seismic design of bridges, the most basic aspect is to ensure that the structural capacity exceeds the structural demand. The structural capacity is the available structural capacity for a particular structure and may be determined either experimentally

or analytically. The structural demand is expressed as the structural requirement for a particular earthquake. The strength-based measures (axial, shear, moment, etc.) for demand and capacity have been used for many years and are well defined. The measures are used to calculate the demand from linear analysis and capacity from code equations. However, research has shown that the strength measures are rational only for moderate earthquakes, for which essentially elastic behavior is expected. For strong earthquakes, substantial inelastic and nonlinear behavior is allowed, and safety should be ensured not by providing strength, but by providing ductility. Hence, deformation-based measures for demand and capacity have been proposed and used in the nonlinear dynamic analysis of bridges (Powell, 1994). A widely accepted deformation-based measure is flexural ductility.

(a) (b)

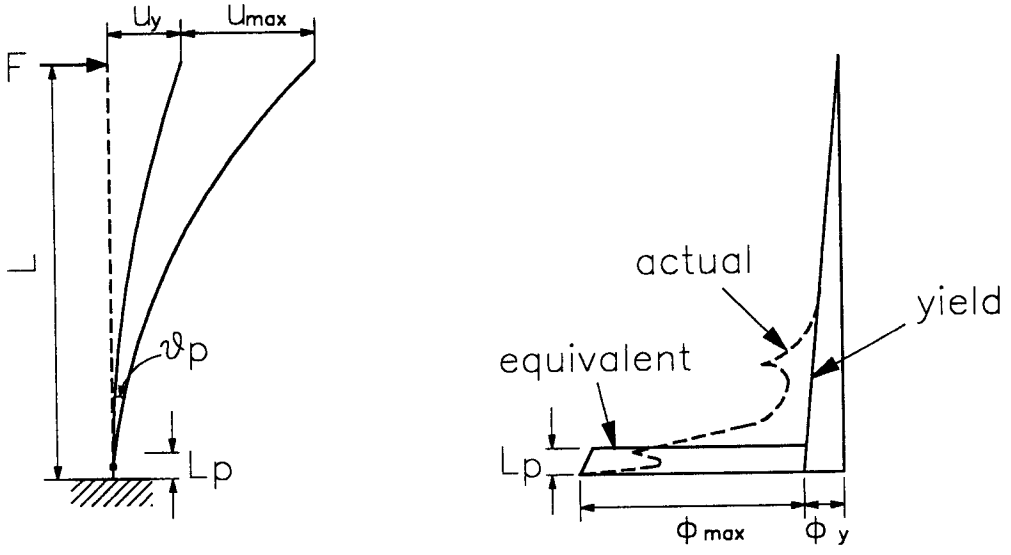

Figure 4.2-1: The Deflection and Curvature of a Simple Cantilever :(a) Deflection; (b) Curvature

Usually, both the curvature ductility factor and the displacement ductility factor may be expressed as the flexural ductility factor (deformation-based) of a bridge member. For instance, for a simple cantilever element supported on a rigid foundation, as shown in Figure 4.2-1a, the curvature ductility factor and the displacement ductility factor can be expressed as:

$$\mu_{\phi} = \frac{\phi_{max}}{\phi_y} \quad \text{.....(4.2.1)}$$

$$\mu_{\Delta} = \frac{u_{max}}{u_y} \quad \text{.....(4.2-2)}$$

where

μ_{ϕ}= the curvature ductility;

μ_{Δ} = the displacement ductility;

ϕ_{max}= the maximum curvature at the bottom resulting from an earthquake-induced support motion;

ϕ_y= the yield curvature at the bottom;

u_{max}= the maximum horizontal displacement at the top resulting from an earthquake-induced support motion;

u_y= the yield displacement.

A relationship between the curvature and displacement ductility factors can be developed for a cantilever. The displacement at the top when the column yields at the base is:

$$u_y = \frac{M_y l^2}{3EI} \quad \text{.....(4.2-3)}$$

where M_y is the column yield moment, EI is the flexural rigidity of the cantilever, and l is the length of the column.

The yield curvature at the column base is $\phi_y = M_y / EI$, thus equation (4.2-3) can be rewritten as:

$$u_y = \frac{\phi_y l^2}{3} \quad \text{.....(4.2-4)}$$

It should be noted that the dashed line in Figure 4.2-1b represents realistic curvatures, and the solid line represents idealized curvatures in which the nonlinear curvature that is caused by the plastic hinge is assumed to be concentrated within the equivalent plastic hinge length l_p and is constant over the length. Thus the plastic rotation may be expressed in terms of the curvature as:

$$\theta_p = (\phi_{max} - \phi_y) l_p \quad \text{.....(4.2-5)}$$

Further assuming that the plastic rotation occurs at the center of the plastic hinge, the plastic displacement resulting from the plastic rotation and the total displacement at the top are:

$$u_p = \theta_p \left(l - \frac{l_p}{2} \right) \quad \text{.....(4.2-6)}$$

$$u_{max} = u_y + u_p = \frac{\phi_y l^2}{3} + \theta_p \left(l - \frac{l_p}{2} \right) \quad \text{.....(4.2-7)}$$

Combining equations (4.2-1), (4.2-2), (4.2-4), (4.2-5), and (4.2-7), a relationship between the displacement ductility factor and curvature ductility factor can be given by:

$$\mu_\Delta = 1 + 3(\mu_\phi - 1)\frac{l_p}{l}\left(1 - 0.5\frac{l_p}{l}\right) \quad \text{.....(4.2-8)}$$

or, conversely:

$$\mu_\phi = 1 + \frac{(\mu_\Delta - 1)}{3\frac{l_p}{l}\left(1 - 0.5\frac{l_p}{l}\right)} \quad \text{.....(4.2-9)}$$

Usually, the plastic hinge length l_p is taken as half the depth of the member. However, recent research by Chai, Priestley, and Seible (1991) suggests the following equation in order to obtain l_p.

$$l_p = 0.08l + \chi d_b \quad \text{.....(4.2-10)}$$

where

l = length from the critical section to the point of contraflexure. For instance it is equal to the member length for the simple cantilever, as shown in Figure 4.2-1a;

d_b= nominal diameter of the longitudinal reinforcement used in the member;

χ= 6 for grade 40 longitudinal reinforcement;

= 9 for grade 60 longitudinal reinforcement.

For a structure as shown in Figure 4.2-2, the stiffness of the top mass is very large such that the rotation at the top is restrained. A contraflexural point will occur in the

middle of the column. In this case, all of the above derived formulas may be used by substituting the half length of the column into the equations.

Usually, the curvature can not be directly obtained in a nonlinear dynamic analysis of the bridge. Tseng and Penzien (1973) used the calculated plastic rotations θ_p from nonlinear analysis and the estimates of the yield rotations θ_y to compute the realistic ductility that is called rotational ductility. The expression is as follows:

$$\mu_\theta = \frac{\theta_{max}}{\theta_y} = \frac{\theta_y + \theta_p}{\theta_p} \quad \text{.....(4.2-11)}$$

where

$$\theta_y = l_p \phi_y = \frac{l_p M_y}{EI} \quad \text{.....(4.2-12)}$$

Equation (4.2-12) is a little bit different compared to that used by Tseng and Penzien, as they simply used member depth as the length of the plastic hinge.

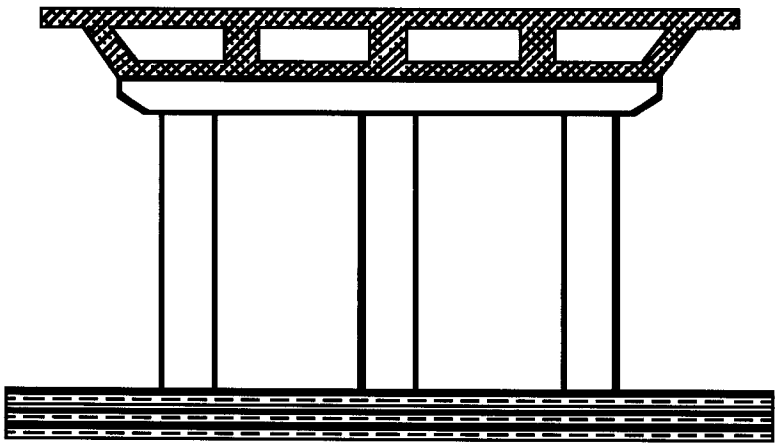

Figure 4.2-2: Multi-Column Bent with Rigid Superstructure

In design codes, the available ductility (capacity) factors are reflected in the response modification factor, R. When designing a bridge, an elastic earthquake response force is first computed. Then, the force for design purposes is obtained by reducing the elastic earthquake response force by the response modification factor. That is:

$$F_u = \frac{F_{eq,el}}{R} \quad \text{.....(4.2-13)}$$

where $F_{eq,el}$ is the elastic earthquake response force when the structure remains elastic, and F_u is the force for design purposes. The design purpose force will allow the structure to develop inelastic and nonlinear behavior. For the NEHRP (1991) provisions, the design force is based on a first significant yield force level. However, UBC (1991) provisions are based on service loads.

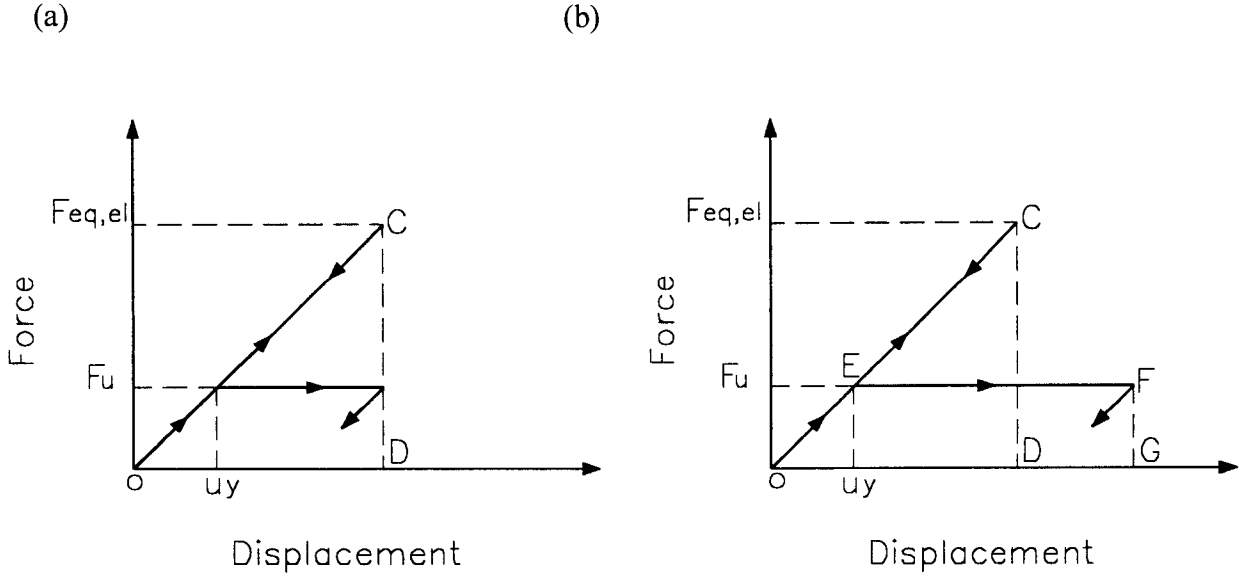

Figure 4.2-3: Assumed Seismic Responses of half Elastic and Elasto-Plastic Structural Systems Subjected to Earthquake Motions: (a) Equal Maximum Displacement Response; (b) Equal Maximum Potential Energy (Imbsen and Penzien, 1986)

A relationship between the displacement ductility factor and the modification factor can be derived by applying the concepts of "equal maximum displacement" and "equal maximum potential energy." When structures respond with a predominantly medium to long period (i.e. $T \geq 0.5$ sec.), the factor may be determined using the concept of "equal maximum displacement," as shown in Figure 4.2-3a, in which the practical maximum displacement of the structure is considered to be equal to the maximum displacement when the structure remains elastic. Thus,

$$\boldsymbol{R = \mu_{\Delta}} \quad \textbf{(4.2-14)}$$

For structures responding with a predominantly short to medium periods (i.e.,T <0.5 sec.), the factor is calculated by using the "equal maximum potential energy," as shown in Figure 4.2-3b, in which the elastic strain energy (i.e., area OACE) and the practical elasto-plastic energy (i.e., area OABD) are equal. That is,

$$E_0 = E_m$$

Thus,

$$\frac{1}{2}ku_0^2 = \frac{1}{2}ku_y^2 + ku_y(\mu_{\Delta} - 1)u_y$$

Using the above equation, one gets,

$$\frac{u_y}{u_0} = \frac{1}{\sqrt{2\mu_{\Delta} - 1}}$$

Thus,

$$\boldsymbol{R = \frac{F_{eq,el}}{F_u} = \frac{u_0}{u_y} = \frac{1}{\sqrt{2\mu_{\Delta} - 1}}} \quad \textbf{(4.2-15)}$$

4.3 Flexural Strength

Based on the experimental work done by Priestley, Seible, and Chai (1992), four models, as shown in Figure 4.3-1, were proposed to represent the strength and ductility of different plastic hinge conditions for column members. The line (1) represents columns that have a comparatively well confined section, in which the nominal moment capacity, M_n, will be reached at $\mu_\Delta = 1$, and then strain-hardening of flexural reinforcement and confinement effects will occur so that the moment reaches an overstrength moment capacity, M_0, that can be attained by moment-curvature analysis. This model is a typical representation of the relationship between strength and ductility for columns with sufficient confinement or retrofitting, i.e., steel jacketing, etc.

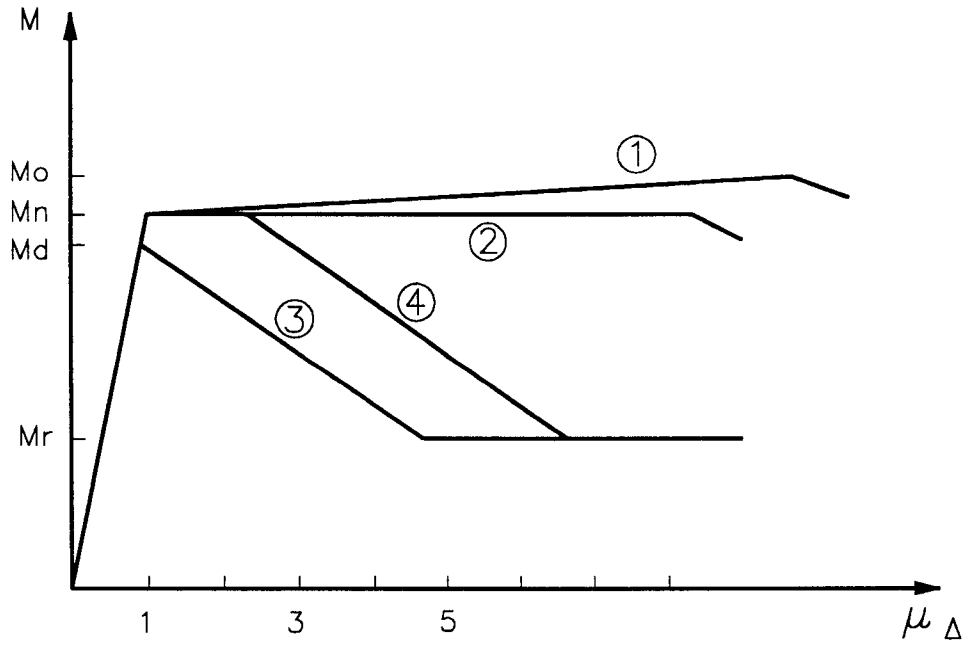

Figure 4.3-1: Flexural Strength and Ductility of Sections (Priestley and Seible 1994)

Line (2) represents a poorly confined column without lap splices in the plastic hinge region, for which the maximum strength is typically equal to the nominal strength. This model is suitable for the columns designed by pre-1971 design codes. Strength degradation will occur if the limit for line (1) or line (2) is reached due to crushing of core concrete and buckling of longitudinal reinforcement.

Line (3) represents degradation of a column with lap splices and poor confinement in the plastic hinge region, in which the nominal moment capacity will not be achieved. The strength starts degrading before $\mu_\Delta = 1$ to a residual flexural strength, M_r, based on the axial load. The cause of the degradation is that the longitudinal bar in the lap splice region can not develop its yield force before rupture.

Line (4) represents degradation of a column with partially confined lap splices, in which the nominal moment capacity M_n can be reached and then a relatively small plastic plateau can be achieved before degradation begins. The degradation occurs when the extreme fiber compression strain ε_c is 0.002. This model indicates that the longitudinal bar in the lap splice region can develop its yield force before the rupture surface fails. The line degrades to M_r, parallel to line (3).

Both lines (3) and (4) show the typical flexural strength and ductility of column sections designed prior to 1971, in which the lap splices were in the range of 20 to 35 longitudinal bar diameters, and confinement reinforcement was inadequate, typically No. 4 reinforcement on 12 in. centers. Columns that are represented by lines (1) and (2) are easily specified. However, computation to identify the columns represented by lines (3)

or (4) is required. At the same time, the evaluation of the reduced maximum flexural strength M_s and the flexural residual strength M_r is also required for nonlinear earthquake analysis. The following is a review of the identification and strength calculation procedures.

Figure 4.3-2 shows two typical "as-built" circular and rectangular bridge columns designed by pre-1971 design codes, and the failure mechanism at the lap splice region. Generally, vertical cracks parallel to the column bars develop first. Then, with the development of these cracks, the second crack surface inside the column bars and parallel to the plane of reinforcement is produced to facilitate the lateral dilation implied by the vertical cracks. According to the failure mechanism, the strength of the lap splices may be determined by postulating the full pattern of cracking that must develop to enable each bar to slide relative to the adjacent bars with which they are lapped. The tensile strength necessary to fracture this surface may be assumed to be equal to the direct concrete tension strength, i.e.,

$$f_t = 4\sqrt{f_c'}\ psi \quad \text{.....(4.3-1)}$$

For a column, the total tensile force on the rupture surface at failure will be:

(1) Circular Column

$$T_b = f_t\left[\frac{\pi D'}{2n} + 2(d_b + c)\right]l_s \quad \text{.....(4.3-2)}$$

where

n= number of vertical bars;

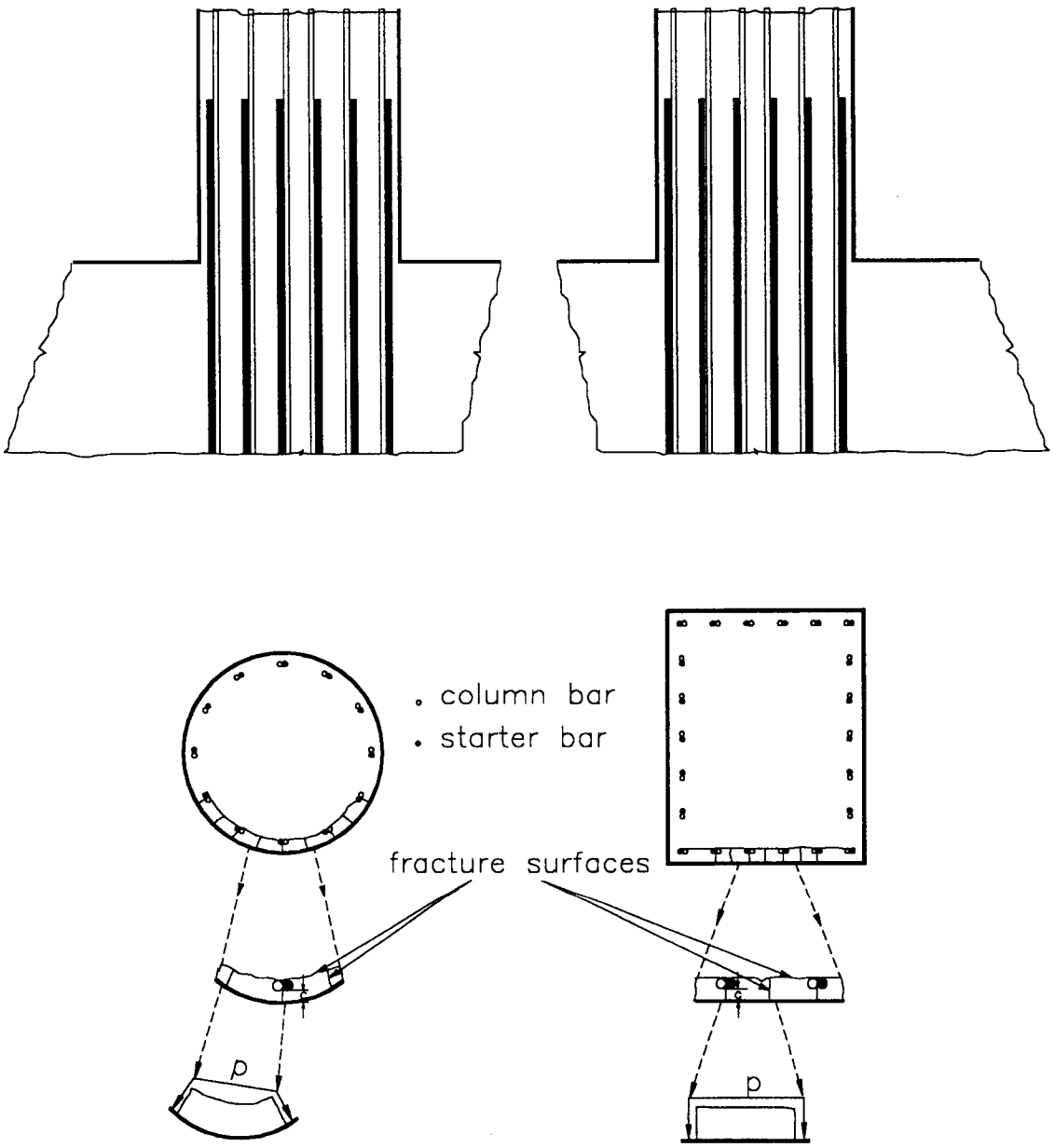

Figure 4.3-2: Lap Splices in Columns and Failure Mechanism (Priestley and Seible 1994)

c= bar cover;

d_b= bar diameter;

D'= bar pitch circle diameter;

l_s= splice length.

(2) Rectangular Column

$$T_b = f_t p l_s \quad \text{.....(4.3-3)}$$

where

p= perimeter of the crack surface.

Theoretically, $A_b f_y$ is the maximum force that can be developed in the column bar. However, this force is often not attained in columns designed prior to 1971 with poor confinement.

If $T_b \langle A_b f_y$, it implies that a bond failure will occur before the nominal flexural strength M_n is reached. After the reduced maximum flexural strength M_s is reached, a rapid degradation will occur. Hence line (3) represents this case. The value of M_s may be calculated using the reduced effective yield stress of $f_s = T_b / A_b$ in the moment-curvature analysis.

Because of the axial compression force on the column, the flexural strength represented by line (3) can be degraded to a residual flexural strength M_r with no contribution from reinforcement. Based on experimental evidence, a reduced effective section after bond failure may be used to calculate the residual strength. As shown in

Figure 4.3-3 for rectangular and circular sections, the reduced section area is taken as the inside of the layer of longitudinal reinforcement. It is assumed that only an equivalent stress block with a depth of a on the top of the reduced effective section carries the axial force, and that the concrete stress of $0.85f_c^{'}$ is uniformly distributed over the equivalent compression zone. Thus, the residual moment capacity based on axial load will be:

(1) Rectangular Column

$$M_r = P\left(\frac{h^{'}}{2} - \frac{a}{2}\right) \quad \text{.....(4.3-4)}$$

where

$a = P/0.85f_c^{'}b^{'}$ is the depth of the equivalent rectangular stress block; and

P =axial load.

(2) Circular Column

$$M_r = P\left(\frac{D^{'}}{2} - x\right) \quad \text{.....(4.3-5)}$$

where x is the centroid of the curved compression zone. The calculation to obtain x is straightforward through the area of the equivalent compression zone and diameter $D^{'}$.

If $T_b \rangle A_b f_y$, it indicates that the longitudinal bars can develop their yield force and initial ideal flexural strength may be achieved. As compression strains adjacent to the

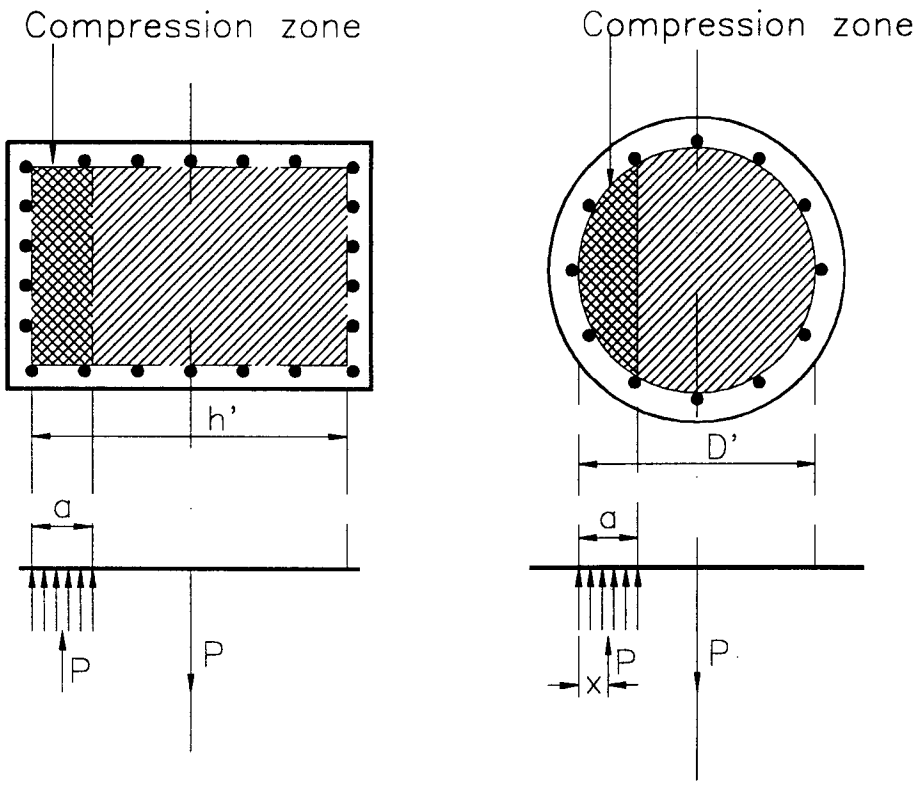

Figure 4.3-3: Residual Moment Capacity of Columns After Lap Splice Failure (Priestley and Seible 1994)

compression reinforcement approach 0.002, extensive longitudinal microcracking will develop. This will clearly degrade the effective tension strength, f_t, in equation (4.3-2) or (4.3-3) on reversal of the direction of seismic response, reducing T_b, and causing bond failure unless sufficient confinement and length of lap l_s are designed. Hence, only a small amount of ductility is achieved before the flexural degradation starts. In this case, the relationship of flexural strength and ductility will be described by line (4). The residual moment capacity may be obtained by using (4.3-4) or (4.3-5).

The method to avoid bond failure is to provide adequate confinement or retrofit measures such as steel jacketing so that the cracks shown in Figure 4.3-2 can be sustained. Because the confinement or retrofit measures provide a clamping pressure across the cracks, the frictional resistance across the crack is sufficient to develop the longitudinal

bar strength. It was found at the University of California, San Diego (Buckle and Friedland, 1995) through tests on various confinement systems that the dilation strain of $\varepsilon_d = 0.001$ of concrete is a limit that can prevent the bond slip. The following suggests an effective lateral pressure for a lap splice with passive confinement:

$$f_l = 0.0005 E_s \rho_s \quad \text{.....(4.3-6)}$$

where E_s is the modulus of elasticity of the confinement and ρ_s is its volumetric ratio. For instance, for a circular column with transverse hoops or spirals of cross-sectional area, A_b, at spacing, s, and $E_s = 200 GPa\,(29{,}000 ksi)$, the effective lateral pressure is:

$$f_l = 0.0005 \times 200 \times 1000 \times \frac{\pi D' A_b}{\frac{1}{4}\pi (D')^2 s} = \frac{400 A_b}{D's}(MPa) = \frac{58 A_b}{D's}(ksi) \quad \text{.....(4.3-7)}$$

The tests also support a friction coefficient of 1.4 across the fractured surface. Thus, the maximum bar force that can be transferred by friction is:

$$T_b = 1.4 f_l p l_s \quad \text{.....(4.3-8)}$$

For example, for a circular column the force should be:

$$T_b = 1.4 f_l \left[\frac{\pi D'}{2n} + 2(d_b + c) \right] l_s \quad \text{.....(4.3-9)}$$

To develop a high value of ductility without bond failure, the limit is:

$$T_b \geq A_b f_u \approx 1.5 A_b f_y \quad \text{.....(4.3-10)}$$

where f_u is ultimate strength of reinforcement.

Although adequate confinement is necessary to ensure that the plastic zone develops high ductility without bond failure, it is not sufficient. The length of lap splices

must exceed a minimum value. Otherwise, bond failure will occur regardless of the confining stress provided by transverse reinforcement. This type of failure is due to the shearing off of a cylinder of concrete of a diameter slightly larger than that of the longitudinal reinforcing steel rather than the mechanism shown in Figure 4.3-2. It was shown by tests (Buckle and Friedland, 1995) that the effective bond stress corresponding to this failure may be taken as:

$$\sigma_u = 1.5\sqrt{f_c'}\,(MPa) = 18\sqrt{f_c'}\,(psi) \quad \text{(4.3-11)}$$

Assuming that the diameter of a cylinder of concrete that will shear off due to the bond failure is approximately equal to the diameter of the longitudinal bar, the total tensile force on the failure surface is:

$$T_b = \pi d_b l_s \sigma_u = 1.5\pi d_b l_s \sqrt{f_c'}\,(kN) = 18\pi d_b l_s \sqrt{f_c'}\,(lb) \quad \text{(4.3-12)}$$

To ensure no "shearing off" bond failure, it must be:

$$T_b \geq A_b f_u = 1.5 A_b f_y = 0.375\pi {d_b}^2 f_y \quad \text{(4.3-13)}$$

Substituting equations (4.3-12) into (4.3-13), one should obtain:

$$l_s \geq \frac{0.25 d_b f_y}{\sqrt{f_c'}}(\,MPa \text{ units}) \approx \frac{0.021 d_b f_y}{\sqrt{f_c'}}(\,psi \text{ units})$$

Thus,

$$l_{s_{\min}} = \frac{0.25 d_b f_y}{\sqrt{f_c'}}(MPa \text{ units}) \approx \frac{0.021 d_b f_y}{\sqrt{f_c'}}(psi \text{ units}) \quad \text{(4.3-14)}$$

where $l_{s_{\min}}$ is the minimum value of length of lap splice to avoid "shearing off" bond failure.

Chapter 5

Seismic Analysis of Bridges with Column Retrofitting

5.1 Moses Lake Bridge (Two-Dimensional Analysis)

To investigate the effects of column retrofitting, a simple two-column bent from a bridge with three spans was analyzed by static and dynamic methods. The emphasis was placed on the investigation of different retrofitting combinations for the columns. The objective was to obtain a basic understanding of current retrofit strategies, where only a few of the substructure elements are retrofitted, could be obtained through a comparison of the dynamic responses.

5.1.1 Introduction

The bridge shown in Figure 5.1 -1 was located on Interstate 90, about 20.9 km east of Moses Lake in Washington State. It was one of a pair of reinforced concrete bridges that were constructed in 1966. To study the deficiencies of pre-1971 designed bridges, including minimal transverse reinforcement, short reinforcing splices, and a lack of top reinforcement in the footing, the bridge was chosen as the subject of a Washington State Department of Transportation (WSDOT) research project. Eberhard, *et al.* (1993) studied the response of the bridge when transverse loads were applied to one of its bents. They conducted a series of in-situ destructive tests and analytical evaluations of the bridge, and concluded that the bridge bents, in spite of their

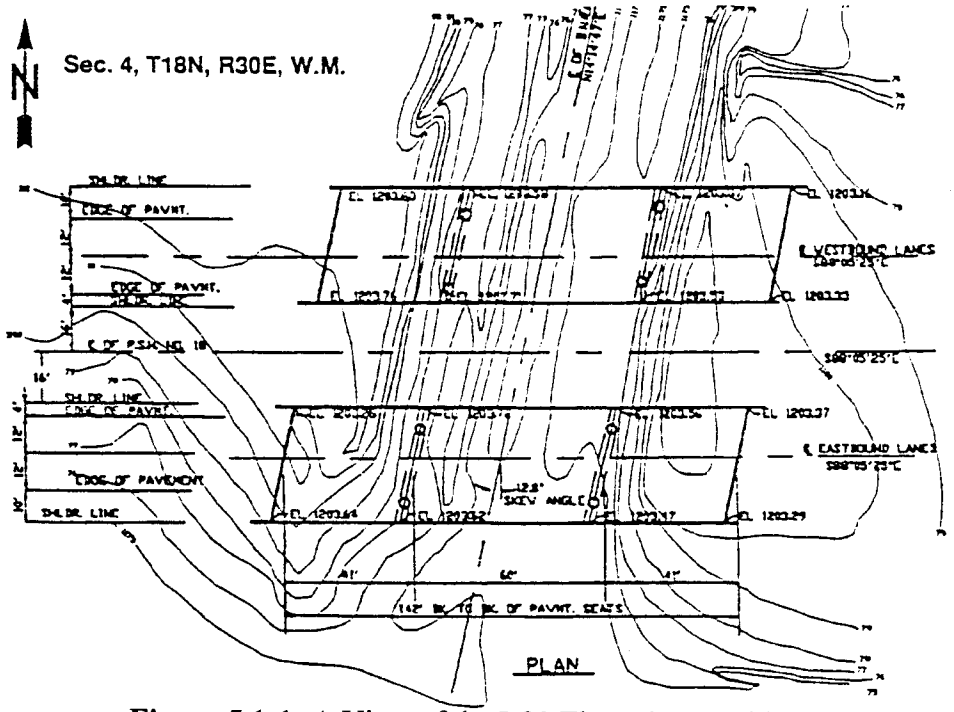

Figure 5.1-1: A View of the I-90 Three-Span Bridge

deficiencies, were capable of resisting significant lateral loads equal to nearly 40% of the bridge's weight at a drift ratio of 3%. The relatively high value of the lateral strength was attributed to the bridge's high stiffness because of its continuous superstructure and stiff abutments. In 1994, Cofer, *et al*, again used the bridge for studying dynamic interaction of a structure and its foundation. In their research, four foundation models that represent the effect of soil-structure interaction were employed to evaluate the structural response of a bridge having spread footings.

In this study, a bent from the bridge was analyzed to assess the benefits from applying different column retrofitting combinations. First, a quasi-static pushover analysis was conducted, in which a static, monotonic loading condition was applied to the bent. Then, a dynamic time-history analysis was performed. The earthquake record in this analysis was that of the 1940 El-Centro earthquake. Finally, conclusions were drawn from the two analyses.

5.1.2 Description of the Bridge and Site

Figure 5.1-2 depicts the plan and elevation of the bridge. The three-span bridge was 43.3 m long. The abutments and the bents that supported a center span of 18.3 m and two end spans of 12.5 m were skewed by 12.8°. The reinforced concrete deck which provided the main lateral stiffness of the superstructure was continuous over the two bents with dimensions of 12.2 m in width and 16.5 cm in thickness. The deck was supported by six 106.7 cm deep prestressed concrete I-girders (Figure 5.1-1) with a spacing of 208.3cm on center. These prestressed girders extended 5.08 cm into the 30.5

cm thick diaphragms at the bents and cast-in-place abutments. These diaphragms were heavily reinforced and cast monolithically with the slab and connected to the underlying bent crossbeam with No. 10 dowels.

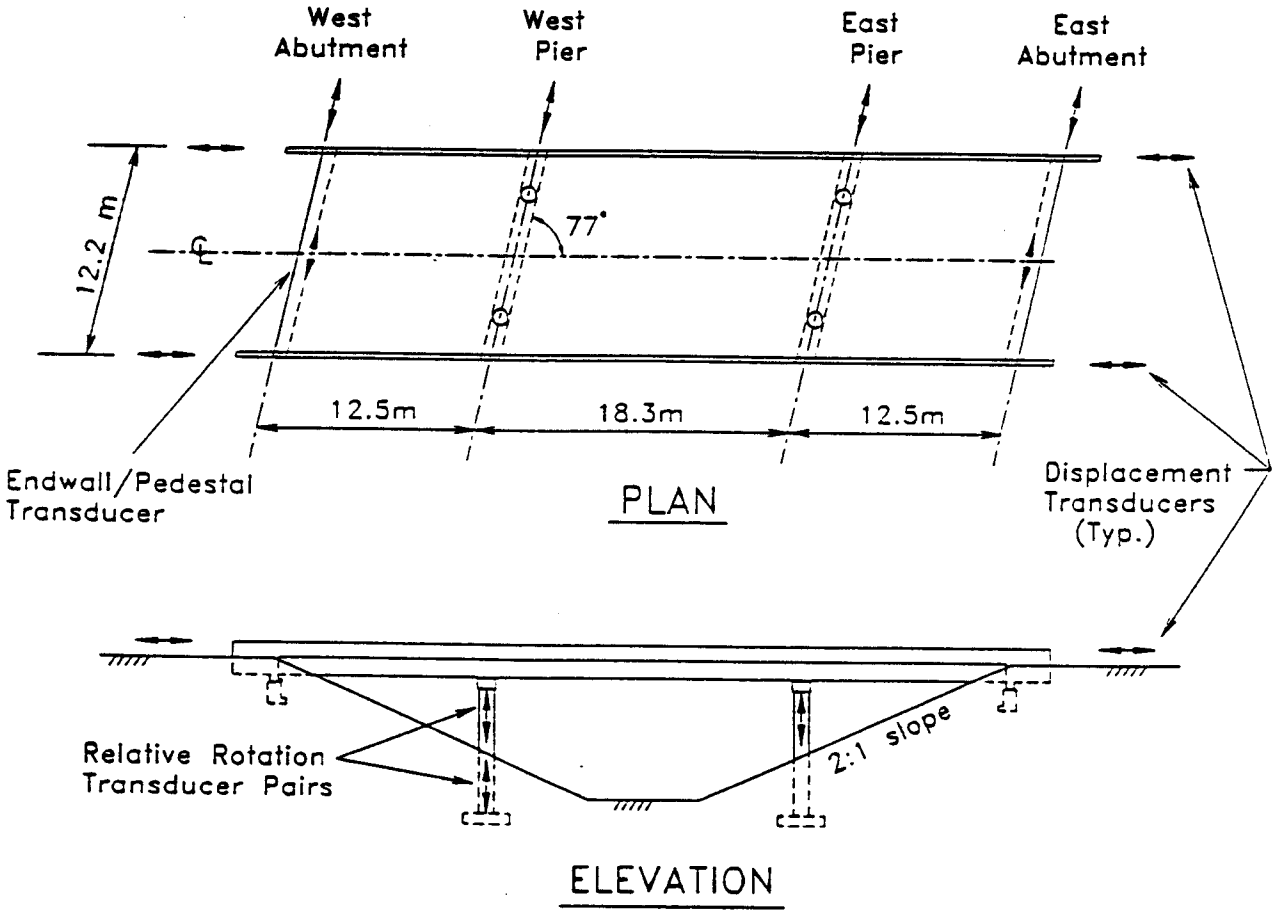

Figure 5.1-2: The Plan and Elevation of the Bridge (Eberhard and Marsh, 1995)

Figure 5.1-3 shows an elevation of the bents with reinforcement detailing. The crossbeam, with a 106.7 cm width and 91.4 cm depth, was monolithic with the two columns. There were ten No. 11 longitudinal bars on the bottom and four No. 10 and six No. 11 bars on the top. The No. 5 stirrups spaced at 30.5 cm were used as confinement.

The length of the crossbeam was 12.05 m, and it supported a static load of 2098 kN. Because the crossbeams were tied together with the slab, I-girders, and diaphragms, they were much stronger and stiffer than the supporting columns.

The two bent columns, supported on spread footings, had clear heights of approximately 7.63 m with 7.32 m centerline spacing in lateral direction. However, compacted fill surrounded the columns, where the soil height was up to 3.72 m from the column bases. It was found by Eberhard and Marsh (1995) that the surrounding soil increased the column shear demand by 25%, causing a redistribution of rotations. The circular columns had 91.4 cm diameters, and they were reinforced longitudinally with eleven No. 9 bars that were spaced evenly around the cross-section perimeter and extended into the crossbeam with no splice. The corresponding longitudinal reinforcement ratio is 1.1%. As was typical in columns designed before the 1970's, lap splices were used in the bases of the columns. The length of the lap splices was 101.6 cm (35 times the longitudinal bar diameter). The columns' transverse reinforcement consisted of No. 3 hoops at 30.5 cm spacing, and it only extended through the lap splice (i.e. no hooks extended into the column core). Compared to the required spiral reinforcement ratio by current seismic design codes (AASHTO 1994), the ratio was only 0.14%, one tenth less than that required. Past earthquakes and tests have proved that such a small confinement ratio and length of lap splice are inadequate for the transfer of moment between the column and footing. A softening plastic hinge with splice breakdown will occur during a major earthquake and will cause column failure.

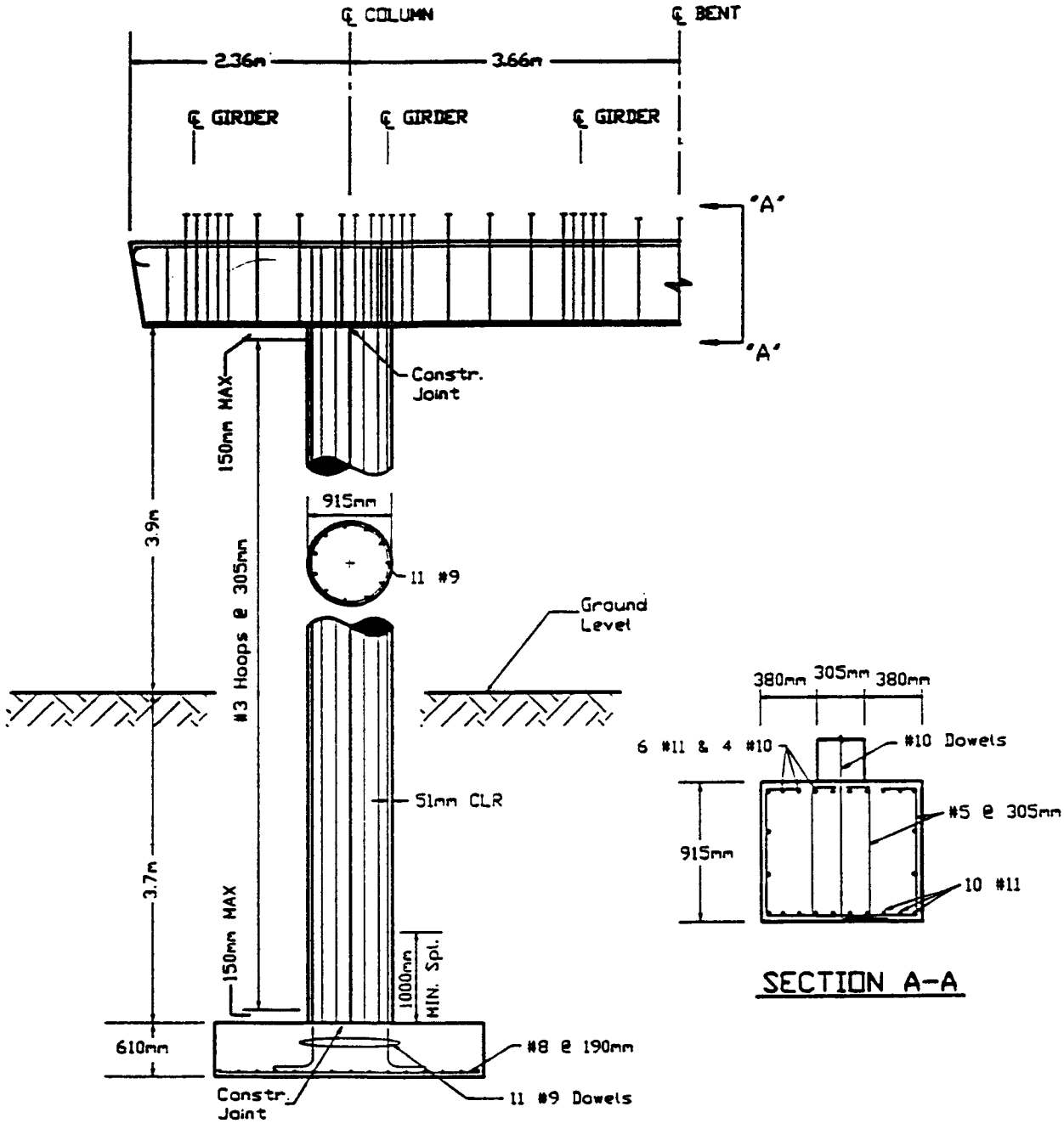

Figure 5.1-3: Bent Elevation and Detailing (Eberhard and Marsh, 1995, in review)

The spread footings were 2.90 m square in the plan and 0.61 m deep with only fourteen No. 8 bars on the bottom layers of each plan direction. The longitudinal bars in the columns were tied into the footings with 90° angles on the bottoms. Recent research shows that a footing failure may occur due to the absence of a top layer of reinforcement and vertical ties in the footings which have the capacity to resist uplift forces (Buckle and Friedland, 1995).

There were two concrete classes used in the bridge. One was a WSDOT Class B mix with a specified compressive strength of $f_c^{'} = 20.67\,MPa$, which was used in the spread footings and abutment walls. The other was a WSDOT Class A mix with a specified compressive strength of $f_c^{'} = 27.56\ MPa$, which was used in all of the remaining members. The steel class used in the bridge was grade 40 with a specified yield strength of $f_y = 275.59\,MPa$. For analytical purposes, Eberhard, *et al.* (1993) measured the in-situ material properties for the concrete, reinforcing steel, and fill surrounding the columns. The concrete strength was measured from twelve approximately 10.2 cm diameter cores taken from the columns, and the steel properties were measured from two No. 9 steel coupons that were also extracted from the columns. The fill's angle of internal friction was measured from undisturbed samples collected at the site and tested under undrained conditions. The measured in-situ material properties are shown in Table 5.1-1.

Table 5.1-1: In-Situ Material Properties

Concrete	Measured Compressive Strength	44 ± 2 *MPa*
	Measured Modulus of Elasticity	32 ± 1.4 *MPa*
Steel	Measured Yield Strength	348.6 *MPa*
	Measured Ultimate Strength	594.6 *MPa*
	Measured Modulus of Elasticity	2.03×10^5 *MPa*
	Strain at Onset of Hardening	0.008
	Strain at Peak Stress	0.035
Fill	In-Situ Unit Weight	$0.017\ N / cm^3$
	Angle of Internal Friction, ϕ	38°

5.1.3 Structural Model

A sketch of the two-dimensional model used to study one of the two bridge bents is shown in Figure 5.1-4. The crossbeam is modeled as an approximately rigid beam element. This consideration is mainly attributed to the composite construction of the 30.5 cm thick cast-in-place diaphragm, deck, I-girder, and bent crossbeam. That makes the crossbeam much stronger and stiffer than the supporting columns. The columns are modeled with nonlinear beam-column elements. The fill surrounding the lower half of the columns is neglected in order to let the conclusions drawn from the nonlinear analysis be

more general for similar kinds of bridges. It is assumed that the bent supports half of the mass of each neighboring span. This mass is specified by assigning an appropriate mass density to the crossbeam.

In a major earthquake, column section cracking will be inevitable, which will decrease the column stiffness. To consider the effect of the cracked column section on column stiffness, use of the effective moment of inertia, I_{eff}, is recommended in a structural analysis rather than the use of gross moment of inertia, I_{gross}. The effective stiffness is a function of the material properties, the longitudinal reinforcement ratio, and the axial load level. In this analysis, the effective moment of inertia is simply taken as half of the gross moment of inertia, as suggested by Buckle et al. (1987). That is $I_{eff} = \frac{1}{2} I_{gross}$. The input parameters required by NEABS to define the axial force-yield moment interaction curve for the columns were obtained using a computer program developed by Marsh (1991). A summary of structural properties of the columns in this analysis is tabulated in Tables 5.1-2 and 5.1-3.

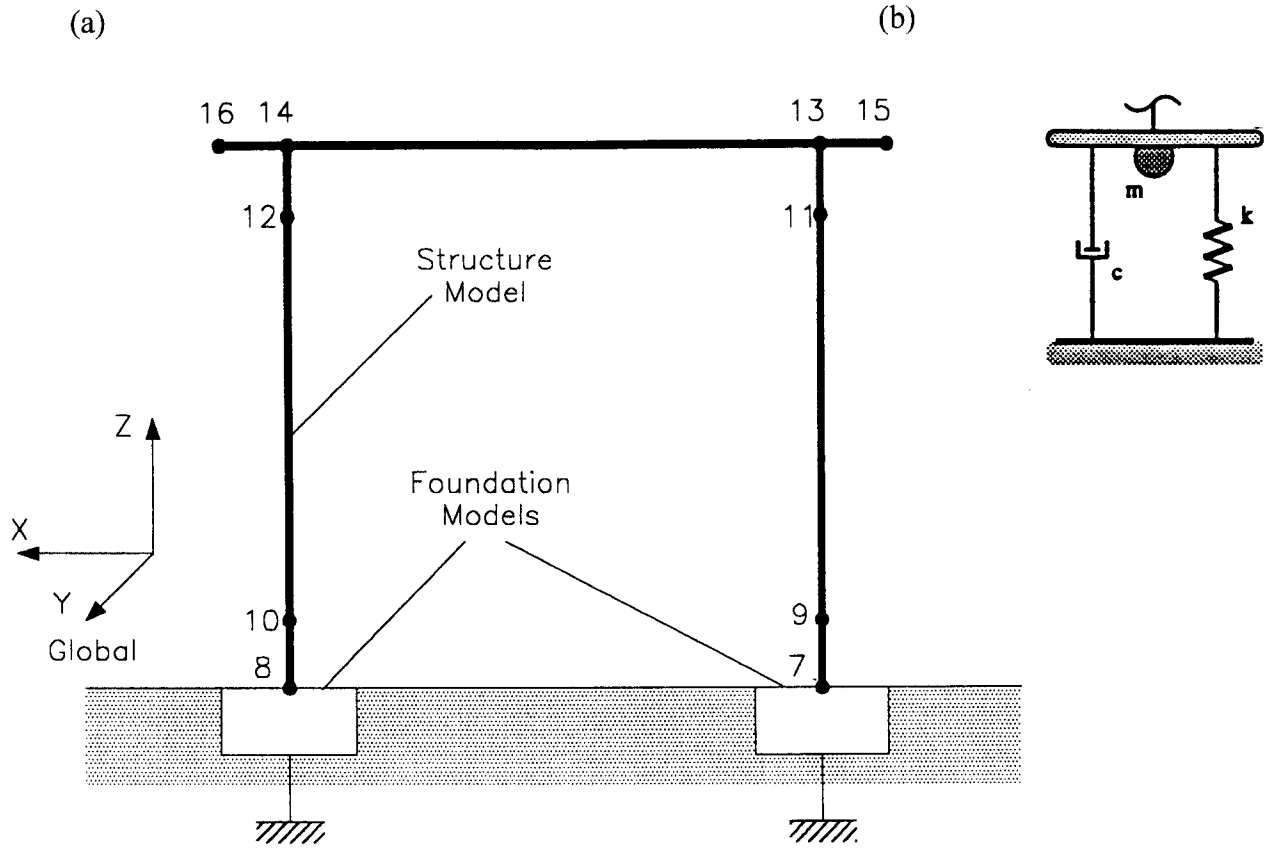

Figure 5.1-4: Structural Model: (a) Bent Model; (b) Foundation Model

Table 5.1-2: Structural Properties for Columns and Crossbeam

	Young's Modulus (kN/cm^2)	Poisson Ratio	Unit Weight (kN/cm^3)	Axial Area (m^2)	Shear Area (m^2)	Bending Inertia (m^4)	Torsional Inertia (m^4)
Columns	3169	0.18	0.0	0.69	0.62	0.017	0.034
Crossbeam	316900	0.18	1.05×10^{-4}	1.67	62.45	1.700	3.400

Table 5.1-3: Yield Function Constants for the Columns

$M_{z0}(kN\cdot m)$	$P_0(kN)$	P_t / P_0	a_0	a_1	a_2	a_3
1016	21709	0.1226	1.0	-6.9732	-9.4420	-1.4688

To consider the influence of soil-structure interaction, a foundation model (Figure 5.1-4b) that represents the elastic half-space is used. The model was developed by Cofer, *et al.* (1994). Note that only the component of the model for the vertical degree-of-freedom is shown in Figure 5.1-4b. A similar arrangement of springs, masses, and dampers is used for the other degrees of freedom. Table 5.1-4 gives the structural properties of the foundation model that represents a relatively stiff soil with a unit weight of $17.59 kN / m^3$, shear wave velocity of $396.5 mps$, shear modulus of $277 MPa$, and Poisson ratio of 0.33.

Proportional damping, known as Rayleigh damping, is used in NEABS. The definition is $\underline{C} = a_0 \underline{M} + a_1 \underline{k}$, where a_0 and a_1 are constants, which are proportional to system mass matrix $\underline{M}$ and stiffness matrix $\underline{k}$. The two Rayleigh damping factors a_0 and a_1 may be evaluated through two specific structural frequencies. Under the assumption that the two control frequencies have the same damping ratio, the proportional factors are given (Clough and Penzien, 1993):

$$\begin{Bmatrix} a_0 \\ a_1 \end{Bmatrix} = \frac{2\xi}{\omega_m + \omega_n} \begin{Bmatrix} \omega_m \omega_n \\ 1 \end{Bmatrix} \quad \text{.....(5.1-1)}$$

where ω_m and ω_n are two control frequencies, and ξ is damping ratio. It is recommended that ω_m generally be taken as the fundamental frequency of the MDOF system and that ω_n be set among the higher frequencies of modes that contribute significantly to the dynamic response. For simplification, it was assumed that only the fundamental frequency controls the dynamic response to obtain the Rayleigh damping factors, that is

$\omega_m = \omega_n = \omega$, where ω is the fundamental frequency of the structural system. Hence, equation 5.1-1 becomes:

$$\begin{Bmatrix} a_0 \\ a_1 \end{Bmatrix} = \xi \begin{Bmatrix} \omega \\ \frac{1}{\omega} \end{Bmatrix} \quad \text{.....(5.1-2)}$$

Cofer, *et al.* (1994) computed the natural period of the bent structure by assuming that the bent columns were fixed at their bases and the columns remained elastic. Using the natural period and a 5% damping ratio ($\xi = 0.05$) for this mode of vibration, the Rayleigh damping factors may be obtained through equation 5.1-2.

Table 5.1-4: Structural Properties of the Foundation Element

	Stiffness	Damping	Mass
Lateral Translation	28476	89.36	0.791
Vertical Translation	32309	134.85	0.210
Rocking	98.65×10^6	125539	484.1

Note: Units are *KN*, *m*, *rad*, and *sec*.

5.1.4 Retrofitting Combinations

The purpose for most column retrofit measures is to increase ductility so that the columns can undergo significant plastic rotation before failure. As described in Section 5.1.2, the longitudinal bars in the columns were extended into the crossbeam with no lap splices at the top. Thus, the tops of the columns are capable of developing plastic hinges with relatively high ductility. The flexural strength and ductility relationship will follow Line (2) (Figure 4.3-1). In the seismic analysis, the plastic hinges that occur at the top are

treated as elastic-perfectly plastic hinges without softening because of the high ductility. However, there was a $35d_b$ (d_b is the longitudinal bar diameter) lap splice and insufficient confinement at the bottom of the column. The methods reported in Chapter 4 were used to identify whether the potential plastic hinge zones at the bases of the columns are able to develop full flexural strength. First, using equations (4.3-1) and (4.3-2), one obtains:

$$f_t = 0.33\sqrt{44} = 2.19 MPa$$

$$T_b = 2.19\times10^3\left[\frac{3.14\times0.756}{2\times11} + 2(0.029+0.051)\right]\times1.016 = 596.1\ kN \rangle A_b f_y = 6.452\times10^{-4}\times348.6\times10^3 = 224.9kN$$

Thus, the longitudinal bars at the bases of the columns can develop their yield force and the nominal flexural strength may be achieved.

To determine if the potential plastic zones at the bases of the columns can develop a high ductility without bond failure, equations (4.3-7) and (4.3-9) may be used.

$$f_l = \frac{400\times7.097\times10^{-5}}{0.803\times0.305} = 0.116\,MPa$$

$$T_b = 1.4\times0.116\times10^3\left[\frac{3.14\times0.756}{2\times11} + 2\times(0.029+0.051)\right]\times1.016 = 43.50kN \langle 1.5A_b f_y = 337.4kN$$

Thus, bond failure will occur at a small value of ductility, and the flexural strength will then degrade to the residual flexural strength even though the nominal flexural strength can be developed. The axial force at the bases of the columns due to the static loading is:

$$P = 1.05\times10^{-4}\times1.67\times10^4\times11.99\times10^2/2 = 1051kN$$

Using equation (4.3-5) and assuming $x = 0.2D' = 0.2\times0.756 \approx 0.15\ m$, the residual flexural strength is:

$$M_r = 1051\left(\frac{0.756}{2} - 0.150\right) = 239.6kN - m.$$

For an axial force of $P = 1051\ kN$ and using equation (6), the ultimate bending moment is:

$$M_{yp} = 1016\times\left[1 - 6.9732\left(\frac{-1051}{21709}\right) - 9.442\left(\frac{-1051}{21709}\right)^2 - 1.4688\left(\frac{-1051}{21709}\right)^3\right]$$
$$= 1336.7kN - m$$

The ratio between residual moment and ultimate bending moment is:

$$r_o = \frac{M_r}{M_{yp}} = \frac{239.6}{1336.7} = 0.18$$

r_o may be used to determine the maximum damage coefficient in equation (1), that is:

$$D_{\max} = 1 - r_o = 1 - 0.18 = 0.82$$

Another means to evaluate the occurence of bond failure before nominal flexural strength is to check the minimum length of lap splice by using equation (4.3-14). That is:

$$l_{s_{\min}} = \frac{0.25\times 0.029\times 348.6}{\sqrt{44}} \approx 0.38\ m. \langle 3.5d_b = 3.5\times 0.029 \approx 1.02\ m$$

Thus, the minimum length requirement for the lap splice is met and no "shearing off" bond failure will occur.

In summary, the pre-1971's designed columns with lap splices and insufficient confinement can reach the nominal moment, but flexural degradation will occur at a small level of ductility. The line (4), as shown in Figure 4.3-1, represents this situation. To improve the seismic resistance and ensure the serviceability of the bridge, some form of column retrofit is required. In this analysis, several retrofit strategies for the two-column bridge bent were evaluated regarding their benefits. For the specific class of columns investigated in this dissertation, failure is assumed to be constrained to occur in the plastic

hinge region at the base of the column and will not be permitted to migrate into the foundation. This assumption usually is reasonable because of the fact that longitudinal bars in the columns were extended into the crossbeams on the top and the foundations were generally designed with significant conservatism.

As reported in Section 1.1.2, a number of bridge column retrofit schemes are available, including welded or bolted cylindrical steel plate jackets, cast-in-place concrete jackets, wrapped epoxy-fiberglass jackets, and tension-wound prestressed confining steel, etc. The first two techniques have been most commonly used in the United States. In this example, the steel jacketing technique will be assumed for parametric retrofit analyses. Figure 5.1-5 shows the retrofit strategies that are designated as Cases 1 to 3 in the analyses. For this retrofit procedure, the as-built column diameter is maintained and successively thicker cylindrical jacketing plates are added to the zone of predicted high damage. The thickness of the steel plate is designed to ensure that the plastic hinge develops at a relatively high level of ductility. The height of the jacket is designed to extend a significant distance above the plastic hinge region to ensure that a localized hinge is not simply translated to the top of the jacket.

Tests have indicated that the partial-height flexural retrofit may affect the column elastic stiffness by a 10 to 15 percent increase. For simplification, this increase is neglected in the analyses. Effectively, jacket provides confinement only and does not act as additional longitudinal reinforcement. In the analyses, any plastic hinge with retrofitting is modeled as an elastic-perfectly plastic hinge without softening because the steel jacketing results in large ductility. Figure 5.1-6 shows the moment-curvature

relationship for the plastic hinges on the top and the plastic hinges at the bases with retrofitting. Regarding the plastic hinges at the bases without retrofitting, as described before, line (4) (Figure 4.3-1) represents the actual moment-curvature relationship, in which a small "plastic plateau" will be developed just after the nominal moment is attained and then the flexural degradation begins. This conclusion is based on the fact that equation (4.3-8) is not satisfied and, thus, high ductility can not be developed before degradation occurs. Figure 5.1-7 shows the moment-curvature relationship for these plastic hinges.

For the modified version of NEABS, the critical plastic rotation θ_{cp} and the maximum theoretical plastic rotation $\theta_{\max}$ defined in Section 2.3.1 are required as input. To obtain the two parameters, in this analysis, the moment-curvature analysis program developed by Marsh (1991) was used again to compute the critical curvature, ϕ_c (Figure 2.3-2) which is corresponding to a strain of 0.002 at the level of the compressive reinforcement. Using the recommendations by Priestley and Seible (1994), in which the flexural strength degrades to a residual flexural capacity at an incremental curvature ductility of $\Delta\mu_\phi = 6$, and the computed critical curvature, the maximum theoretical curvature, $\phi_{\max}$ was obtained. Equations (2.3-2) and (2.3-3) may then be used to evaluate the value of θ_c and $\theta_{\max}$. The computations are as follows:

$\phi_c = 3.66\phi_y$ (from Marsh's program)

$\phi_{\max} = 10.98\phi_y$ (from ϕ_c and Priestley's recommendations)

$l_p = 0.08 \times 381 + 9 \times 2.865 = 56.265$ cm. (from equation (4.2-10))

Thus, by using equations (2.3-2) and (2.3-3), the critical plastic rotation and maximum theoretical plastic rotation are:

$$\theta_c = (\phi_c - \phi_y) l_p = (3.66 - 1) \times \frac{1336.7}{3169 \times 10^4 \times 1.715 \times 10^{-2}} \times 56.265 \times 10^{-2} = 3.68 \times 10^{-3} rad$$

$$\theta_{\max} = (\phi_{\max} - \phi_y) l_p = (10.98 - 1) \times \frac{1336.7}{3169 \times 10^4 \times 1.715 \times 10^{-2}} \times 56.265 \times 10^{-2} = 1.38 \times 10^{-2} rad$$

.

(1)

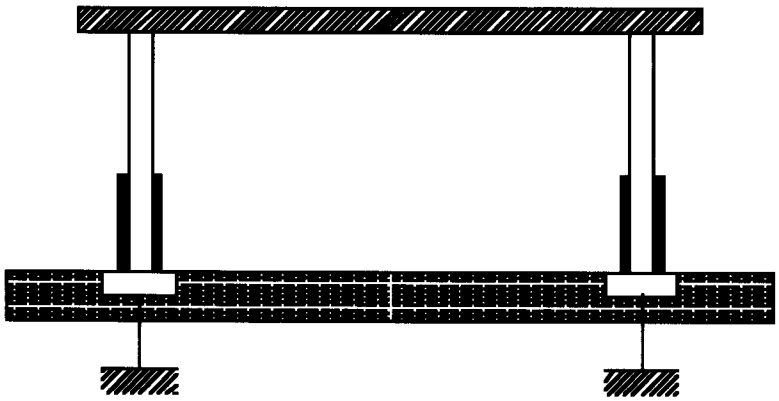

(2)

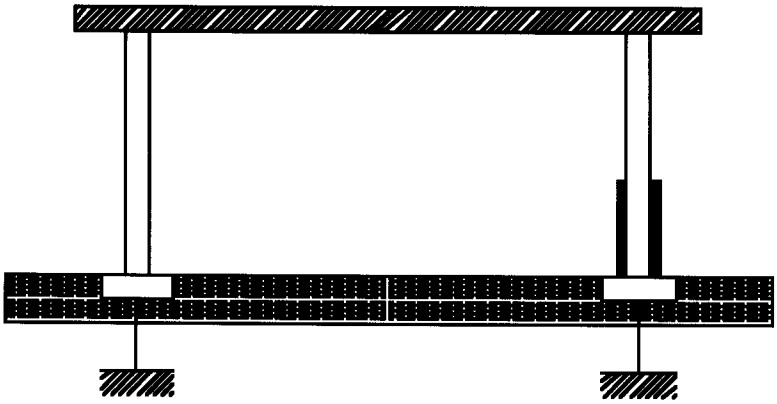

(3)

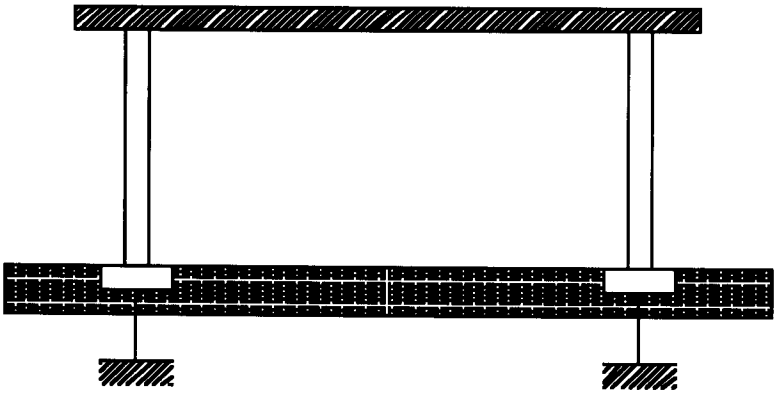

Figure 5.1-5: The Bent Retrofit Strategies: (1) Case 1; (2) Case 2; (3) Case 3

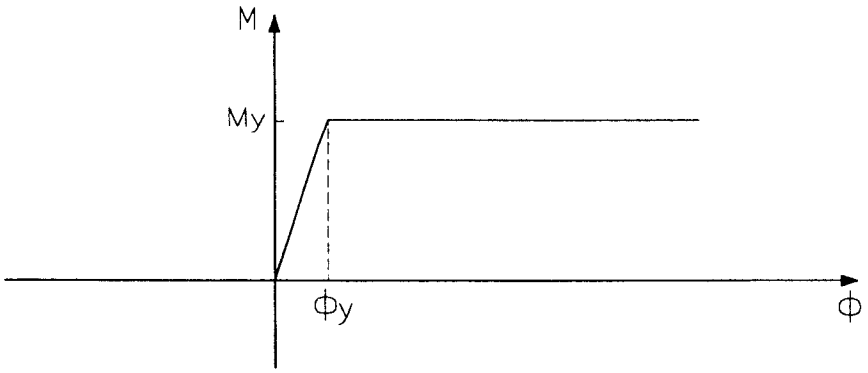

Figure 5.1-6: Elastic-Perfectly Plastic Hinge Model

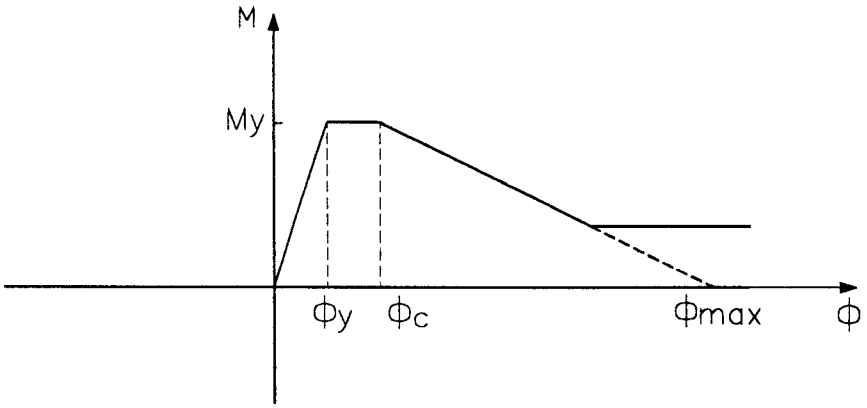

Figure 5.1-7: Plastic Hinge with Softening Model

5.1.5 Seismic Excitation

The seismic loading used in the time-history analysis was the S00E component of the El Centro acceleration record of the 1940 Imperial Valley Earthquake (referred to as the "El Centro" record). The objective is to let the seismic loading be representative of an

actual earthquake. The 1940 Imperial Valley earthquake was of 6.7 Richter magnitude, and the peak ground acceleration was 0.35g. Figure 5.1-8 shows the acceleration history for the earthquake record. A plot of the response spectra, for four damping ratios, of the El Centro record is included Figure 5.1-9.

In the analyses, the acceleration record was scaled to an intensity of 0.40g effective peak acceleration, or EPA. The EPA of a record is related to the average spectral acceleration the record produces over a certain system period range rather than to the ground motion itself. Thus, it is a more characteristic measure of intensity than peak ground acceleration for engineering purposes (Cofer, *et al.*, 1994).

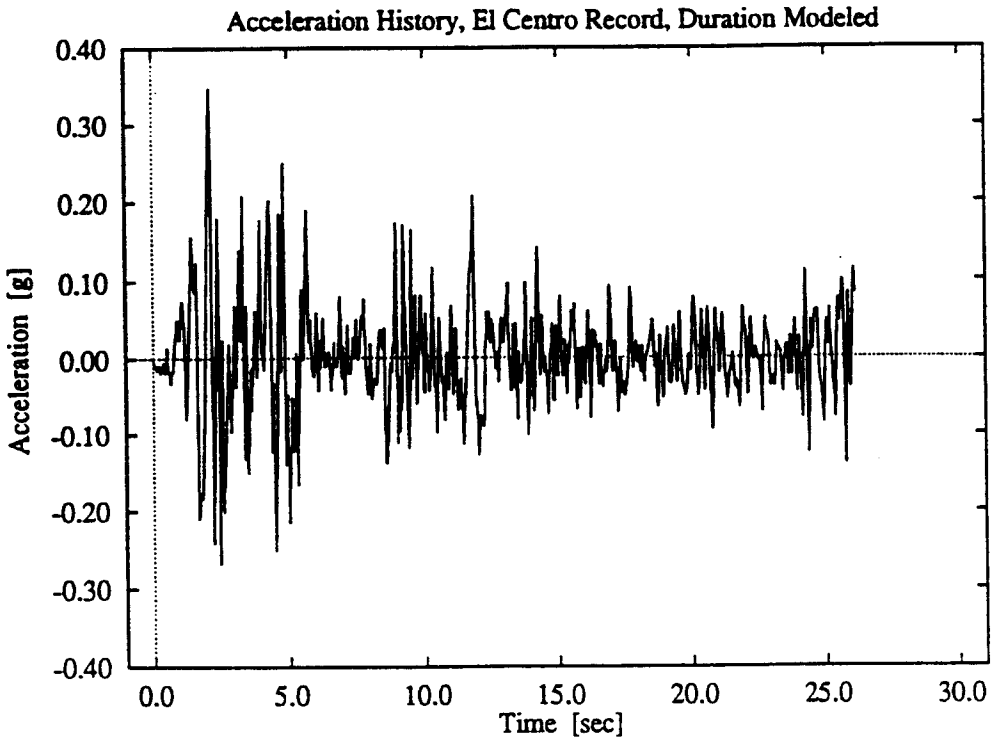

Figure 5.1-8: Ground Acceleration Time History of the El Centro Earthquake (Cofer, *et al.*, 1994)

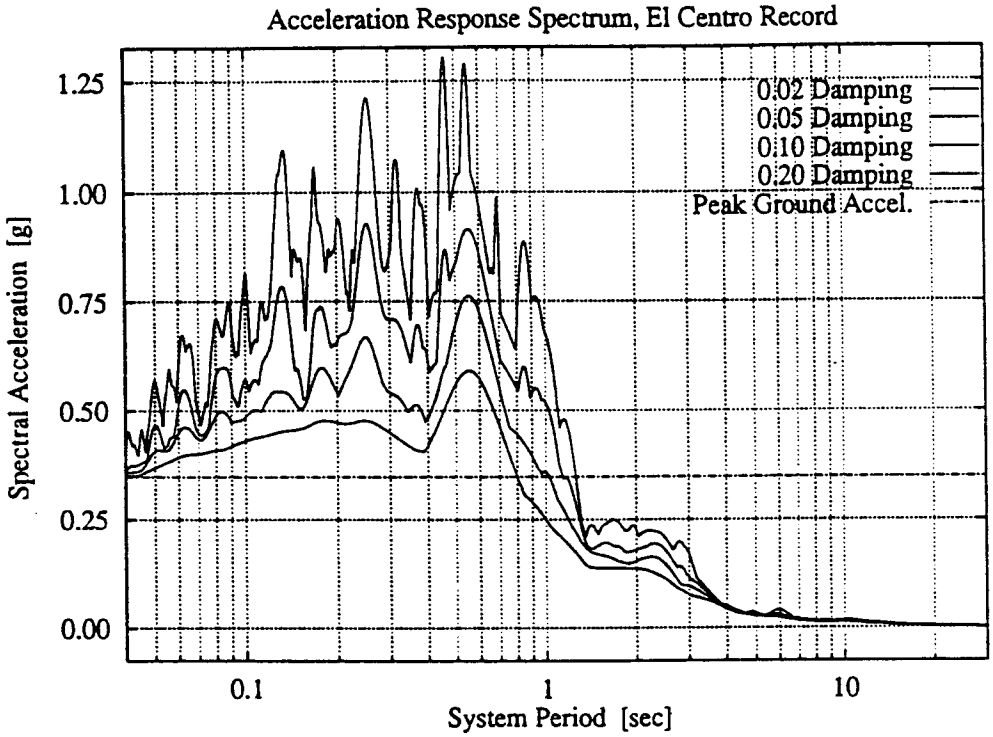

Figure 5.1-9: Acceleration Response Spectra for El Centro Earthquake Record (Cofer, *et al.*, 1994)

5.1.6 Analytical Results and Interpretation

Selected results from both the static and nonlinear time-history analyses are presented in this section. The performance of each of the various retrofitted conditions is assessed in terms of its effects on the response of the bent structure. The results presented are those selected in support of the objectives of the case studies and those believed to be generally of greatest interest to bridge designers. The pertinent results reported in the following sections include: the top displacement of the bent, the plastic rotations of the plastic hinge at the column bases, internal column moment, and ductility.

5.1.6.1 Static Analysis

In this analysis, a lateral monotonic loading is applied to the top of the bent for the various retrofitting combinations. The purpose of this quasi-static pushover type of analysis was to evaluate the collapse performance of different retrofit combinations. Because the bent will collapse when the monotonic load exceeds the yielding load at which the moment at both bases reaches its nominal value, the softening properties cannot be obtained with this load-controlled analysis. To solve this problem, a translational linear spring was connected to the right end of the crossbeam, as shown in Figure 5.1-10a. The function of the spring was to carry the extra force released by the bent due to the softening of the plastic hinges; hence the lateral load carried by the bent is the difference between the total load and the internal force of the spring. The stiffness of the linear spring was chosen to equal the lateral elastic stiffness of the bent, that is

$k_s = 2 \times (12EI / l^3) = 294.81 kN / cm$

Figure 5.1-10b shows the equivalent structural model of the bent-spring system.

Figure 5.1-11 shows the load carried by the bent versus the bent displacement for each retrofit case. This graph shows that the retrofit method has a significant influence on structural resistance. For Case 1, because no damage is allowed at the bases of the columns, the load versus deflection curve is basically elastic-perfectly plastic. For Cases 2 and 3, in which some damage was allowed at the bottom of the columns, the total lateral stiffness of the bent decreased with softening, and the force carried by the bent decreased with increasing deflection until the residual flexural strength capacity was reached. Then, the force carried by the bent remained essentially unchanged. It can be observed that the two curves look like line (4) in Figure 4.3-1.

From Figure 5.1-11, one also can see that a partial retrofit (i.e. retrofitting only one column) is somewhat effective in increasing both the residual strength of the bent and the energy that would be dissipated, as defined by the area under the curves.

(a)

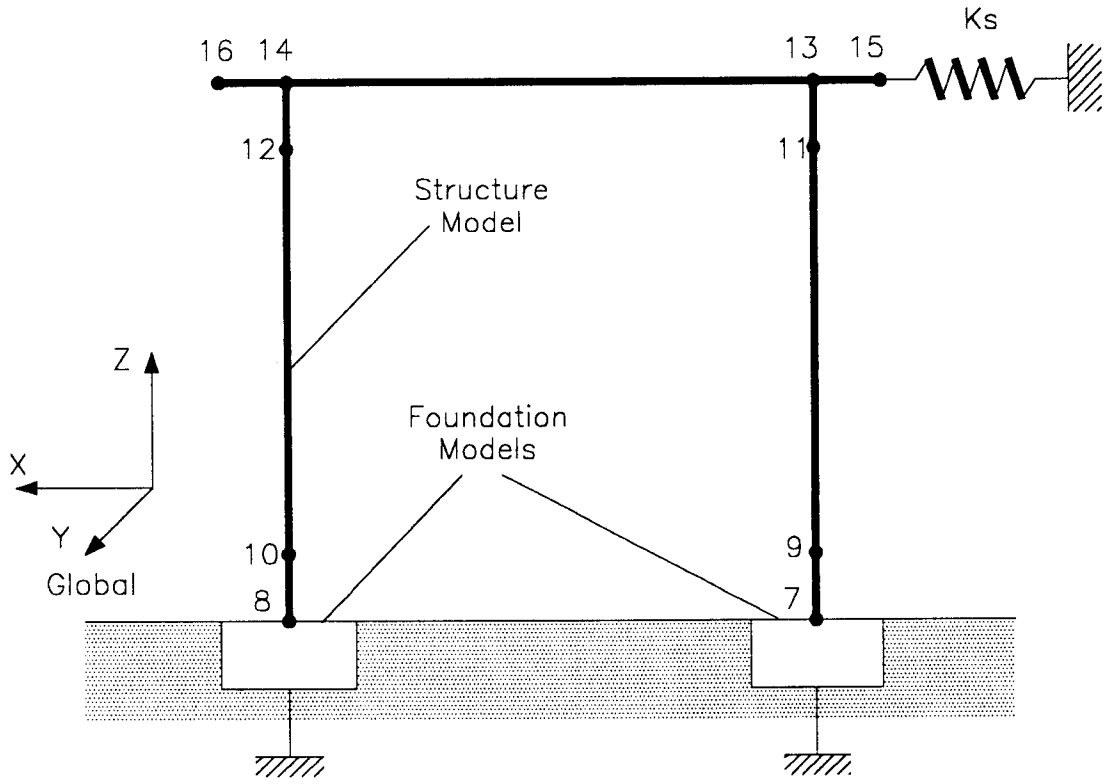

(b)

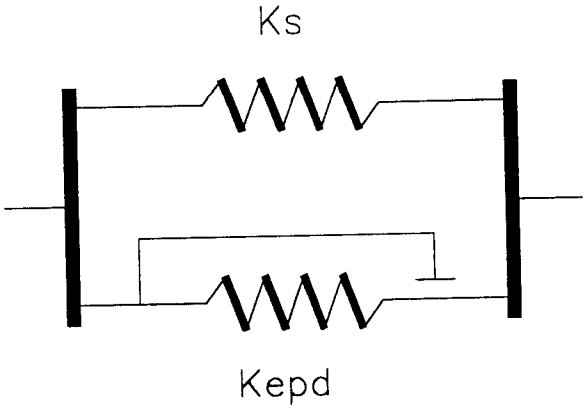

Figure 5.1-10: Structural Model and Equivalent Structural Model of the Bent-Spring System: (a) Structural Model; (b) Equivalent Structural Model

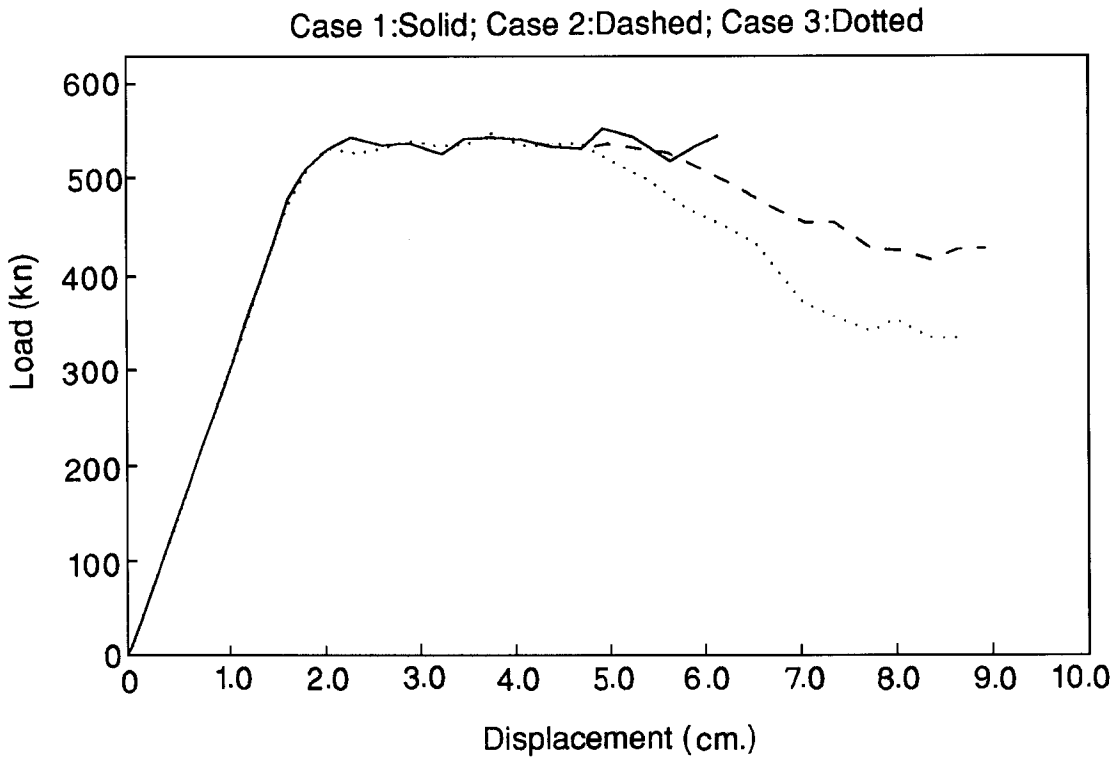

Figure 5.1-11: Load vs Displacement

5.1.6.2 Seismic Analysis

Three cases were analyzed by applying the El Centro earthquake record with an intensity of 0.40g EPA. The output of the NEABS program is in the form of time histories. Selected analytical results from the nonlinear time-history analyses are presented in Figures 5.1-12 through 5.1-16. In Figure 5.1-12, the horizontal displacement time-history of the top of the bent is shown. The plastic hinge rotations at the bottom of the columns are given in Figures 5.1-13 and 5.1-14, while the moment response is shown in Figures 5.1-15 and 5.1-16. Note that the base of the left column is assumed to be

retrofitted in only Case 1, and the base of the right column is assumed to be retrofitted in Cases 1 and 2.

As shown in the figures, the displacement, plastic deformations, and moments for all cases are fairly similar at the beginning phase of the earthquake because little or no damage has occurred. At a time of approximately two seconds, the peak ground acceleration occurs and the response for each case diverges from the others due to damage and softening at the column bases that were assumed to be unretrofitted. From Figures 5.1-12 to 5.1-14, one can note that the models of Cases 2 and 3 are subject to increased horizontal displacements and plastic hinge rotations compared to Case 1. However, because the base of the right column in Case 2 was retrofitted, the increases for that case are less than those of Case 3, in which both column bases were allowed to experience softening and degradation of stiffness, but greater than those of Case 1, in which both column bases were retrofitted. A similar situation also occurred for the left column in Case 2; however, because this column was unretrofitted for the case, the plastic deformation is more like the left column in Case 3.

The time-history response plots of the moments at the bases of the two columns for each case are shown in Figures 5.1-15 and 5.1-16. It was found that a significant decrease in the moments occurred at about 4.5 seconds for the left column of Cases 2 and 3. After six seconds, the moment capacities for Cases 2 and 3 were softened to the residual flexural strength and correspondingly large plastic deformations (Figure 5.1-13) developed because of the small flexural resistance. For the right column, because it was retrofitted at the bases for Cases 1 and 2, the flexural strength remained unchanged (Figure

5.1-16) and both time-history curves are basically the same. Regarding Case 3, similar behavior is observed for both the right and left columns.

To compare and summarize these results, the maximum displacement-based ductility demand and rotational ductility demand factors were computed by using equations 4.2-2 and 4.2-11. The results are tabulated in Table 5.1-5. As expected, the sequence of values of displacement-based ductility demands for Cases 3, 2, and 1 are highest, medium, and lowest, respectively. Compared to the completely retrofitted bent (Case 1), there is a 65% displacement ductility demand increase for the partially retrofitted bent (Case 2) and a 112% increase for the unretrofitted bent (Case 3). Regarding the rotational demand ductility factors, as described in Table 5.1-5, one may observe that these factors at the bottoms of the columns have an effective decrease for the retrofitted column in Cases 1 and 2 compared to those in Case 3. However, the level of decrease for the right retrofitted column in Case 1 is much more pronounced compared with that in Case 2. Moreover, a relatively large rotation was still observed at the unretrofitted column base for Case 2. This results from the flexural strength softening making the connection as if it was pinned, and the column shape is one of single curvature rather than double curvature.

All rotational ductility demand factors at the tops of columns are smaller than the rotational ductility capacity, $\mu_{\theta_{cap}}$ which was computed by using the moment-curvature analysis program (Marsh, 1991) when the concrete compressive strain at extreme fiber, ε_c, equals 0.005. This proves that the elastic-perfectly plastic assumption for the

tops of the columns is correct and the softening would not occur at the tops of columns for the earthquake record input.

Table 5.1-5: Displacement-Based Ductility Demand Factors (μ_Δ) at the Top of the Bent and the Rotational Ductility Demand Factors (μ_θ) at the Top and Bottom of the Columns

		Case No.		
		1	2	3
μ_Δ	On the Top of Bent	2.20	3.62	4.66
μ_θ(top)	Left Column	2.72	4.79	5.94
	Right Column	1.91	4.85	5.72
μ_θ(bottom)	Left Column	2.68	11.03	13.82
	Right Column	1.89	4.97	10.65

Note: $\mu_{\theta_{cap}} = 8.66$ at top of the column.

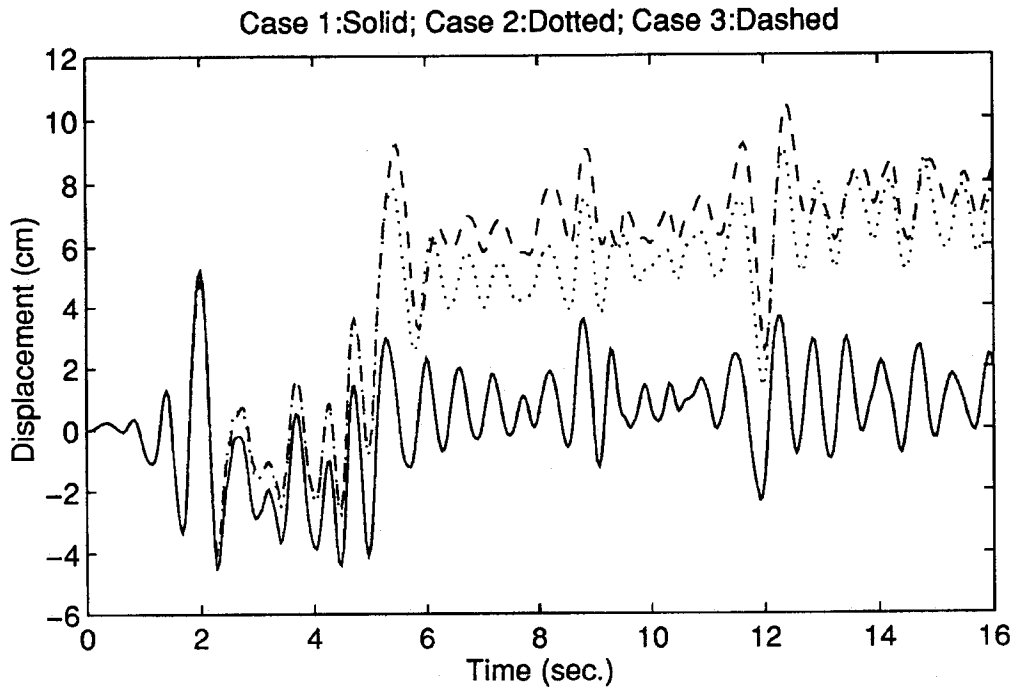

Figure 5.1-12: Time-History Response at Top of the Bent for Different Retrofit Models

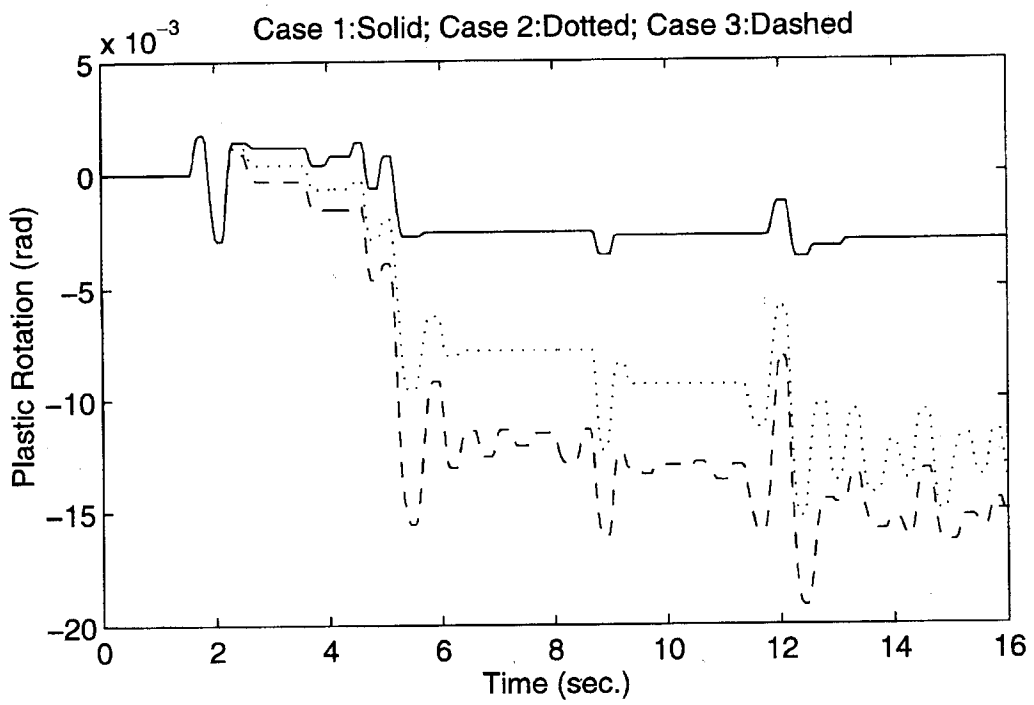

Figure 5.1-13: Plastic Hinge Rotations at Bottom of Left Column for Different Retrofit Models

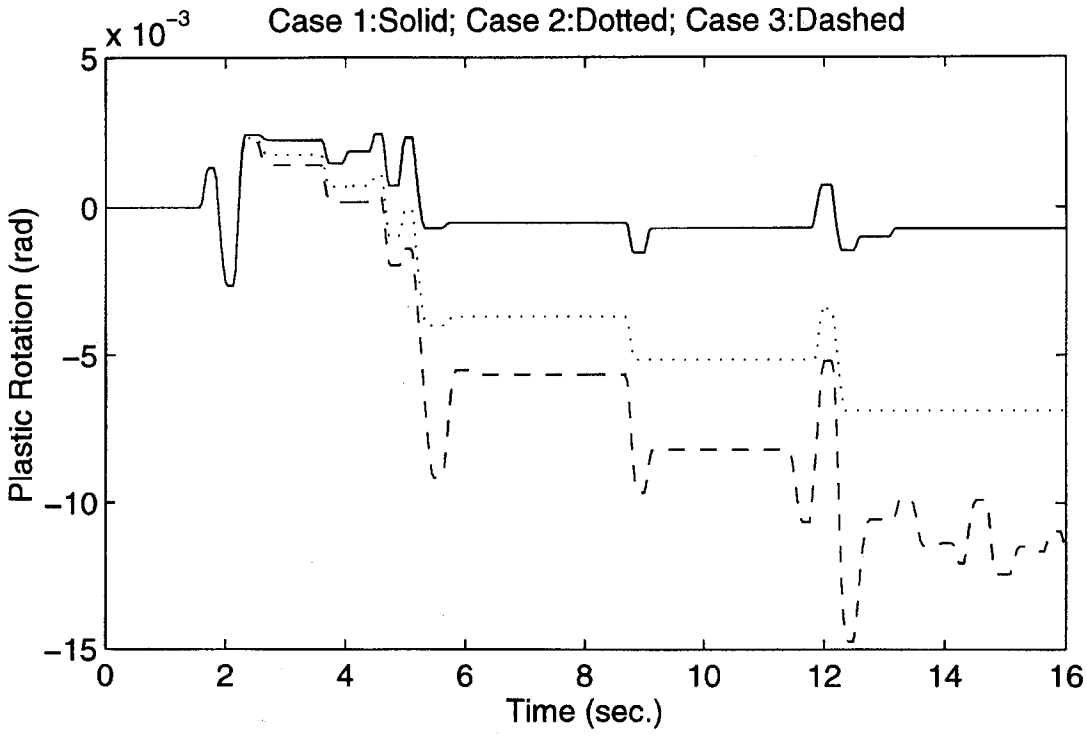

Figure 5.1-14: Plastic Hinge Rotations at Bottom of Right Column for Different Retrofit Models

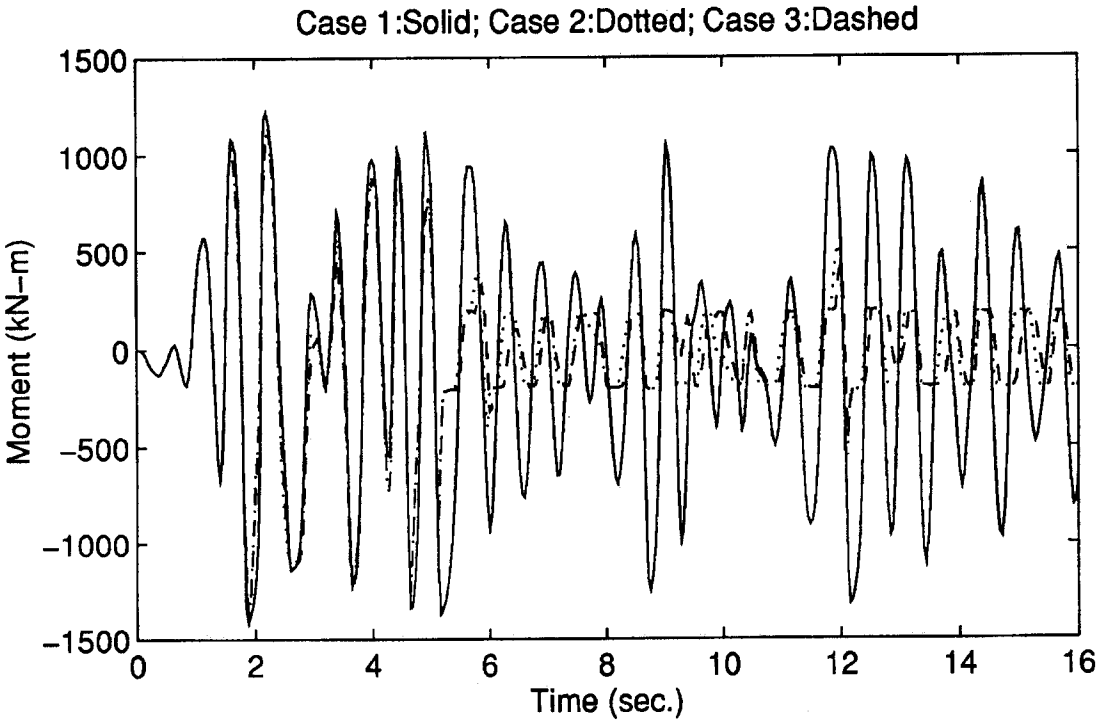

Figure 5.1-15: Moment Responses at Bottom of Left Column for Different Retrofit Models

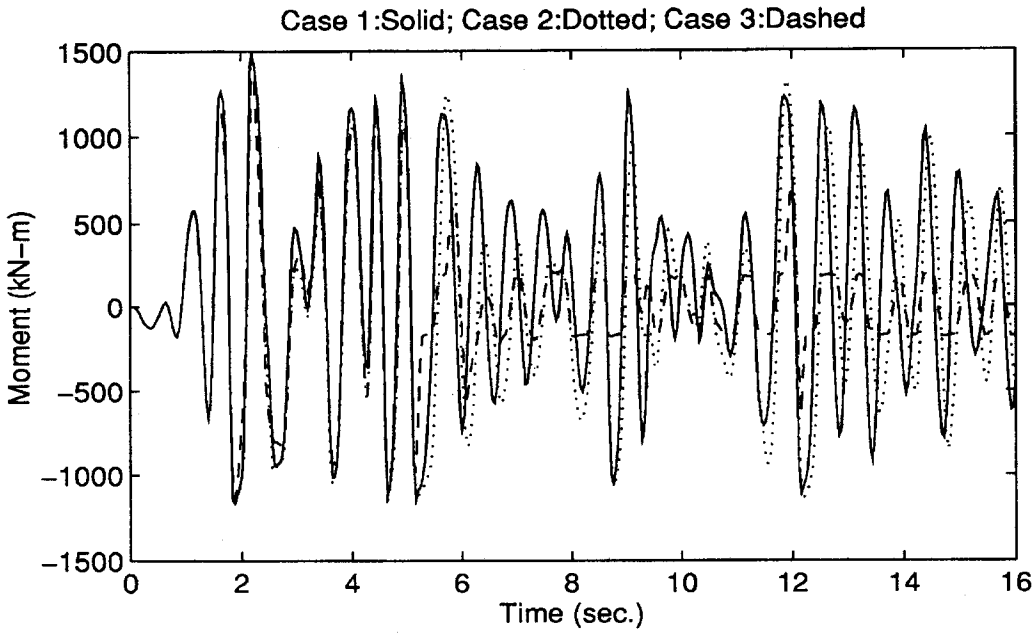

Figure 5.1-16: Moment Responses at Bottom of Right Column for Different Retrofit Models

5.1.7 Conclusions and Recommendations

In all three computed cases, plastic hinges developed at the bases of columns for the input earthquake record. However, softening occurred for the left column of Case 2 and both columns of Case 3 so that only residual flexural strength was left. Therefore, the damage was serious. However, both columns in Case 1 performed very well because of the retrofit strategy used. Although the retrofit strategy used in Case 2, in which only the right column was retrofitted, caused a decrease in the total displacement-based ductility to a certain degree, the cost may be very high with respect to benefit because of the serious damage of the unretrofitted right column. The magnitude of the damage may be unacceptable because of the high repair cost and long construction time. Hence, it is recommended that full column retrofit will be more suitable for this type of bridge with only two columns in a bent.

5.2 Mercer Slough Highway Bridge (2-Dimensional Structural Analysis)

This section may be considered as a continuation of Section 5.1 for investigating the retrofitting effect of the columns. In this section, a relatively complicated bridge bent with five column is analyzed with various retrofit strategies. This bridge was selected because it has multiple bent columns and it was constructed prior to the introduction of modern seismic design criteria. Hence, there are a number of possible column retrofit strategies and the analytical results will be useful for their evaluation.

5.2.1 Introduction

The bridge studied here supports the Mercer Slough Westbound Lanes, which is located on Interstate 90 where it crosses Mercer Slough in south Bellevue, Washington. Figure 5.2-1 is an aerial view of the Interstate 90 Mercer Slough crossing, in which the darker lanes are the Westbound Lanes. The bridge was constructed in 1939 to carry traffic in both directions, and it is an important element of Interstate 90, linking Seattle to points east of the city. Because of the peat soil type upon which the structure is founded, the variation in soil profile from one end of the bridge to the other, the soil-pile nonlinear behavior, and the large size of the structure, the seismic analysis for the bridge poses a number of challenges. McLean and Cannon (1992) studied the seismic behavior of this bridge by using linear and somewhat nonlinear dynamic analyses. They predicted that the most likely failure modes of the bridge were moment failure and ductility in the columns, failure of timber pile footings, and excessive displacements in the expansion joints. In 1993, Cofer, McGuire, and McLean again used the bridge to investigate the effects of soil-structure interaction.

In this analysis, six column retrofitting combinations were applied to a typical bridge bent. The primary purpose of the analyses is to evaluate the influence of the various retrofitting strategies, flexural softening, and degradation of stiffness on the seismic response of the bridge. The earthquake record used in this analysis is again the 1940 El-Centro earthquake record. Based on the analytical results, conclusions and recommendations are drawn.

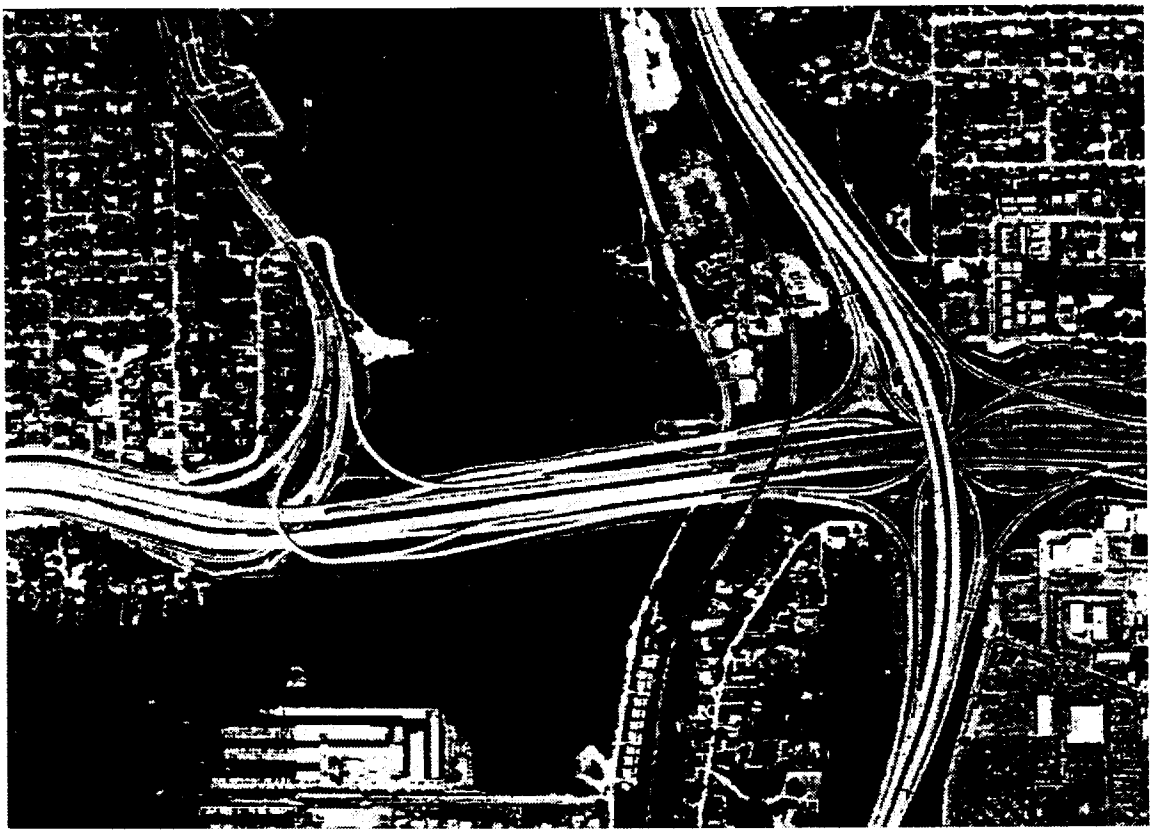

Figure 5.2-1: An Aerial View of Mercer Slough Crossing

5.2.2 Description of the Bridge and Site

The bridge structure consists of T-girder spans which are continuous over four spans and separated by an expansion joint at every fourth bent. The 85-span bridge is approximately 854 meters long. Most of the spans are 18.3 meters wide. The spans are typically supported on pile-founded, five column, reinforced concrete bents. Typically, each span length is 9.15 meters except for the longer end spans. Figure 5.2-2 shows the

side elevation and cross-section of the spans. The spans have a 15.24-cm-thick slab and nine 40.64-cm-wide webs spaced at about 2.29 meters center-to-center. The section is typically 83.82 cm deep from the bottom of the web to the top of the slab. The bent cap beams form diaphragms between the T-girder webs.

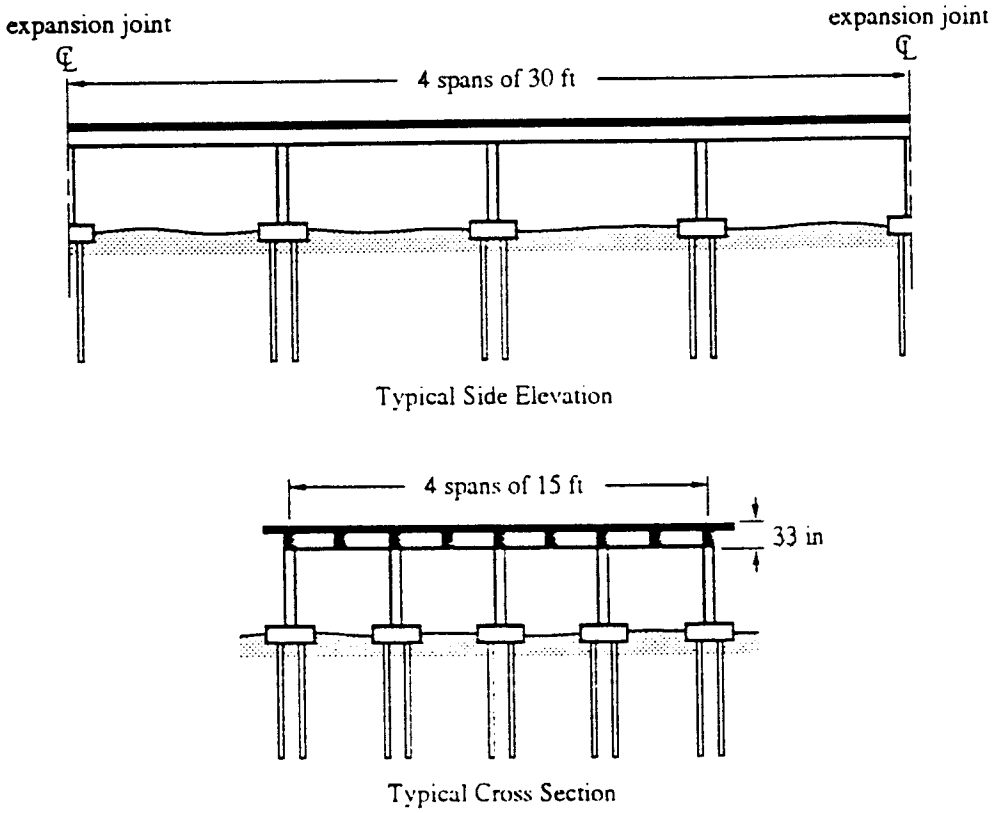

Figure 5.2-2: Span Elevation and Cross Section (Cofer, *et al.*, 1994)

A typical bridge bent consists of five columns, each on a separate foundation. The columns are evenly spaced across the width of the bridge. Figure 5.2-3 shows the detail of a typical column, the cross section, and pile cap. The column cross-section is 50.8 cm square, and eight No. 7 longitudinal bars are evenly spaced around the perimeter with 38.10 mm clear cover. The corresponding longitudinal reinforcement ratio is 1.2%. The columns are constructed monolithically with the foundation and bridge superstructure. The longitudinal bars are tied into the diaphragm directly in the T-girder system, but only into the bent cap beam at the expansion joints. At the bottom, the longitudinal reinforcement is spliced with the same amount of steel from the pile cap. The length of the lap splice is 35 times the longitudinal bar diameter. The columns' transverse reinforcement only consists of No. 4 stirrups spaced 30.48 cm apart over its entire length. There is no additional confinement at the lap splice zone in order to insure continued performance of the longitudinal bar. The lack of sufficient transverse reinforcement and the short splice length at the base of the column can not allow the formation of a ductile plastic hinge. When a major earthquake occurs, the moment strength will degrade rapidly.

As shown in Figure 5.2-3, the pile cap is supported on four timber piles. Each direction of the pile cap contains eight No. 8 bars. The location of the bars are indicated in Figure 5.2-3. No mechanical connection is provided between the piles and pile cap. It was reported by McLean and Cannon (1992) that the flexural strength of the pile cap is greater than that of the column; thus the pile cap will not fail before the column.

The expected in-situ material strengths are $f_c^{'} = 31\,MPa$ for the concrete and $f_y = 310 MPa$ for the steel. As per ACI318-89 § 8.5.1, the modulus of elasticity of $E_c = 57{,}000\sqrt{f_c^{'}}(psi) = 26{,}344\,MPa$ is used for the columns.

The soil condition at Mercer Slough varies from soft peat and loose sand to dense sand. The main part of the bridge rests on very soft peat and organic silt. Through the study by Kramer (1992), it was found that soft soils could potentially amplify ground motion and provide little resistance to lateral bridge movement.

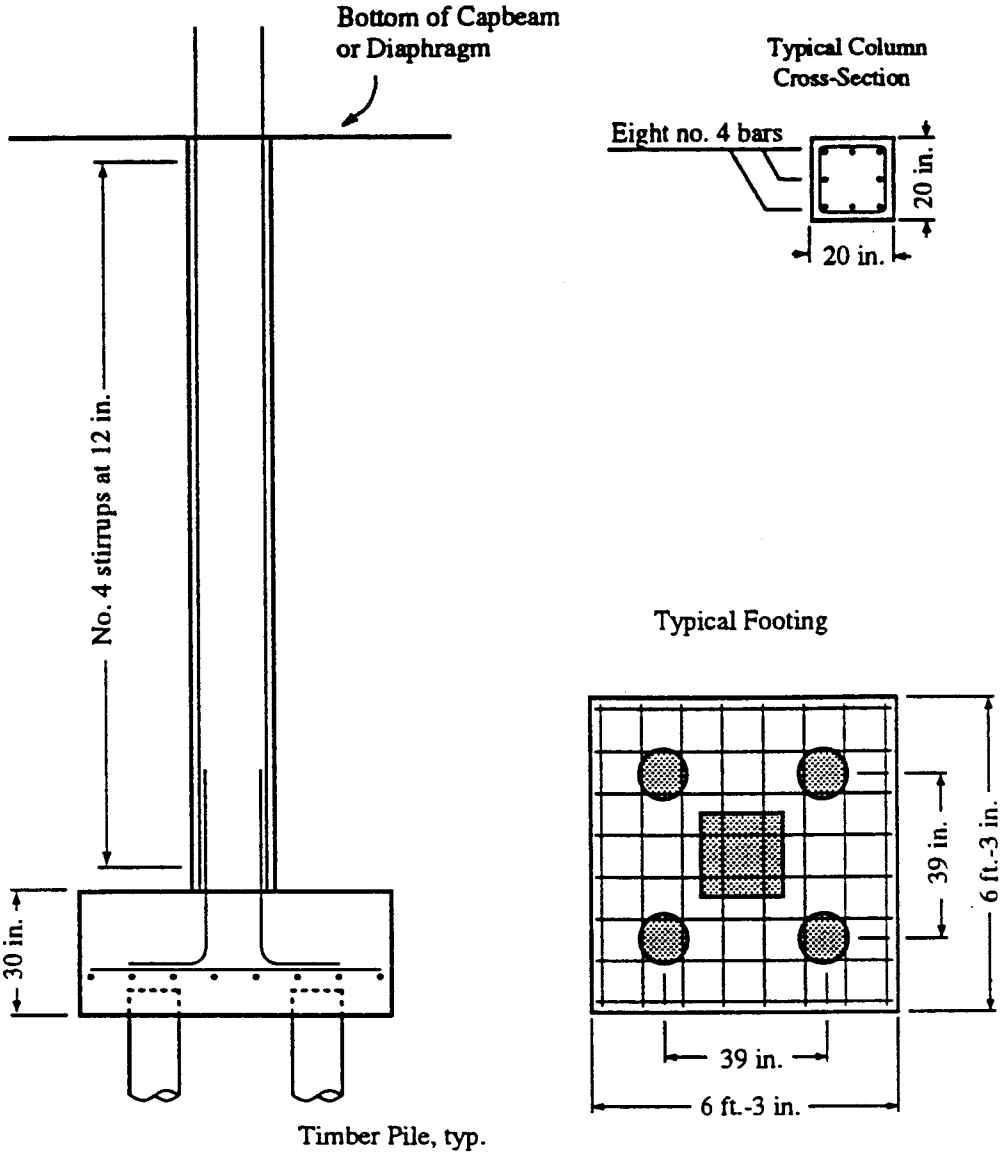

Figure 5.2-3: Typical Columns and Pile Cap Details (Cofer, *et al.*, 1994)

5.2.3 Structural Model

To study the retrofit strategies, a typical Mercer Slough bridge bent was used as a nonlinear analysis model. Figure 5.2-4 shows the idealized structural model. To clearly identify the effect of column retrofitting on structural response, the base of each column is assumed to be fixed to the footing. This assumption makes it easier to draw conclusions that are related to the column retrofitting.

Two types of elements are used to model the bent structure. Because of the monolithic construction of columns, bent cap beams, and diaphragm, the cross-beam is modeled as an approximately rigid beam with very large stiffness as with the previous analysis of the Moses Lake bridge bent. The mass supported by the bent is applied by specifying an appropriate density for the crossbeam elements. The columns are modeled with nonlinear beam-column elements. The effective elastic stiffness for the cracked column is assumed to be $E_c I_{eff} = \frac{1}{2} E_c I_{gross}$. Crossbeam and column masses are lumped at the corresponding nodes.

As in the study of the Moses Lake bridge, the computer program developed by Marsh (1991) was again used to obtain the axial force-yield moment interaction curve. Tables 5.2-1 and 5.2-2 show the parameters required by NEABS.

To apply Rayleigh damping to the bent, the fundamental period of the bent with fixed bases and rigid crossbeam is calculated to be 0.33 seconds. 5% damping ratio ($\xi = 0.05$) is assumed for this mode of vibration. Using equation 5.1-2, the damping factors required by NEABS may be obtained.

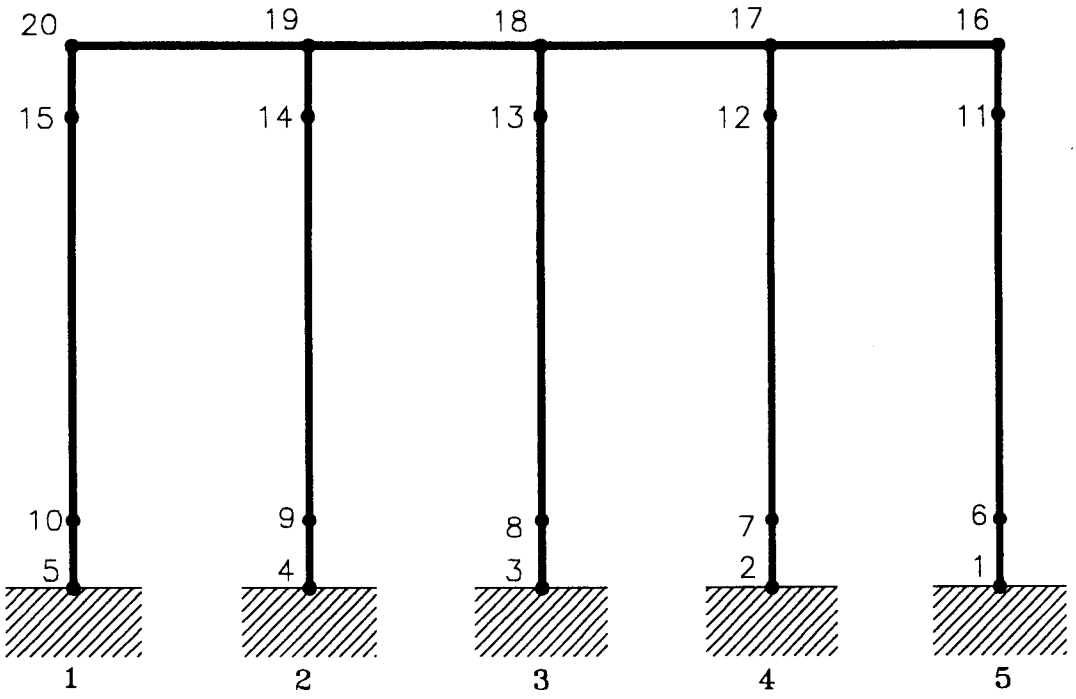

Figure 5.2-4: Structural Model

Table 5.2-1: Structural Properties for Columns and Cross-beam

	Young's Modulus (kN/cm^2)	Poisson Ratio	Unit Weight (kN/cm^3)	Axial Area (m^2)	Shear Area (m^2)	Bending Inertia (m^4)	Torsional Inertia (m^4)
Column	2635	0.18	0.2355×10^{-4}	0.279	0.251	0.003	0.006
Crossbeam	263500	0.18	0.2614×10^{-5}	27.90	25.10	0.300	0.600

Table 5.2-2: Yield Function Constants for the Columns

$M_{z0}(kN\cdot m)$	$P_0(kN)$	P_t / P_0	a_0	a_1	a_2	a_3
207	7174	0.1143	1.0	-7.5969	-9.9330	-1.2261

5.2.4 Retrofitting Combinations

The purpose of this analysis is to compare the results of the time-history analyses using various column retrofit combinations. Based on this comparison, the effectiveness of the retrofit strategies can be evaluated.

The column steel is continued into the cap beam or diaphragm; therefore, at the top of the column, the yield moment and subsequent relatively high ductility probably can be developed. At the bottom, the column steel was lap spliced to the same amount of steel placed in the pile cap. The $35d_b$ long lap splice and No.4 confinement at the bases of columns will not allow the columns to develop fully ductile plastic hinges. Softening will occur once the flexural strength is reached. As discussed in the Moses Lake bridge bent study, it is assumed that the top of the columns will follow the elastic-perfectly plastic model. The same procedure described in Section 5.1.4 is used to decide whether the potential plastic hinge zones on the bases of the columns can develop full strength.

First the concrete tension strength needs to be calculated by equation (4.3-1).

$f_t = 0.33\sqrt{31} = 1.84\ MPa$

The perimeter of the crack surface defined in Section 4.3 may be computed as:

$p = (0.508 - 0.038 \times 2 - 3 \times 0.022)/4 + 2 \times (0.022 + 0.038) = 0.212\ m$

Moreover,

$l_s = 35d_b = 35 \times 0.022 \approx 0.770\ m$

Thus, using equation (4.3-3), the total tensile force on the rupture surface at failure is:

$T_b = 1.84 \times 10^3 \times 0.212 \times 0.770 = 300.36\ kN \rangle A_b f_y = 3.871 \times 10^{-4} \times 310 \times 10^3 = 120.00\ kN$

The above inequality indicates that the longitudinal bars at the bases of the columns can develop their yield force and that the nominal flexural strength may be achieved.

Using equations (4.3-6) and (4.3-9), one may determine whether the potential plastic zones at the bases of the columns can develop high ductility without bond failure.

$$f_l = 0.0005 \times 310 \times 10^3 \times \frac{(0.508 - 0.076) \times 1.290 \times 10^{-4} \times 4}{(0.508 - 0.076)^2 \times 0.305} = 0.607\ MPa$$

$$T_b = 1.4 \times 0.607 \times 10^3 \times 0.212 \times 0.770 = 138.72\ kN\ (1.5 A_b f_y = 180.00\ kN$$

The above inequality means that the bond failure will occur at small ductility and that the flexural strength will then start to degrade to the residual flexural strength even though the nominal flexural strength can be developed. The residual flexural strength may be obtained through the following calculation. The axial force at each base of a column due to the static loading is:

$$P = 0.279 \times 4.572 \times 0.2355 \times 10^{-4} \times 10^6 + 27.90 \times 4.572 \times 4 \times 0.2614 \times 10^{-5} \times 10^6 / 5 = 296.79\ kN$$

The depth of the equivalent rectangular stress block which produces residual moment is:

$$a = \frac{P}{0.85 f_c' b'} = \frac{296.79}{0.85 \times 31 \times 10^3 \times 0.387} = 0.029\ m$$

Thus, using equation (4.3-4), the residual flexural strength is:

$$M_r = 296.79 \times \left(\frac{0.387}{2} - \frac{0.029}{2} \right) = 53.13\ kN - m$$

The ratio between residual flexural strength and the ultimate bending moment may be obtained through first computing the ultimate moment for an axial force of $P = 296.79\ kN$.

$$M_{yp} = 207 \times \left[1 - 7.596 \left(\frac{-29.679}{7174} \right) - 9.933 \left(\frac{-29.679}{7174} \right)^2 - 1.336 \left(\frac{-29.679}{7174} \right)^3 \right]$$
$$= 268.56 kN - m$$

Thus,

$$r_o = \frac{M_r}{M_{yp}} = \frac{53.13}{268.56} = 0.20$$

r_o may be used to define the maximum damage coefficient that the Modified NEABS requires as input.

$$D_{\max} = 1 - r_o = 1 - 0.20 = 0.80$$

To avoid bond failure before nominal flexural strength is reached, the minimum length of lap splice must be met. Using equation (4.3-14), the minimum length of lap splice is:

$$l_{s_{\min}} = \frac{0.25 \times 0.022 \times 310}{\sqrt{31}} = 0.306 m$$

The length of lap splice is $35 d_b = 0.787 m$ and greater than $l_{s_{\min}}$. Hence, the "shearing off" bond failure will not occur.

The above calculation indicates that softening will occur in a potential earthquake after a small ductility is exceeded even though the nominal moment can be reached. The primary reason is the column design deficiencies, i.e., lap splices and inadequate confinement at base plastic hinge zones. The relationship between the moment and ductility at the bases of columns will follow line (4), as shown in Figure 4.3-1. A possible retrofitting effort to overcome these deficiencies is to provide steel jacketing in the potential plastic hinge zone. Figure 5.2-5 shows a cross section at the base of a retrofitted

column. A circular steel jacket is used to provide continuous confinement acting similar to that of a circular column. The space between the steel jacket and the column is filled with grout. The thickness of the steel jacket is designed to insure that the plastic hinge develops a high ductility. The height of the jacket is equal to two times the side length of the square column cross section.

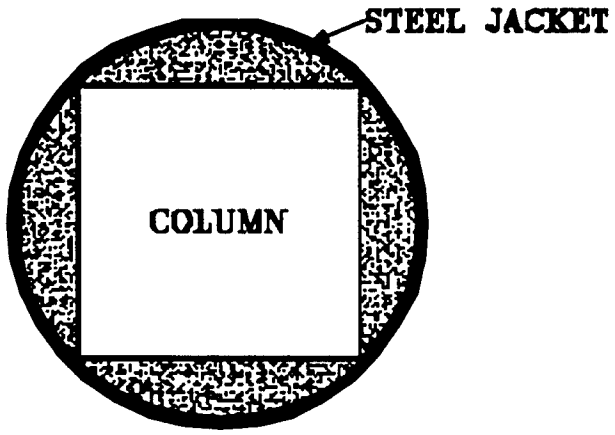

Figure 5.2-5: The Cross Section of A Retrofitted Column

Six retrofitting combinations, as shown in Figure 5.2-6, in the sequence of Case 1 to 6 are analyzed. In this analysis, at the bases of the columns, the hinges with retrofitting are modeled as elastic-perfectly plastic hinges without softening; however, the hinges without retrofitting are modeled as elastic-plastic-softening hinges. On the top, because the column reinforcement is tied directly into the bent cap, the hinges also are modeled as elastic-perfectly plastic hinges. The relationship of moment and curvature is the same as in Figure 5.1-6 for elastic-perfectly plastic hinges, but that of Figure 5.1-7 for elastic

plastic softening hinges. The increase of column stiffness caused by the retrofitting is ignored once again.

The same procedure as described in Section 5.1.4 was used to calculate the critical plastic rotation θ_c and maximum theoretical plastic rotation θ_{max}. These computations are as follows:

$\phi_c = 5.63\phi_y$ (from Marsh's program)

$\phi_{max} = 13.13\phi_y$ (from ϕ_c and Priestley's recommendations)

$l_p = 0.08 \times 228.6 + 9 \times 2.223 = 38.30$ cm. (from equation (4.2-10))

Using equations (2.3-2) and (2.3-3), the critical and max. theoretical plastic rotations are:

$$\theta_c = (\phi_c - \phi_y) l_p = (\mu_{\phi_c} - 1)\frac{M_{yp}}{EI} l_p = (5.63 - 1) \times \frac{268.56}{2635 \times 10^4 \times 3.063 \times 10^{-3}} \times 38.30 \times 10^{-2}$$

$$= 5.89 \times 10^{-3} rad$$

$$\theta_{max} = (\phi_{max} - \phi_y) l_p = (\mu_{\phi_{max}} - 1)\frac{M_{yp}}{EI} l_p = (13.13 - 1) \times \frac{268.56}{2635 \times 10^4 \times 3.063 \times 10^{-3}} \times 38.30 \times 10^{-2}$$

$$= 0.016 \; rad.$$

θ_{cp} and θ_{max} are the parameters that are required as input by the modified version of NEABS.

(1)

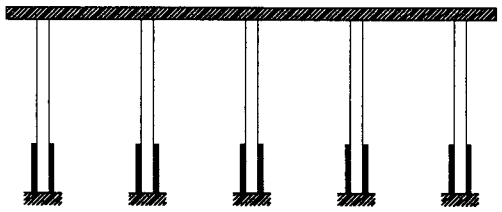

(2)

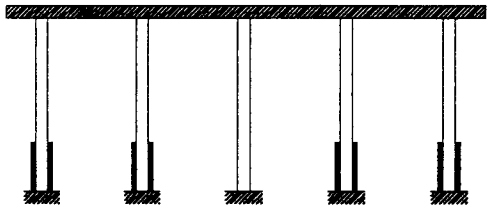

(3)

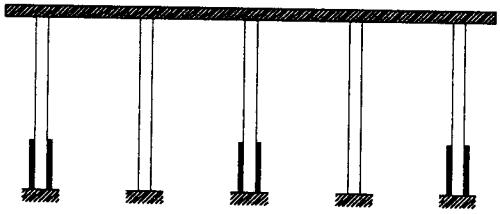

(4)

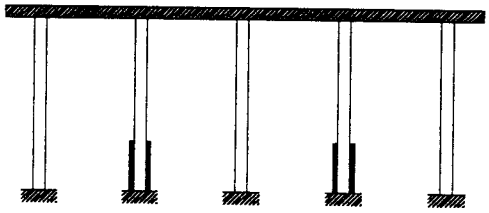

(5)

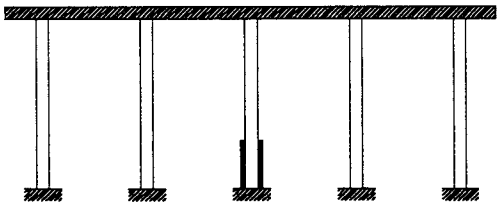

(6)

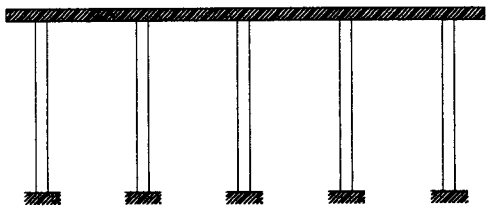

Figure 5.2-6: The Bent Retrofitting Strategies: (1) Case 1; (2) Case 2; (3) Case 3; (4) Case 4; (5) Case 5; (6) Case 6

5.2.5 Seismic Excitation

In this analysis, the S00E component of the El Centro acceleration record of the 1940 Imperial Valley Earthquake (referred to as the "El Centro" record), described in Chapter 5.1.5, is again used as the earthquake record. Because the bridge structure is weaker than that of the Moses Lake bridge, the effective peak acceleration (EPA) is set equal to 0.25g rather than 0.40g, as used before.

5.2.6 Analytical Results and Interpretation

Selected nonlinear time-history analysis results are presented in this section. The performance of various retrofitted combinations is assessed on the the basis of comparisons between responses of the bent structures. The results that are presented were chosen to answer question related to the objectives of the case studies and generally of greatest interest to bridge engineers. The results from the dynamic analysis include the top displacement of the bent, the plastic rotation of plastic hinge at the bases of the columns, internal moment, and displacement-based and rotational ductility demands.

A total of six analyses were performed. No results are reported for Cases 5 and 6 because very large deformations were observed, indicating that the two bent models collapsed during the input earthquake.

5.2.6.1 Displacement

Figure 5.2-7 shows the top displacement response for Cases 1 to 4. At the beginning phase of three seconds, the displacements for all four cases are very similar;

however, an apparent divergence for each case occurred after that time. Compared to Case 1, in which all bases of the columns were retrofitted, the displacement magnitudes of all other cases increase. However, the increased amplitude for each case is different. Because only two columns were retrofitted in Case 4, the increase of the response is the largest. Case 2 had four retrofitted columns; hence, the increase is the least. The increased amplitude for Case 3 is between that of Case 2 and Case 4. The cause of the response increases is the softening and stiffness degradation that occurred in the unretrofitted columns. Naturally, the more columns that are retrofitted, the stronger the structure. In general, the flexural capacity of the bent with all columns retrofitted is the highest. The collapse runs for Cases 5 and 6 had the lowest flexural capacities compared to the other cases.

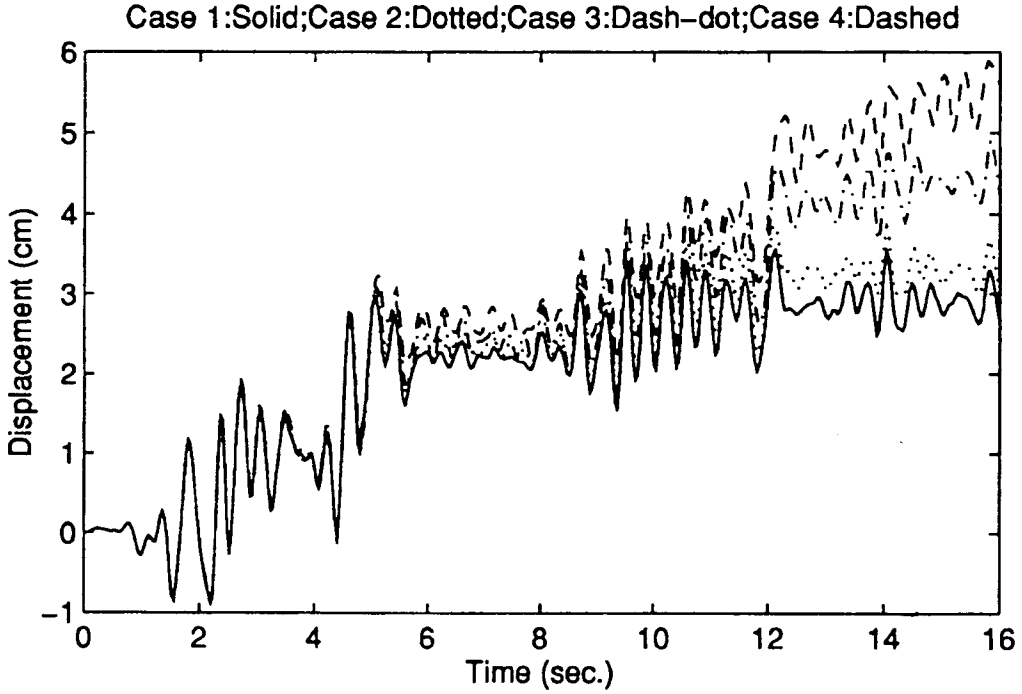

Figure 5.2-7: Time-History Response at Top of the Bent for Different Retrofit Models

To evaluate the benefit from each case, the maximum displacements and corresponding displacement-based ductility demand factors are tabulated in Table 5.2-3. The column top displacement-based ductility demand factor is significantly more severe for Case 4 than for Cases 1, 2 and 3. Compared to Case 1, the increase percentages for other cases are 28%, 33%, and 50%, successively. The increased amplitudes for Cases 2 and 3 are approximately same.

Table 5.2-3: Maximum Displacements (cm) and Corresponding Ductility Demand Factors

	Case No.			
	1	2	3	4
Displacement	3.56	4.54	4.75	5.33
Ductility Demand	3.08	3.93	4.10	4.61

5.2.6.2 Plastic Hinge Rotation

The time-histories of the plastic hinge rotations at the bottom of the columns are given in Figures 5.2-8 through 5.2-12. The columns are identified as columns 1 to 5, starting from the left column of the bent. As discussed in Section 5.2.6.1, the difference in plastic hinge rotations is not obvious in the first three seconds for all four cases. The response time-histories of columns 1 and 5, or columns 2 and 4, for each case are

relatively similar because of symmetry. If the plastic hinge rotation in Case 1 is used as a reference to which the plastic responses are compared, the increase of the plastic hinge rotations for the retrofitted columns in Case 2 is observed to be the smallest, but for the unretrofitted middle column in this case the increase is greater. For Case 3, the time-histories of the plastic hinge rotations for the three retrofitted columns are approximately same, and the aforementioned conclusion also is drawn for the two unretrofitted columns. Because softening has occurred at the bases of the two unretrofitted columns for Case 3, the plastic hinge rotations for these columns are larger than those for the retrofitted columns. The increase of the plastic hinge rotation for each column in Case 4 is the largest, when compared to Case 1. The reason is that the bent for this case only had two retrofitted columns, fewer than the other cases. Thus, flexural softening occurred in the three unretrofitted columns, which caused the redistribution of the earthquake force. The released earthquake force by the softening columns was transmitted to the retrofitted columns and superstructure. Therefore, large plastic rotations were increased, as expected.

Table 5.2-4 gives the maximum plastic rotations θ_{max} and corresponding rotational ductility factors μ_θ at the top and bottom of the columns for each case. One can look at the results from the bottom of the columns shown in this table in two ways. One way is to compare the results from case to case. With a decrease in the number of columns that are retrofitted in a bent, the plastic rotations for all columns in a bent increase. Another way is to compare the results from within a case. If a column was unretrofitted in a case, its plastic rotation is larger than that for the retrofitted column in the same case. Compared with Case 1 for the plastic rotations at the bottom of the columns, there are

approximate rotational ductility increases of 35% for the retrofitted columns and 40% for the unretrofitted column in Case 2, 42% for the retrofitted column and 51% for the unretrofitted columns in Case 3, and 65% for the retrofitted columns and 83% for the unretrofitted columns in Case 4.

Comparing the plastic rotation capacity computed from the moment-curvature analysis program (Marsh, 1991) with the plastic rotational ductility demand factors at the top of the columns in Table 5.2-4, it is found that no softening occurred at the top of the columns. The elastic-perfectly plastic assumption is reasonable for these seismic analyses.

Table 5.2-4: Maximum Plastic Rotations (rad$\times 10^{-3}$) and Corresponding Rotational Ductility Demand Factors at the Top and Bottom of the Columns

			Column No.				
			1	2	3	4	5
Top	Case 1	θ_{max}	5.603	5.623	5.611	5.623	5.623
		μ_θ	4.404	4.419	4.410	4.419	4.419
	Case 2	θ_{max}	7.947	7.662	7.572	7.766	8.098
		μ_θ	6.246	6.022	5.951	6.104	6.365
	Case 3	θ_{max}	8.405	7.817	8.094	7.956	8.522
		μ_θ	6.606	6.144	6.362	6.253	6.698
	Case 4	θ_{max}	8.876	9.291	8.556	9.369	9.113
		μ_θ	6.976	7.302	6.725	7.364	7.162
Bottom	Case 1	θ_{max}	*5.564	*5.589	*5.625	*5.623	*5.636
		μ_θ	*4.373	*4.393	*4.421	*4.419	*4.430
	Case 2	θ_{max}	*7.471	*7.698	7.886	*7.650	*7.449
		μ_θ	*5.872	*6.050	6.198	*6.013	*5.855
	Case 3	θ_{max}	*7.888	8.498	*8.115	8.414	*7.866
		μ_θ	*6.200	6.679	*6.378	6.613	*6.182
	Case 4	θ_{max}	10.220	*9.300	10.50	*9.253	9.994
		μ_θ	8.032	*7.309	8.252	*7.272	7.855

Note: * represents that column under retrofitted condition; $\mu_{\theta_{cap}}$.=13.00 at the top of the column.

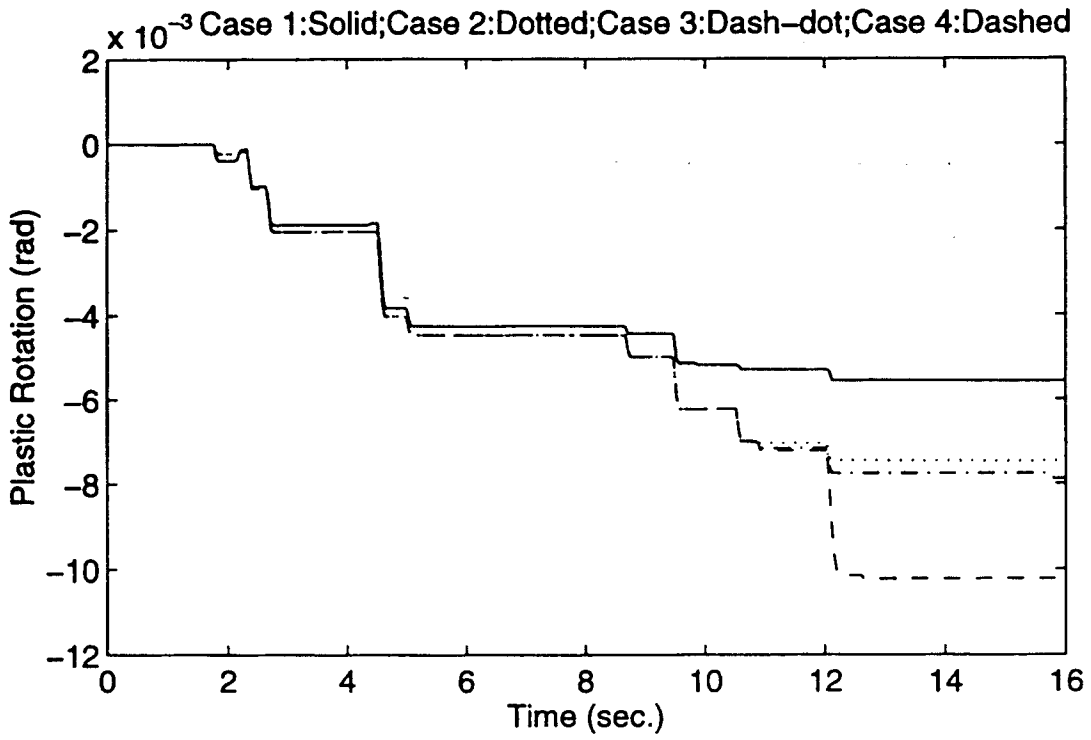

Figure 5.2-8: Plastic Hinge Rotations at the Bottom of Column One for Different Retrofit Models

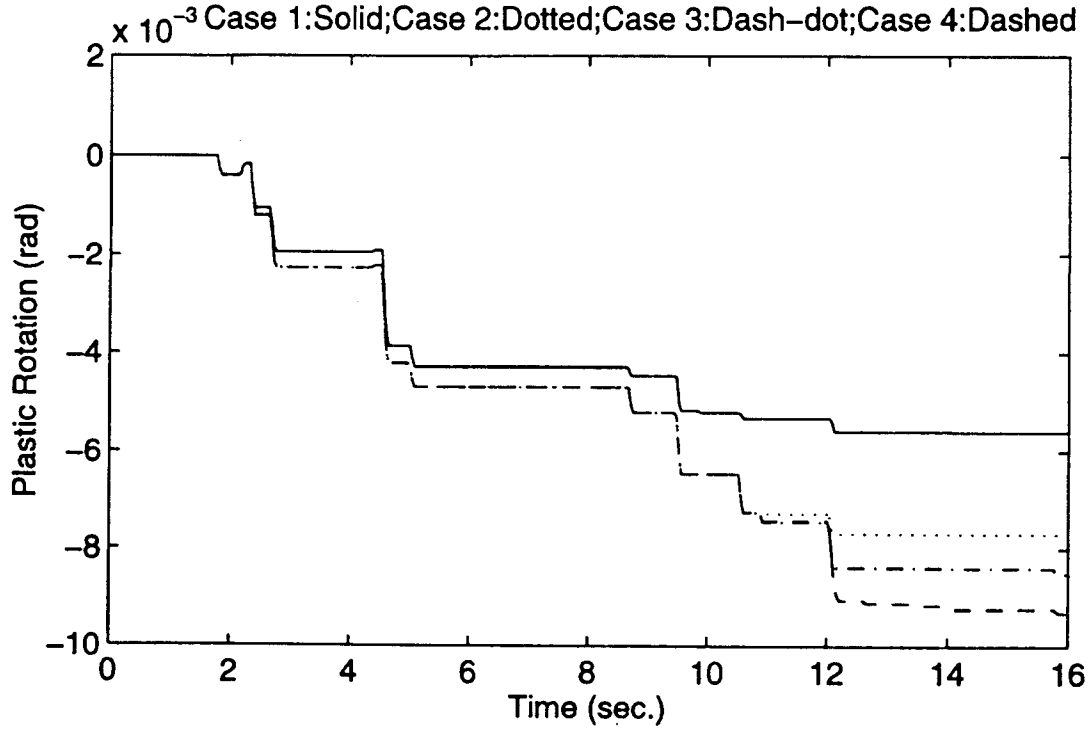

Figure 5.2-9: Plastic Hinge Rotations at the Bottom of Column Two for Different Retrofit Models

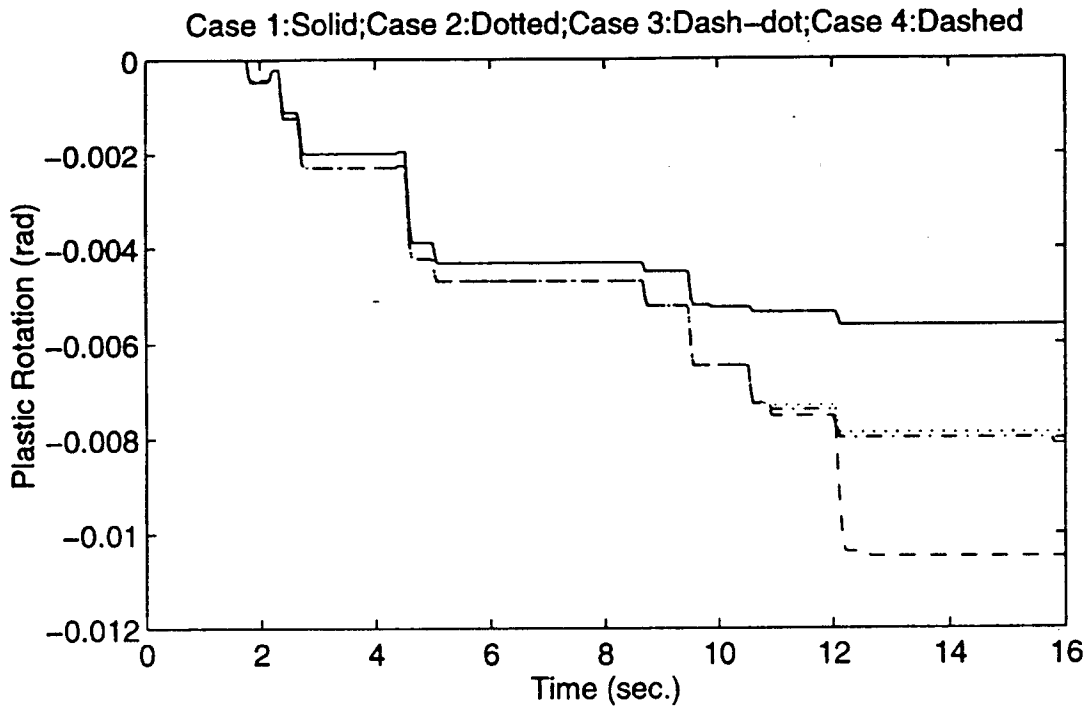

Figure 5.2-10: Plastic Hinge Rotations at the Bottom of Column Three for Different Retrofit Models

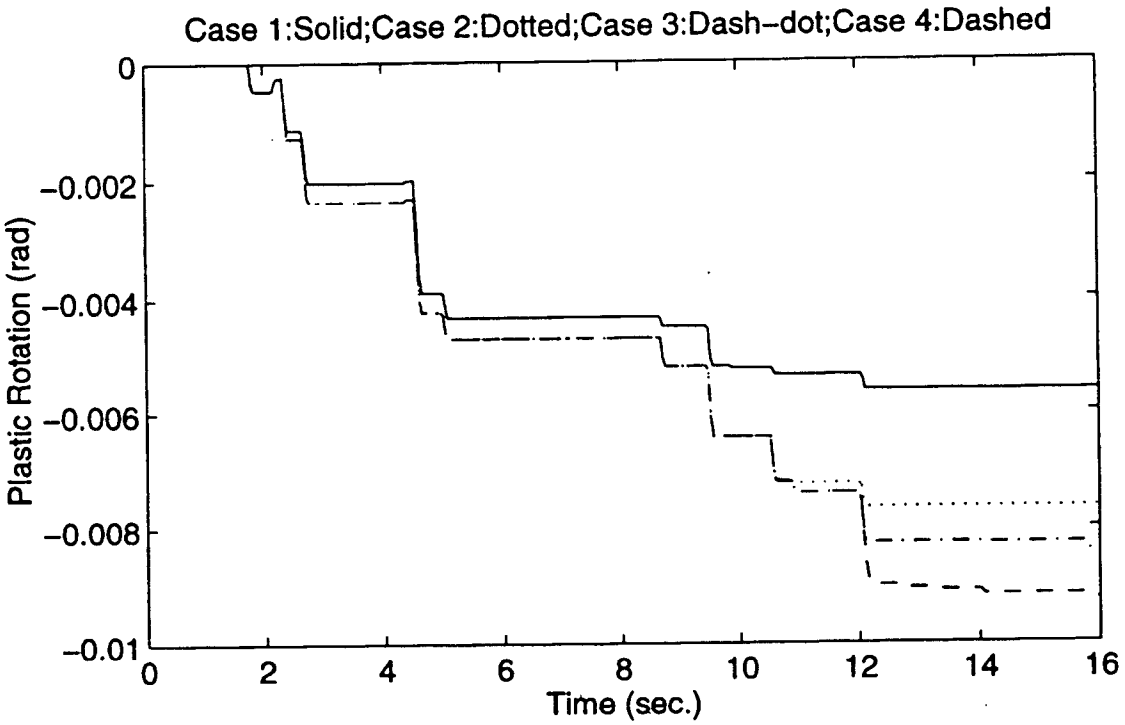

Figure 5.2-11: Plastic Hinge Rotations at the Bottom of Column Four for Different Retrofit Models

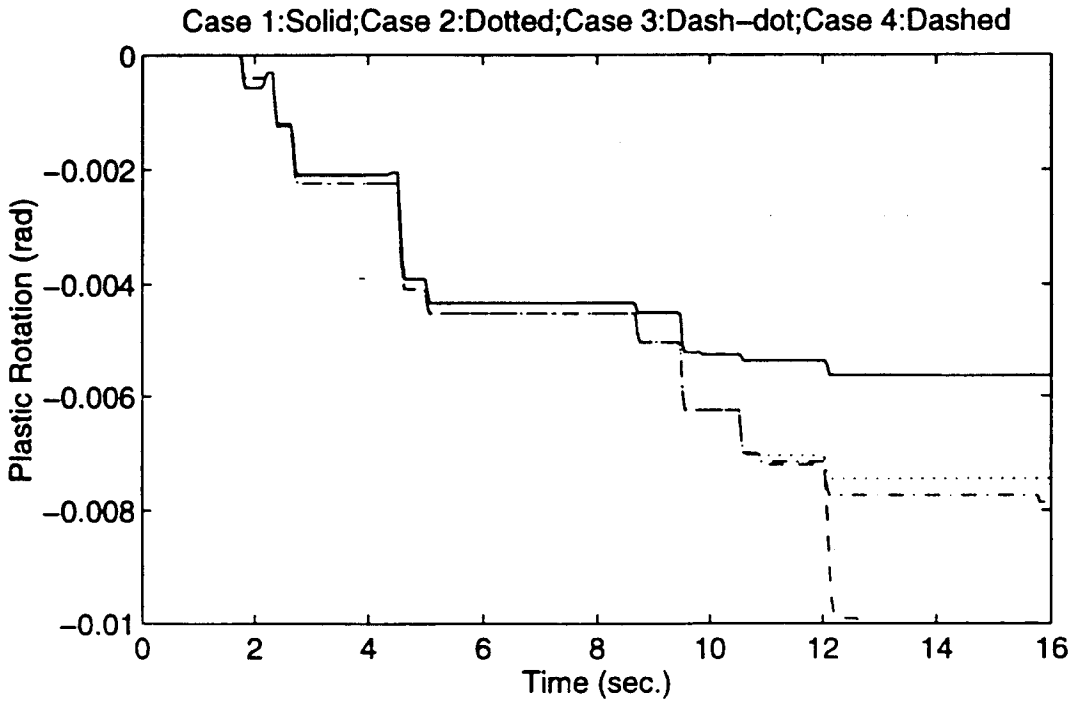

Figure 5.2-12: Plastic Hinge Rotations at the Bottom of Column Five for Different Retrofit Models

5.2.6.3 Moment

Figures 5.2-13 through 5.2-17 show the moment time-histories at the bottom of each column for different cases. From these figures, it can be concluded that the softening for the unretrofitted columns in each case occurred after approximately three seconds. However, the level of damage was not the same from case to case. The worst damage is observed in the three unretrofitted columns for Case 4, in which the residual flexural strength was nearly reached. Therefore, the flexural damage in the unretrofitted columns was relatively serious. Although some flexural capacity was lost in the unretrofitted columns for Cases 2 and 3 due to the softening, a relatively significant part was still retained.

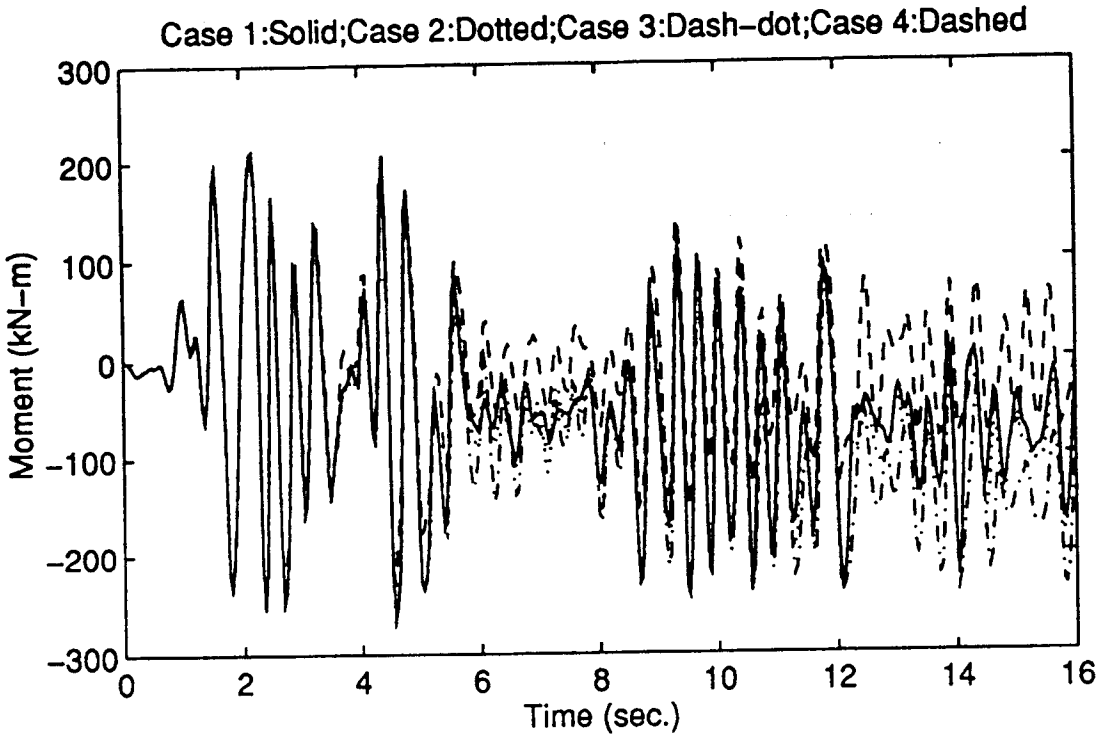

Figure 5.2-13: Moment Responses at the Bottom of Column One for Different Retrofit Models

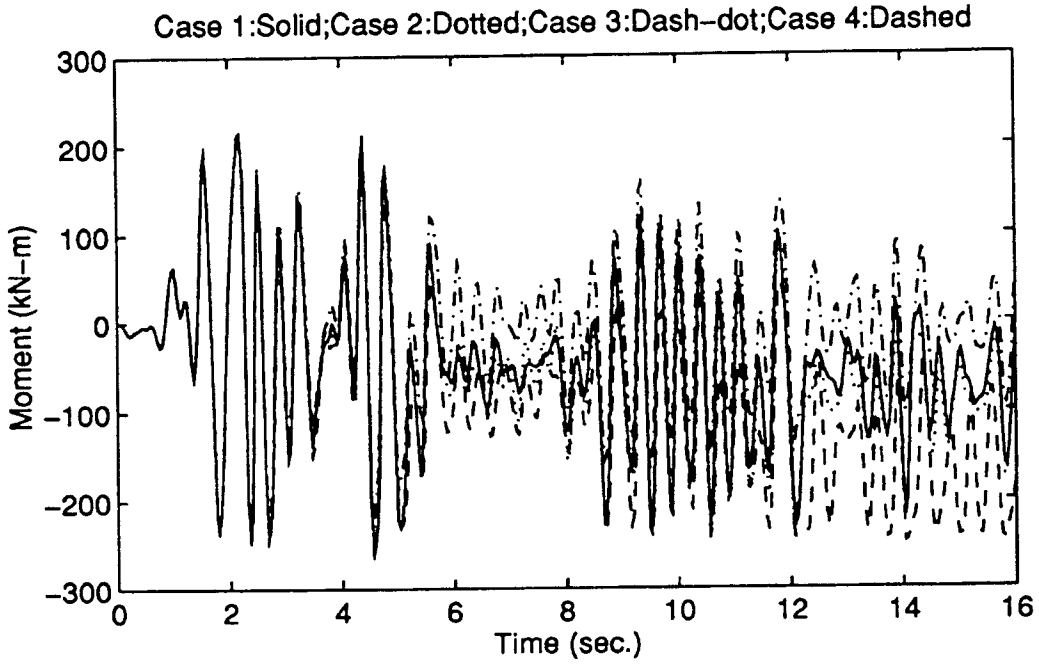

Figure 5.2-14: Moment Responses at the Bottom of Column Two for Different Retrofit Models

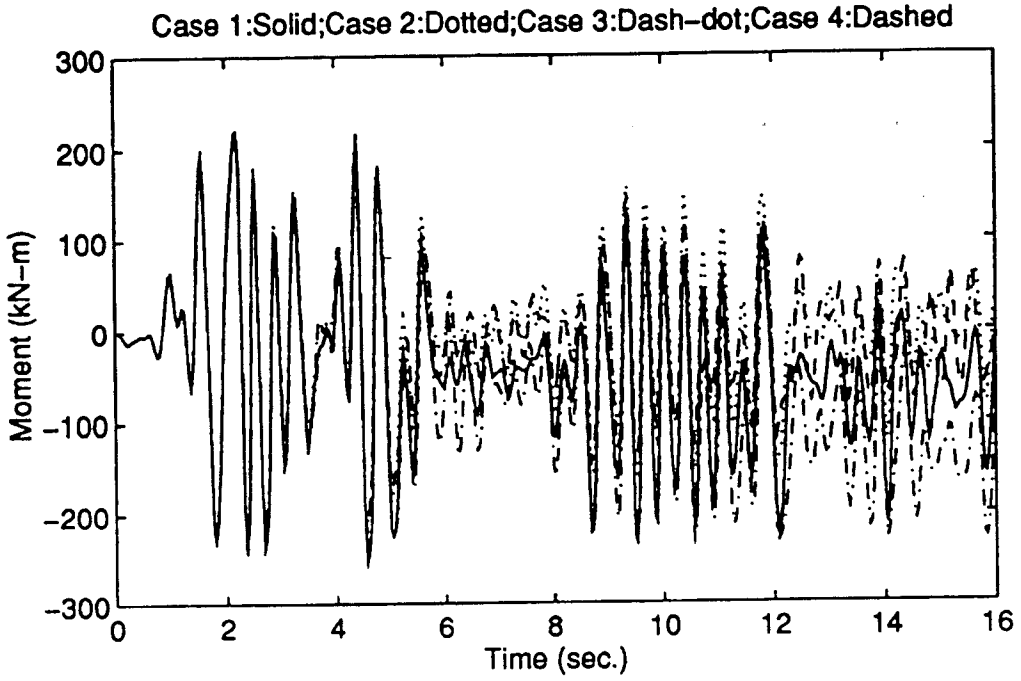

Figure 5.2-15: Moment Responses at the Bottom of Column Three for Different Retrofit Models

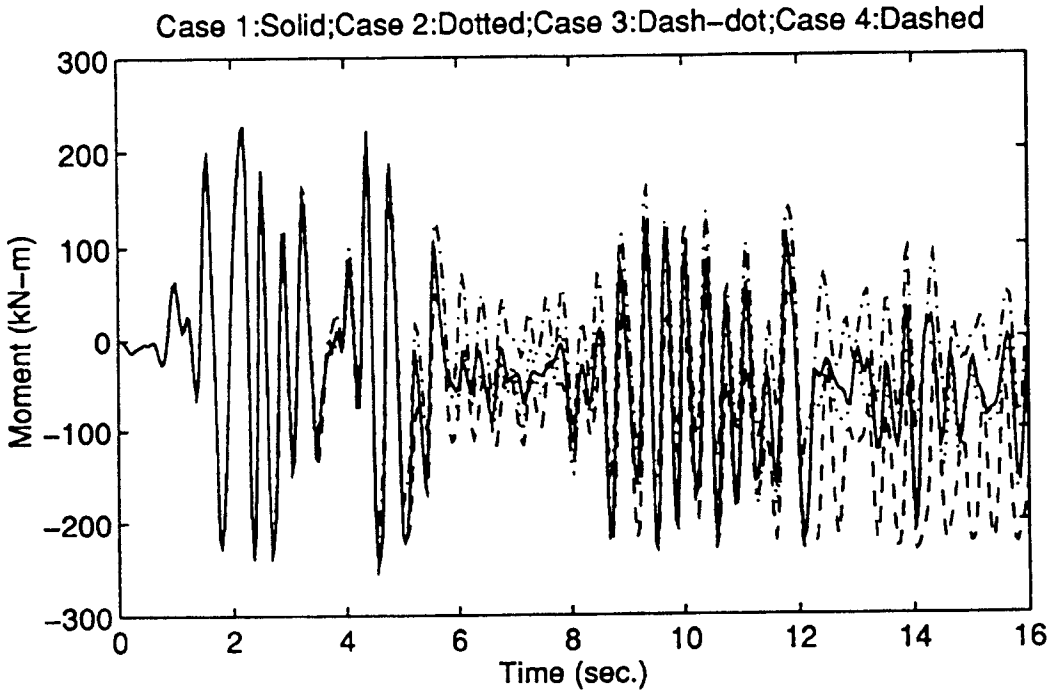

Figure 5.2-16: Moment Responses at the Bottom of Column Four for Different Retrofit Models

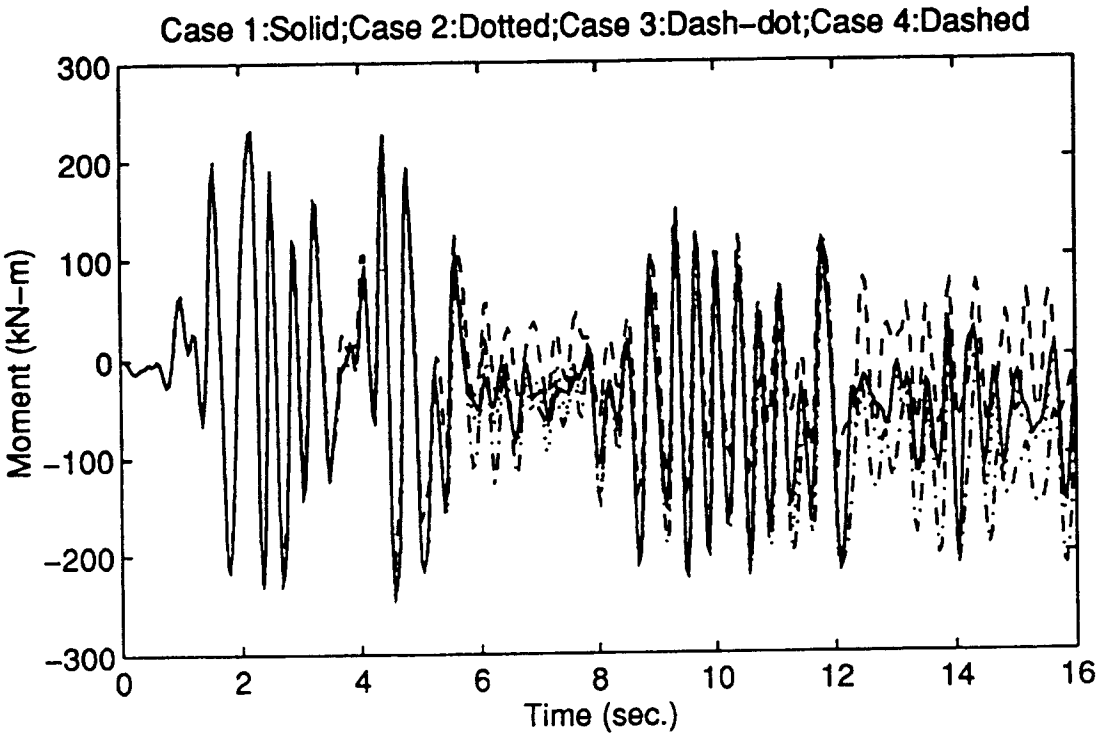

Figure 5.2-17: Moment Responses at the Bottom of Column Five for Different Retrofit Models

5.2.7 Conclusions and Recommendations

Through the six case studies, there were repeated indications that the seismic response of a bridge may be significantly influenced by flexural softening and degradation of stiffness. From the analysis, it is found that the unretrofitted bent (i.e. Case 6) would collapse during the input earthquake because of the pre-1971 non-ductile column designs. Although many retrofit combinations are available to decrease the seismic response, their effectiveness needs to be evaluated. The retrofitting strategy used in Case 5, in which

only one column was retrofitted, was not effective in avoiding the bridge bent failure because excessive deformation was observed in this case.

The deformation response from Case 4 is the largest among the four viable case results. However, as discussed in Section 5.2.6.3, because of the extremely large plastic deformation around the bases of the columns, most of the flexural capacity for the three unretrofitted columns was lost. The damage is relatively severe. Because most columns (i.e. three columns out of five columns) in Case 4 were in the severely unacceptable damage situation, the retrofit strategy used in Case 4 is not recommended. When economic and time considerations are main factors in choosing retrofit strategies, the retrofit strategy used in Case 3 is an effective one and may be considered. Of course, if the financial situation allows, the full retrofit measure used in Case 1 and nearly full retrofit strategy used in Case 2 still are the choices that designers should consider.

Chapter 6

Seismic Analysis of Bridge with Expansion Joint Retrofitting

6.1 Mercer Slough Highway Bridge (Three-Dimensional Structural Analysis)

In this chapter, a three-dimensional analysis of the Mercer Slough bridge was conducted to investigate the performance of longitudinal cable restrainers at the expansion joints. To complete the objectives, the restrainers were first designed according to current design methodology used by Caltrans. Then, the expansion joint element within NEABS was used to model the behavior of the joints. The focus of the study was to evaluate the relative displacements at the expansion joint hinge, restrainer stresses, and earthquake force redistribution caused by the installation of the restrainers.

6.1.1 Introduction

Since the San Fernando earthquake in 1971, restrainers have been generally incorporated in highway bridges in California and other states to prevent superstructures from falling off their support seats during major earthquakes. It may be said that this retrofit measure is the oldest and most successful for bridge retrofitting. However, many aspects of the restrainer behavior, including the design method and influence on bridge structural response, have not been studied in detail. As reported by Cooper and Buckle (1995) in reviewing the Kobe earthquake, the force transmitted by restrainers should be applied to the strongest structural members rather than the weakest ones. Therefore, the

correct and effective installation of restrainers is critical to avoid bridge collapse during earthquakes.

6.1.2 Properties of the Bridge

Most of the bridge properties, especially the substructure properties, were discussed in Section 5.2; therefore, they will not be repeated again. The following two sections will mainly describe the properties of the superstructure, the expansion joints, and the bearings that support the superstructure.

6.1.2.1 Superstructure

A cross-section of the 83.8-cm deep superstructure is shown in Figure 6.1-1. The superstructure consists of a 15.2-cm-thick slab and nine 40.6-cm-wide webs spaced at about 2.29 meters center-to-center. As described in Section 5.2, the bents are monolithic with the superstructure, tying directly into a transverse diaphragm in the T-girder system except at the expansion joints. Table 6.1-1 gives the superstructure properties.

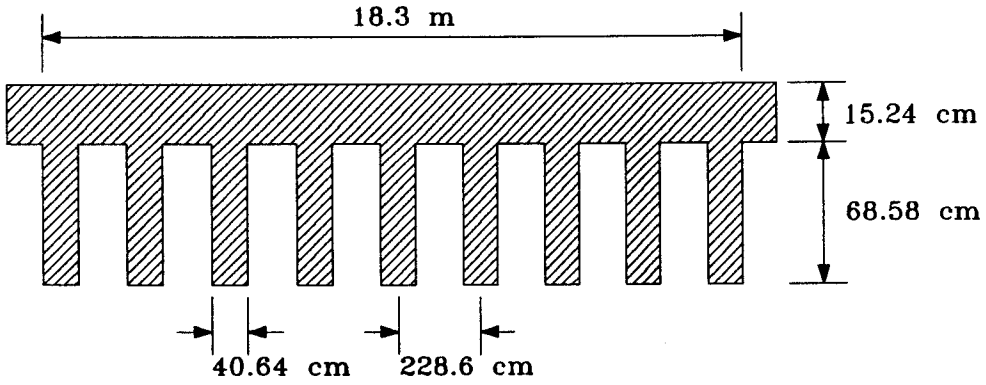

Figure 6.1-1: Cross Section of the Superstructure

Table 6.1-1: Bridge Superstructure Properties

A	I_x	I_y	I_z	E	A_{sy}	A_{sz}	f_c'	ρ
5.36	0.146	1.70×10^{2}	0.429	2.63×10^{7}	2.37	3.07	3.10×10^{7}	0.24×10^{2}

Note: A_{sy} and A_{sz} represent the shear areas about y and z-axes, respectively, and all units are kN, and meter.

6.1.2.2 Expansion Joints and Bearings

Figure 6.1-2 shows a typical expansion joint. Usually, there is a joint at every fourth bent. At the expansion joint, one span inlays the bent cap, and the other span is supported by a rocker located on the bent cap. The rocker allows the span to have a small amount of rotation and longitudinal joint translation before adjacent spans contact each other. The gap between the two adjacent spans is approximately 2.54 cm.

There is a ledge (Figure 6.1-2) on the bottom of each girder web for the span that is joined to the bent cap, and the intruding part inlays the bent cap. The space between the web and bent cap is filled. Moreover, the reinforcement from the bent cap is directly tied into the web. The relatively strong connection between the span and bent cap exists because the ledge restricts the longitudinal translation of the span. For the nonlinear analysis requirements, the connection may be idealized as a longitudinal spring. The equivalent spring stiffness due to the ledges is estimated by the shear strength provided by the concrete. The following is basis for the estimation.

The cross sectional area for each ledge is approximately equal to:

$$A_s \approx 12.7\times40.64 = 516.13\ cm^2$$

Neglecting the shear strength provided by the bars tying into the ledge, the shear strength attributed to the concrete for each ledge is:

$$V_c = 0.166\sqrt{f_c'}A_s = 0.166\sqrt{31}\times 516.13\times\frac{1}{10000}\times 10^3 = 47.70\ kN$$

Thus, the corresponding shear strain is

$$\gamma_c = \frac{V_c}{A_s G} = \frac{2(1+v)V_c}{EA_s} = \frac{2(1+0.18)\times 47.70}{2.64\times 10^7 \times 516.13\times 10^{-4}} = 8.26\times 10^{-5}$$

As shown in Figure 6.1-2, the depth of the ledge that inlays the bent cap is approximately taken as $h_l \approx 3.81\ cm$. Therefore, the longitudinal deformation of the ledge is:

$$\Delta l = \gamma_c h_l = 8.26\times 10^{-5}\times 3.81 = 3.147\times 10^{-4}\ cm$$

Based on the shear strength and corresponding longitudinal deformation, one may obtain the longitudinal stiffness for each ledge:

$$k_l = \frac{V_c}{\Delta l} = \frac{47.70}{3.147\times 10^{-4}} = 151573\ kN/cm$$

Because there are nine webs for the T-girder system, the total stiffness is:

$$k_l' = 9k_l = 9\times 151573 = 1364157\ kN/cm$$

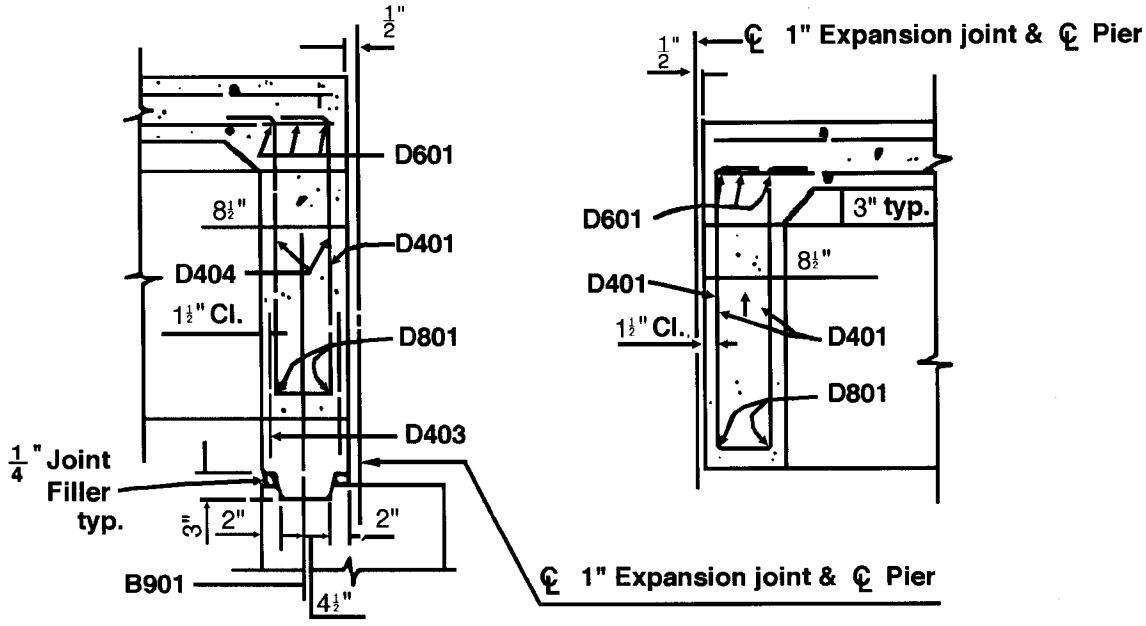

Figure 6.1-2: Expansion Joint and Elevation (from Cofer, *et al.*, 1994)

6.1.3 Retrofitting

Retrofitting of this bridge consisted of tying two adjacent girders together with four steel cable units. The cable is 0.75 galvanized steel wire rope (6 strands with 19 wires per strand), which is one of two standard materials used in current Caltrans restrainer design. The properties and location of the retrofit restrainer units are included in Table 6.1-2. The equivalent tensile stiffness of the restrainer for each span was computed and tabulated using the modulus of elasticity, yield strength, and length for the cable.

Table 6.1-2: Properties of the Retrofit Restrainer Units

Number of Restrainer Units	4
Number of Cables Per Unit	2
Transverse Location of Units (m)	±3.05, ±6.10
Length of Restrainer Units (m)	1.83
Yield Strength of the Cable (kN/cm^2)	143
Modulus of Elasticity of the Cable (kN/cm^2)	12402
Cross Section Area of the Cable (cm^2)	1.432
Total Tensile Stiffness Per Restrainer (kN/cm)	193.9
Total Tensile Capacity Per Restrainer (kN)	409
Restrainer Gap ($in.$)	0

6.1.4 Structural Model

Two three-dimensional models were used for the nonlinear time-history analyses, one each for the unretrofitted and the retrofitted superstructure conditions. As reported by McLean and Cannon (1994), because the actual bridge is over 80 spans, it is likely that abutment effects will be significant only in a few spans near each end. Therefore, a model of twenty spans was selected for the nonlinear analysis. These spans are typical of the geometry in the center region of the bridge so that the results were not dependent on the modeling of the abutments.

Figure 6.1-3 shows the structural model. Expansion joints were incorporated at the two ends and between each four-span section. The boundary conditions at both ends were designed to be the same as those in the report by McLean and Cannon (1994), in which the bridge is allowed to move longitudinally, but transverse motion is restricted. Rotational motion is also allowed. Three types of elements provided in NEABS were used to model the bridge. The monolithic bents were modeled as continuous frames. The superstructure and crossbeam were simply modeled using elastic beam elements, and the structural properties for the superstructure were included in Table 6.1-1. Except for at the expansion joints, the connection between the superstructure and bent cap was rigid. The columns were modeled as nonlinear column elements with an elastic-perfectly plastic assumed behavior. These elements had the properties that were included in Tables 5.1-1 and 5.1-2. The base of each column was assumed fixed at the footing.

Each expansion joint at the bent was idealized by three expansion-joint elements placed at each bent, as shown for a typical bent in Figure 6.1-4. The element numbered 1

in this figure was placed between the bent cap and the end of the left span to model the "rocker" connection effect. Element 2 in this figure was placed between the bent cap and the end of the right span to model the "ledge" connection effect. These elements provided for vertical support and relative movements between the bent cap and the spans. Element 3 in the figure was placed between the ends of the two adjacent spans and was used to model the effects of the two spans impacting one another because of closure of the gap. As suggested by Imbsen, *et al.* (1979), the impact spring for the purposes of modeling impacting of the superstructure was assumed to have the axial stiffness of the superstructure. All properties of the nonlinear expansion joint elements used to idealize the connection at the bents with retrofitting and without are tabulated in Table 6.1-3. The difference between a non-retrofitted bridge and a retrofitted one is the addition of tie-bar element properties for the retrofitted bridge.

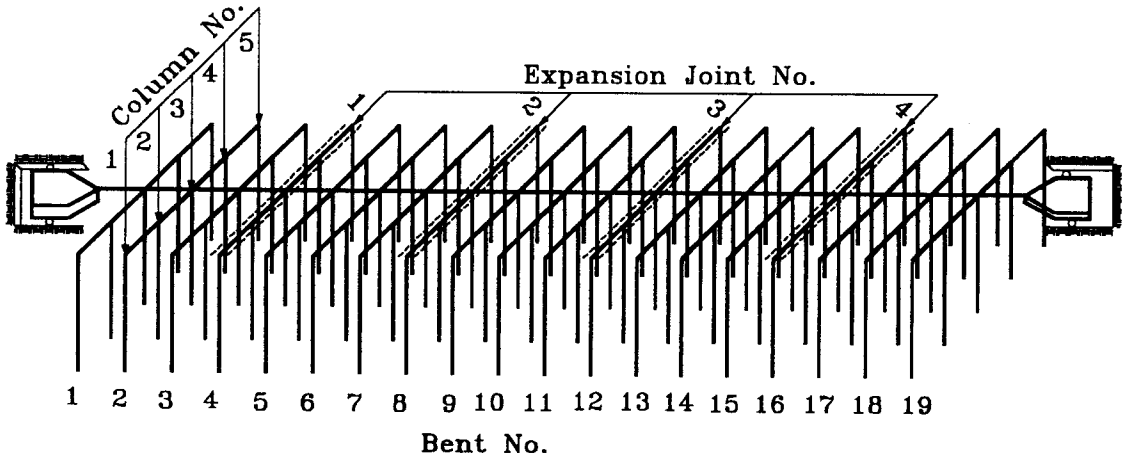

Figure 6.1-3: Three Dimensional Bridge Model

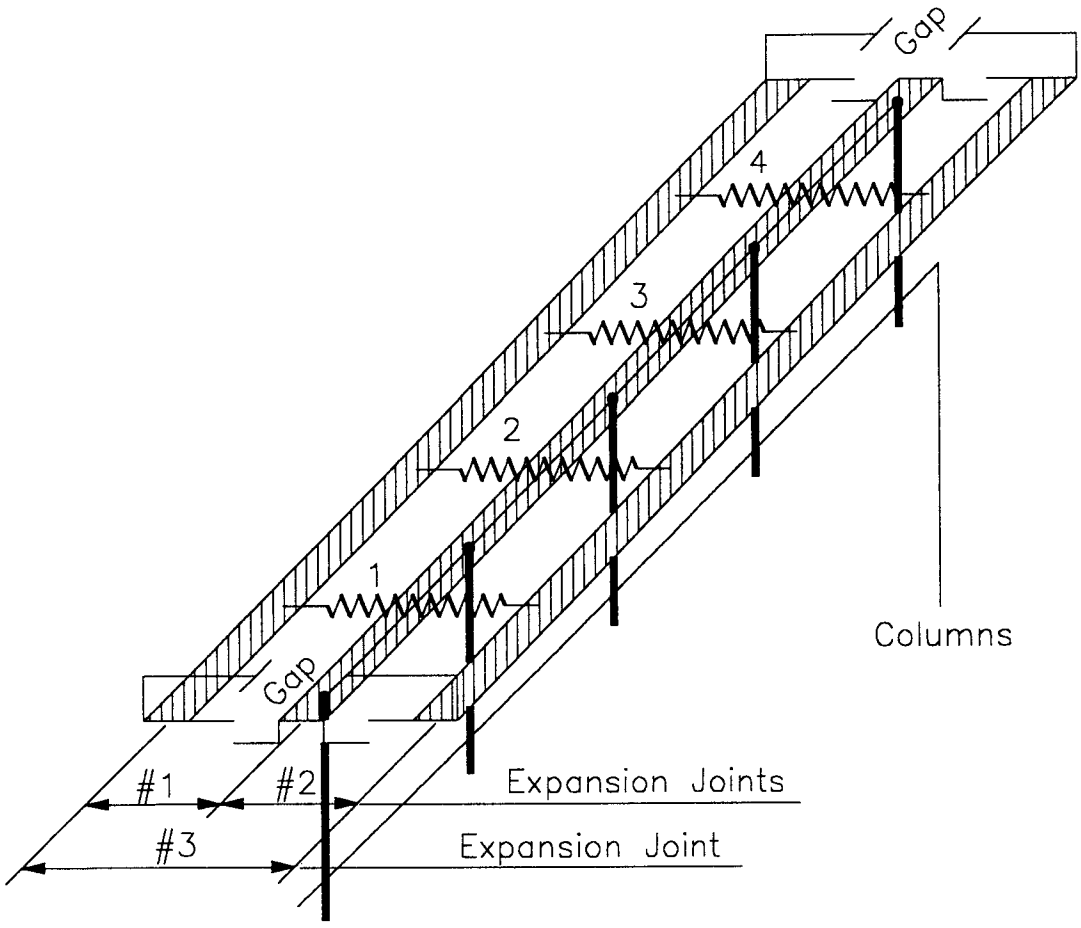

Figure 6.1-4: Bearing Idealization of the Two Adjacent Spans at the Bent Using Expansion Joint Elements

Table 6.1-3: Input Parameters for Nonlinear Hinges Used to Model the Expansion Joints at the Bents

	Support	Hinge	Impacting Hinge	Cable
Bearing Type	Ledge	Rocker	NA	NA
Element Width (m), d	18.30	18.30	18.30	NA
Skew ($^\circ$)	0.00	0.00	0.00	NA
Impacting Spring Stiffness (kN/cm), k_I	1.00	1.00	1.52×10^4	NA
Bearing Friction Stiffness (kN/cm), k_F	1.00	1.00	1.00	NA
Coefficient of Friction of Bearing, c_F	0.00	0.02	0.00	NA
Stiffness of Tie Bar (kN/cm), k_T	0.00	000	0.00	193.90
Tie Bar Yield Force (kN), Y_T	0.00	0.00	0.00	409.00
Tie Bar Gap (cm), G_T	0.00	0.00	0.00	0.00
Seat Gap (cm), G_S	0.00	0.00	1.00	NA
Number of Tie Bars	0	0	0	4
Vertical Stiffness (kN/cm), k_3, k_6	4.03×10^6	4.03×10^6	0.00	NA
Longitudinal Stiffness (kN/cm), k_1, k_4	7.70×10^4	0.00	0.00	NA
Transverse Stiffness (kN/cm), k_2	3.87×10^5	3.87×10^5	0.00	NA
Rotational Stiffness (kN/cm), k_5	0.00	0.00	0.00	NA

All symbols that are shown in Table 6.1-3 are included in the NEABS User Manual. For conservatism, in the nonlinear analysis, the stiffness of the longitudinal spring for ledge bearing is taken as one tenth of the calculated value of Section 6.1.2.2 because of the imperfect connection between the deck and bent cap.

Damping constants proportional to mass and stiffness were computed using Equation 5.1-2 as described in Section 5.1-3. The fundamental period (0.33 sec.) was used to calculate damping constants corresponding to a five-percent damping ratio.

6.1.5 Seismic Excitation

To evaluate the performance of the restrainers, the S00E component of the El Centro record of the 1940 Imperial Valley Earthquake, described in Section 5.1.5, was applied in the transverse direction with respect to the centerline of the bridge. The effective peak acceleration was 0.25g.

6.1.6 Analytical Results and Interpretation

The results from two analyses are presented in this section. The first analysis was for the unretrofitted superstructure, in which no restrainers were installed, and the second analysis was for the retrofitted superstructure, in which the restrainers were installed at the expansion joints. The results presented are those selected relevant to the objectives of the case studies and those believed to be of greatest interest to bridge designers. The pertinent results reported in the following sections include the relative longitudinal displacements at the expansion joints, tensile forces in the restrainers, and the column moments and shears.

6.1.5.1 Time-Histories of the Joint Openings and Maximum Deck Separations

The expansion joints in the bridge structural model are identified as expansion joints 1 to 4, starting from the expansion joint on the extreme left, as shown in Figure 6.1-3. The time-history responses of the relative longitudinal displacements at the expansion joints for the left and right edge-of-deck are shown in Figures 6.1-5 through 6.1-8. When the relative displacement is positive, it indicates that the two adjacent decks are opening;

when negative, it indicates that the two adjacent decks are closing. The maximum deck separations at both edges of the expansion joints are tabulated in Table 6.1-4. It should be noted that the two maximum deck separations for each expansion joint did not necessarily occur at the same time. From Figure 6.1-5b, one can see that the closure of the joint gap for the right edge-of-deck at expansion joint 1 occurred after about six seconds for the unretrofitted condition. That means that there was a collision between the two neighboring decks during this earthquake. At the same time, relatively large separation for the left edge-of-deck at this expansion joint is observed (see Figure 6.1-5a). The large joint opening is much more significant considering the available seat width of only 7.62 cm for the expansion joints. In addition, relatively large closing and opening also were observed for left and right edge-of-deck at expansion joint three for the unretrofitted condition (see Figure 6.1-6), and the gap for the left edge-of-deck is nearly closed.

The relative displacements at expansion joints 2 and 4 for the unretrofitted condition are not significant when compared to those for expansion joints 1 and 3, and no collision between decks was found. As indicated in these figures and Table 6.1-4, all of the separations at the edges are reduced by the retrofitting. Substantial reductions in the separations are observed for expansion joints 1 and 3.

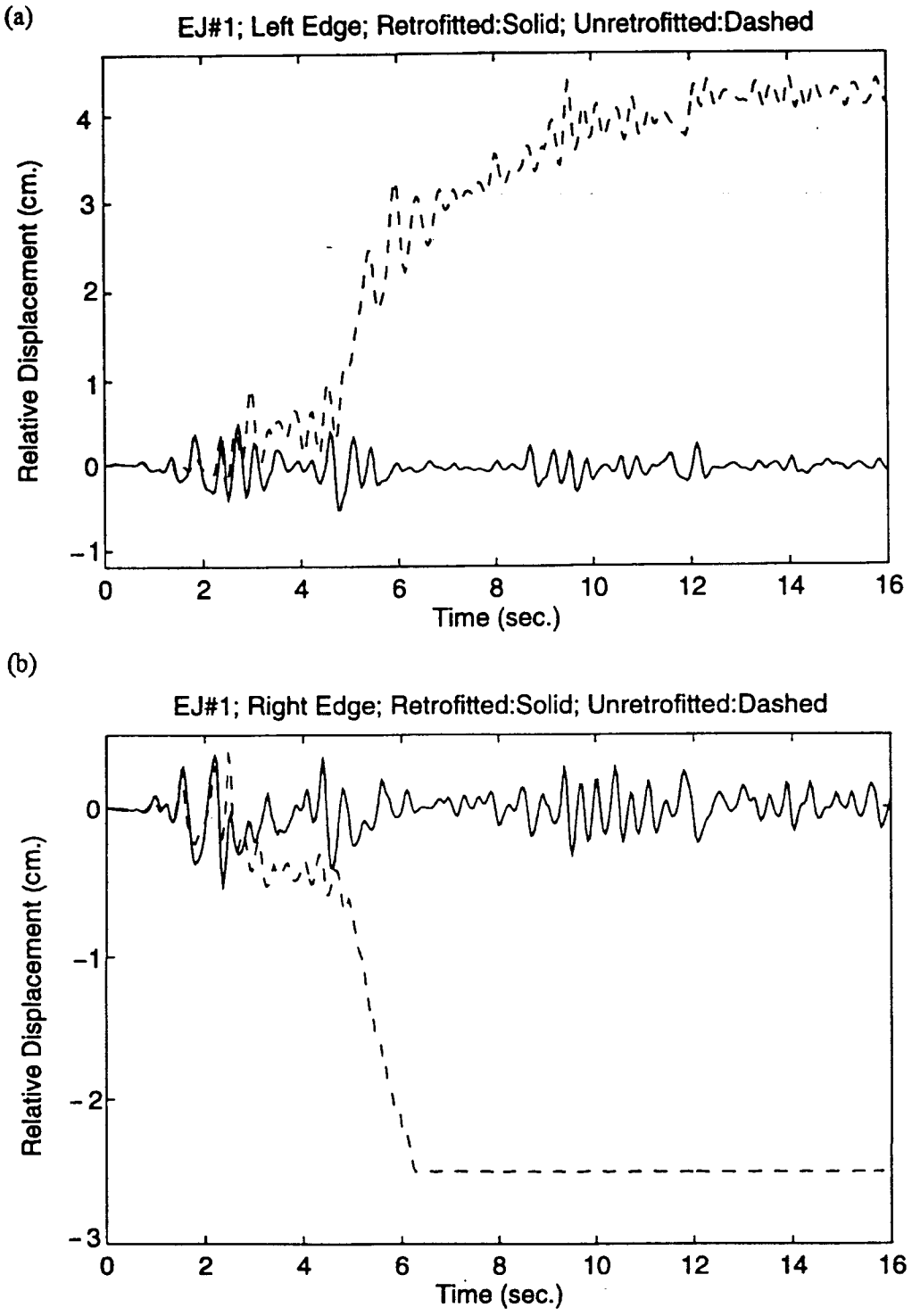

Figure 6.1-5: Hinge Relative Displacements of Expansion Joint 1: (a) Left Edge-of-Deck; (b) Right Edge-of-Deck

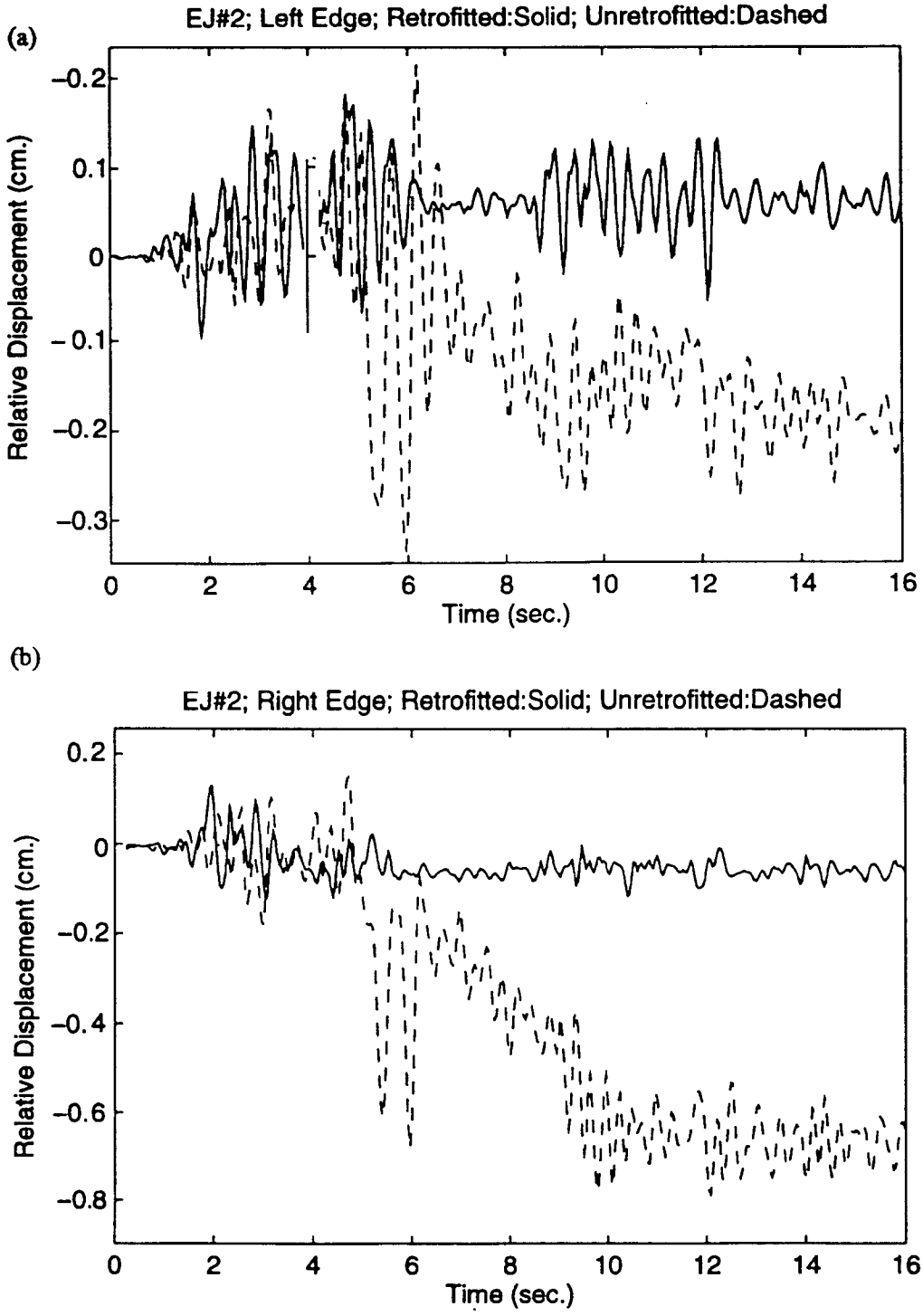

Figure 6.1-6: Hinge Relative Displacements of Expansion Joint 2: (a) Left Edge-of-Deck; (b) Right Edge-of-Deck

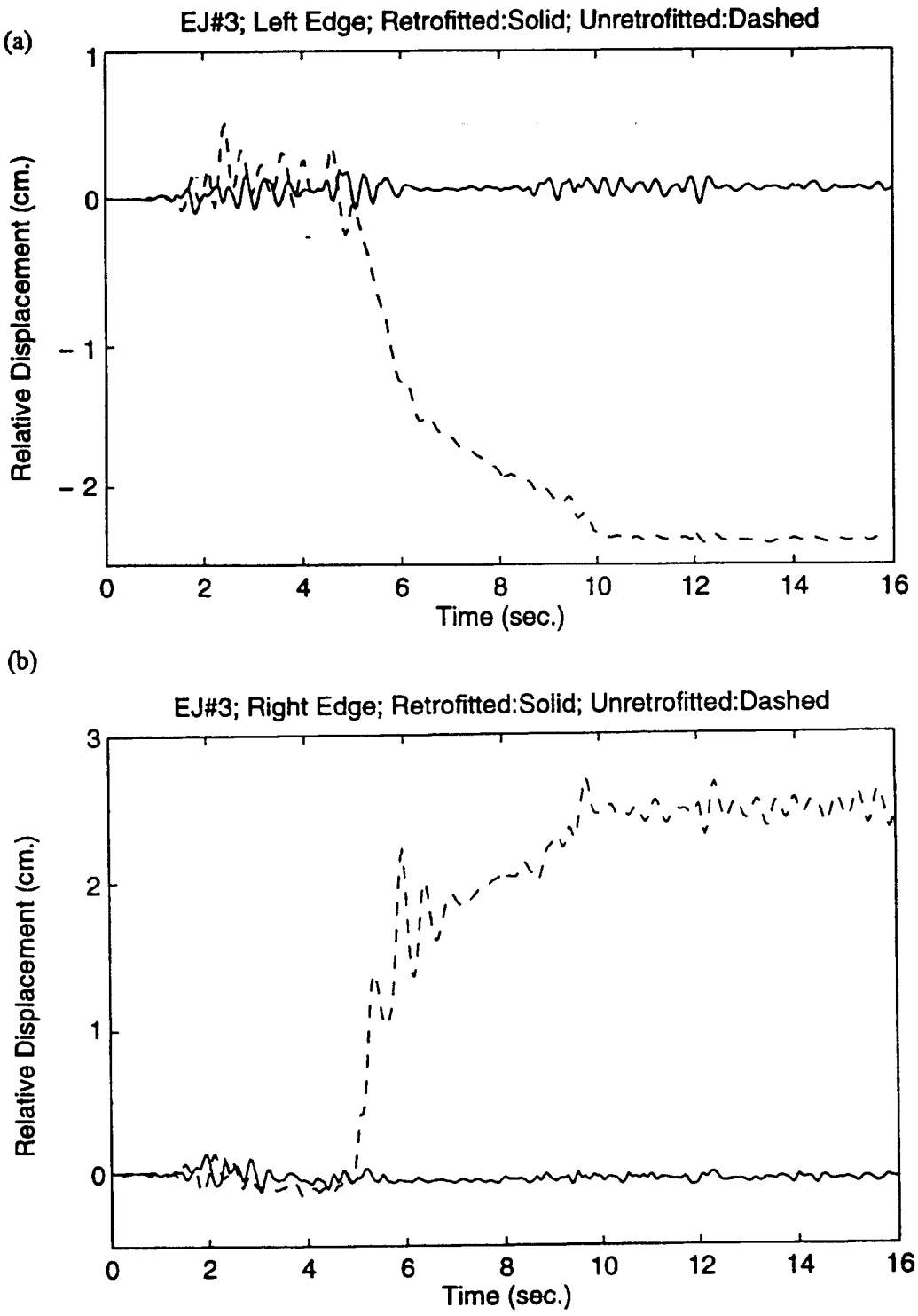

Figure 6.1-7: Hinge Relative Displacements of Expansion Joint 3: (a) Left Edge-of-Deck; (b) Right Edge-of-Deck

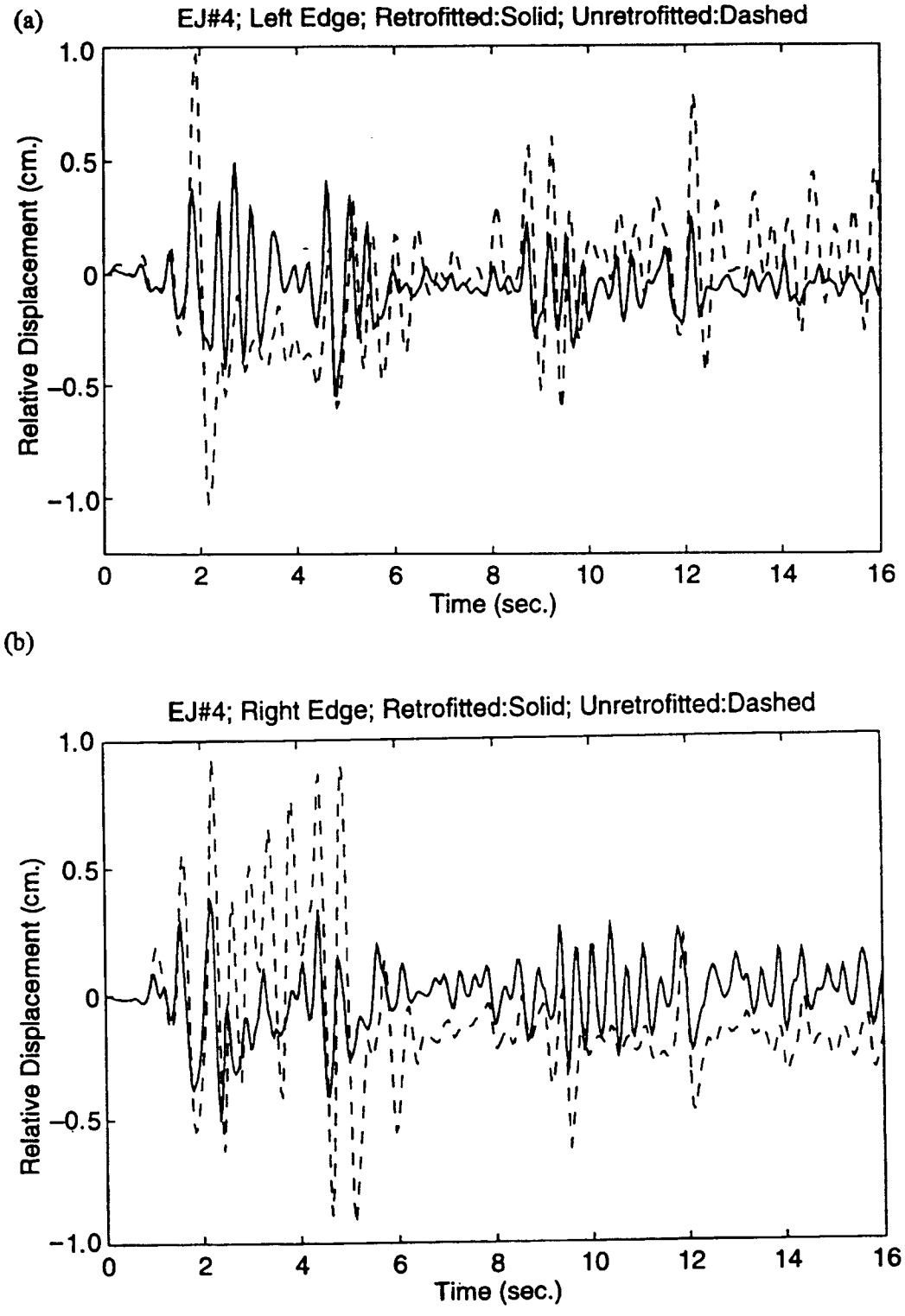

Figure 6.1-8: Hinge Relative Displacements of Expansion Joint 4: (a) Left Edge-of-Deck; (b) Right Edge-of-Deck

Table 6.1-4: Maximum Separation (cm) at the Expansion Joints

	EJ#1		EJ#2		EJ#3		EJ#4	
	Left	Right	Left	Right	Left	Right	Left	Right
Unretrofitted	4.7854	0.3609	0.2317	0.1547	0.5161	2.7407	0.9822	0.9523
Retrofitted	0.5037	0.3637	0.1905	0.1349	0.1920	0.1349	0.4890	0.3708

Left: Left Edge-of-Deck; Right: Right Edge-of-Deck

6.1.5.2 Time-Histories of the Restrainer Forces and Maximum Restrainer Forces

Plots of the time-histories of responses for the restrainer forces are included in Figures 6.1-9 through 6.1-12. Four cable forces on each expansion joint are shown on a plot. As assumed in Chapter 3, the tie bar is activated only when the adjacent decks are opening. That means that the cables had no compressive stiffness. From these figures, it also can be seen that the restrainer forces are only tensile. The cables were designed in this study with a yield force of 409.0 kN (Table 6.1-3). The maximum value of the restrainer force for each cable is tabulated in Table 6.1-5. No cable was found to yield during the earthquake. All the maximum restrainer forces were well below the yield strength of 409.0 kN.

Table 6.1-5: Maximum Restrainer Forces (kN)

		Cable No.			
		1	2	3	4
Expansion Joint No.	One	47.339	28.648	45.072	71.387
	Two	21.554	21.678	26.123	31.097
	Three	21.585	22.621	27.390	31.302
	Four	48.806	28.541	44.850	71.076

Note: The cable number in each expansion joint is shown in Figure 6.1-4.

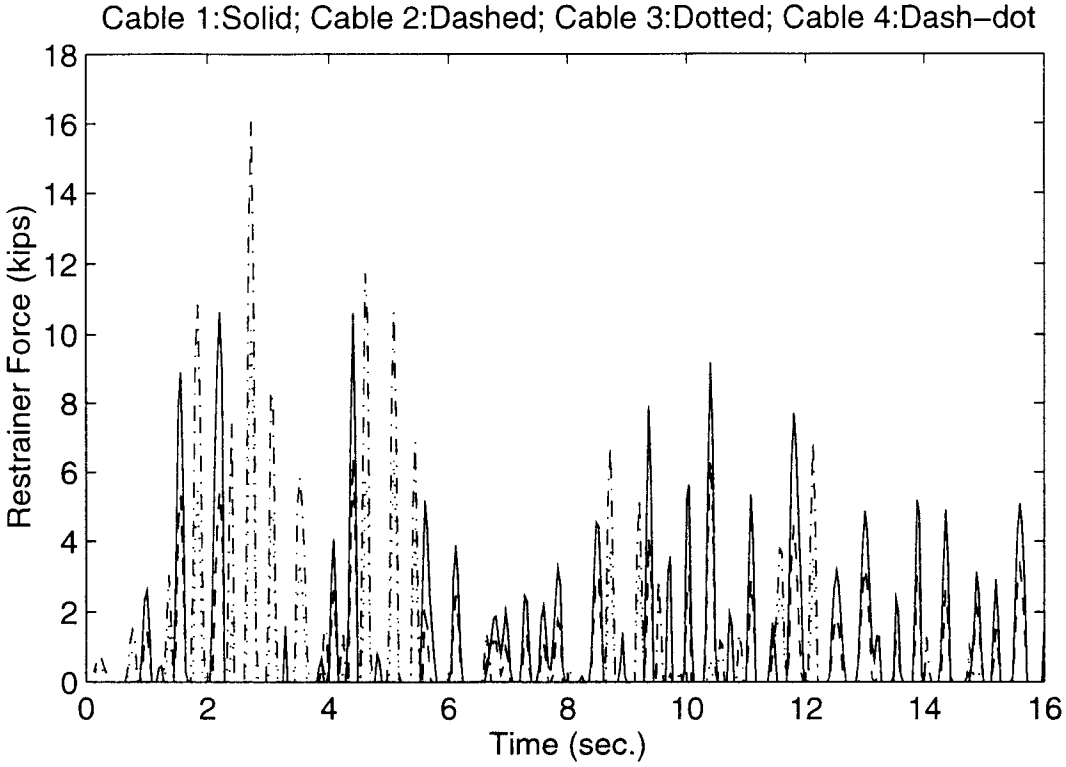

Figure 6.1-9: Restrainer Force Responses at Expansion Joint 1

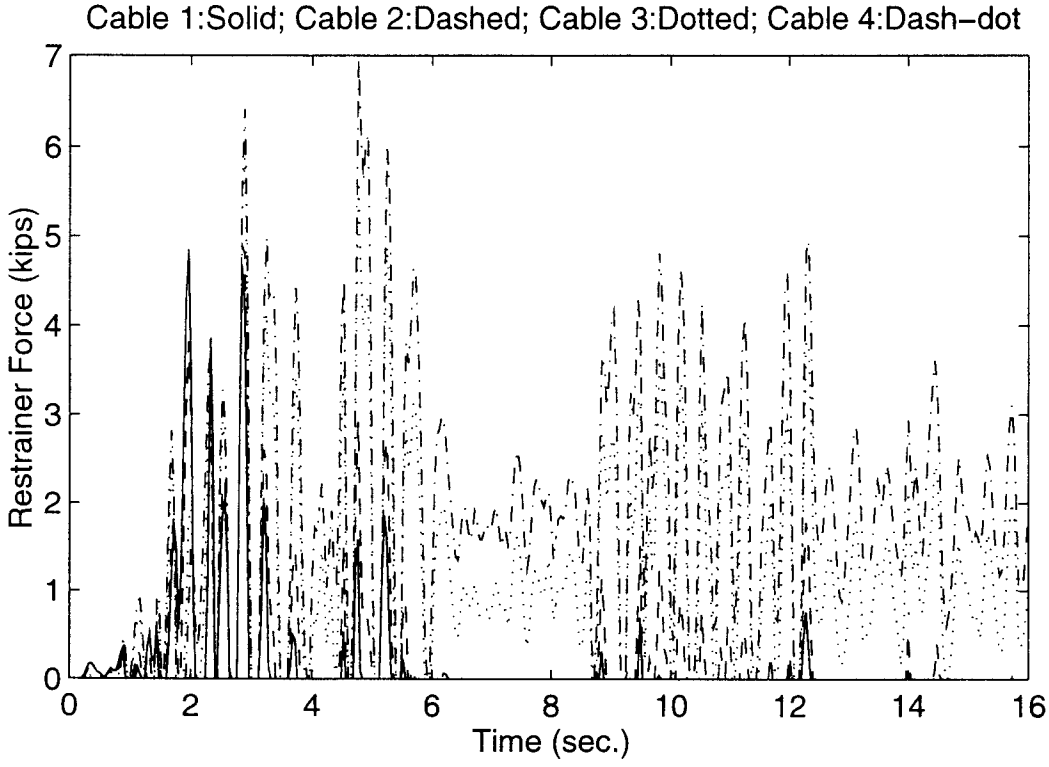

Figure 6.1-10: Restrainer Force Responses at Expansion Joint 2

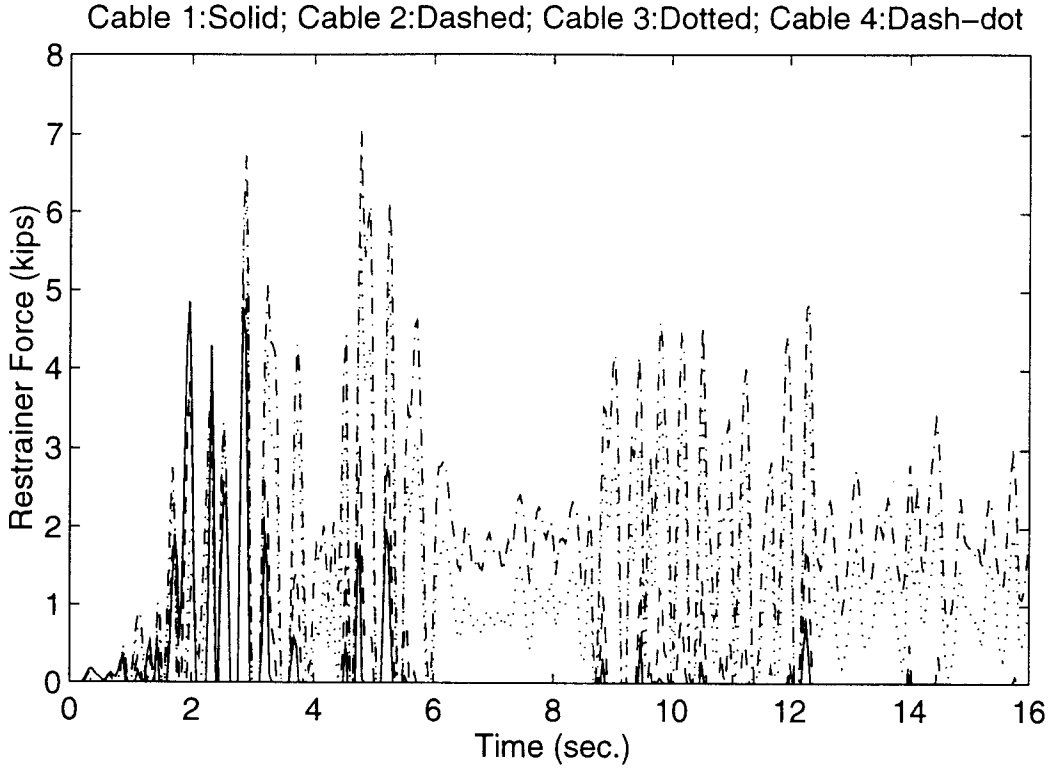

Figure 6.1-11: Restrainer Force Responses at Expansion Joint 3

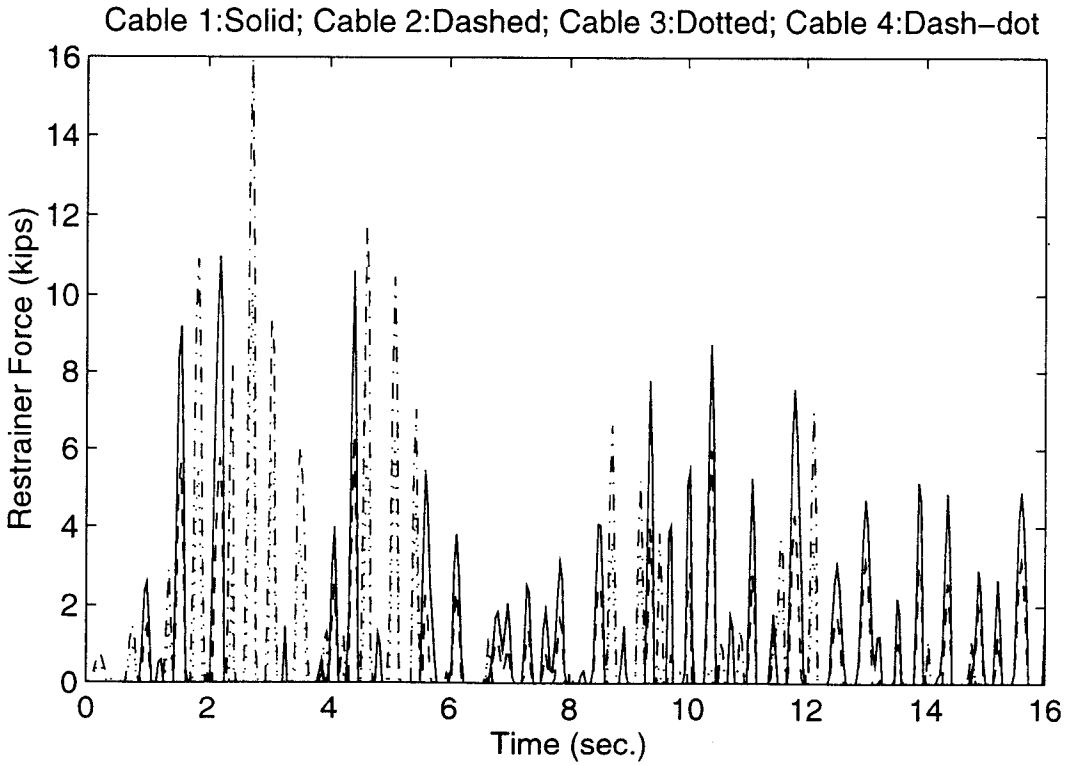

Figure 6.1-12: Restrainer Force Responses at Expansion Joint 4

6.1.5.3 Maximum Column Moments and Shears

The maximum values of column moments and shears are tabulated for the bottom of columns in Tables 6.1- 6 and 6.1-7, respectively. Only the maximum column moment values that occur about the axis normal to the direction of the base motion, and the shear values that occur parallel to the direction of the base motion, are tabulated. The tabulated maximum values of moment and shear are considered to be control values. The bent number included in tables 6.1-6 and 6.1-7 is counted from the bent on the far left to the bent on the far right, as shown in Figure 6.1-3. The column number for each bent included in tables 6.1-6 and 6.1-7 is also shown in Figure 6.1-3.

The results tabulated in Tables 6.1-6 and 6.1-7 indicate that values of the maximum moments and shears for the middle column in a bent are typically the largest compared to those with other columns in the bent. Under the unretrofitted condition, the maximum values of moment and shear between the first three and the last three bents is significantly different. The possible explanation for this difference is the influence of the rockers. As described before, the deck on the extreme left is supported by the rockers located on the fourth bent cap, but the deck on the extreme right inlays the sixteenth bent cap. The rocker cannot provide stiffness in the longitudinal direction. Therefore, the free movement between the deck on the extreme left and the fourth bent cap prevented the earthquake force from entering the other bridge sections to a certain degree. Contrarily, the strong ledge connection between the deck on the extreme right and the sixteenth bent cap made the earthquake force redistribute more easily. It is interesting to note that the addition of restrainers has substantially lowered the maximum moments and shears at

Table 6.1-6: Maximum Moments ($kN-m$) at the Bottoms of Columns

		Column No.				
Bent No.	Case No.	1	2	3	4	5
1	1	233	230	384	246	203
	2	94	102	98	94	94
2	1	237	264	382	274	241
	2	188	199	195	192	188
3	1	245	304	516	285	244
	2	233	234	293	240	230
4	1	236	247	290	251	239
	2	239	263	361	257	237
5	1	213	237	414	249	234
	2	240	263	398	254	237
6	1	238	253	367	288	239
	2	239	260	394	251	237
7	1	244	282	419	435	243
	2	239	258	411	249	237
8	1	239	252	337	277	240
	2	239	254	378	246	237
9	1	205	239	404	249	233
	2	238	258	414	248	237
10	1	237	252	370	287	239
	2	239	257	396	247	236
11	1	244	283	419	423	243
	2	238	258	414	248	236
12	1	243	260	352	276	242
	2	237	254	378	246	237
13	1	233	238	232	235	223
	2	239	258	411	249	237
14	1	237	250	361	258	239
	2	239	260	394	251	237
15	1	241	277	411	280	244
	2	240	263	397	254	237
16	1	248	264	342	262	245
	2	240	263	361	257	237
17	1	229	229	258	237	225
	2	232	234	293	240	230
18	1	166	176	172	169	166
	2	188	199	195	192	188
19	1	83	90	86	82	83
	2	94	102	98	94	94

Note: Case 1: Unretrofitted; Case 2: Retrofitted.

Table 6.1-7: Maximum Shears (kN) at the Bottoms of Columns

		Column No.				
Bent No.	Case No.	1	2	3	4	5
1	1	101	100	167	106	88
	2	40	45	42	40	40
2	1	102	115	166	119	104
	2	80	87	85	83	80
3	1	106	132	225	124	106
	2	100	101	127	104	97
4	1	101	107	127	108	103
	2	103	114	157	112	102
5	1	90	103	178	108	101
	2	103	114	172	110	102
6	1	102	109	158	125	103
	2	103	112	171	109	102
7	1	105	122	182	190	105
	2	103	112	178	108	102
8	1	103	109	146	121	104
	2	103	110	164	106	102
9	1	89	104	173	108	101
	2	103	112	180	107	102
10	1	102	109	160	125	103
	2	103	111	172	107	102
11	1	105	123	182	185	105
	2	103	112	180	107	102
12	1	105	112	152	120	105
	2	103	110	164	106	102
13	1	100	98	100	102	95
	2	103	112	178	108	102
14	1	102	108	156	111	103
	2	103	112	171	109	102
15	1	104	120	179	121	105
	2	103	114	172	110	102
16	1	107	115	148	114	106
	2	103	114	157	111	102
17	1	99	99	112	103	96
	2	100	101	127	104	97
18	1	71	77	75	73	71
	2	80	87	84	83	80
19	1	35	40	37	35	36
	2	40	45	42	40	40

Note: Case 1: Unretrofitted; Case 2: Retrofitted.

Bents 1, 2, and 3; however, for Bents 18 and 19, the maximum moments and shears have a slight increase with the retrofitted conditions. This increase is not considered to be significant because none of the columns in the two bents developed yielding under the retrofitted condition (static yielding moment = 268 $kN-m$). The changes of maximum moments and shears for columns in other bents under unretrofitted and retrofitted conditions are minor.

6.2 Conclusions and Recommendations

As expected, a substantial reduction in deck separation resulted when the longitudinal restrainers were installed at expansion joints. In most bents, the redistribution of earthquake forces caused by the addition of restrainers was not very significant. For the unretrofitted condition, relatively large separations were observed at two expansion joints. The large separation was considered to be serious because the available seat width for each expansion joint is only 7.62 cm. In addition, impacting also occurred for the unretrofitted condition. It has been pointed out (Imbsen and Penzien, 1986) that if the impacting forces can not be absorbed by any energy-dissipating mechanism, the impacting will produce high shear forces at bearings and cause those bearings to fail. Therefore, retrofit effort toward decreasing the effects of colliding should be considered.

Chapter 7

Summary and Recommendations

7.1 Summary and Conclusions

Two actual highway bridges modeled with three structural models were analyzed with a modified version of the nonlinear analysis program, NEABS. The computational results indicated that the nonlinear elastic-plastic analysis is significantly influenced by including softening behavior and degradation of stiffness in which the bending moment capacity and elastic stiffness are allowed to degrade. Because concrete columns designed using pre-1971 codes are typically deficient in flexural strength from inadequate lap splices in critical regions due to premature termination of longitudinal reinforcement, these effects, i.e. softening and degradation of stiffness, have special significance for older columns. In the absence of physical test data on the nonlinear behavior of actual highway bridges subjected to dynamic loads of an earthquake, the effective analysis of these bridges built before 1971, i.e., including the flexural softening and stiffness degradation effects, will help bridge designers to evaluate more exactly the structural demand of the bridges.

Although a number of column retrofit strategies for multi-column bridges currently are available in the United States, the optimal selection of these strategies strongly relies on the development of energy absorption in the non-ductile components to dissipate earthquake-induced forces. Because the partial column retrofit strategies on pre-1971

constructed bridges allow for the existence of some old and unretrofitted columns, an accurate beam-column element representing the true structural behavior is neccessary for the nonlinear analysis of partially retrofitted bridges. The beam-column element developed herein, which includes the softening effect, is a more realistic idealization of a reinforced concrete column constructed by the pre-1971 design codes than the elastic-perfectly plastic idealization originally used in NEABS. Moreover, the hysteresis rule for cyclic loadings proposed and then implemented into NEABS is also more realistic for the nonlinear analysis. Therefore, the modified NEABS program, including the effects of flexural softening and degradation of stiffness, provides a practical method for evaluating the effectiveness of column retrofit measures when earthquake records are applied to highway bridges.

Through the analysis of the two actual highway bridges under unretrofitted conditions, it was found that flexural yielding and softening occurred at the base of the columns, leaving only residual flexural strength. Thus, the plastic deformation of the columns was considerable due to the softening. Indeed, the unretrofitted Mercer Slough bridge bent collapsed during the input earthquake because of unacceptable displacement levels. To reduce the plastic deformation and increase ductile capacity of the bridges, both partial and full retrofit measures used in the study were effective; however, the levels of effectiveness were not the same. Generally speaking, with an increase in the number of retrofitted columns in a bridge bent, the ductility demand is reduced. Although some partial retrofit strategies analyzed in the study can improve the seismic resistance of bridges to a certain degree, at the same time substantial damage was found at the bases of

the unretrofitted columns. On the basis of plastic hinge rotation, this damage is considered to be unacceptable. For practical purposes, those partial retrofit measures that cause severe column damage are not recommended. A careful examination of the available retrofit measures will therefore be required through comparison of responses and by checking the level of damage.

The discontinuity caused by the presence of the expansion joints greatly complicates the structural properties of bridges. A rational model that includes the main behavior of the expansion joints during dynamic loading is critical to exactly predict the response of bridges. The expansion joint element provided by NEABS includes behavior such as sliding friction between superstructure and substructure, impacting, and tie bars. These components are capable of capturing the primary nonlinear factors of the expansion joints. In the absence of a more accurate model, the expansion joint element may be used to estimate the opening and closing of the expansion joints.

The performance of the cable restrainers used in this study basically achieved the goals for which they were designed. Substantial reductions in the separations were observed. However, the force redistribution caused by the installation of cable restrainers was not significant in the case that was studied. As reported by McLean and Cannon (1994), the bridge may collapse because of the inadequate ability of the expansion joints to sustain large relative displacements of adjacent bridge units during a major earthquake. The analytical results from the three-dimensional analysis of the bridge, in which the superstructure was not retrofitted, support that conclusion. Large relative displacements between the decks were seen despite the fact that the earthquake used in this analysis was

only a moderate one. Moreover, impacting between the adjacent decks was also observed. Collisions can cause high shear forces at the connection between the superstructure and substructure, resulting in failure of the bearings prior to the development of plastic hinges in the columns.

7.2 Recommendations

As described, flexural softening and the degradation of stiffness were added to the beam-column element in NEABS. Based on the results of this research effort, the following recommendations are made regarding improvements of earthquake resistance for highway bridges:

1. Due to the unique dynamic characteristics of bridge structures, retrofit efforts for the members of highway bridges should be based on the dynamic response from nonlinear analyses using appropriate nonlinear models to represent the true structural system.
2. The modified computer program, NEABS, may be used as a tool to evaluate seismic retrofit strategies, e.g., column or superstructure retrofitting. The program provides two models dealing with flexural strength and ductility for the beam-column element. One model is based on the elastic-perfectly plastic assumption, and the other is based on the elastic plastic softening assumption. For the columns that were designed by post-1971 design codes with adequate confinement or strengthened by retrofit measures at plastic hinge zones, it is suitable to select the first model; otherwise the latter one should be used.

3. To ensure the accuracy of the predicted response, it is important that the column ductility and strength should be assessed thoroughly. Use of the methods described in Chapter 4 are recommended in order to achieve these assessments.
4. Once the elastic plastic softening model is chosen, the critical curvature that indicates the point at which softening begins and maximum theoretical curvature for which the maximum capability is equal to zero should be defined for the nonlinear analysis. According to the conclusions drawn by Jaradat (1996) in his Ph.D. dissertation, the flexural strength model proposed by Priestley and Seible (1994) and used in this study closely predicted the flexural behavior of the platic hinge regions with poor confinement with lap splices. Thus, it may be used to define these two parameters.
5. It was assumed in this research that the shear strength of the column in the plastic hinge region would remain intact in the nonlinear analyses. However, the testing conducted by Jaradat, McLean, and Marsh (1995) on bridge column specimens that incorporated pre-1971 design under seismic loading indicated that column shear failure may occasionally occur because of diagonal cracks that can form at low and high displacement levels. Obviously, this type of brittle failure will have an influence on the response of the bridges. Therefore, further research is needed to include shear softening effects in the beam-column element of NEABS.
6. Impacting effects should be studied carefully because they occurred to the unretrofitted superstructure of the Mercer Slough bridge for the input earthquake record. Retrofitting methods should be proposed to reduce these effects. This is

particularly important when nonductile bearing components separate the superstructure mass from the energy-absorbing ductile columns.

7. The evaluation of seismic response for highway bridges is complicated and may be influenced by many factors. Additional parametric studies should be conducted so that more general conclusions can be reached. These analyses should include various soil conditions, soil-structure interaction on typical bridge foundations, and different earthquakes.
8. In this research, it was assumed that the failure is constrained to occur in the columns and will not be permitted to migrate into the foundation. However, since any retrofit of a column will necessarily increase the loading on the foundation, further study is required to determine if failure may occur in the foundation and what subsequent strengthening would be required of the foundation in that case.

References

AASHTO LRFD Bridge Design Specification, American Association of State Highway and Transportation Officials, Washington, DC.

Al-Sulaimani, G.J., and Roessett, J.M., "Design Spectra for Degrading Systems," Journal of Structural Engineering, ASCE, Vol. 111, No. 12, December 1985, pp. 2611-2623.

Atalay, B., and Penzien, J., "The Seismic Behavior of Critical Regions of Reinforced Concrete Components as Influenced by Moment, Shear and Axial Force," EERC-Report No. 75-19, Earthquake Engineering Research Center, University of California, Berkeley, California, 1975.

Bresler, B., "Design Criteria for Reinforced Columns under Axial Load and Biaxial Bending," ACI, Vol. 32, No. 5, November 1960.

Buckle, I.G., and Friedland, I.M., Editors, "Seismic Retrofitting Manual for Highway Bridges," US Department of Transportation, Federal Highway Administration, Publication No. FHWA-RD-94-052, May 1995.

Buckle, I.G., Mayes, R.L., and Button, M.R., "Seismic Design and Retrofit Manual for Highway Bridges," Final Report, Federal Highway Administration, 1987.

Chai, Y.H., Priestley, M.J.N., and Seible, F., "Flexural Retrofit of Circular Reinforced Concrete Bridge Columns by Steel Jacketing," University of California, San Diego, Structural Systems Research Project, Report No. SSRP 91/06, October 1991, pp. 151.

Chen, M.C., and Penzien, J., "Analytical Investigation of Seismic Response of Short, Single or Multiple-Span Highway Bridges," Report No. FHWA-RD-75-10, Earthquake Engineering Research Center, University of California, Berkeley, California, January 1975.

Chen, W.F., and Han, D.J., "Plasticity for Structural Engineers," Springer-Verlag, New York, 1988.

Clough, R.W., "Effect of Stiffness Degradation on Earthquake Ductility Requirements," Report 66-16, Structural and Materials Research, Structural Engineering Laboratory, University of California, Berkeley, California, 1966.

Clough, R.W., and Penzien, J., Dynamics of Structures, Second Edition, McGraw-Hill, Inc., New York, 1993.

Cofer, W.F., McLean, D.I., and McGuire, J.W., "Analytical Modeling of Foundations for Seismic Analysis of Bridges," Research Report T9234-02, Washington State Department of Transportation, February 1994.

Cooper, J.D., and Buckle, I., "Lessons from the Kobe Quake," Public Roads, Autumn 1995, Vol. 59, No. 2, pp. 28-37.

Cooper, J.D., Friedland, I.M., Buckle, I. G., Nimis, R.B., and Bobb, N.M., "The Northridge Earthquake: Progress Made, Lessons Learned in Seismic Resistant Bridge Design," Public Road, Summer 1994, Vol. 58, No. 1., pp. 26-36.

Darvall, P.L., "Stiffness Matrix for Elastic-Softening Beams," Journal of Structural Engineering, Vol. 111, No. 2, February 1985, pp. 469-473.

Darvall, P.L., and Mendis, P.A., "Elastic-Plastic-Softening Analysis of Plane Frames," Journal of Structural Engineering, Vol. 111, No. April 1985, pp. 871-888.

Eberhard, M.O., and Marsh, M.L., (in review) "Lateral-Load Response of Two Reinforced Concrete Bents," Journal of Structural Engineering, ASCE.

Eberhard, M.O., Maclardy, J.A., Marsh, M.L., and Hjartarson, G., "Lateral-Load Response of A Reinforced Concrete Bridge," Washington State Department of Transportation, Technical Report WA-RD 305.2, Olympia, WA, 1993.

Idriss, I.M., Sun, J.I., and Dirrim, P., "User's Manual for SHAKE91, A Computer Program for Conducting Equivalent Linear Response Analysis of Horizontally Layered Soil Deposits," Department of Civil Engineering, University of California, Davis, California, 1992.

Imbsen, R., and Nutt, R.V., and Penzien, J., "Seismic Response of Bridges-Case Studies," Report No. FHWA-RD-78-157, Earthquake Engineering Research Center, University of California, Berkeley, California, June 1978.

Imbsen, R., and Penzien, J., "Evaluation of Energy Absorption Characteristics of Highway Bridges Under Seismic Conditions," Volume I, UCB/EERC-84/17, Earthquake Engineering Research Center, University of California, Berkeley, California, September, 1986

Imbsen, R.A., Nutt, R.V., and Penzien, J., "Evaluation of Analytical Procedures Used in Bridge Seismic Design Practice," Workshop on Earthquake Resistance of Highway Bridges Proceedings, Palo Alto, California, 1979, pp. 467-496.

Iwasaki, T., Penzien, J., and Clough, R., "Literature Survey-Seismic Effects on Highway Bridges," EERC 71-11, Earthquake Engineering Research Center, University of California, Berkeley, California, November, 1972.

Jaradat, O.A., "Seismic Evaluation of Existing Bridge Columns," Ph.D. Dissertation, Department of Civil and Environmental Engineering, Washington State University, Pullman, USA, 1996.

Jaradat, O.A., McLean, D.I., and Marsh, M.L., "Strength Degradation of Existing Bridge Columns under Seismic Loading," Transportation Research Record, Transportation Research Board, In Press, 1996.

Kawashima, K., and Penzien, J., "Correlative Investigations on Theoretical and Experimental Dynamic Behavior of A Model Bridge Structure," Report No. FHWA-W RD-77-57, Earthquake Engineering Research Center, University of California, Berkeley, California, July 1976.

Kramer, S.L., "Seismic Response-Foundation in Soft Soils," Draft Report for Washington State Transportation Center, Seattle, WA, July 1992.

Kunnath, S.R., Reinhorn, A.M., and Lobo, R.F., "IDARC Version 3.0, A Program for the Inelastic Damage Analysis of Reinforced Concrete Structures," Report No. NCEER-92-0002, National Center for Earthquake Engineering Research, State University of New York at Buffalo, Buffalo, New York, 1992.

Marsh, M.L., Effects of Flexural Strength Variations on the Seismic Performance of Reinforced Concrete Multiple Column Bridge Bents, Doctoral Thesis, University of Washington, 1991.

McLean, D.I., and Cannon, I.B.S., Seismic Analysis of the Westbound Lanes of the I-90 Bridges Crossing Mercer Slough, Washington State Department of Transportation, Technical Report WA-RD 299.1, Olympia, WA, 1992.

NEHRP Recommended Provisions for the Development of Seismic Regulations for New Buildings-Part 1 Provisions, Federal Emergency Management Agency, National Earthquake Hazards Reduction Program, 1991.

Park, Y.J., and Ang, H-S., "Mechanistic Seismic Damage Model for Reinforced Concrete," Journal of Structural Engineering, Buckle Vol. 111 No. 4, April 1985, pp. 722-739.

Penzien, J., Imbsen, R.A., and Liu, W.D., NEABS (Nonlinear Earthquake Analysis of Bridge Systems), A Computer Program Source Code and User's Manual, National Information Service for Earthquake Engineering, EERC, University of California, Berkeley, California, 1981.

Powell, G.H., "Modeling of Reinforced Concrete Bridge Column," the Third Caltrans Workshop, Sacramento, June 27-29, 1994.

Prakash, V., Powell, G.H., and Filippou, F.C., "DRAIN-2DX Base Program User's Guide," Report No. UCB/SEMM-92/29, Department of Civil Engineering, University of California, Berkeley, California, 1992.

Priestley, M.J.N., and Seible, F., "Design of Seismic Retrofit Measures for Concrete Bridges," Seismic Assessment and Retrofit of Bridges, SSRP 91/03, 1988.

Priestley, M.J.N., and Seible, F., "Seismic Assessment of Existing Bridges," Seismic Design and Retrofitting of Reinforced Concrete Bridges, Proceedings of the Second International Workshop, Queenstown, New Zealand, August, 1994, pp. 447-471.

Priestley, M.J.N., and Seible, S., "Retrofitting," Proceeding, "International Workshop on Seismic Design and Retrofitting of Reinforced Concrete Bridges," G. M. Calvi and M. J. N. Priestley, Editors, Bormio 1991, pp. 529-568.

Priestley, M.J.N., Seible, F., and Chai, Y.H., "Design Guidelines for Assessment Retrofit and Repair of Bridges for Seismic Performance," Report No. SSRP-92/01, Department of Applied Mechanics and Engineering Sciences, University of California, San Diego, California, 1992 pp. 266, 1992.

Roberts, J.E., "Improved Seismic Details for Highway Bridges," California Department of Transportation, Sacramento, California, 1995.

Rodriguez-Gomez, S., Chung, Y.S., and Meyer, C., "SARCF-II User's Guide: Seismic Analysis of Reinforced Concrete Frames," Report No. NCEER-90-0027, National Center for Earthquake Engineering Research, State University of New York at Buffalo, Buffalo, New York, 1990.

Saiidi, M., Maragakis, E., and Feng, S., "Parameters in Bridge Restrainer Design for Seismic Retrofit," Journal of Structural Engineering, Vol. 122, No. 1, January 1996.

Sanjayan, G., "Dynamic Response of Reinforced Concrete Structures with Softening Behavior," Ph.D. Dissertation, Department of Civil Engineering, Monash University, Clayton, Victoria, Australia, 1988.

Sanjayan, G., and Darvall, P.L., "Singularities in RC Beam Elements with Finite Length Hinges," Journal of Structural Engineering, Vol. 121, No. 1, pp. 39-47, January 1995.

Stone, W.C., and Taylor, A., "ISDP: Integrated Approach to Seismic Design of Reinforced Concrete Structures," Journal of Structural Engineering, Vol. 120, No. 12, December 1994, pp. 3548-3566.

Tan, B.S., and Wilson, J.C., "Models for Seismic Response of Highway Bridge Abutments," 5th Canadian Conference of Earthquake Engineering, Ottawa, Canada, 1987.

Todd, D., Nicholas, N., Chung, R.M., Lew, H.S., Taylor, A.W., Walton, W.D., Cooper, J.D., and Nimis, R., "1994 Northridge Earthquake, Performance of Structures, Lifelines, and Fire Protection Systems," NIST Special Publication 862, United States Department of Commerce, Technology Administration, National Institute of Standards and Technology, May 1994.

Tseng, W., and Penzien, J., "Analytical Investigations of the Seismic Response of Long Multiple-Span Highway Bridges," Earthquake Engineering Research Center, University of California, Berkeley, California, June, 1973.

Uniform Building Code, Structural Engineering Design Provisions, International Conference of Building Officials, Volume 2, 1991.

Williams, D., and Godden, W.G., "Experimental Model Studies on the Seismic Response of High Curved Overcrossings," Report No. FHWA-RD-77-91, Earthquake Engineering Research Center, University of California, Berkeley, California, June 1976.

Wood, R.H., "Some Controversial and Curious Developments in the Plastic Theory of Structures," Engineering Plasticity, J. Heyman and F. A. Leckie Editors, Cambridge University Press, London, England, 1968, pp. 665-691.

Appendix A

NEABS User's Guide Supplement

A.1 Introduction

This appendix is supplementary to the modified NEABS User's Guide by Cofer, McLean, and McGuire in 1994 in order to include the softening and stiffness degradation effects in the beam-column element. Users must first refer to the NEABS Guide (Penzien, Imbsen, and Liu, 1981) and the NEABS User's Guide Supplement (Cofer, McLean, and McGuire, 1994).

A.2 Additions to the Required Input Data

A new card is added to Nonlinear Property Cards for Elasto-Plastic Flexural Beam Elements behind Card 2, called Card 3. The format and meaning of the parameters for Card 3 are:

Card 3:

Columns		
1-10	ENPROP(N,13)	Critical plastic rotation angle at I-end
11-20	ENPROP(N,14)	Maximum theoretical plastic rotation angle at I-end
21-30	ENPROP(N,15)	Critical plastic rotation angle at J-end

31-40	ENPROP(N,16)	Maximum theoretical plastic rotation angle at J-end

Appendix B

Elastic & Release Stiffness Matrices for Beam-Column Element

B.1 Introduction

This appendix lists the elastic stiffness matrix used in NEABS for the beam-column element. Moreover, the release matrices used in Section 2.5 to include the stiffness degradation effect for cyclic loading are also listed. The physical meaning for these release matrices can be found in this chapter.

B.2 Elastic Stiffness Matrix

For a three dimensional beam-column element, as shown in Figure 2.3-6, the elastic stiffness matrix is:

$$
\underline{k}^e = \begin{bmatrix}
\frac{EA}{L} & & & & & & & & & & & \\
0 & \frac{12EI_z}{L^3(1+\phi_y)} & & & & & & & & & & \\
0 & 0 & \frac{12EI_y}{L^3(1+\phi_z)} & & & & & & & & & \\
0 & 0 & 0 & \frac{GJ}{L} & & & & & & & & \\
0 & 0 & -\frac{6EI_y}{L^2(1+\phi_y)} & 0 & \frac{(4+\phi_y)EI_y}{L(1+\phi_z)} & & & & & & & \\
0 & \frac{6EI_z}{L^2(1+\phi_y)} & 0 & 0 & 0 & \frac{(4+\phi_y)EI_z}{L(1+\phi_y)} & & & & & & \\
-\frac{EA}{L} & 0 & 0 & 0 & 0 & 0 & \frac{EA}{L} & & & & & \\
0 & -\frac{12EI_z}{L^3(1+\phi_y)} & 0 & 0 & 0 & -\frac{6EI_z}{L^2(1+\phi_y)} & 0 & \frac{12EI_z}{L^3(1+\phi_y)} & & & & \\
0 & 0 & -\frac{12EI_y}{L^3(1+\phi_z)} & 0 & \frac{6EI_y}{L^2(1+\phi_z)} & 0 & 0 & 0 & \frac{12EI_y}{L^3(1+\phi_z)} & & & \\
0 & 0 & 0 & -\frac{GJ}{L} & 0 & 0 & 0 & 0 & 0 & \frac{GJ}{L} & & \\
0 & 0 & -\frac{6EI_y}{L^2(1+\phi_z)} & 0 & 0 & \frac{(2-\phi_z)EI_y}{L(1+\phi_z)} & 0 & 0 & 0 & \frac{6EI_y}{L^2(1+\phi_z)} & \frac{(4+\phi_z)EI_y}{L(1+\phi_z)} & \\
0 & \frac{6EI_z}{L^2(1+\phi_y)} & 0 & 0 & 0 & \frac{(2-\phi_y)EI_z}{L(1+\phi_y)} & 0 & -\frac{6EI_z}{L^2(1+\phi_y)} & 0 & 0 & 0 & \frac{(4+\phi_y)EI_z}{L(1+\phi_y)}
\end{bmatrix}
$$

where,

A =cross sectional area of the beam-column element;

E =modulus of elasticity;

G =shear modulus;

I_y =bending inertia about the local y-axis;

I_z =bending inertia about the local z-axis;

$$\phi_y = \frac{12EI_z}{GA_{sy}L^2};$$

$$\phi_z = \frac{12EI_y}{GA_{sz}L^2};$$

A_{sy} =shear area in the local y-direction;

A_{sz} =shear area in the local z-direction.

B.3 Release Stiffness Matrices

The release matrices $\underline{k}^e_{miy}$, $\underline{k}^e_{miz}$, $\underline{k}^e_{mjy}$, and $\underline{k}^e_{mjz}$ used in Section 2.5 are:

$$\underline{k}^e_{miy} = \begin{bmatrix}
0 & & & & & & & & & & & \\
0 & 0 & & & & & & & & & & \\
0 & 0 & \frac{36EI_y}{L^3(1+\phi_z)(4+\phi_z)} & & & & & & & & & \\
0 & 0 & 0 & 0 & & & & & & & & \\
0 & 0 & -\frac{6EI_y}{L^2(1+\phi_y)} & 0 & \frac{(4+\phi_y)EI_y}{L(1+\phi_z)} & & & & & & & \\
0 & 0 & 0 & 0 & 0 & 0 & & & & & & \\
0 & 0 & 0 & 0 & 0 & 0 & 0 & & & & & \\
0 & 0 & 0 & 0 & 0 & 0 & 0 & 0 & & & & \\
0 & 0 & -\frac{36EI_y}{L^3(1+\phi_z)(4+\phi_z)} & 0 & \frac{6EI_y}{L^2(1+\phi_z)} & 0 & 0 & 0 & \frac{36EI_y}{L^3(1+\phi_z)(4+\phi_z)} & & & \\
0 & 0 & 0 & 0 & 0 & 0 & 0 & 0 & 0 & 0 & & \\
0 & 0 & -\frac{6(2-\phi_z)EI_y}{L^2(1+\phi_z)(4+\phi_z)} & 0 & -\frac{(2-\phi_z)EI_y}{L(1+\phi_z)} & 0 & 0 & 0 & -\frac{6(2-\phi_z)EI_y}{L^2(1+\phi_z)(1+\phi_z)} & 0 & \frac{(2-\phi_z)^2EI_y}{L(1+\phi_z)(4+\phi_z)} & \\
0 & 0 & 0 & 0 & 0 & 0 & 0 & 0 & 0 & 0 & 0 & 0
\end{bmatrix}$$

$$\underline{k}^{e}_{miz} = \begin{bmatrix}
0 & & & & & & & & & & & \\
0 & \frac{36EI_z}{L^3(1+\phi_y)(4+\phi_y)} & & & & & & & & & & \\
0 & 0 & 0 & & & & & & & & & \\
0 & 0 & 0 & 0 & & & & & & & & \\
0 & 0 & 0 & 0 & 0 & & & & & & & \\
0 & \frac{6EI_z}{L^2(1+\phi_y)} & 0 & 0 & 0 & \frac{(4+\phi_y)EI_z}{L(1+\phi_y)} & & & & & & \\
0 & 0 & 0 & 0 & 0 & 0 & & & & & & \\
0 & -\frac{36EI_z}{L^3(1+\phi_y)(4+\phi_y)} & 0 & 0 & 0 & -\frac{6EI_z}{L^2(1+\phi_y)} & 0 & \frac{36EI_z}{L^3(1+\phi_y)(4+\phi_y)} & & & & \\
0 & 0 & 0 & 0 & 0 & 0 & 0 & 0 & 0 & & & \\
0 & 0 & 0 & 0 & 0 & 0 & 0 & 0 & 0 & 0 & & \\
0 & 0 & 0 & 0 & 0 & 0 & 0 & 0 & 0 & 0 & 0 & \\
0 & \frac{6(2-\phi_y)EI_z}{L^2(1+\phi_y)(4+\phi_y)} & 0 & 0 & 0 & \frac{(2-\phi_y)EI_z}{L(1+\phi_y)} & 0 & -\frac{6(2-\phi_y)EI_z}{L^2(1+\phi_y)(4+\phi_y)} & 0 & 0 & 0 & \frac{(2-\phi_y)^2 EI_z}{L(1+\phi_y)(4+\phi_y)}
\end{bmatrix}$$

$$\underline{k}^{e}_{mjy} = \begin{bmatrix}
0 & & & & & & & & & & & \\
0 & 0 & & & & & & & & & & \\
0 & 0 & \frac{36EI_y}{L^3(1+\phi_z)(4+\phi_z)} & & & & & & & & & \\
0 & 0 & 0 & 0 & & & & & & & & \\
0 & 0 & -\frac{6(2-\phi_z)EI_y}{L^2(1+\phi_z)(4+\phi_z)} & 0 & \frac{(2-\phi_y)^2 EI_y}{L(1+\phi_z)(4+\phi_z)} & & & & & & & \\
0 & 0 & 0 & 0 & 0 & 0 & & & & & & \\
0 & 0 & 0 & 0 & 0 & 0 & 0 & & & & & \\
0 & 0 & 0 & 0 & 0 & 0 & 0 & 0 & & & & \\
0 & 0 & -\frac{36EI_y}{L^3(1+\phi_z)(4+\phi_z)} & 0 & \frac{6(2-\phi_z)EI_y}{L^2(1+\phi_z)(4+\phi_z)} & 0 & 0 & 0 & \frac{36EI_y}{L^3(1+\phi_z)(4+\phi_z)} & & & \\
0 & 0 & 0 & 0 & 0 & 0 & 0 & 0 & 0 & 0 & & \\
0 & 0 & -\frac{6EI_y}{L^2(1+\phi_z)} & 0 & 0 & \frac{(2-\phi_z)EI_y}{L(1+\phi_z)} & 0 & 0 & 0 & \frac{6EI_y}{L^2(1+\phi_z)} & \frac{(4+\phi_z)EI_y}{L(1+\phi_z)} & \\
0 & 0 & 0 & 0 & 0 & 0 & 0 & 0 & 0 & 0 & 0 & 0
\end{bmatrix}$$

and

$$\underline{k}^{e}_{mjz} = \begin{bmatrix}
0 & & & & & & & & & & & \\
0 & \frac{36EI_z}{L^3(1+\phi_y)(4+\phi_y)} & & & & & & & & & & \\
0 & 0 & 0 & & & & & & & & & \\
0 & 0 & 0 & 0 & & & & & & & & \\
0 & 0 & 0 & 0 & 0 & & & & & & & \\
0 & \frac{6(2-\phi_y)EI_z}{L^2(1+\phi_y)(4+\phi_y)} & 0 & 0 & 0 & \frac{(2-\phi_y)^2 EI_z}{L(1+\phi_y)(4+\phi_y)} & & & & & & \\
0 & 0 & 0 & 0 & 0 & 0 & 0 & & & & & \\
0 & -\frac{36EI_z}{L^3(1+\phi_y)(4+\phi_y)} & 0 & 0 & 0 & -\frac{6(2-\phi_y)EI_z}{L^2(1+\phi_y)(4+\phi_y)} & 0 & \frac{36EI_z}{L^3(1+\phi_y)(4+\phi_y)} & & & & \\
0 & 0 & 0 & 0 & 0 & 0 & 0 & 0 & 0 & & & \\
0 & 0 & 0 & 0 & 0 & 0 & 0 & 0 & 0 & 0 & & \\
0 & 0 & 0 & 0 & 0 & 0 & 0 & 0 & 0 & 0 & 0 & \\
0 & \frac{6EI_z}{L^2(1+\phi_y)} & 0 & 0 & 0 & \frac{(2-\phi_y)EI_z}{L(1+\phi_y)} & 0 & -\frac{6EI_z}{L^2(1+\phi_y)} & 0 & 0 & 0 & \frac{(4+\phi_y)EI_z}{L(1+\phi_y)}
\end{bmatrix}$$